CHEMISTRY OF CHELATE-STABILIZED TUNGSTEN(VI) DIALKYL COMPLEXES

By

SHU-YU STEVE WANG

A DISSERTATION PRESENTED TO THE GRADUATE SCHOOL
OF THE UNIVERSITY OF FLORIDA IN PARTIAL FULFILLMENT
OF THE REQUIREMENTS FOR THE DEGREE OF
DOCTOR OF PHILOSOPHY

UNIVERSITY OF FLORIDA

1998

To my wife Becky and my son Kyle

ACKNOWLEDGMENTS

My sincere appreciation is extended to my research advisor, Dr. Jim Boncella, for his excellent guidence and support. Jim helped me from understanding fundamental concepts to developing self-confidence and self-reliance. His advice, patience, and encouragement motivated me during those frustration periods and reminded me to be humble when things went well. I am eternally grateful for what I learned from Jim, professionally and personally.

I am also grateful to Dr. Khalil Abboud for his help, enthusiasm and patience. He taught me everything I know about crystallography, from the basic concepts to how to get high quality crystals. He also helped me solve all the nine X-ray crystal structures in this dissertation, including the one with R_1=1.65%.

I would like to thank the members of my committee, Professors Lisa McElwee-White, David Richardson, Ken Wagener and Anthony Brennan for their help, advice and encouragement. Discussions with Professors Phil Brucat, Bill Weltner, and Bill Dolbier are also instrumental for the kinetics and mechanism work in Chapter 4.

Sincere thanks and affection is also extended to past and present members of the Boncella group. Dr. Dan VanderLende and Dr. Will Vaughan taught me how to work with air- and moisture-sensitive chemicals and how much fun it can be working day and night. Dr. Faisal Shafiq and Dr. Dave Knoeppel helped with my experimental technique, provided me with valuable insight into chemistry and showed me what a professional chemist should be. Percy Doufou, Jerrold Miller, Jon Penney, Perla Izsak, Carlos Ortiz, Leigh Huff, Ryan Mills, Ken Weakley, and Tim Foley have created an enjoyable research environment and helped me with my English and understanding of American Cultures.

My parents have been the biggest push for my desire to learn and strengthen myself. Their love, guidance and support helped me to bring out the best of myself. The important values they instilled in me will always help me with my life.

Finally, and most importantly, I would like to thank my wife and my best friend, Becky. She has been very understanding and supportive throughout these years and never complained about spending numerous nights alone because I had another "overnighter." Her love has made my life wonderful and worthwhile. And the best gift she gave me, our son Kyle, has been the best cure when my experiments did not work and the biggest inspiration helping me through those difficult times.

TABLE OF CONTENTS

ACKNOWLEDGMENTS iii

ABSTRACT viii

CHAPTERS

1. INTRODUCTION AND BACKGROUND 1

Synthesis of Transition Metal Alkyl Complexes 1
Decomposition of Transition Metal Alkyl Complexes 4
β-H Elimination and Abstraction 4
Decomposition of Metallacycles 7
α-H Elimination 8

2. SYNTHESIS, STRUCTURE AND REACTIVITY OF DIALKYL COMPLEXES 13

Synthesis of W(VI) Dialkyl Complexes 13
Structure Study for W(VI) Dialkyl Complexes 15
Pentacoordinated Complexes 25
Berry Pseudorotation 26
Turnstile Process 26
Fluxionality of Compounds with Bulky Alkyl Groups 28
Equilibrium Between SP and TBP Isomers of **7** 31
Coordination of Trimethylphosphine 35
Insertion Reaction of Isocyanide and **6** 49

3. METATHESIS REACTION AND THE CHEMISTRY OF TUNGSTA(VI)METALLACYCLOPENTANE 52

Synthesis of the Alkylidene Complex 52
Olefin Metathesis 53
Metathesis Reactions of 1-Pentene 56
Formation of Metallacyclopentane Complex 58
Mechanism of the Formation of Metallacyclopentane Complex 63
Conclusions 70

4. MECHANISTIC INVESTIGATIONS OF THE DECOMPOSITION OF β-H CONTAINING W(VI) DIALKYL COMPLEXES 72

Introduction 72
Synthesis of Tungsten(IV) Olefin Complexes 73
Mechanistic Studies 77

Phosphine Dependence 82
Deuterium Labeling Experiment 84
Mechanistic Study of the Formation of ethylene complex, **39** 89
Mechanistic Study of the Formation of styrene complex, **40** 91
Calculation of Entropy of Activation 99
α- vs β-Abstraction Reactions 102
Discussion and Conclusion 104

5. HYDROGENOLYSIS AND HYDROGENATION REACTIONS 106

Introduction 106
Synthesis of Hydridotungsten(VI) Complexes 107
Reactivity of W(VI) Dihydrides, **44** and **45** 112
Catalytic Hydrogenation Reactions 114
Introduction 114
Catalytic Hydrogenation of Alkenes by **44** or **40** 115
Synthesis and Reactivity of W(NPh)[*o*-$(Me_3SiN)_2C_6H_4$](η^6-PhEt), **43** 118

6. EXPERIMENTAL PROCEDURES 122

Materials and Methods 122
Syntheses 123
Preparation of [*o*-$(Me_3SiNH)_2C_6H_4$, **1** 123
Preparation of W(NPh)[*o*-$(Me_3SiN)_2C_6H_4$]$(Cl)_2$, **2** 123
Preparation of W(NPh)[*o*-$(Me_3SiN)_2C_6H_4$]$(CH_3)_2$, **3** 124
Preparation of W(NPh)[*o*-$(Me_3SiN)_2C_6H_4$]$(CH_2CH_3)_2$, **4** 124
Preparation of W(NPh)[*o*-$(Me_3SiN)_2C_6H_4$]$(CH_2CD_3)_2$, **4-*d*$_6$** 125
Preparation of W(NPh)[*o*-$(Me_3SiN)_2C_6H_4$]$(CH_2CH_2CH_3)_2$, **5** 125
Preparation of W(NPh)[*o*-$(Me_3SiN)_2C_6H_4$]$(CH_2CH_2Ph)_2$, **6** 126
Preparation of W(NPh)[*o*-$(Me_3SiN)_2C_6H_4$]$(CH_2CD_2Ph)_2$, **6-*d*$_4$** 127
Preparation of W(NPh)[*o*-$(Me_3SiN)_2C_6H_4$]$(CH_2CH(CH_3)_2)_2$, **7** 127
Preparation of W(NPh)[*o*-$(Me_3SiN)_2C_6H_4$]$(Ph)_2$, **8** 128
Preparation of W(NPh)[*o*-$(Me_3SiN)_2C_6H_4$]$(CH_2Ph)_2$, **9** 129
Prepararion of W(NPh)[*o*-$(Me_3SiN)_2C_6H_4$]$(CH_2C(CH_3)_3)_2$, **10** 129
Prepararion of W(NPh)[*o*-$(Me_3SiN)_2C_6H_4$]$(CH_2C(CH_3)_2Ph)_2$, **11** 130
Prepararion of W(NPh)[*o*-$(Me_3SiN)_2C_6H_4$]$(CH_2Si(CH_3)_3)_2$, **12** 131
Preparation of W(NPh)[*o*-$(Me_3SiN)_2C_6H_4$]$(CH_2CH_3)Cl$, **13** 131
Preparation of W(NPh)[*o*-$(Me_3SiN)_2C_6H_4$]$(CH_2CH_2Ph)Cl$, **14** 132
Prepararion of W(NPh)[*o*-$(Me_3SiN)_2C_6H_4$]$(CH_2C(CH_3)_3)Cl$, **15** 133
Preparation of W(NPh)[*o*-$(Me_3SiN)_2C_6H_4$][η^2-(tBu)NC$CH_2CH_2Ph]_2$, **26** 133
Preparation of W(NPh)[*o*-$(Me_3SiN)_2C_6H_4$][(tBu)NC(CH_2CH_2Ph)= C(CH_2CH_2Ph)N(tBu)] , **27** 134
Preparation of W(NPh)[*o*-$(Me_3SiN)_2C_6H_4$]$(CHCMe_3)(PMe_3)$, **34** 134
Preparation of W(NPh)[*o*-$(Me_3SiN)_2C_6H_4$]$(CH_2CH_2CH_2CH_2)$, **35** 135
Preparation of W(NPh)[*o*-$(Me_3SiN)_2C_6H_4$](CHt-BuCH_2CH_2), **36** 136
Preparation of W(NPh)[*o*-$(Me_3SiN)_2C_6H_4$](η^2-C_2H_4)$(PMe_3)_2$, **39** 136
Preparation of W(NPh)[*o*-$(Me_3SiN)_2C_6H_4$](η^2-CH_2=CHPh)$(PMe_3)_2$, **40** 137
Preparation of W(NPh)[*o*-$(Me_3SiN)_2C_6H_4$](η2-CH_2=$CHCH_3$) $(PMe_3)_2$, **41** 137

Preparation of W(NPh)[*o*-$(Me_3SiN)_2C_6H_4$]$(H)_2(PMe_3)_2$, **44**. 138
Preparation of W(NPh)[*o*-$(Me_3SiN)_2C_6H_4$]$(H)_2$(DPPE), **45**. 139
Kinetics Study 140
Phosphine Dependence 142
Hydrogenation Reaction 142
Crystallographic Studies 143
X-ray data collection and structure refinement for compounds **3**, **10** and **21** 143
X-ray data collection and structure refinement for compounds **35** and **39** 144
X-ray data collection and structure refinement for compound **6**. 144
X-ray data collection and structure refinement for compound **7**. 145

APPENDICES

A TABLES OF CRYSTALLOGRAPHIC DATA 146

B TABLES OF KINETICS STUDIES 226

C INPUT FOR KINFIT SIMULATION PROGRAM 230

D SCHEMATIC SUMMARY OF THE REACTIVITIES OF TUNGSTEN(VI) DLALKYL COMPLEXES 232

LIST OF REFERENCES 234

BIOGRAPHICAL SKETCH 244

Abstract of Dissertation Presented to the Graduate School
of the University of Florida in Partial Fulfillment of the
Requirements for the Degree of Doctor of Philosophy

CHEMISTRY OF CHELATE-STABILIZED TUNGSTEN(VI)
DIALKYL COMPLEXES

By

Shu-Yu Steve Wang

May, 1998

Chairman: James M. Boncella
Major Department: Chemistry

A number of tungsten(VI) imido dialkyl complexes containing the chelating diamido ligand, [*o*-$(NSiMe_3)_2C_6H_4$], have been synthesized with the formulae : W(NPh)[*o*-$(NSiMe_3)_2C_6H_4]R_2$, R = Me(**3**), Et(**4**), *n*-Pr(**5**), CH_2CH_2Ph(**6**), CH_2CHMe_2(**7**), Ph(**8**), CH_2Ph(**9**), CH_2CMe_3(**10**), CH_2CMe_2Ph(**11**), CH_2SiMe_3(**12**). Mono alkyl complexes, W(NPh)[*o*-$(NSiMe_3)_2C_6H_4$]RCl, R = Et, CH_2CH_2Ph, CH_2CHMe_2, **13** - **15**, were also isolated by reacting the dichloride complex, W(NPh)[*o*-$(NSiMe_3)_2C_6H_4]Cl_2$, **2**, with one equivalent of appropriate Grignard reagent.

The structures of these compounds have been fully characterized by NMR spectroscopy and the X-ray crystal structures of **3**, **6**, **10**, and **15** have been determined. All complexes display fluxional behavior between the the trigonal bipyramidal (TBP) and square pyramidal (SP) geometries in solution. The solid state structures reveal the preference for SP structure for small alkyls (e.g. **3**) and the preference of TBP structure for bulky alkyls (e.g. **10**). Lewis base, PMe_3 and *t*-BuNC, adducts can be observed and the coordination modes are discussed.

Mechanisms for the β-H transfer reactions of **4** and **6** with added PMe_3 are proposed. In the diethyl (**4**) case, the reaction involves pre-coordination of PMe_3 followed by rate-limiting β-H abstraction. The reaction of **6** with PMe_3 follows two competing pathways. One is phosphine independent β-H abstraction, and the other is PMe_3 induced β-H elimination/reductive elimination.

Other reactions involving these dialkyl complexes, such as the metathesis reactions of α-olefins, insertion of *t*-BuNC, isomerization and hydrogenation of unsaturated hydrocarbons are also discussed in this dissertation.

CHAPTER 1
INTRODUCTION AND BACKGROUND

Much attention and effort has been focused on transition metal alkyl complexes because of their involvement in many organic and organometallic transformations as well as in catalytic reactions with hydrocarbons in homogeneous and heterogeneous systems.[1,2] Examples include the use of early transition metal (group 3-6) alkyls in olefin polymerization and metathesis reactions,[3] Fischer-Tropsch reactions that are catalyzed by iron and ruthenium alkyls,[4] cobalt and rhodium alkyls used in hydroformylation and acetic acid synthesis,[5] palladium and platinum alkyls used in the copolymerization of CO and ethylene and hydrogenation of alkenes.[6] The study of the properties and reactivities of these compounds is essential to develop an understanding of their role in these transformations and for the design of novel catalysts for further applications.

Synthesis of Transition Metal Alkyl Complexes

The study of metal-alkyl complexes originated with Frankland's discovery of $ZnEt_2$ in 1849. Numerous attempts to prepare transition metal analogs were largely unsuccessful. A few thermally stable compounds such as $[PtIMe_3]_4$ and $[AuBrEt_2]_2$ were isolated and characterized, but most of the work only resulted in the formation of organic decomposition products and low-valent metal species.[7]

It was later realized that thermally stable alkyls could be prepared when "stabilizing" ligands, such as C_p (η^5-cyclopentadienyl), CO, or PR_3 are present. Examples of such

compounds include [$TiPh_2C_{p2}$], [$MnMe(CO)_5$], and *cis*-[$PtEt_2(PMe_3)_2$].[8] The kinetic stability of these compounds arises because the ancillary ligands block the usual decomposition pathways of metal alkyl complexes.

Thermal decomposition of alkyl complexes containing β-hydrogens is usually facile because of β-H elimination reactions (equation 1.1). The complex [$Cr(^tBu)_4$] displays remarkable thermal stability.[9] This is owed to a cog-wheel effect in which the interlocking *t*-butyl groups are rigidly held in a conformation which prevents the β-H atoms from approaching the metal center. Another series of stable complexes were prepared using bridgehead ligands such as 1-norbornyl or 1-adamantyl (**Figure 1.1**),[10] in which β-H elimination is unfavorable because a high energy intermediate, unsaturation at a bridgehead carbon, would be necessary (Bredt's rule). The use of alkyl groups without β-hydrogens, such as neopentyl (-CH_2CMe_3), trimethylsilylmethyl (-CH_2SiMe_3), and benzyl (-CH_2Ph) has allowed the isolation of a variety of transition metal alkyl complexes.[11]

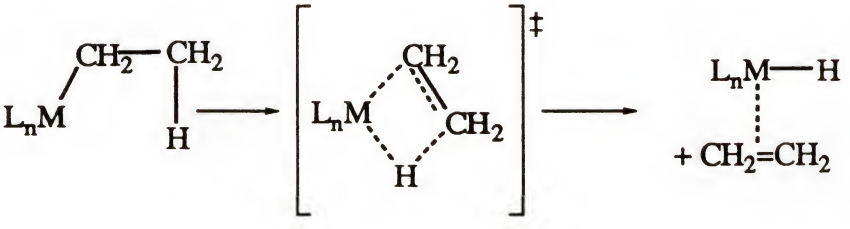

1.1

1-norbornyl 1-adamantyl

Figure 1.1. Structures of 1-norbornyl and 1-adamantyl ligands.

The most widely used method for the synthesis of metal alkyls is the use of alkyl transfer reagents such as alkyllithium, Grignard reagents, or milder alkylating reagents

such as dialkylzinc or tetraalkyltin derivatives. Other synthetic methods such as oxidative addition, cyclometallation, insertion of alkenes and alkynes, and attack on coordinated ligands are extensively discussed in many books and comprehensive reviews.[12] The variety of synthetic methods available (**Table 1.I**) makes viturally every class of organic compound a potential source for the preparation of metal alkyl complexes.

Table 1.I. Synthetic methods for transition metal alkyl complexes.

Alkylating reagent	
Oxidative addition	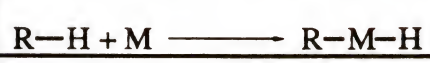
Cyclometallation	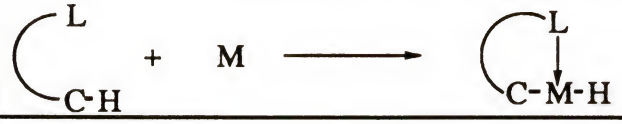
Metathesis	
1,2-Addition	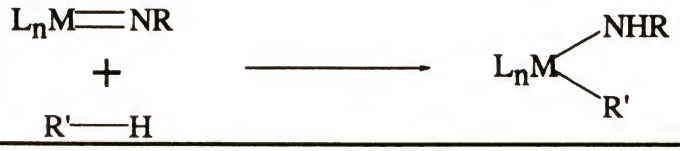
Oxidative coupling of alkenes and alkynes	
Insertion	
Elimination	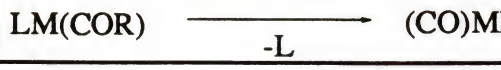
Attack on coordinated ligand	
Acidic hydrocarbon	

Decomposition of Transition Metal Alkyl Complexes

Transition metal alkyl complexes have been used for a variety of transformations. Much of the interest in these complexes derives from the fact that the σ-bond between a transition metal and carbon can be easily made and broken. In addition, spectroscopic studies of the new compounds formed and mechanistic investigations of metal-carbon bond reactivities have enriched our understanding of the nature of these processes, leading to dramatic extensions of the range of descriptive transition-metal chemistry. Transition metal alkyl complexes can promote a variety of organometallic and organic transformations or serve as precursors to catalysts which carry out a wide range of catalytic reactions. Furthermore, studies of the decomposition of transition metal alkyl derivatives also provide substantial practical applications.

As discussed above, transition metal alkyls that have no readily transferable β-hydrogens are more stable than related β-hydrogen containing complexes. However, the existence of low energy decomposition pathways makes many metal alkyls unstable, despite the fairly strong M-C bonds (30-65 Kcal/mol). Studying those pathways and ways to inhibit them is essential for designing thermally stable alkyls.

β-H Elimination and Abstraction

β-Elimination and its microscopic reverse, olefin insertion into the metal-hydride bond, are among the most fundamental transformations that occur in organometallic chemistry.[13] There is much evidence[14] that provides compelling support for olefin insertion into the metal-hydride bond as an initiation step in Ziegler-Natta polymerization of

ethylene and α–olefins, while β-H elimination serves as a chain-transfer or termination step in olefin polymerization.

β-H elimination is unquestionably the most important decomposition reaction which converts a metal alkyl into a hydrido metal olefin (which may or may not dissociate from the metal center) complex (equation 1.1). This reaction readily occurs not only for alkyls, but also for acyls and alkoxides.[15] Indeed, the facility of this pathway often precludes isolation of alkyl complexes with β-hydrogen atoms, especially when the complexes are coordinatively unsaturated.[12a] A concerted, four-center transition state is usually proposed for this transformation.

We[16] and others[17-20] have focused on the preparation of complexes of early transition metals in group 3 - 6 at their highest oxidation states that contain β-hydrogens on one or more substituents. Decomposition of these complexes and mechanistic investigations were also carried out in order to gain some insight into the olefin polymerization reactions in which β-H elimination serves as a key termination step. The majority of those decomposition pathways and mechanistic studies fall into two categories (**Figure 1.2**). One is the well-known β-H elimination pathway[18] in which the hydrido olefin intermediate is formed followed by reductive elimination of the alkane. The other pathway proposed is β-H abstraction[16,18] in which the β-hydrogen is transferred from the β-carbon to another alkyl group in one step, without the formation of the hydrido intermediate. This mechanism was also proposed by Buchwald,[21] Erker,[22] Marks[23] and Schrock[24] for the direct β-hydrogen abstraction process from an sp^2-hybridized carbon in the formation of alkyne or aryne complexes.

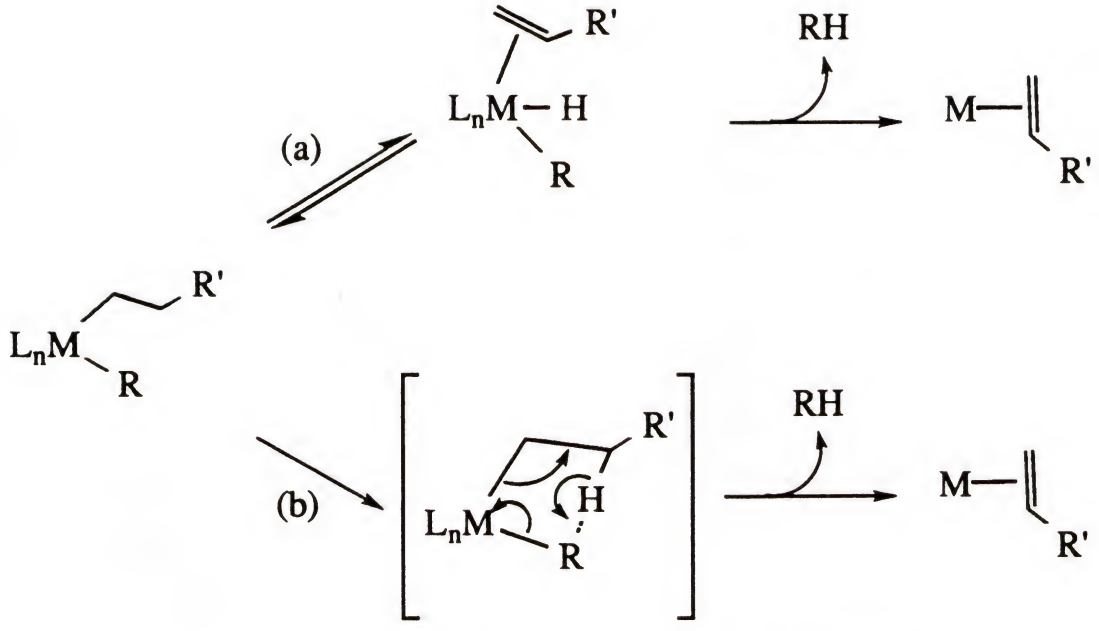

Figure 1.2. Possible Pathways for β-H Transfer.

As can be seen in **Figure 1.2**, the two pathways take place through distinct transition states (bent for elimination and linear for abstraction), which will result in different amplitudes of H vibration at the transition states.[25] Therefore, the best way to distinguish these two pathways is by the primary kinetic isotope effect. For a bent transition state (elimination pathway), the isotope effect (k_H/k_D) is usually temperature independent and has a magnitude of ≥1.4. The isotope effect for a β-H elimination reaction usually falls into the range of 1.4-2.5 at room temperature. β-H elimination followed by reductive elimination involves two steps in which there is C-H bond breaking or bond making. Thus, the isotope effect observed when reductive elimination is rate limiting is the product of the isotope effects for each step. Examples include $PdEt_2(PMePh_2)_2$ (KIE=1.4),[26] $CoEt_2(acac)(PMe_2Ph)_2$ (KIE=2.3),[27] $PtEt_2(PEt_3)_2$ (KIE=1.4-1.7),[28] $Cp^*_2ScCH_2CH_2Ph$ (KIE=2.0)[29] and $(CO)(PPh_3)_2IrCH_2CH_2C_6H_{13}$ (KIE=2.3).[30] On the other hand, the isotope effect for a linear, symmetrical transition state is usually found to be

5-8 at room temperature.[31] Experimental data reported for $Cp_2Zr(SCH_2Ph)(Me)$,[18a] KIE = 5.2, and $[Me_3SiNCH_2CH_2]_3NTa(Et)_2$,[18b] KIE = 5.7, are consistent with the proposed near linear transition state for the direct β-hydrogen abstraction pathway.

Due to the high reactivities of these β-H containing complexes, most complexes can only be observed as intermediates when they are coordinatively unsaturated or can be isolated when sterically protected by bulky groups, such as $[(Me_3SiNCH_2CH_2)_3N]^{3-}$,[18b] are used as ancillary ligands. Green,[19] Schrock,[20] and Bercaw[17] have reported the ethyl complexes of d^0, early transition metals (Ti, Ta, and Sc), stabilized by β-agostic interactions.

It is worth noting that β-H-elimination is reversible, and both the formation and the breaking of M-C bonds by this route are important in a variety of transformations. Insertion of an olefin into a metal-hydride bond is a key step in the hydrogenation of unsaturated hydrocarbons, hydroformylation, hydroboration, hydrosilylation, and alkyl isomerization. The β-H elimination process, breaking the M-C bond, serves as a key chain termination pathway in Ziegler-Natta type olefin polymerization.[2]

Decomposition of Metallacycles

The β-H containing cyclic complexes, metallacycles, are relatively more stable than the related alkyl complexes. This is due to the ring strain that makes it difficult to achieve the optimal M-C-C-H dihedral angle of 0° that is necessary for the concerted, planar, four-center transition state β-H elimination. The formation of 1-butene from metallacyclopentanes (equation 1.2) have been reported with Ni(II),[32] Pd(II),[33] Pt(II),[34] Pt(IV),[35] Ta[36] and Ti.[37]

1.2

Whitesides proposed a chain transfer process for the decomposition of a platinacyclopentane initiated by ligand-cyclometallation (**Figure 1.3**).[38,39] This mechanism is compatible with the observations that hydrogen transfer between C_4 moieties proceeds by an intermolecular process implies that platinum hydrides are intermediates.

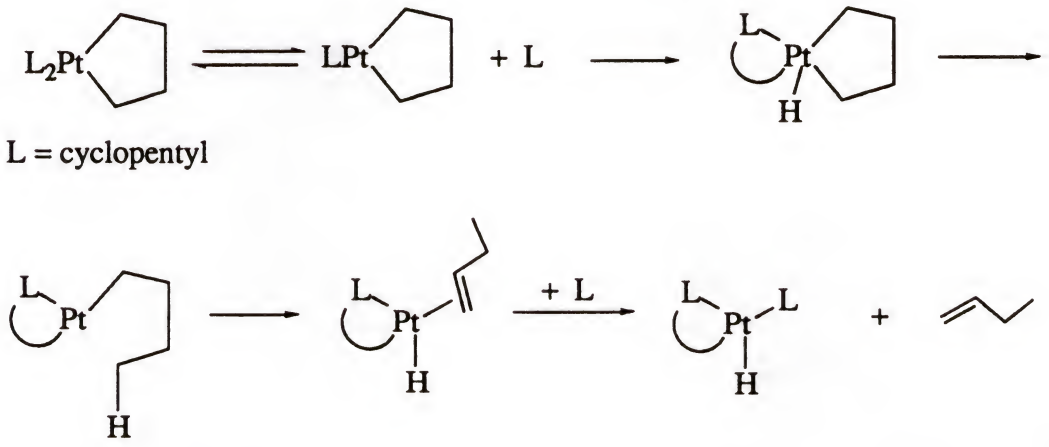

Figure 1.3. Proposed mechanism for the decomposition of a platinacyclopentane.

α-H Abstraction

The α-H abstraction, activation of α-CH bond by metal center, converts a metal alkyl into an alkylidene functionality (M=C) with the loss of alkane molecules (equation 1.3). The reaction is believed to occur through a four-center transition state in which M-C and C-H bonds are being both broken and formed. This idea is supported by the theoretical studies by Hoffmann,[40] which suggests that the reaction proceeds through a concerted pathway where the α-H is transfered to the leaving group with no net change in the metal oxidation state.

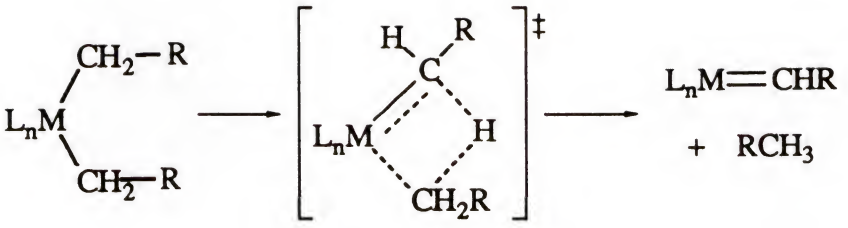

1.3

Although it is considered to be a "decomposition" of a dialkyl complex, the consequence of this transformation is the generation of an alkylidene complex. The alkylidene complex is widely used in metathesis reactions (see Chapter 3), converting α-olefins (C_n) to internal olefins (C_{2n-2}) with the liberation of ethylene. It is also used in polymerization reactions of alkenes, such as ring opening metathesis polymerization (ROMP),[41] a chain-growth polymerization of ring-strained cyclic or bicyclic olefins, and acyclic diene metathesis polymerization (ADMET),[42] a step propagation condensation type polymerization.

Concerted 1,2-RH-addition across a metal carbon double bond has also been reported. This occurs in an intramolecular fashion through the metallation of other ligands.[43] However, α-H abstraction is usually irreversible since the reverse would result in the unfavorable intermolecular C-H activation across the metal-carbon double bond. Recently, Tran and Legzdins reported the example of the reverse of an α-H abstraction reaction.[44] Thermolysis of a 16 e^- dialkyl complex, $Cp^*W(NO)(CH_2CMe_3)_2$, **A**, in tetramethylsilane results in the formation of a mixed dialkyl complex, $Cp^*W(NO)(CH_2SiMe_3)(CH_2CMe_3)$, **C**. This is believed to form via C-H activation of tetramethylsilane by the alkylidene intermediate, **B** (**Figure 1.4**).

For both α- and β-H transfer reactions, the metal centers must have available empty orbitals of the correct symmetry to interact with the C-H bond in the transition state. This is usually accessible for coordinatively unsaturated, early transition metal d^0 complexes. However, the lack of *d* electrons to back-donate into the σ* orbital of the C-H bond also results in the observed agostic interaction.[17,19,20] Whether the C-H bond is only

weakened (agostic interaction) or completely broken (elimination) involves a combination of effects,[12] including the σ-acidity and π-basicity of the metal, the electronics and sterics of ancillary ligands, and the relative bond strength of the bonds that are broken and formed. Other hydrogen transfer reactions such as γ-H elimination, leading to the formation of a metallacycle (equation 1.4),[45] and H-abstraction from non-alkyl ligands (equation 1.5)[46] have also been reported as the decomposition pathways for metal alkyl complexes.

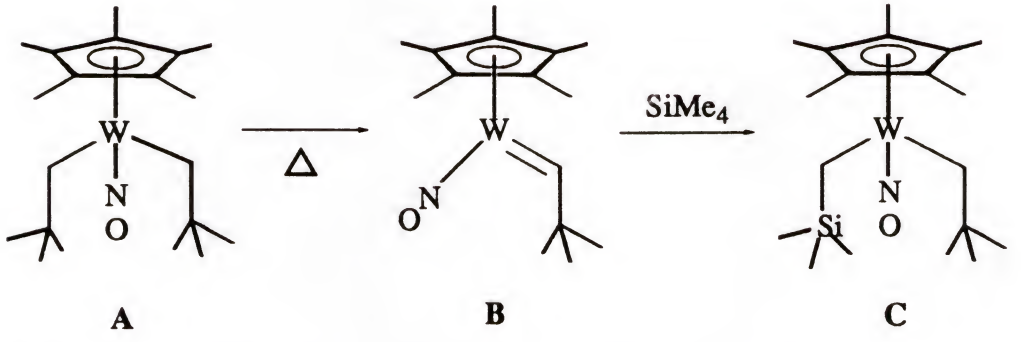

Figure 1.4. Example for cyclometallation hindered by steric repulsion.

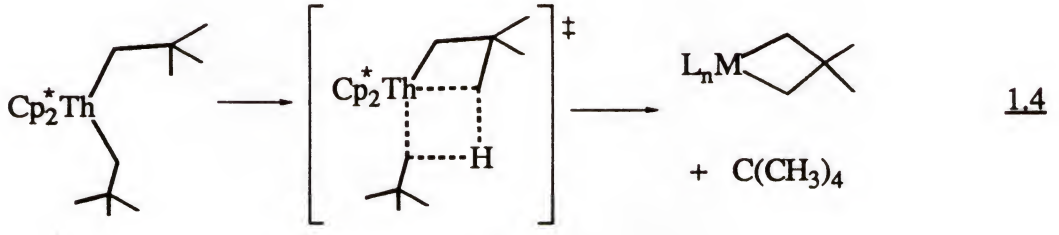

1.4

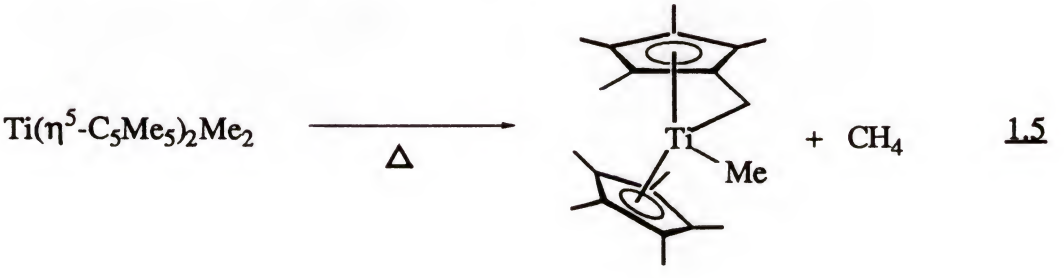

1.5

The other common decomposition pathway of metal alkyls is reductive elimination (equation 1.6), resulting in a decrease (two less) of the formal oxidation state of the metal. Reductive elimination of alkyl hydrides (X=H) is usually both kinetically facile and thermodynamically favorable, which is why those alkyl hydride complexes are usually unstable. The reaction is of particular interest because of its relation to processes involved in catalytic hydrogenation. The reductive coupling of two alkyl groups (X=R) is kinetically less favorable and hence proceeds at a much slower rate than elimination of alkyl hydrides. This is owed to the required rehybridization of the sp^3 orbital of the carbon atom for bond breaking and making in the transition state. Reductive elimination of alkyl halides is usually not observed, which can be explained by the much stronger metal-halogen bonds (110-120 Kcal/mol for M-Cl) compared to metal alkyl bonds (30-65 Kcal/mol).

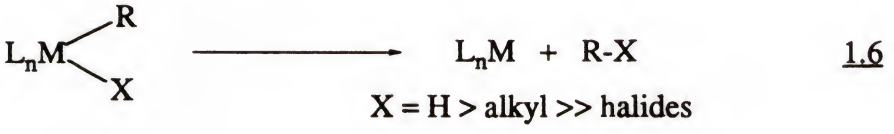

1.6

The instability of *cis* alkyl hydride complexes can be demonstrated by the observed decomposition of *cis*-$Pt(PPh_3)_2(CH_3)H$ at -25^{0}C, liberating methane.[47] Although *cis* alkyl hydride complexes have been isolated from the oxidative addition of alkanes,[48] the predominant kinetic pathway by which these complexes react is still the reductive elimination of alkanes. In order to overcome the kinetic preference of *cis* alkyl hydrides towards reductive elimination over other productive transformations, proper ligand design is essential that will provide another low kinetic barrier pathway. The low barrier pathway has been achieved by the associative ring slippage (η^5 to η^3) pathway made available by the indenyl ligand (**Figure 1.5**).[49] In the attempt to promote migratory insertion of CO with the iridium complex (η^5-Ind)$(PMe_3)Ir(CH_3)(H)$, **A**, liberation of methane (the product of reductive elimination) is observed. When **A** reacts with ethylene and alkynes, the insertion of ethylene and alkynes into the Ir-H bond in the *cis*-hydridomethyl complex, **A**, is

preferred over the reductive elimination pathway. Presumably, the ring slippage (η^5 to η^3) pathway made available by the indenyl ligand provides a low kinetic barrier for the insertion reaction to occur.

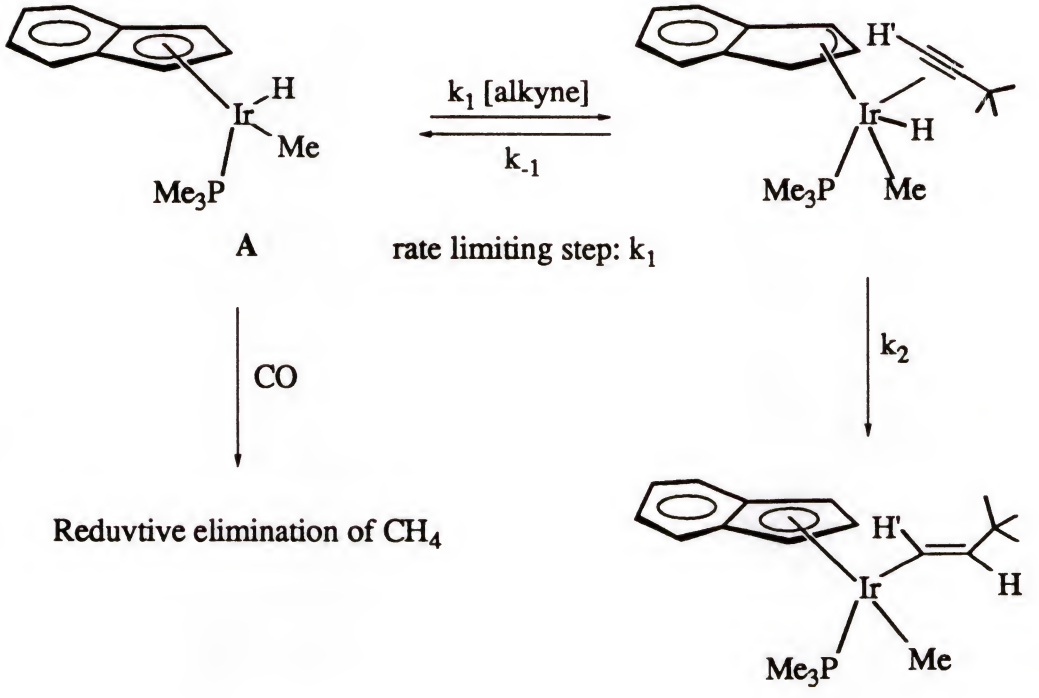

Figure 1.5. Indenyl ring slip (η^5 to η^3) assisted insertion reaction.

In this dissertation my research on chelate-stabilized tungsten(VI) dialkyl complexes is presented, including the syntheses and fluxional behavioral studies; kinetic *vs.* thermodynamic preferences of coordination of PMe_3 and ^{t}BuNC; productive metathesis reactions; isolation of β-hydrogen containing complexes and their reactivities towards PMe_3; steric-controlled mechanisms for the formation of olefin complexes; reactions catalyzed by these complexes; and the comparison of reactivities with different ligand environments.

CHAPTER 2
SYNTHEISIS, STRUCTURE AND REACTIVITY OF DIALKYL COMPLEXES

Synthesis of W(VI) Dialkyl Complexes

This work has been focused on the chemistry of W(VI) imido dichloride, dialkyl, and alkylidene compounds stabilized by a chelating diamido ligand derived from N,N'-bis-trimethylsilyl-*o*-phenylenediamine [*o*-$(Me_3SiNH)_2C_6H_4$].[50] It has been shown that the synthesis of a large variety of compounds can be carried out by using the H_2pda ancillary ligand.[16] Recently, related group 4 and 5 complexes containing disubstituted-pda ligands have also been reported.[51,52]

The synthesis of the dichloride precursor, $W(NPh)Cl_2[(NSiMe_3)_2C_6H_4]$, **2**, is achieved by the reaction of the dilithium salt of $[(TMS)_2pda]^{2-}$, generated *in situ* from H_2pda and *n*-BuLi, with $(PhN=)WCl_4 \cdot OEt_2$[50] in diethyl ether as shown in **Scheme 2.A**. This is a high yield reaction that has been successfully carried out using up to 20 g of $(PhN=)WCl_4 \cdot OEt_2$.

Compound **2** is an air and water sensitive, orange microcrystalline solid which is indefinitely stable in the solid state or in solution if stored under an inert atmosphere. Compound **2** is a convenient starting material for the synthesis of a variety of alkyl complexes. As shown in **Scheme 2.A**, carbanions cleanly displace the chloride ligands of **2** giving the corresponding dialkyl complexes, **3 - 12** . These reactions are most successful when Grignard reagents are employed as the alkylating agents. When lithium reagents are used, reduced yields are obtained and are accompanied by the formation of uncharacterizable decomposition products which have proven difficult to separate.

Scheme 2.A. Synthesis of the dialkyl complexes.

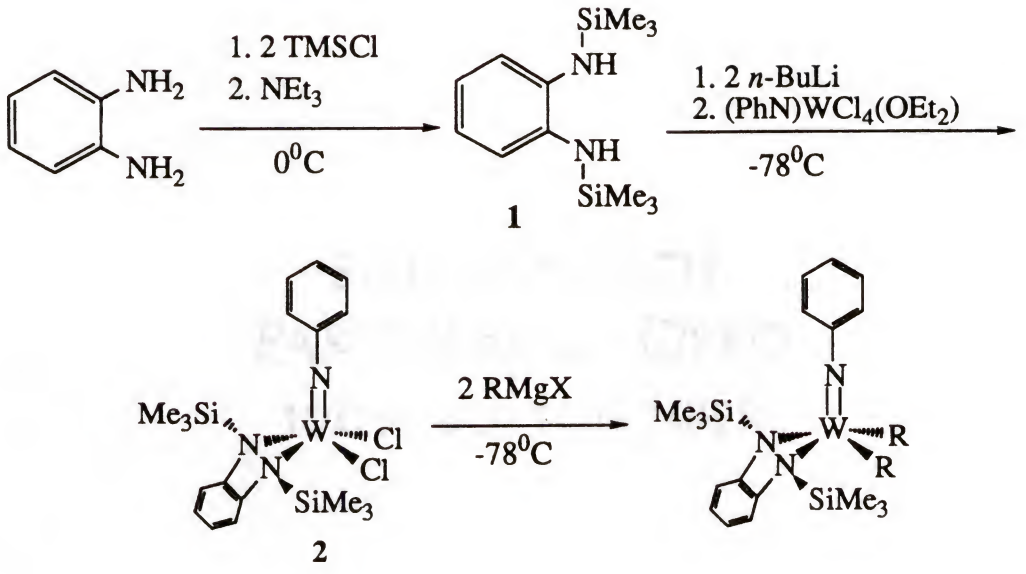

R = Me(**3**), Et(**4**), *n*-Pr(**5**), CH_2CH_2Ph(**6**), CH_2CHMe_2(**7**), Ph(**8**), CH_2Ph(**9**), CH_2CMe_3(**10**), CH_2CMe_2Ph(**11**), CH_2SiMe_3(**12**),

The dialkyl complexes, **3** - **12**, are extremely soluble in hydrocarbon solvents which tends to complicate their isolation and purification. All of these compounds are air and moisture sensitive solids with the exception of **4** and **5,** which are oils at room temperature. Despite their coordinative unsaturation, **3** - **12** are indefinitely stable at room temperature if stored under an inert atmosphere. This is particularly surprising for **4-7,** which are five coordinate, electronically unsaturated complexes containing β-hydrogen atoms.

The room temperature ^1H and ^{13}C NMR spectra of **3** - **12** display equivalent TMS methyl groups and alkyl groups as well as aa'bb' patterns for the protons of the $(TMS)_2$pda phenyl group (see experimental section). These observations are consistent with either a square pyramidal structure with the imido group occuping the apical position or with rapidly exchanging trigonal bipyramidal and square pyramidal structures.

The alkylation reactions can also be performed with only one equivalent of Grignard reagent, resulting in monoalkyl, monochloride complexes, **13** - **15**, as shown in equation 2.1. Subsequent alkylation of the monoalkyl complexes, **13** to **15**, gives dialkyl compounds, **16** - **20**, with two different alkyl groups (equation 2.2).

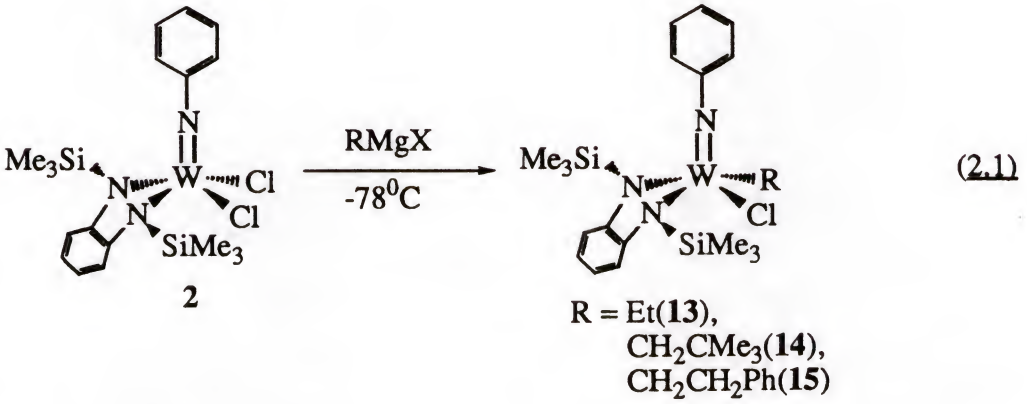

2

R = Et(**13**), CH_2CMe_3(**14**), CH_2CH_2Ph(**15**) (2.1)

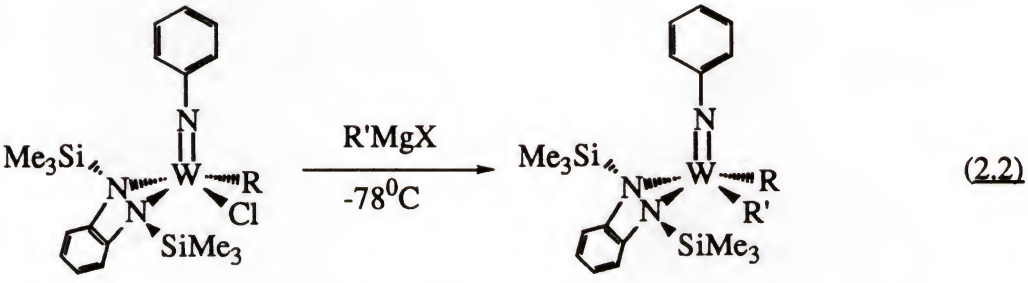

R = CH_2CMe_3(**14**), R' = Me(**16**), Et(**17**), CH_2CHMe_2(**18**), CH_2CH_2Ph(**19**)

CH_2CH_2Ph(**15**), R' = Et (**20**) (2.2)

Structure Study for W(VI) Dialkyl Complexes

Single crystal X-ray diffraction studies were performed on compounds **3**, **6**, **10**, and **14**. Thermal ellipsoid plots of the compounds are shown in **Figures 2.1 - 4**, while

selected bond lengths and angles are found in **Tables 2.I - IV**. Some general comments about these structures are warranted. All compounds have short W-N(imido) bond lengths (1.73 - 1.78Å), indicating that there is significant interaction between the imido nitrogen atom lone pair and the W center, with W-N-Ph angles being close to linear. These bond lengths and angles are within normal ranges for tungsten-imido complexes[53,54] in which the W-N bond can be considered to be triply bound, with the lone pair of the N atom donating to an empty $d\pi$ orbital of the d^0 W atom. The W-alkyl bond lengths (2.14 - 2.19Å) are also within the ranges expected for W(VI)-C distances.[55] Despite the coordinatively unsaturated nature of the complexes, there is no evidence for α or β agostic W-H-C interactions either structurally or spectroscopically.

The five coordinate complexes **3** and **6** have square pyramidal coordination about the W atom with the imido group in the axial position. The mean deviations from the basal plane occupied by two amido nitrogens and two α-carbons are 0.023 and 0.080Å for **3** and **6**, respectively. In both structures, the $(TMS)_2$pda ligand is obviously folded about the vector that connects the two amido N atoms. This results in a dihedral angle of 130^0 between the phenyl ring of the $(TMS)_2$pda ligand and the plane defined by W and the amido N atoms in both **3** and **6**. The folding of the phenyl ring results in close contacts between the *ortho* carbon atoms of the phenyl ring of the $(TMS)_2$pda ligand and the metal center that range between 2.58 and 2.64 Å.

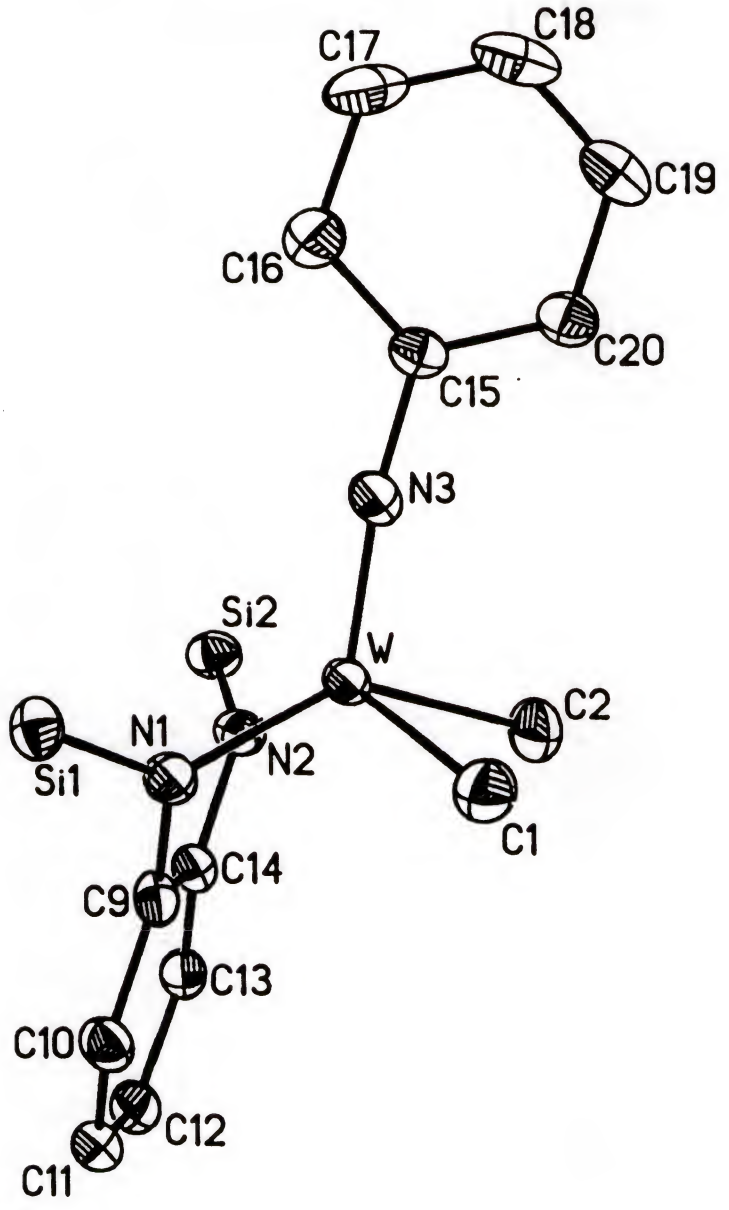

Figure 2.1. Molecular structure of W(NPh)[*o*-$(Me_3SiN)_2C_6H_4$]Me_2, **3.** with 50% probability ellipsoids and showing the atom numbering scheme. All hydrogen and silyl methyl atoms are omitted for clarity.

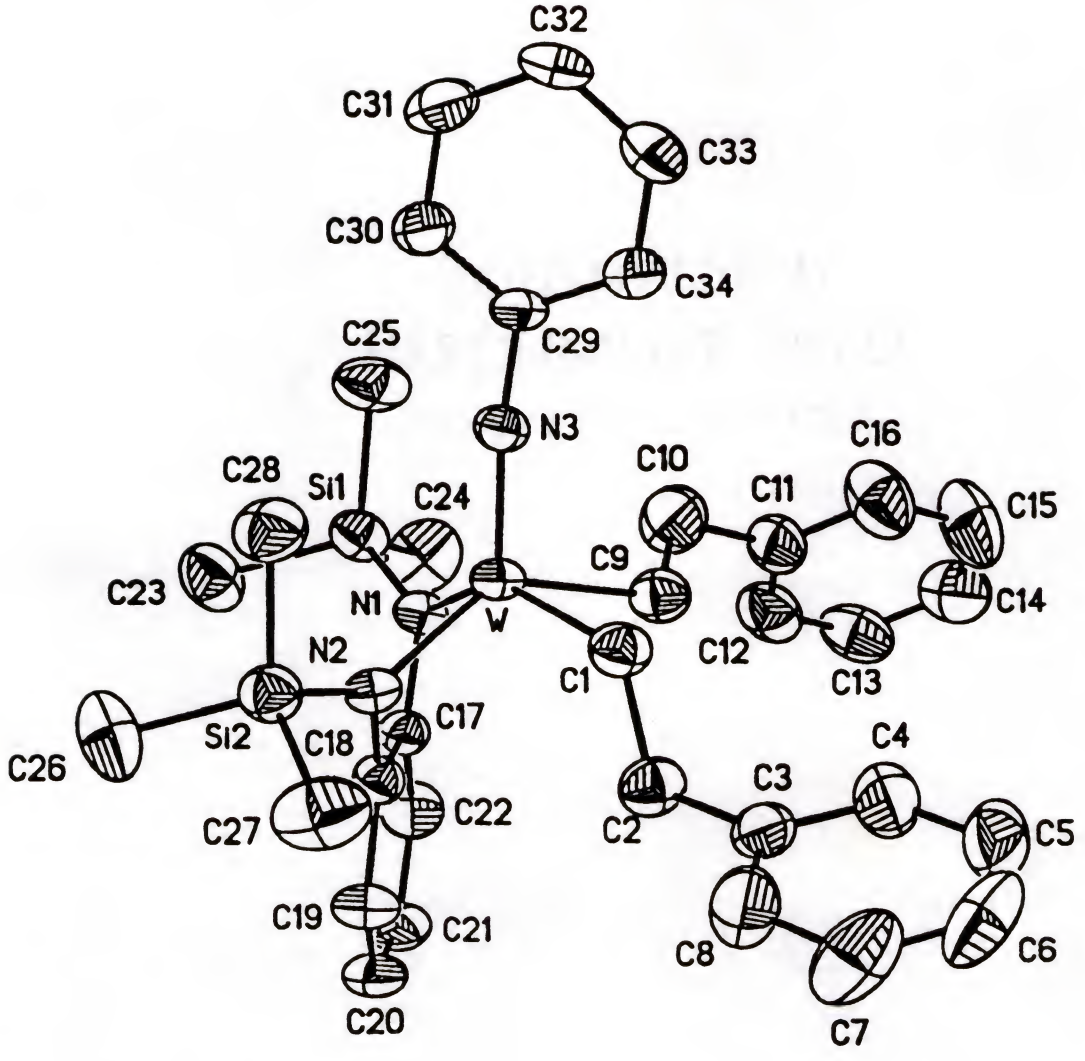

Figure 2.2. Molecular structure of W(NPh)[*o*-$(Me_3SiN)_2C_6H_4$]$(CH_2CH_2Ph)_2$, **6.** with 40% probability ellipsoids and showing the atom numbering scheme. All hydrogen atoms are omitted for clarity.

Table 2.I. Selected Bond Lengths (Å) and Angles (°) for W(NPh)[*o*-$(Me_3SiN)_2C_6H_4]Me_2$, **3**.

1	2	3	1-2	1-2-3
N1	W	C1	2.007(3)	84.98(14)
N1	W	C2		141.7(2)
N2	W	N1	2.006(3)	82.55(11)
N2	W	C1		138.87(14)
N2	W	C2		85.5(2)
N3	W	N1	1.738(3)	117.64(13)
N3	W	N2		117.81(13)
N3	W	C1		102.7(2)
C1	W	C2	2.173(4)	80.5(2)
C2	W	N3	2.176(4)	100.2(2)

Table 2.II. Selected Bond Lengths (Å) and Angles (°) for W(NPh)[*o*-$(Me_3SiN)_2C_6H_4](CH_2CH_2Ph)_2$, **6**.

1	2	3	1-2	1-2-3
N1	W	C1	2.000(4)	145.0(2)
N1	W	C9		85.1(2)
N2	W	N1	2.003(4)	82.9(2)
N2	W	C1		85.4(2)
N2	W	C9		135.8(2)
N3	W	N1	1.728(4)	117.1(2)
N3	W	N2		120.7(2)
N3	W	C1		97.2(2)
C1	W	C9	2.189(5)	80.6(2)
C9	W	N3	2.175(5)	102.6(2)

As can be seen in **Figure 2.3**, the W atom in **10** adopts a trigonal bipyramidal coordination geometry with the imido N and one amido N occupying the two axial sites. The three equatorial sites are occupied by the bulky neopentyl groups and the remaining amido N. In response to the greater steric demands of the ligands in **10**, the folding of the TMS_2pda ligand has decreased relative to the other compounds resulting in a dihedral angle between the phenyl ring of the $(TMS)_2$pda ligand and the plane defined by W and the amido N atoms of 164°. The W-N2 bond (2.133(3)Å) is significantly longer than the W-N3 bond (1.981(3)Å), reflecting the strong *trans* influence that is exerted by the imido group. The amido group *trans* to the imido group causes the W-N1 bond to be slightly longer in **10**. However, the W-N1 bond length is still within the range expected for a triply bonded imido group. The W-C1-C2 and W-C6-C7 angles (126.2^0 and 120.6^0, respectively) are within the expected range for undistorted neopentyl groups.

Given the π bonding demands of the imido group as well as its strong *trans* influence, the square pyramidal geometry found in **3**, and **6** is expected to be the most stable in this class of five coordinate molecules because it maximizes the imido-W π interaction.[53,54] Thus, the trigonal bipyramidal coordination geometry found in complex **10** most likely arises from the steric bulk of the neopentyl groups. As expected, the most sterically encumbered groups occupy the equatiorial plane of the trigonal bipyramid and the smaller imido group occupies the axial position. The structure is clearly related to that of W(=NPh)(CH_2-*t*-Bu)$_3$Cl which has not been structurally characterized, but has been assigned a trigonal bipyramidal structure with equatorial neopentyl groups using NMR data.[56] The steric effect on the preference of geometry can also be seen in the structure of [*o* -$C_6H_4(NSiMe_3)_2$](PhN)W(CH_2CMe_3)Cl, **14**.[57]

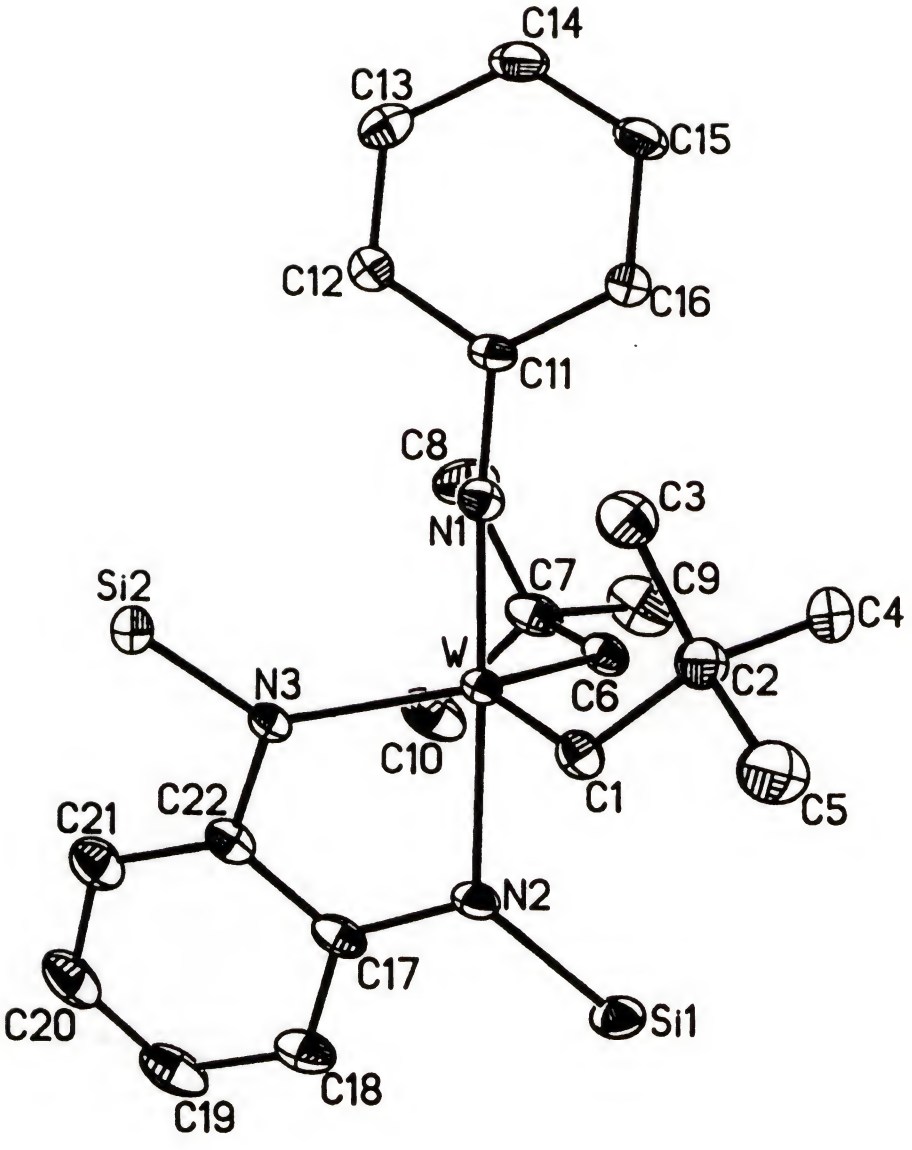

Figure 2.3. Molecular structure of W(NPh)[*o*-$(Me_3SiN)_2C_6H_4$]$(CH_2CMe_3)_2$, **10.** with 50% probability ellipsoids and showing the atom numbering scheme. All hydrogen atoms are omitted for clarity.

Table 2.III. Selected Bond Lengths (Å) and Angles (°) for W(NPh)[*o*-$(Me_3SiN)_2C_6H_4$]$(CH_2CMe_2)_2$, **10**.

1	2	3	1-2	1-2-3
N1	W	N2	1.775(3)	170.89(12)
N1	W	N3		99.58(12)
N1	W	C1		98.47(13)
N1	W	C6		88.62(13)
N2	W	C1	2.133(3)	90.40(12)
N2	W	C6		84.83(12)
N3	W	N2	1.981(3)	79.35(11)
N3	W	C1		108.93(12)
C1	W	C6	2.135(3)	122.40(13)
C6	W	N3	2.165(3)	126.15(12)
C2	C1	W		126.2(2)
C7	C6	W		120.6(2)

The coordination geometry of **14** around the W atom is a distorted square pyramid with the imido ligand occupying the axial position (**Figure 2.4**). The mean deviation of the basal plane defined by N1-N2-Cl-C19 is 0.2993 Å with the distances between the atoms and the plane being N1: 0.3305Å, N2: -0.3208Å, Cl: 0.2681Å, and C19: -0.2778Å. The W atom sits 0.6750Å above the plane and the W-N3 vector deviates 7.9^0 from the normal vector of the plane. As can be seen in **Figure 2.4**, the N2 atom is clearly distorted from the equatorial plane of the square pyramid and found 1.0809 Å below the plane defined by N1-Cl-C19. The distortion is due to the bulkiness of the neopentyl group, resulting in an intermediate structure between square pyramid, **3**, and trigonal bipyramid, **10**, when two neopentyl groups are incorporated. The W-N3 bond length is 1.741(4) Å and the phenyl ring on the imido ligand leans away from trimethylsilyl groups, resulting in the W-N3-C7 bond angle of $165.1(4)^0$. Those data are still within the range considered for W-N triple bonds. The coordination geometry around the W atom can also be viewed as a

trigonal bipyramid with N1 and Cl occupying the axial positions, in which the N1-W-Cl bond angle is 160.21(11)^0. The mean deviation of the equatorial plane defined by W-N2-N3-C19 is only 0.02Å compared with the mean deviation of 0.299Å in the basal plane defined by N1-N2-Cl-C19 in the square pyramid.

Table 2.IV. Selected Bond Lengths (Å) and Angles (°) for W(NPh)[*o*-($Me_3SiN)_2C_6H_4$](CH_2CMe_3)Cl, **14**.

1	2	3	1-2	1-2-3
N1	W	Cl	1.973(4)	160.21(11)
N1	W	C19		88.0(2)
N2	W	N1	2.013(4)	82.6(2)
N2	W	Cl		86.42(11)
N2	W	C19		124.5(2)
N3	W	N1	1.741(4)	103.9(2)
N3	W	N2		126.6(2)
N3	W	Cl		95.88(12)
Cl	W	C19	2.182(5)	84.69(14)
C19	W	N3	2.4216(11)	108.8(2)

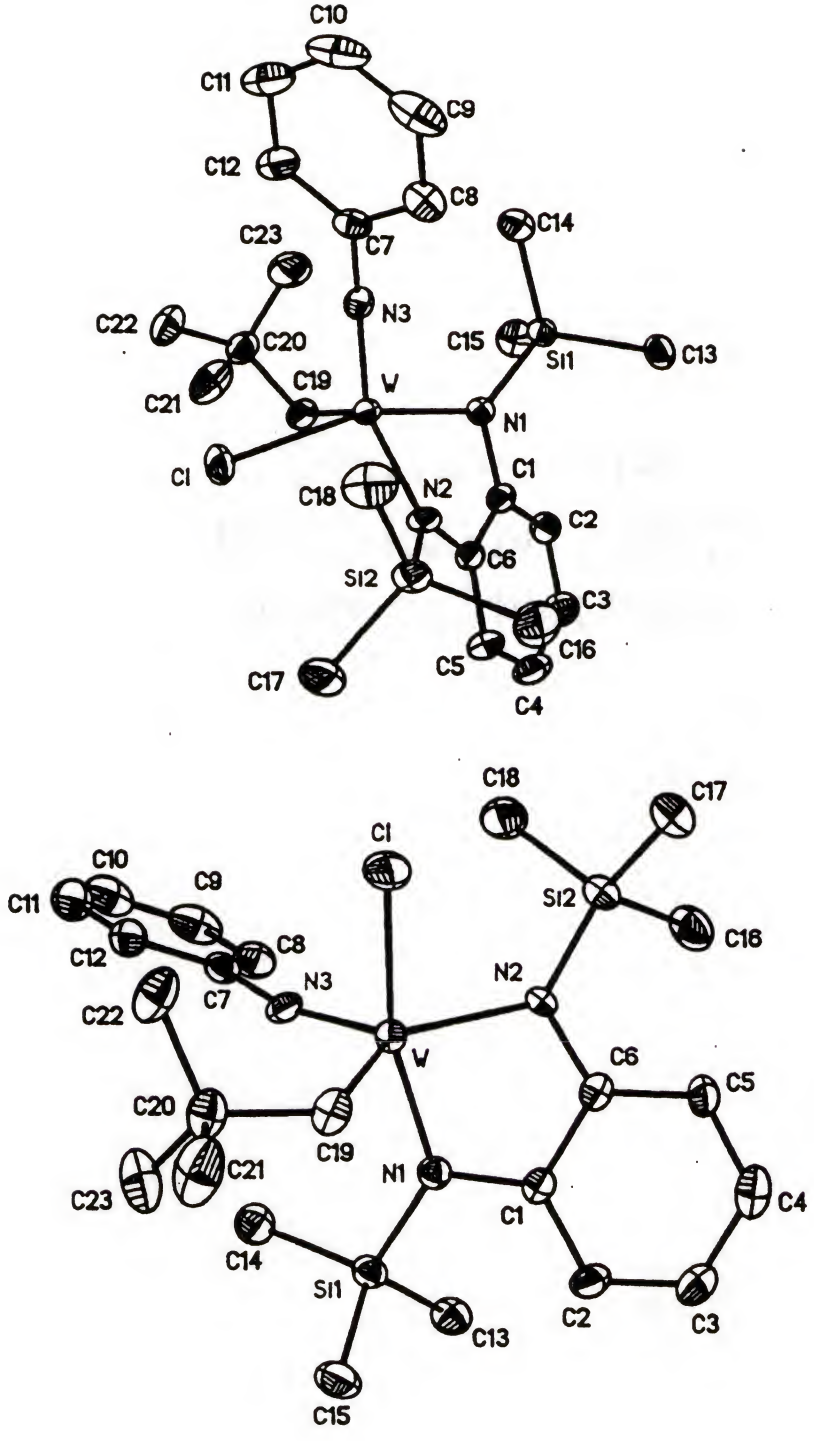

Figure 2.4. Molecular structure of W(NPh)[*o*-$(Me_3SiN)_2C_6H_4$](CH_2CMe_3)Cl, **14.** in the SP geometry (**top**) and TBP structure (**bottom**) with 50% probability ellipsoids and showing the atom numbering scheme. All hydrogen atoms are omitted for clarity.

Pentacoordinated Complexes

All the dialkyl and alkyl chloride complexes, **3** to **20**, are pentacoordinated, possessing either a trigonal bipyramidal (TBP) or square pyramidal (SP) structure. The ^1H NMR of the bisneopentyl complex, **10**, at room temperature reveals a singlet for the trimethylsilyl groups, indicating that the two silyl groups are equivalent. However, the solid state structure shows a trigonal bipyramidal structure with the two nitrogens of the diamide ligand occupying different sites (one equitoral and the other axial). The inconsistency of the findings suggests that this molecule maybe undergoing a fluxional process that equilibrates the trimethylsilyl groups. Stereochemical nonrigidity associated with five-coordinated species is usually observed, because the structural isomers undergo fast intramolecular ligand exchange.

In general, d^0 and d^{10} metal complexes should favor the trigonal bipyramid when acyclic ligands are present as predicted by valence shell electron pair repulsion (VSEPR) theory. The angular overlap model[58] also predicts the preferred structure being the one that minimizes electron pair and ligand-ligand repulsions in the case of d^0 and d^{10} metal complexes, rather than the one that minimizes the role of d_{σ^*} antibonding electrons. As ring strain is imposed by chelating ligands, or ligands with different donating and accepting strength are present, the structural preference becomes a delicate balance between electronic and steric effects.[59] The preference for the square pyramidal structure seen in our system due to the demand of maximizing the imido-W π interaction is just one of the many examples. Details of the preference for other *d*-orbital configurations is also reported.[60] Similar observations of differences between solid-state and solution structures of other fluxional molecules are also attributed to lattice interactions.[61] This packing effect will distort the pentacoordinated structure along its lowest energy path, presumably the one

existing in solution that gives rise to the fluxional behavior that is observed spectroscopically.

Berry Pseudorotation

Berry first proposed an intramolecular exchange mechanism[62] initiated by an internal vibrational process to account for the fluxionality observed in 5 coordinate complexes by NMR spectroscopy. It was noted that a vibrational bending mode involving both axial and equatorial ligands can provide a suitable exchange coordinate, from which a square pyramidal transition state is formed (**Scheme 2.B**). On reforming the trigonal bipyramid, the two axial ligands, **4** and **5**, have exchanged with two of the equatorial ligands, **2** and **3**. Further aspects, such as theoretical treatment[63] and vibrational potential function calculation[64] have also established that this process is a low energy exchange coordinate for pentacoordinated molecules.

Scheme 2.B. Berry intramolecular ligand exchange process.

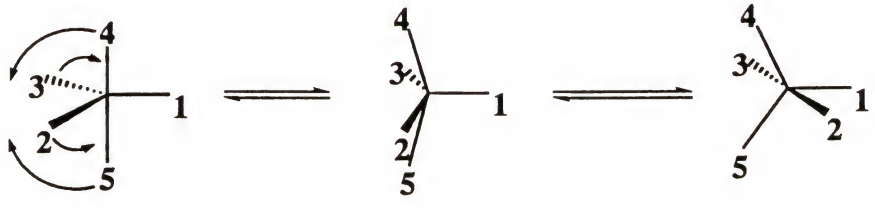

Turnstile Process

The turnstile process[65] is also used to explain the same intramolecular exchange phenomena. This process corresponds to an internal rotation of one axial, **4**, and one equatorial, **2**, ligand rotating as a pair. While the three remaining ligands rotate in the opposite direction as illustrated in **Scheme 2.C(a)**. Another way to look at this process

is by viewing the trigonal bipyramid above the **2**-**4** edge(**Scheme 2.C(b)**). A 30^0 rotation of the **2**-**4** edge relative to the base **1**-**3**-**5** will yield a square pyramidal transition state, with the **1** at apical position, similar to that of the Berry process. Further rotation and ligand reorganization leads to a trigonal bipyramidal structure with the new axial ligands being **2** and **3**.

Scheme 2.C. Turnstile Rotation Process.

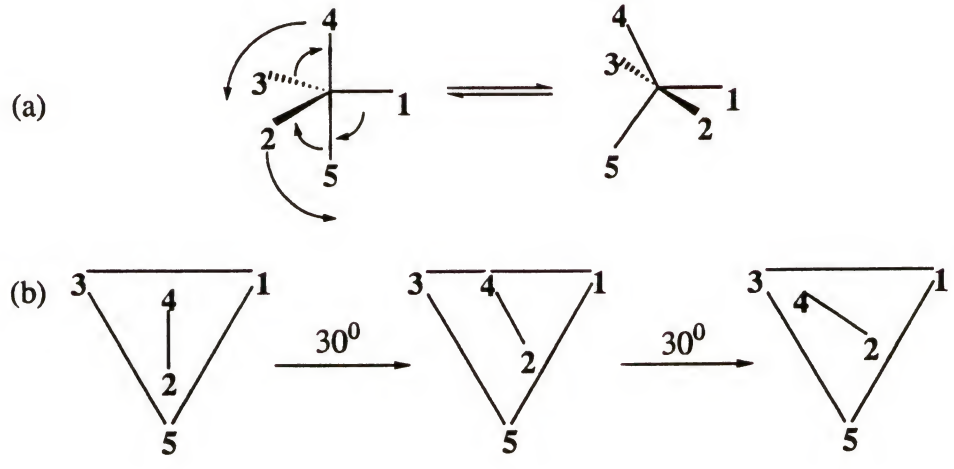

Although the final results of both processes are essentially equal, there are fundamental differences between them. All of the differences relate to the fact that Berry pseudorotation is a process that does not involve any sort of internal rotation about an axis through the central atom and the turnstile process is an internal rotation process, resulting in two mechanistic pathways proceding through entirely different sets of states differing in geometry, symmetry, and potential energy.[65] Recent *ab initio* calculations show that the turnstile mechanism is an energetically allowed pathway for isomerization in some pentacoordinated palladium(II) complexes.[66] Espinet[67] also reported experimental evidence supporting this mechanism.

Fluxionality of Compounds with Bulky Alkyl Groups

The ^{1}H NMR spectra of complexes **3** - **6** are invarient as the temperature is decreased from room temperature to -80°C in d_8-toluene. These observations are consistent with **3** - **6** having a square pyramidal structure at all temperatures and are consistent with the crystal structures of **3** and **6**. The ^{1}H NMR spectrum of complex **10** at room temperature reveals only one peak for the two "inequivalent" trimethylsilyl groups as suggested by the solid state structure. A variable temperature NMR study was performed on a d_8-toluene solution of **10**. When **10** is cooled to -80°C, the trimethylsilyl methyl resonaces broaden and decoalesce (T_c= -45°C) into two peaks that integrate as 9 protons each (**Figure 2.5**), while the $(TMS)_2$pda phenyl protons split into four separate one proton resonances. Given that the crystal structure of compound **10** shows that it has a trigonal bipyramidal structure with the imido N and one amide group of the $(TMS)_2$pda ligand occupying axial positions, the observed NMR behavior of **10** is consistent with this structure at low temperature.

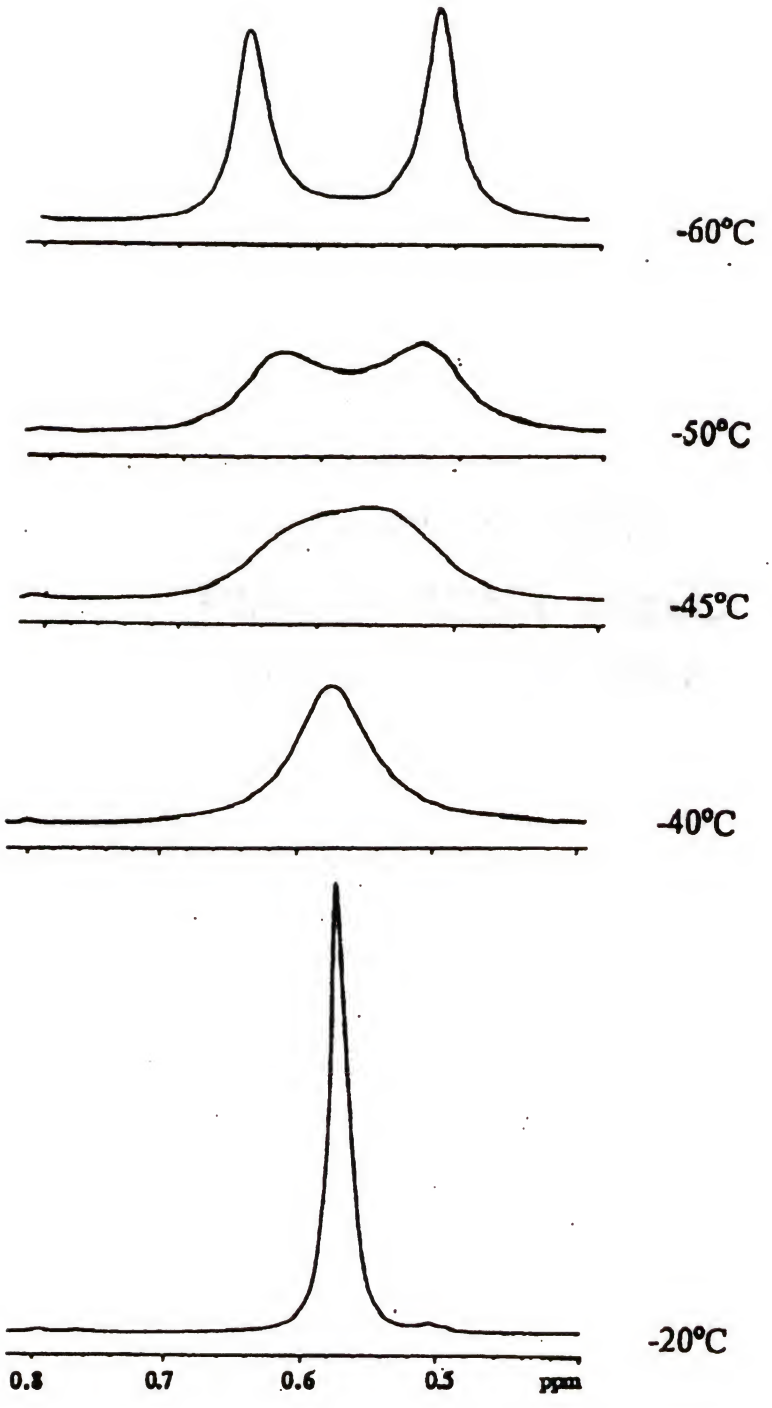

Figure 2.5. Variable temperature NMR spectra, showing the fluxional preperty of **10**.

An intramolecular exchange process results in the exchange of the amide TMS groups ($\underline{N_1}$ and $\underline{N_2}$ in **Scheme 2.D**). A turnstile motion involving internal rotation of one axial, $\underline{N_1}$, and one equatorial, $\underline{N_2}$, ligands rotating as a pair *vs.* the other rotating trio of the three remaining ligands ($\underline{N_3}$, $\underline{C_1}$ and $\underline{C_2}$) is illustrated in **Scheme 2.D-(a)**. This results in the exchange of the two diamido nitrogens, $\underline{N_1}$ (*ax* -> *eq*) and $\underline{N_2}$ (*eq* -> *ax*). The Berry pseudorotation (**Scheme 2.D-(b)**) will exchange two axial groups with two equitorial groups, forming **A**. Further motion will generate intermediate **B**, which then followed by another process to yield **C** with $\underline{N_2}$ at the axial position. The other possibility, where one arm of the $(TMS)_2pda$ ligand dissociates and re-coordinates following the rotation of W-N bond, will also result in the exchange of the amide TMS groups. Unfortunately, no further evidence has been obtained to determine which mechanism best represents the fluxional process that **10** undergoes in solution.

Scheme 2.D. Intramolecular motions for the fluxional property.

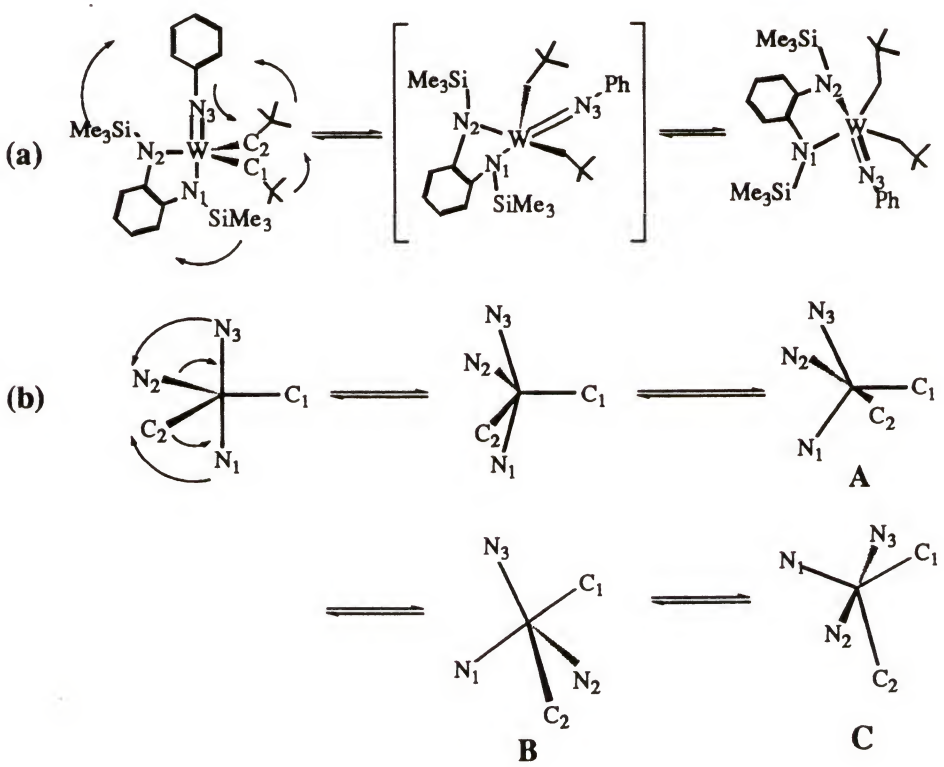

The coalescence temperature obtained from the variable temperature NMR study allows us to calculate the free energy of activation for this fluxional process by applying the two site exchange approximation (equation 2.3).[68] Fluxional behavior is also observed for other dialkyl complexes with bulky alkyl groups. The activation barriers for these compounds are reported in **Table 2.V**.

$$\Delta G_c^{\ddagger} = aT_c[\ 9.972 + \log(T_c/\delta\upsilon)\ ] \qquad 2.3$$

$$\begin{cases} a = 0.004575 \text{ Kcal/mol} \\ T_c : \text{coalescence temperature (K)} \\ \delta\upsilon : \text{peak separation (Hz) at low temperature limit} \end{cases}$$

Table 2.V. Free energy of activation for compounds containing bulky alkyl groups.

	T_c(K)	$\Delta G_c^{\ddagger}$(Kcal/mol)
$W(CH_2CMe_3)_2$, **10**	228	11.13
$W(CH_2CMe_2Ph)_2$, **11**	231	10.90
$W(CH_2SiMe_3)_2$, **12**	225	11.02
$W(CH_2CMe_3)(CH_2CHMe_2)$, **18**	260	12.78

Equilibrium Between SP and TBP Isomers of 7

We have shown that the geometry of these dialkyl complexes is dependent on the size of the alkyl groups. For small alkyls (*e.g.* methyl), the complex possesses a square

pyramidal geometry with the imido N in the axial position. For large alkyls (*e.g.* neopentyl), a trigonal bipyramidal structure with the imido N and one of the two N of the diamido ligand at the axial positions. Complexes **3** - **6** are all square pyramidal, as determined by the equivalence of the trimethylsilyl groups in their ^{1}H and ^{13}C NMR spectra at various temperatures. Complexes **10**, **11**, **12** and **18** are trigonal bipyramidal and exhibit fluxional behavior in solution. Complex **7**, [*o* -$C_6H_4(NSiMe_3)_2$](PhN)W $(CH_2CHMe_2)_2$, is also square pyramidal, according to the single crystal X-ray study (**Figure 2.6; Table 2.VI**), but shows an equilibrium between square pyramidal and trigonal bipyramidal geometries (equation 2.4) at low temperature.

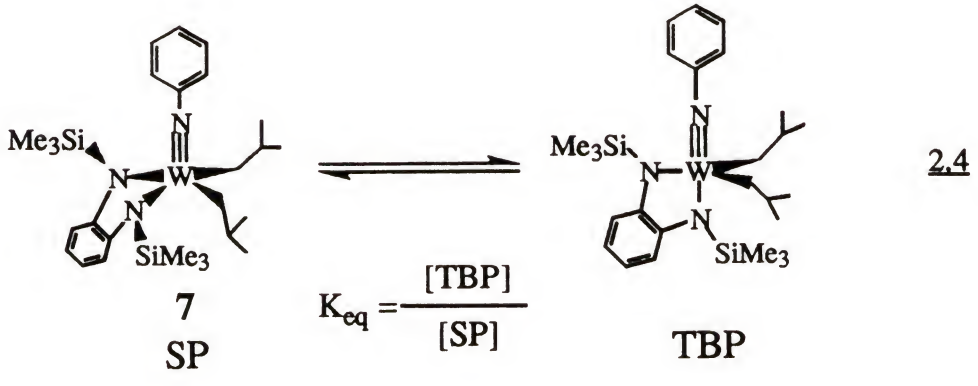

2.4

Table 2.VI. Selected Bond Lengths (Å) and Angles (°) for W(NPh)[*o*-$Me_3SiN)_2C_6H_4$] $(CH_2CHMe_2)_2$, **7.**

W-N(1)	1.738(2)	W-C(1)	2.182(5)
W-N(2)	2.013(2)	W-C(9)	2.195(2)
W-N(3)	2.023(2)		
N(1)-W-N(2)	114.77(8)	N(3)-W-C(1)	139.31(8)
N(1)-W-N(3)	120.17(8)	N(3)-W-C(5)	83.13(8)
N(1)-W-C(1)	100.35(8)	C(1)-W-C(5)	85.47
N(1)-W-C(5)	101.54(9)	W-N(1)-C(9)	174.9(2)
N(2)-W-N(3)	81.43(7)	W-C(1)-C(2)	120.0(2)
N(2)-W-C(1)	85.09(8)	W-C(5)-C(6)	127.0(2)
N(2)-W-C(5)	143.55(8)		

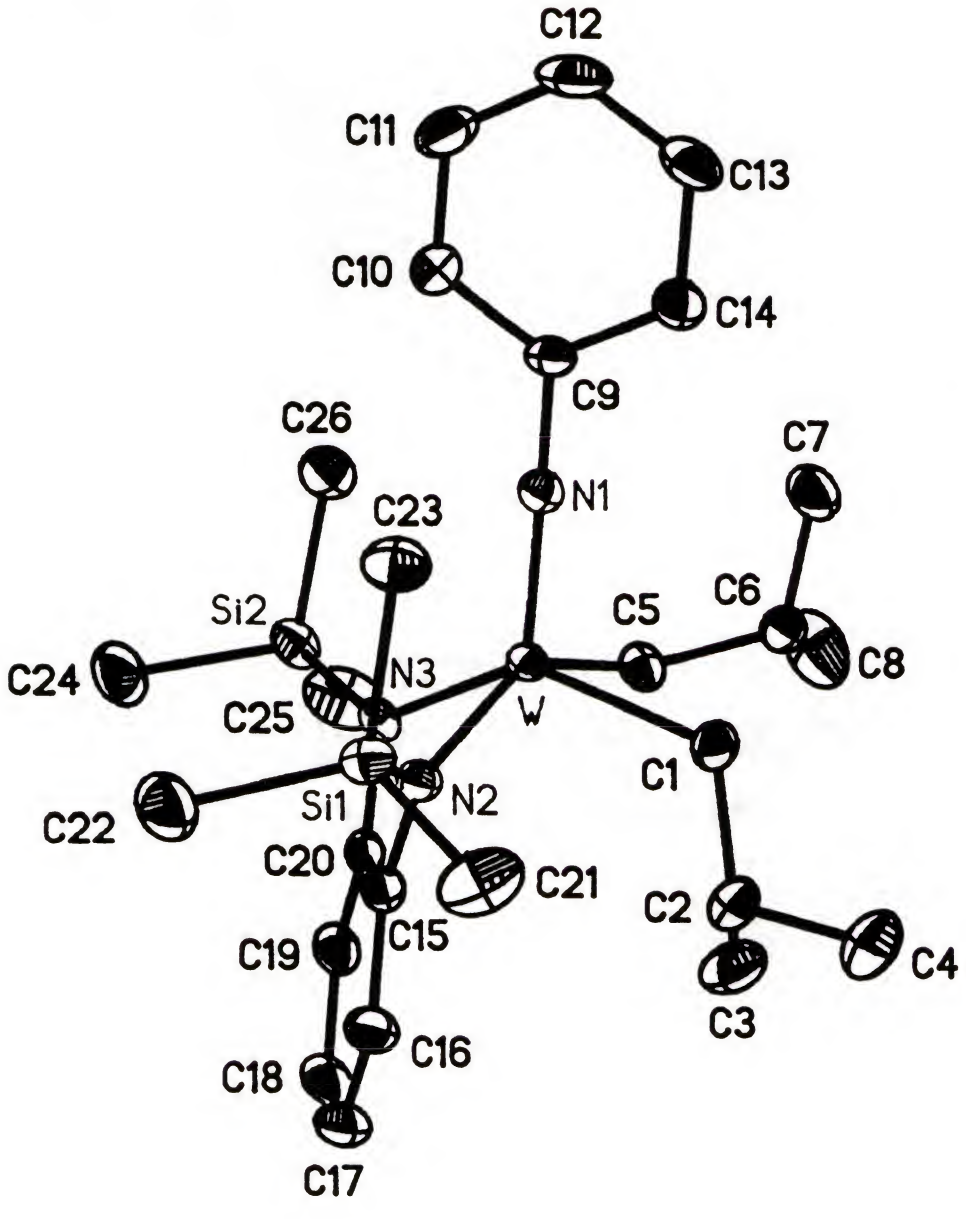

Figure 2.6. Molecular structure of W(NPh)[*o*-$(Me_3SiN)_2C_6H_4$]$(CH_2CHMe_2)_2$, **7**, with 50% probability ellipsoids and showing the atom numbering scheme. All hydrogen atoms are omitted for clarity.

At room temperature, the ^1H NMR of **7** shows only one trimethylsilyl peak at 0.34 ppm, indicating the two silyl groups are equivalent because of the mirror plane bisecting the W-N2-N3 plane (**Figure 2.6**) in the SP geometry. At -70^{0}C, another specie with two trimethylsilyl peaks (0.43, 0.59 ppm) is also observed, suggesting the formation of the TBP isomer in which the two silyl groups are inequivalent. The equilibrium constants at three different temperature are obtained by integrating the silyl peaks of the two isomers in the ^1H NMR spectra (**Table 2.VII**). Thermodynamic parameters (ΔH° = -0.66(3)Kcal/mol, ΔS° = -4.3(4) cal/mol·K) are also obtained from a van't Hoff plot of lnK *vs.* 1/T (**Figure 2.7**).

Table 2.VII. Selected Bond Lengths (Å) and Angles (°) for W(NPh)[*o*-$Me_3SiN)_2C_6H_4$] $(CH_2CHMe_2)_2$, **7.**

T(K)	K_{eq}	ΔG^0 (Kcal/mol)
233.15	0.49	0.33
223.15	0.52	0.29
193.15	0.66	0.16

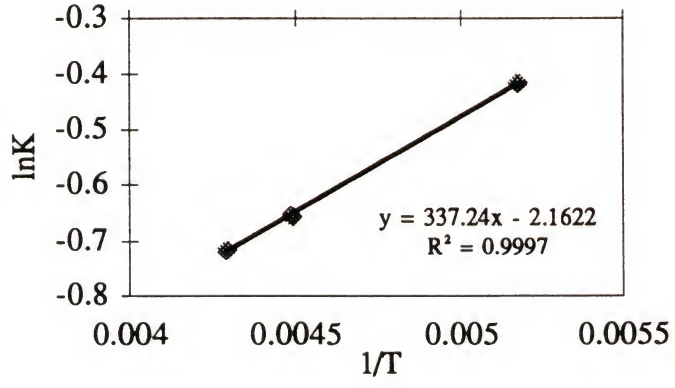

Figure 2.7. van't Hoff plot for the isomerization (SP<=>TBP) of W(NPh)[*o*-$Me_3SiN)_2C_6H_4$]$(CH_2CHMe_2)_2$, **7.** ($\Delta G = -RT\ln K$, => $\ln K = (\Delta S/R) - (\Delta H/R)(1/T)$)

Coordination of Trimethylphosphine

Complexes **2-20** are coordinatively-unsaturated tungsten species. It is reasonable to assume that coordination of Lewis bases to the d^0 metal center would be facile. We have shown that complex **2** reacts instantaneously with Lewis bases giving purple, six coordinate, Lewis base adducts as shown in equation 2.5.[69] Weak Lewis bases such as diethyl ether can be removed from the complex under reduced pressure at room temperature, while stronger Lewis bases form isolable adducts.

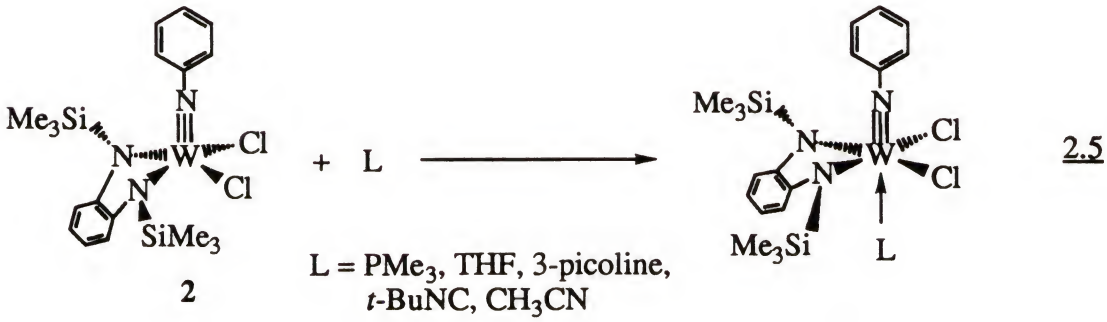

2 2.5

Solutions of dimethyl complex, **3**, change color from yellow-orange to red in the presence of PMe_3. Crystals of the complex $(TMS_2pda)W(=NPh)Me_2(PMe_3)$, **21**, can be isolated by cooling a pentane solution of **3** that contains excess PMe_3 to -40°C. These crystals readily lose PMe_3 under reduced pressure, and consequently, they are isolated by filtration followed with drying under a gentle stream of nitrogen gas. The ^1H NMR spectrum of a C_6D_6 solution of **21** displays shifted methyl (0.31 to 0.33 ppm) and TMS groups (1.12 to 0.90 ppm) relative to **3**. The chemical shift of the PMe_3 is identical to that of free PMe_3, suggesting that exchange between bound and free PMe_3 is rapid on the NMR timescale and is consistent with weak binding of PMe_3 to **3**.

A single crystal X-ray study of **21** was performed and confirmed a six-coordinate structure with an octahedral geometry. Selected bond lengths and angles can be found in **Table 2.VIII**. As can be seen in **Figure 2.8**, the phosphine coordinates *trans* to the imido ligand and the molecule has a mirror plane containing the imido N, W and phosphorus atoms, resulting in the equivalency of the two trimethylsilyl groups (equation 2.6). The coordination of PMe_3 to give the six coordinate complex, **21**, results in a reduction in the fold of the $(TMS)_2$pda ligand as demonstrated by the increased dihedral angle between the phenyl ring of the $(TMS)_2$pda ligand and the plane defined by W and the amido N atoms of 150°. The reduction in the fold of the ligand moves the *ortho* carbon atoms of the $(TMS)_2$pda ligand away from the metal center. Complex **21** has a rather long W-P bond of 2.72Å and has increased bond lengths between W and the other ligands as is expected with the increased coordination number relative to **3**.

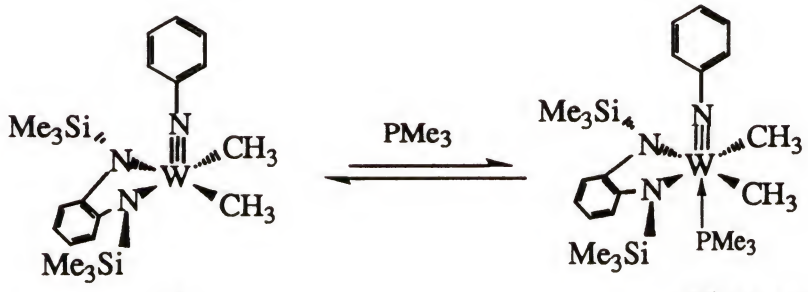

3 **21** (*cis*-alkyls) 2.6

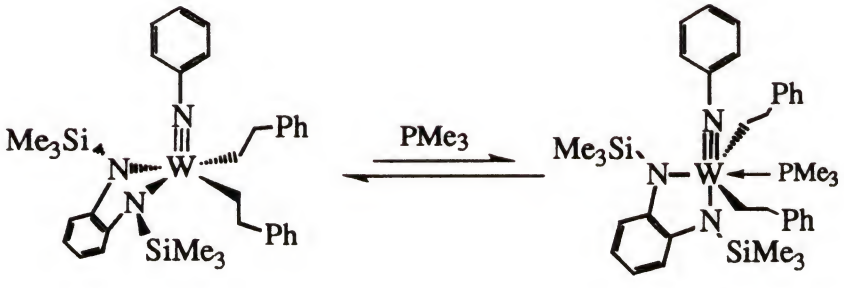

6 **22** (*trans*-alkyls) 2.7

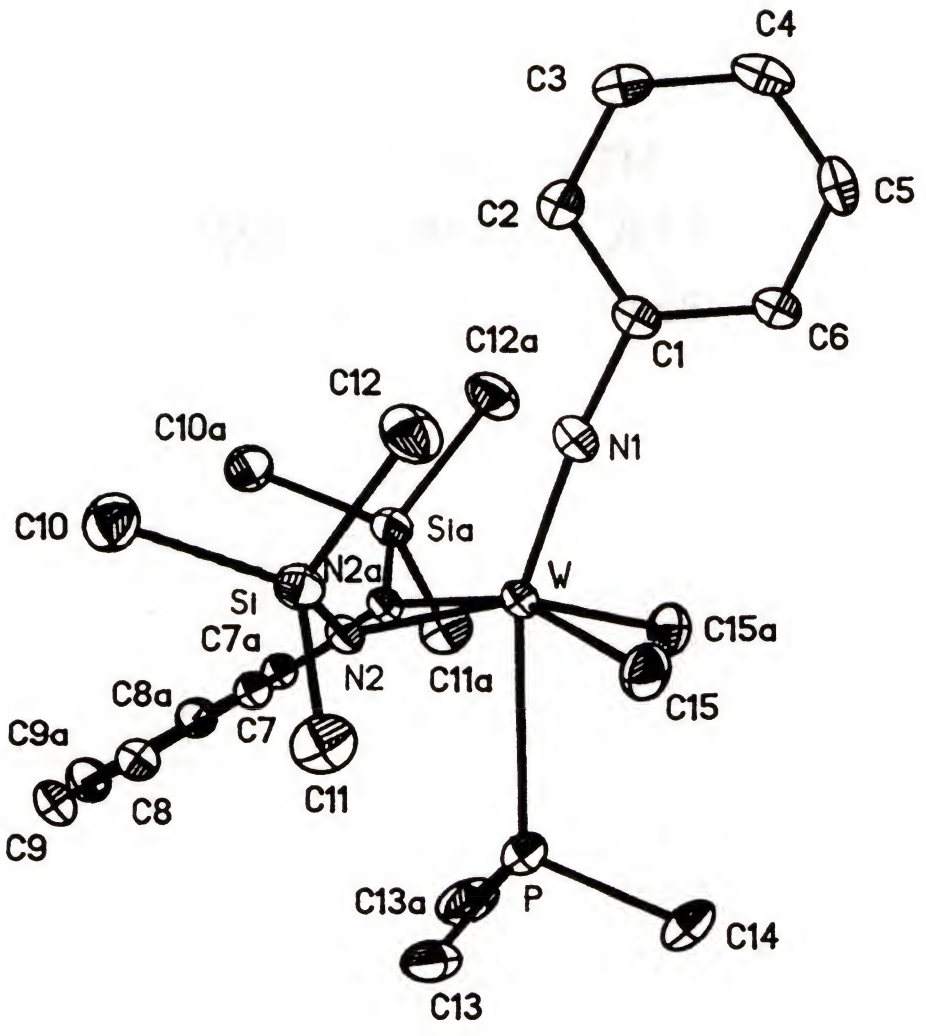

Figure 2.8. Molecular structure of W(NPh)[*o*-$(Me_3SiN)_2C_6H_4$]$(PMe_3)Me_2$, **21.** with 50% probability ellipsoids and showing the atom numbering scheme. All hydrogen atoms are omitted for clarity.

Table 2.VIII. Selected Bond Lengths (Å) and Angles (°) for W(NPh)[*o*-$(Me_3SiN)_2C_6H_4$]$(PMe_3)Me_2$, **21**.

1	2	3	1-2	1-2-3
N1	W	N2	1.760(4)	110.99(12)
N1	W	N2a		110.99(12)
N1	W	C15		91.03(12)
N1	W	C15a		91.03(12)
N1	W	P		160.04(13)
N2	W	N2a	2.067(2)	77.30(14)
N2	W	C15		90.13(12)
N2	W	C15a		157.34(12)
N2	W	P		84.28(7)
N2a	W	C15	2.067(2)	157.34(12)
N2a	W	C15a		90.13(12)
N2a	W	P		84.28(7)
C15	W	C15a	2.218(3)	94.9(2)
C15a	W	P	2.218(3)	75.67(10)
P	W	C15	2.7148(12)	75.67(10)

Although no PMe_3 adduct can be observed for the other dialkyl complexes **4-20** at room temperature, adducts can be observed by ^1H, ^{13}C, and ^{31}P NMR spectroscopy at low temperature. The spectrum of a toluene-d_8 solution of **6** at -80°C, in the presence of excess PMe_3, reveals two new peaks at 0.49 and 0.58 ppm (**Figure 2.9**), corresponding to the two silyl groups of **22**. The alkyl groups are observed to be equivalent. This suggests that PMe_3 coordinates to the metal center cis to the imido group and between the two alkyl groups, resulting in a change of geometry related to **21** (equation 2.7).

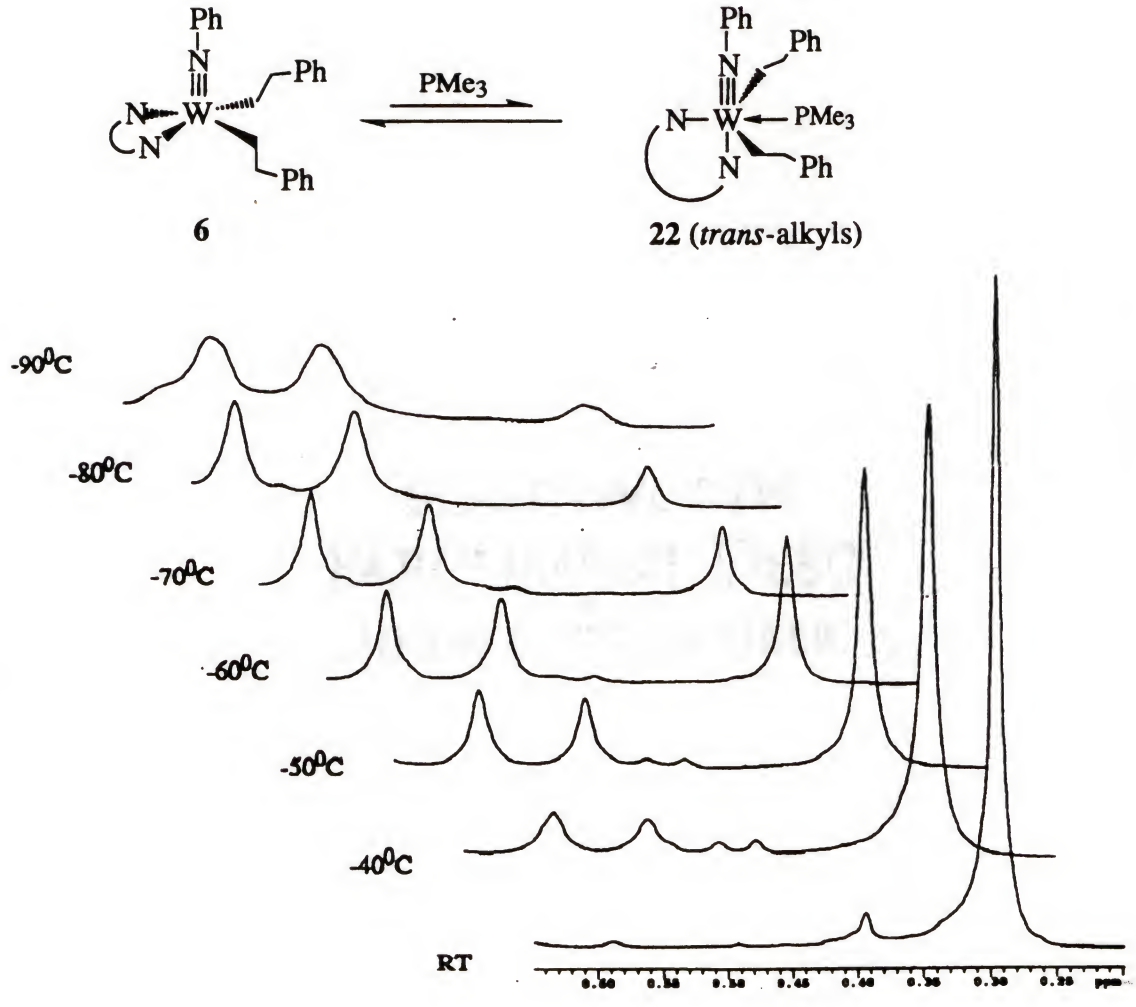

Figure 2.9. Variable temperature NMR (silyl region) of **6** in the presence of excess PMe_3.

The variable temperature NMR study (**Figure 2.10**) of the formation of W(NPh)[*o*-$(Me_3SiN)_2C_6H_4$]$(PMe_3)Et_2$, **23**, on the other hand, shows only one new peak for the two silyl groups. This implies that the PMe_3 coordinates to **4** trans to the imido group, similar to the dimethyl case. However, ^{13}C NMR spectrum of an ether-d_{10} solution of **23** (**Figure 2.11**) displays two silyl peaks at 4.66 and 5.48 ppm, which suggests that the coordination of PMe_3 is actually *cis* to the imido ligand. The peak corresponding to PMe_3 is observed at ~δ15, overlapping with solvent peaks, and other peaks are assigned as follows: **23**: δ21.23-$CH_2\underline{C}H_3$; 44.15-$\underline{C}H_2CH_3$; **4**: δ0.93-$SiMe_3$; 16.80-$CH_2\underline{C}H_3$; 57.10-$\underline{C}H_2CH_3$($J_{W\text{-}C}$=77.05Hz)). The inability to observe the inequivalent silyl peaks in the ^1H NMR is due to the faster PMe_3 exchange and ligand reorganization processes relative to the NMR time scale.

A variable temperature (room temperature to -80^{0}C) ^{13}C NMR study was also performed of the formation of W(NPh)[*o*-$(Me_3SiN)_2C_6H_4$]$(PMe_3)Me_2$, **21**. Upon the addition of ca. 20 equivalents of PMe_3 to a toluene-d_8 solution of **3**, the silyl peak shifts from 0.64 to 2.51ppm and the methyl peak shifts from 41.92 to 28.43 ppm at all temperatures, corresponding to the formation of **21**. When less PMe_3 (ca. 5 eq.) is used, the methyl peak is observed as a broad peak at 36.04 at room temperature. As the temperature decreases, the methyl peak becomes sharper and shifts upfield. At -80^{0}C, the spectrum looks exactly the same as the 20 eq. PMe_3 case with the methyl peak observed at 28.44ppm. The broadness and shifting of the peak corresponding to temperature strongly suggest weak bonding between W and PMe_3 and a fast exchange process between free and coordinated PMe_3, resulting in the observed averaged spectrum at ambient temperature. This is also verified by the observed broad PMe_3 peak at all temperatures. No peaks corresponding to the *trans* alkyl isomer of **21** was observed via ^{13}C NMR in all experiments.

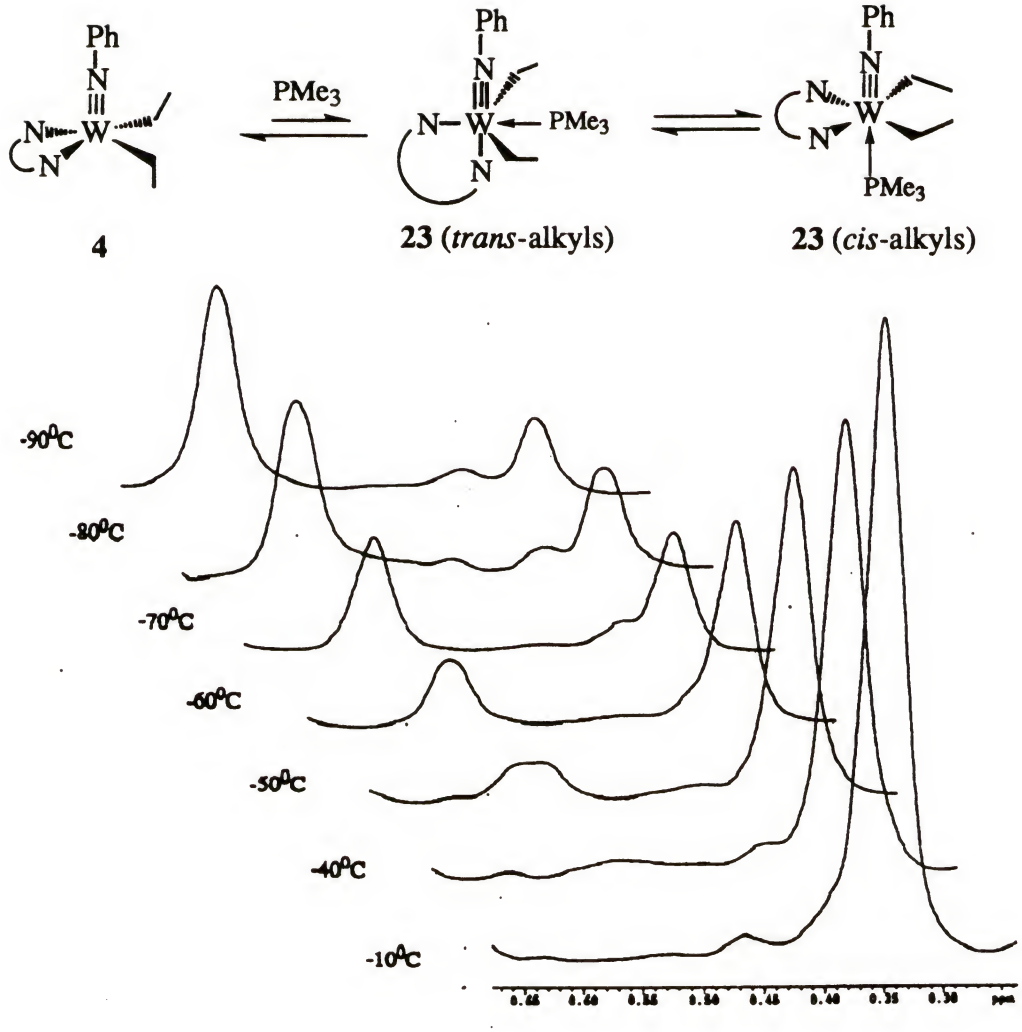

Figure 2.10. Variable temperature NMR (silyl region) of **4** in the presence of excess PMe_3.

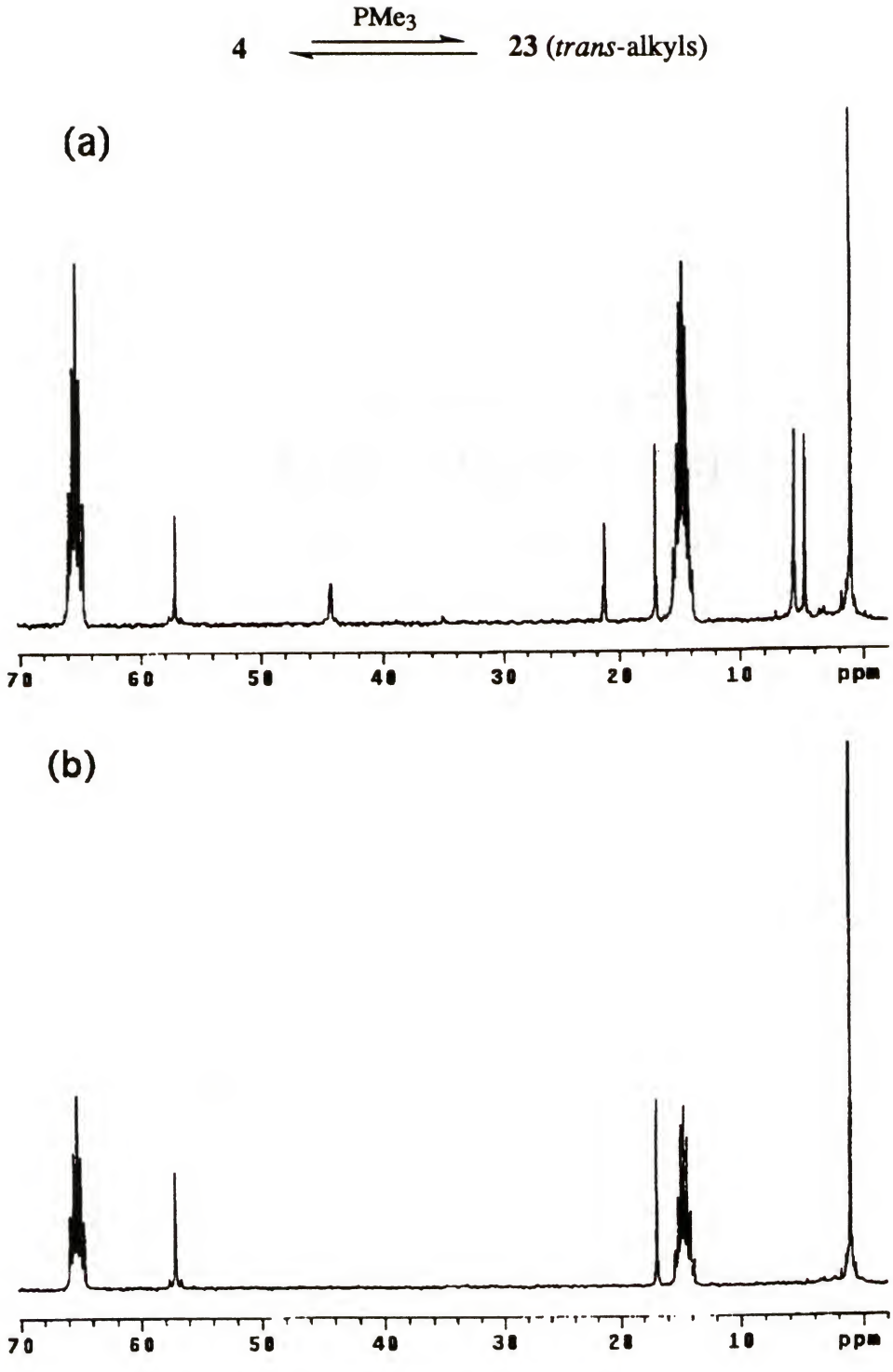

Figure 2.11. ^{13}C NMR spectra (-80^{0}C) in diethyl ether-d_{10}.(δ14, 65) (a) **4** + excess PMe3. (b) **4**.

The formation of **22** and **23** can also be observed by ^{31}P NMR spectroscopy. No peak corresponding to the coordinated PMe_3 in **22** can be observed above -70°C. At -90°C, the toluene-d_8 solution of **6** in excess PMe_3 displays a new peak at -27.05ppm, which is assigned to the coordinated PMe_3 (**Figure 2.12**). The broadness of the peak is due to fast PMe_3 exchange with free PMe_3. Both isomers were observed for the PMe_3 adduct of **4**, W(NPh)[*o*-$(Me_3SiN)_2C_6H_4$]$(PMe_3)Et_2$. ^{31}P NMR of a toluene-d_8 solution of **4** in the presence of 15 eq. of PMe_3 at -80°C reveals two distinct peaks (**Figure 2.13**) in a ratio of *ca.* 20:1 at δ -21.9 ($^1J_{P\text{-}W}$ = 240 Hz, major isomer, PMe_3 *cis* to imido and ethyl groups mutually *trans*) and δ -28.1 (broad, minor isomer with PMe_3 *trans* to imido and ethyl groups mutually *cis*). We believe that both *cis* and *trans* isomers can exist in solution for each complex with the major species being the *trans* isomer. The spectroscopic data of the PMe_3 coordinated adducts is reported in **Table IX**.

Table 2.IX. Spectroscopic data (-80°C) for PMe_3 coordinated complexes.

Compound	^{31}P (ppm)
(NPh)[*o*-$(Me_3SiN)_2C_6H_4$]$W(PMe_3)Me_2$, **21**	-23.78; -26.08
(NPh)[*o*-$(Me_3SiN)_2C_6H_4$]$W(PMe_3)Et_2$, **23**	-21.87; -28.11
(NPh)[*o*-$(Me_3SiN)_2C_6H_4$]$W(PMe_3)(CH_2CH_2Ph)_2$, **22**	-27.05
(NPh)[*o*-$(Me_3SiN)_2C_6H_4$]$W(PMe_3)Et(CH_2CH_2Ph)$, **24**	-20.19
(NPh)[*o*-$(Me_3SiN)_2C_6H_4$]$W(PMe_3)Et(CH_2CMe_3)$, **25**	-20.02; -28.20

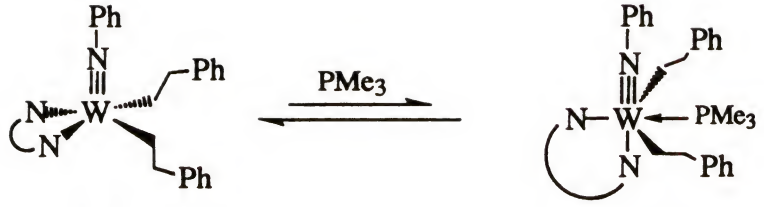

6 **22** (*trans*-alkyls)

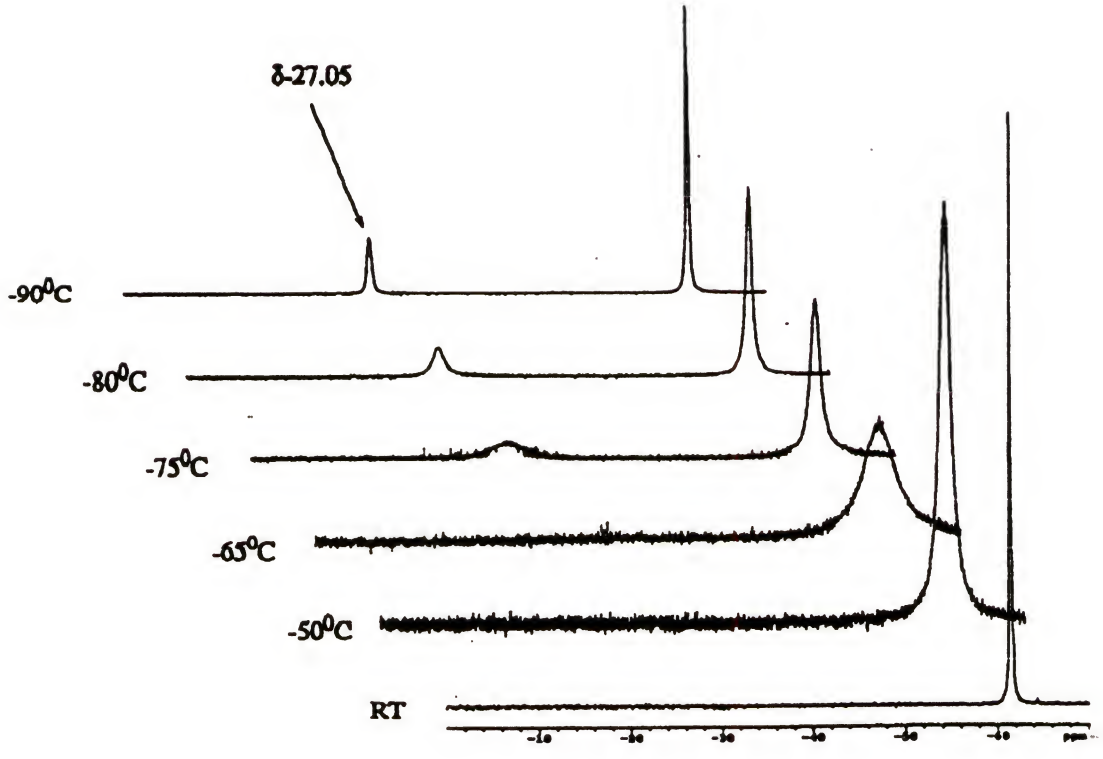

Figure 2.12. Variable temperature ^{31}P NMR of **6** in the presence of excess PMe_3.

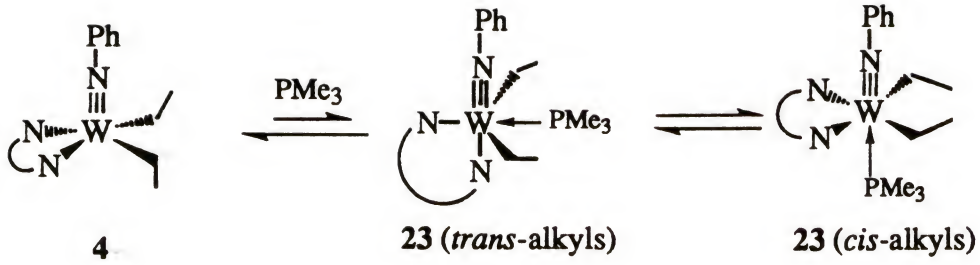

4 **23** (*trans*-alkyls) **23** (*cis*-alkyls)

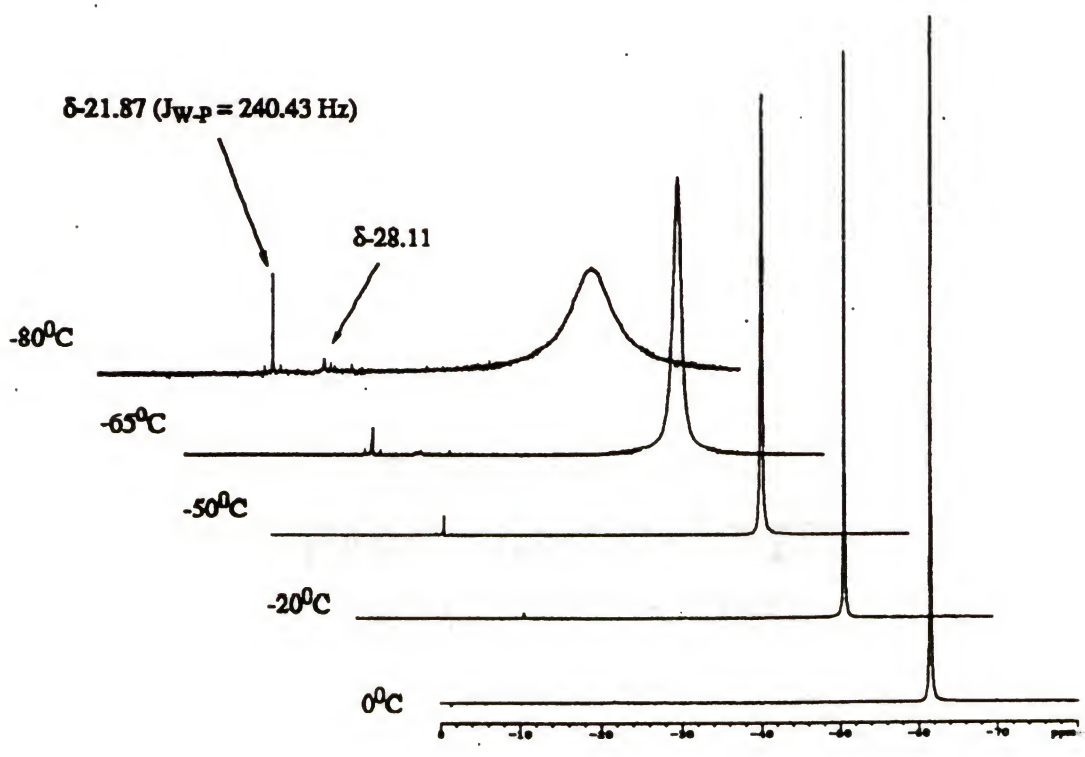

Figure 2.13. Variable temperature ^{31}P NMR of **4** in the presence of excess PMe_3.

It is worthwhile to note that in the 5-coordinate SP complexes **3-7**, the LUMO is the d_{xy} orbital which directs the coordination of PMe_3 between the two alkyl ligands, as demonstrated in the bis-β-phenylethyl case, **6**.[70] For the dimethyl complex, **3**, the coordination of PMe_3 is sterically controlled at the less hindered site, d_{z2} orbital, rather than the LUMO which will result in the repulsion between the phosphine and the methyl groups. In an extended Huckel calculation, using the crystal structure coordinates of **3**, the d_{z2} orbital (LUMO + 7) lies approximately 3.7 eV higher in energy than the LUMO (d_{xy}). For larger alkyl groups, the coordination site *trans* to the imido is also hindered, resulting in the coordination of PMe_3 at the LUMO and the *trans* alkyl isomer being the major species in solution (**Scheme2.E**).

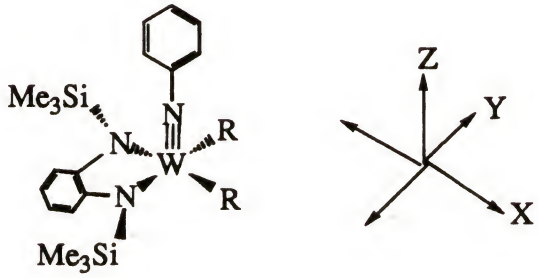

Another explanation for the formation of *trans* alkyl isomer is to consider the fast isomerization between square pyramidal and trigonal bipyramidal structures for these pentacoordinated complexes. The coordination of PMe_3 occurs at the LUMO site (between two alkyl groups) of the trigonal bipyramidal isomer, forming the *trans* alkyl PMe_3 adduct. In addition, the packing effect is probably also a factor to cause the significant difference in the coordination modes of PMe_3 from a small steric difference of the methyl and ethyl groups.

Scheme 2.E Diagram for the orbitals interacting with PMe_3.

Square pyramid

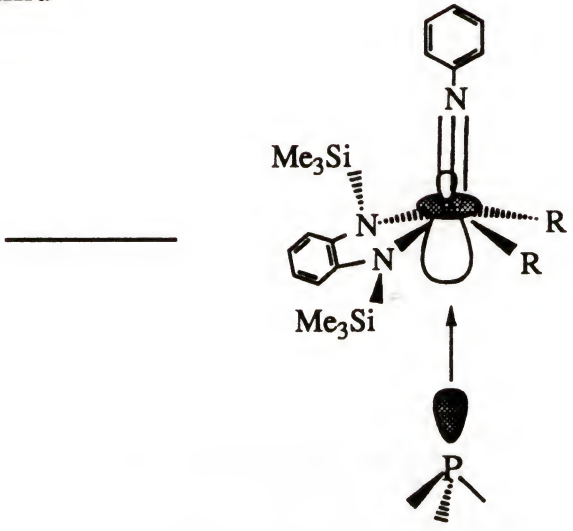

LUMO

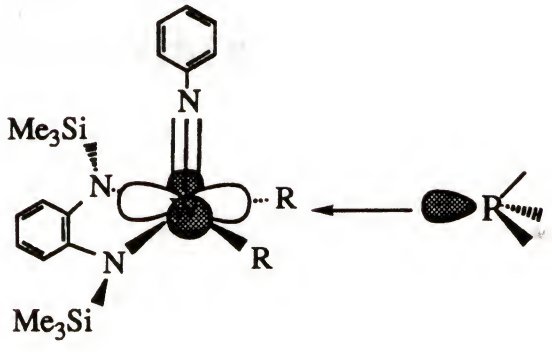

Trigonal bipyramid

LUMO

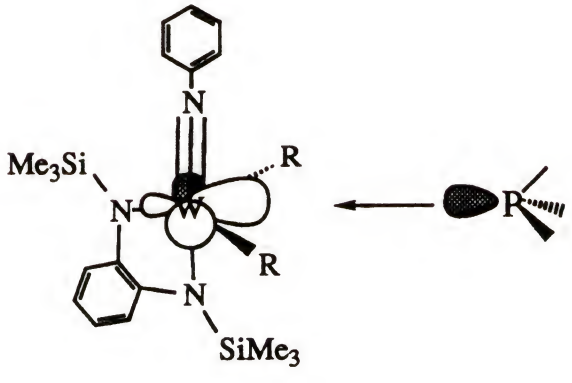

Different preferences for the coordination of isocyanides have also been observed. For the dichloride complex, **2**, both the coordination of PMe_3 and ^tBuNC are *trans* to the imido ligand as shown in **Figure 2.14**. However, the ^tBuNC only coordinates *cis* to the imido ligand in the dimethyl, **3**, and bisneopentyl, **10**, complexes. This is in contrast to earlier results where PMe_3 coordinates preferencially *trans*to the imido ligand of **3** and does not coordinate to **10**. The differences can be attributed to the different steric and electronic properties of the ligands. The poorer σ-donor properties of Cl^- relative to Me^- render the metal center more electrophilic. This is reflected in the stronger coordination of Lewis bases to the dichloride complex, **2**. The smaller σ-donor, ^tBuNC, can coordinate between two alkyl groups with less steric repulsions, compared to the coordination of PMe_3, which results in the different isomers observed. The coordination of ^tBuNC, but not PMe_3, to **10** is considered also due to this size effect.

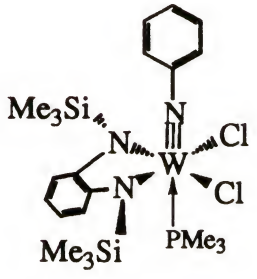

28 (*cis*-Cl)

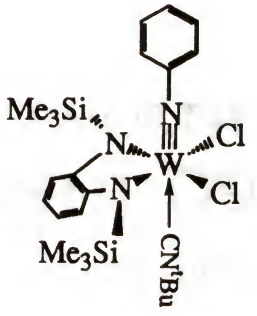

29 (*cis*-Cl)

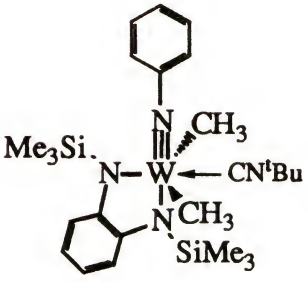

30 (*trans*-alkyls)

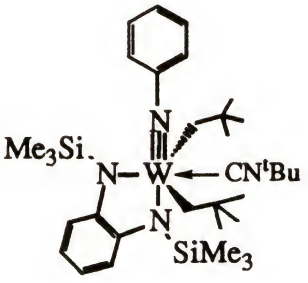

31 (*trans*-alkyls)

Figure 2.14. Preferences of the coordination of Lewis bases.

Insertion Reaction of Isocyanide and **6**

Insertion reactions of isocyanide, isoelectronic with CO, into metal-carbon bonds has been extensively studied over the past few decades.[71] Unlike carbon monoxide, isocyanide readily undergoes multiple insertions into various metal-carbon σ-bonds, providing useful synthetic routes to nitrogen containing organic compounds.[72] Furthermore, isocyanides are better σ-donors[71a] than CO and can function as ligands in metal complexes where carbon monoxide does not. For high-valent early transition metal alkyls, the insertion of isocyanides usually forms the η^2-iminoacyl moiety as shown in equation 2.8.[73] Recently, the insertion reactions of isocyanide into metal-sulfur[74] and metal-hydride[75] bonds have also been reported.

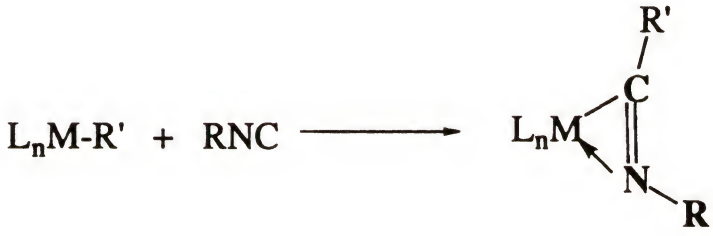

2.8

When 2 equivalents of ^{t}BuNC are added to a solution of **6**, the orange solution turns green within a few minutes. NMR scale experiments indicate that this reaction is immediate and quantitative upon addition of isocyanide. Concentration and cooling of this solution affords a green solid, **26**, which is extremely soluble in hydrocarbon solvents and ethers (**Scheme 2.F**). Compound **26** is air and moisture-sensitive but is indefinitely stable in the solid state under an inert atmosphere. The ^{1}H NMR spectrum of **26** in C_6D_6 reveals peaks at 0.33 ppm (9H) and 0.82 ppm (9H), identified as inequivalent trimethyl

silyl groups. A singlet at 1.46 ppm (18H) is assigned to equivalent *t*-butyl groups, shifted downfield from free ^{t}BuNC (0.94 ppm) and overlapping multiplets in the aromatic region integrate to a total of 19 protons.

The ^{13}C NMR spectrum of **26** in C_6D_6 displays inequivalent TMS groups and equivalent *t*-butyl groups. Additionally, a single peak at 211.48 ppm indicates the presence of an η^2-imino-acyl moiety.[23b] The NMR data for compound **26** are consistent with the 18e$^-$ trigonal bipyramidal bis-η^2-imino-acyl complex, [(TMS)$_2$pda](NPh)W[η^2-(^{t}Bu)NC(CH$_2$CH$_2$Ph)]$_2$ (**Scheme 2.F**), with one (TMS)$_2$pda nitrogen axial, *trans* to the imido ligand, similar to the solid state structure of the related compound, [(TMS)$_2$pda](NPh)W[η^2-(^{t}Bu)NC(Me)]$_2$.[16]

Heating a solution of **26** to 70°C for 3 days causes complete conversion to a new complex, **27**, which can be isolated as a red, air and moisture-sensitive solid. Compound **27** is indefinitely stable in both the solid state and in solution under inert conditions. The ^{1}H NMR spectrum of **27** in C_6D_6 shows a singlet at 0.47 ppm (18H), attributed to equivalent TMS groups, and a singlet at 1.33 ppm (18H) which is assigned to equivalent *t*-butyl groups. The {^{1}H}^{13}C NMR spectrum confirms the equivalent TMS and *t*-butyl groups, showing singlets at 4.38 and 32.59 ppm respectively. The NMR spectra of **27** are consistent with a symmetric complex with square pyramidal geometry about the W atom. Complex **27**, [(TMS)$_2$pda](NPh)W[(^{t}Bu)NC(CH$_2$CH$_2$Ph)=C(CH$_2$CH$_2$Ph)N(^{t}Bu)], is considered to be a metallacycle with the imido moiety in the apical position, similar to the solid state structure of the related compound, [(TMS)$_2$pda](NPh)W[(^{t}Bu)NC(Me)=C(Me)N(^{t}Bu)].[16] The thermolysis of **26** involves an intramolecular coupling of the two η^2-iminoacyl groups to produce the cyclic enediamidate complex, **27**.[23b] Similar results have also been observed for dimethyl, **3**, and bisneopentyl, **10**, complexes, with the exception that the bis-η^2-iminoacyl compound of **10** does not undergo further coupling reaction to form the metallacyclic enediamidate, presumably due to the steric bulk of the neopentyl group.[16]

It is clear that compound **2** is a convenient starting material for a variety of new W(VI) complexes. The steric flexibility of the $(TMS)_2$pda ligand may prove useful in the stabilization of coordinatively unsaturated complexes. This is demonstrated by the change in the degree of folding of the $(TMS)_2$pda ligand observed in the structures reported herein. The ability to fold along the N-N vector allows the $(TMS)_2$pda ligand to possess a variable steric "footprint" depending upon the needs of the metal center. Our studies on the thermolysis of **10**[76] have demonstrated that new alkylidene complexes that are useful olefin metathesis catalysts containing the $(TMS)_2$pda ligand are accessible. Further studies directed toward understanding how the structural preferences identified here affect and control the reactivity of these compounds with substrates such as H_2 and ethylene will be discussed later.

Scheme 2.F. Reaction of **6** with ^{t}BuNC and subsequent isomerization of **26** to produce compound **27**.

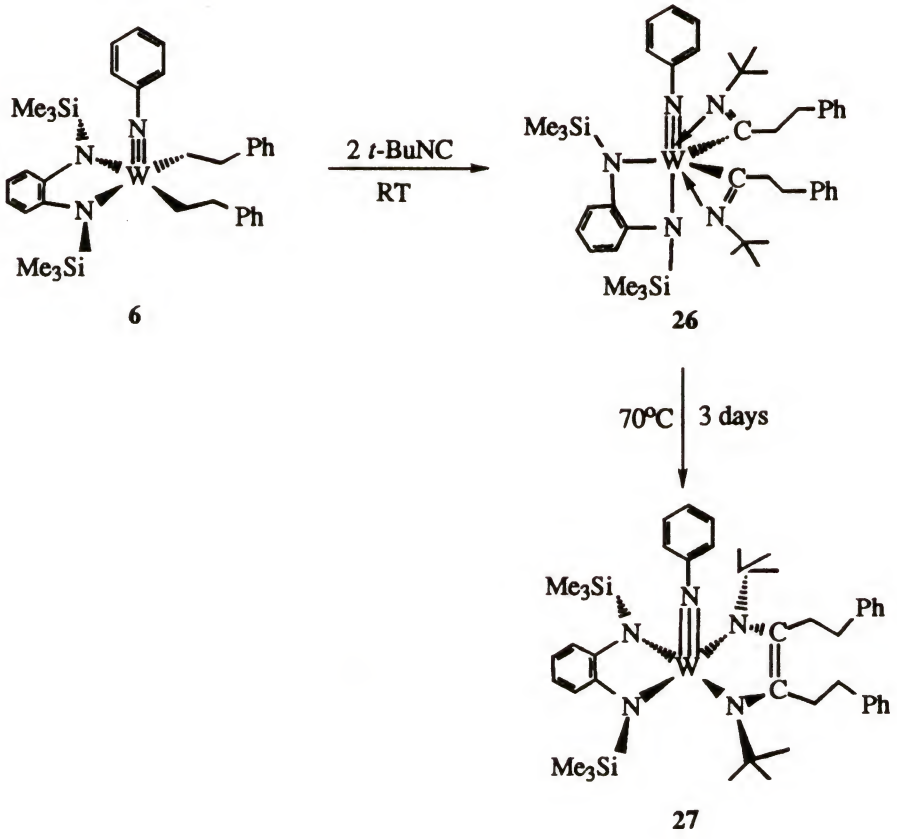

CHAPTER 3
METATHESIS REACTION AND THE CHEMISTRY OF TUNGSTA(VI)METALLACYCLOPENTANE

Synthesis of the Alkylidene Complex

Alkylidene complexes ($L_nM{=}C(R)R'$) have been shown to be active intermediates in a variety of important transition metal catalyzed reactions such as olefin metathesis,[3a] rearrangement of strained hydrocarbons,[77] and biochemical oxidation.[78]

The most widespread strategy of forming an alkylidene bond is the abstraction of an α-proton from a metal alkyl ligand.[53] Schrock reported the formation of an alkylidene complex, $Ta(CHC(CH_3)_3)(CH_2C(CH_3)_3)_3$, from the reaction of two equivalents of neopentyl lithium with $Ta(CH_2C(CH_3)_3)_3Cl_2$.[79] Intramolecular α-hydrogen abstraction from one alkyl ligand by another occurs most readily if coordination about the metal center is crowded. For example, $Ta(CH_3)_5$[80] can be readily prepared, but $Ta(CH_3C(CH_3)_3)_5$, which can only be observed at low temperature, decomposes to $Ta[CH_3C(CH_3)_3]_3[CHC(CH_3)_3]$ with the loss of neopentane.[81] Intermolecular α-hydrogen abstraction can also be used to prepare alkylidene complexes if intramolecular abstraction fails or can not be controlled.[82] A ligand-induced α-abstraction process is also observed when trimethylphosphine is added to $W(NPh)(CH_2C(CH_3)_3)_2(PMe_3)(Cl)_2$ to give $W(NPh)(CHC(CH_3)_3)(PMe_3)_2(Cl)_2$.[56]

The alkylidene complex, $W(NPh)[o\text{-}(Me_3SiN)_2C_6H_4](CHCMe_3)(PMe_3)$, **34**, can be synthesized via heating the bisneopentyl complex, **10**, in the presence of PMe_3.[50a] The reaction is found to proceed by competing α- and γ-H abstractions (**Scheme 3.A**) with the formation of two intermediates: tungsten metallasilacycle, **32**, and the base-free

alkylidene species, **33**.[76] Addition of trimethylphosphine yields the neopentylidene complex, **34**.

Scheme 3.A

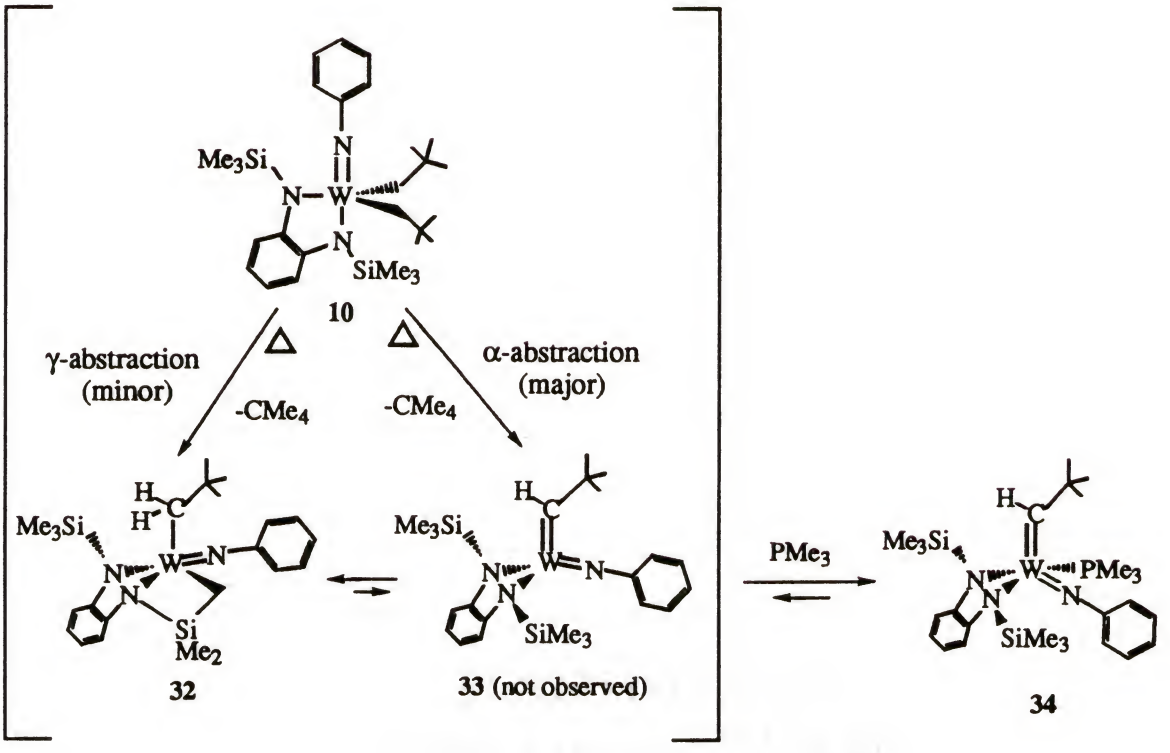

Olefin Metathesis

There has been a wide range of interest in transition metal alkylidene complexes, primarily focused on their reactions with olefins. The olefin metathesis reaction, which is catalyzed by alkylidene complexes, interchanges the carbon fragments of olefins to give new olefins.[3a,83] Herrison and Chauvin[84] proposed that the active catalytic species consists of a metal alkylidene and the mechanism involves the formation of metallacyclobutane complexes. The mechanism (**Scheme 3.B**) involves the initial

formation of an alkylidene-olefin complex (step (a)), followed by a [2+2] cycloaddition to give metallacyclobutanes (step(b)), which then undergo a [2+2] cycloreversion to form a new olefin and a scrambled alkylidene fragment (step (c)).

Scheme 3.B

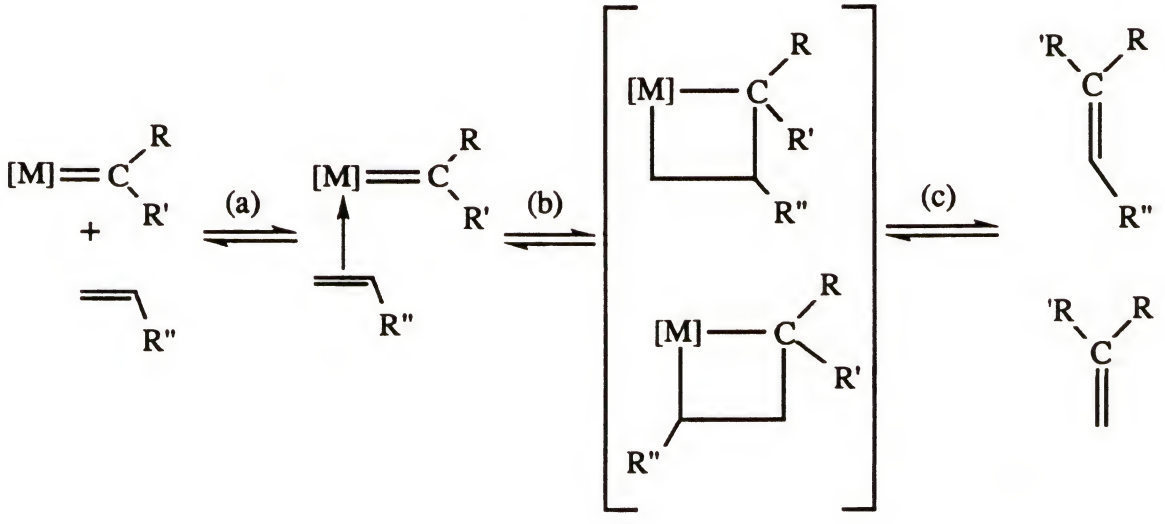

In catalytic reactions, the initial metathesis product, $R'CH=CH_2$ is formed, followed by coupling of two terminal olefins ($RCH_2=CH_2$) to give internal olefins (RCH=CHR, **Scheme 3.C**).[85] This reaction can be driven by removal of the ethylene liberated, which is productive only if the amount of internal olefins (RCH=CHR) exceeds the amount of the initial metathesis product, $R'CH=CH_2$.

Scheme 3.C

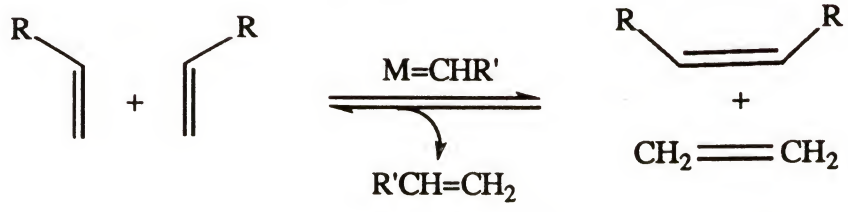

There are several decomposition pathways[86] which terminate the metathesis chain in classical metathesis systems, such as (a)-bimolecular decomposition of alkylidene complexes (especially of methylidene, $M=CH_2$),[82] (b)-rearrangement of metallacyclobutane rings to olefins,[87] and (c)-rearrangement of alkylidene ligands to olefins[87a] (**Scheme 3.D**).

Scheme 3.D

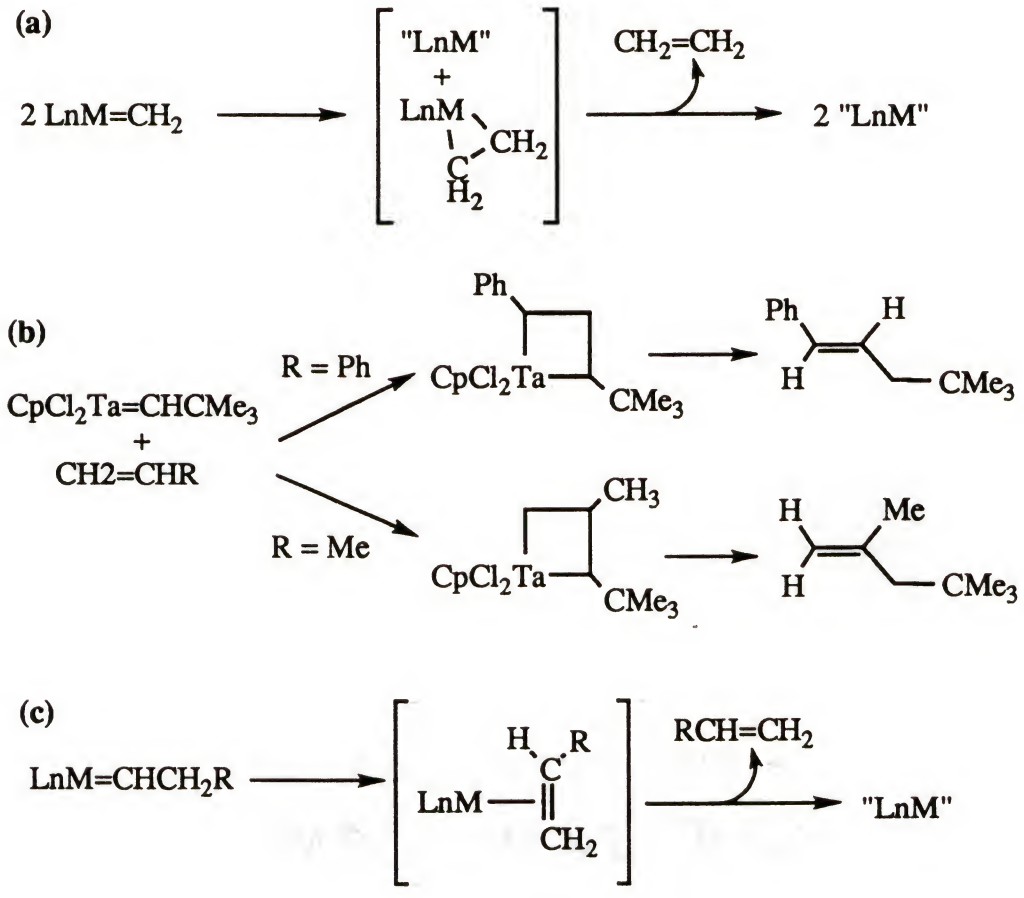

Metathesis Reactions of 1-Pentene

The metathesis reaction of 1-pentene was carried out by reacting the alkylidene complex, **34**, with excess 1-pentene (ca. 40 equivalent) at 80°C. The initial metathesis product, 3,3-dimethyl-1-butene, was observed upon the addition of 1-pentene, and the metathesis product (90% yield) was identified as 4-octene by GC-MS (equation 3.1).

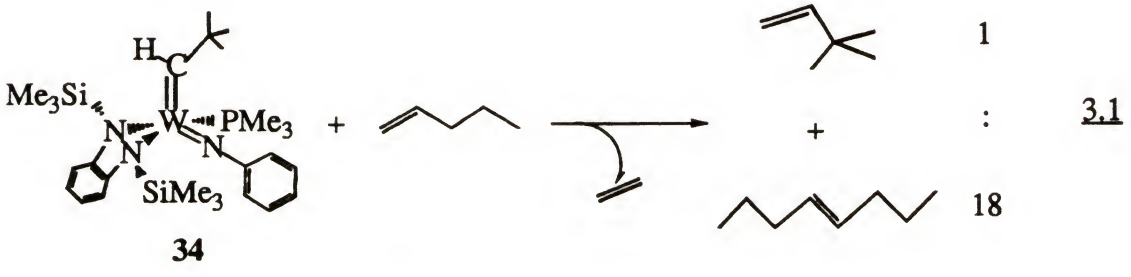

34

The mechanism illustrated in **Scheme 3.E** accounts for the formation of 1-octene. The initial reaction between 1-pentene and **33** selectively forms the α, α'-disubstituted metallacyclobutane, **A**. The formation of intermediate **A** instead of the α, β-disubstituted compound is due to the steric of bulkiness of the *t*-butyl group. Therefore the α'-position is less crowded than the β-position (bond length of C-C bond: ~1.5Å; W-C bond: ~2.2Å), leading to the formation of **A**. Similar preference for the formation of an α, α'-disubstituted metallacyclobutane[88] was also reported in the metathesis reaction of $(NAr)(OR)_2Mo{=}CHSiMe_3$ and $CH_2{=}CHSiMe_3$.[88a] Neohexene is released from metal center (**A**), resulting in the formation of a new butylidene complex, **B**, which starts the catalytic cycle. Gassman and Johnson[89] have pointed out that the chain-carrying specie in the metathesis reaction is a substituted metal alkylidene complex rather than a nonsubstituted methylidene complex, based on their interpretation of the formation of "degenerate metathesis" products (i.e., the M-C and C-C bonds of the metallacyclobutane

cleave in the way to yield back the original olefin and alkylidene complex) in their study of metathesis reactions of terminal olefins.

Scheme 3.E

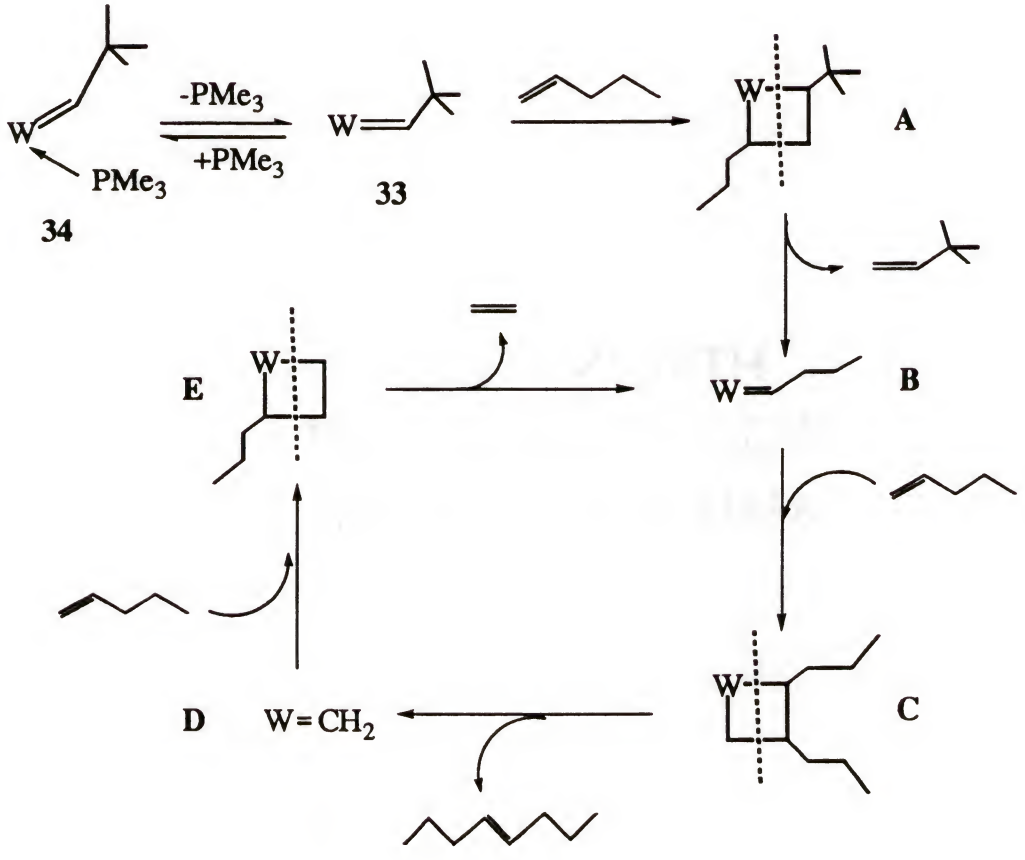

The next metathesis step between **B** and 1-pentene yields an α, β-disubstituted metallacyclobutane, **C**. The α, α'-analog will result in degenerate metathesis. The formation of **C** is consistent with the nucleophilic properties of the alkylidene α-carbon and a polarization which places partial positive charge on the metal and partial negative charge on the unsubstituted olefinic carbon of 1-pentene as a single bond forms between the alkylidene α-carbon and the substituted olefinic carbon. The following cycloreversion step

produces the internal olefin, 4-octene, and a methylidene intermediate, **D**. Transition metal methylidene complexes have been considered as highly reactive intermediates in the metathesis reaction. The involvement of methylidene complexes is supported by the successful isolation of methylidene complexes of Ta,[90] Zr,[91] and Mo,[92], which showed high reactivity towards electrophiles, π-bonding ligands, and silanes.[93] Further metathesis reaction of **D** results in the formation of ethylene and **B**, which completes the catalytic cycle. The reaction can also be carried out by directly activating the catalyst precursor, bisneopentyl complex, **10**, by heating it in the presence of 1-pentene.

Formation of Metallacyclopentane Complex

Earlier work in our group demonstrated that the alkylidene complex, **34**, can initiate the ROMP of cycloalkenes.[50a] However, it only catalyzes the oligomerization of α,ω-dienes via ADMET chemistry. Furthermore, **34** can also be used for the metathesis degradation of poly-1,4-butadiene with an internal olefin (equation 3.2). If the same degradation conditions are used and ethylene is substituted for the internal olefin, very little degradation (as measured by reduction in molecular weight of the polymer) is observed.[50b,94]

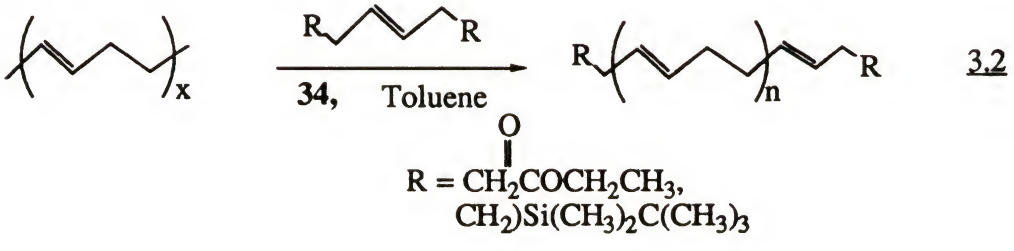

3.2

In order to find an explanation for these observations and a possible explanation for the general observation that tungsten containing catalysts tend to be inferior for the metathesis of terminal olefins,[3a] a series of experiments were carried out. Thermolysis of bisneopentyl complex, **10**, in the presence of excess ethylene results in the formation of neopentane, 3,3-dimethyl-1-butene, and a metallacyclopentane complex $W(CH_2CH_2CH_2CH_2)(NPh)[o\text{-}(Me_3SiN)_2C_6H_4]$, **35**, as shown in equation 3.3. Complex **35** can also be synthesized independently on a preparative scale (equation 3.4) by allowing the dichloride complex, $W(NPh)[o\text{-}(Me_3SiN)_2C_6H_4](Cl)_2$, **2**, to react with the Grignard reagent, $BrMg(CH_2)_4MgBr$.

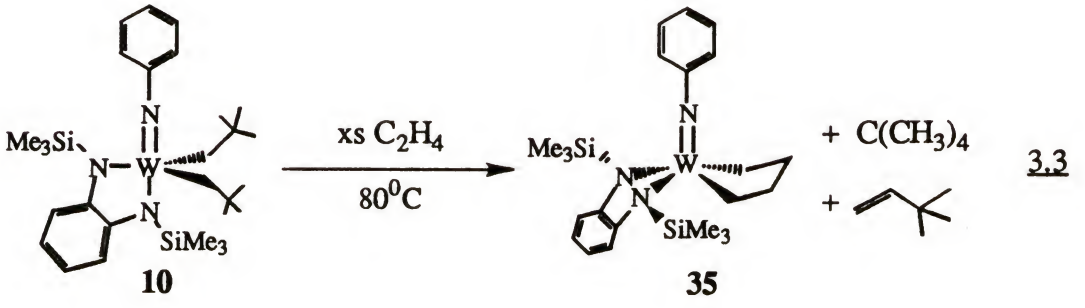

10 **35** 3.3

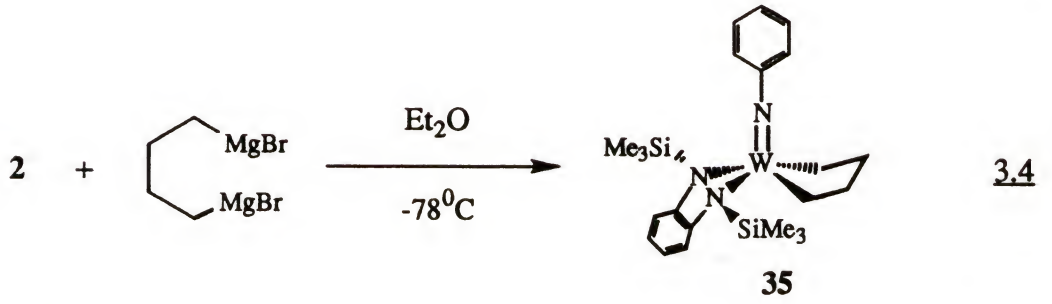

35 3.4

The ^{1}H-NMR spectrum of **35** in benzene-d_6 displays broad resonances with unresolved fine structure that are assigned to the CH_2 protons at 2.93, 2.91, 2.42, and 1.54 ppm, respectively, in a 2:2:2:2 ratio. The silyl methyls are observed as a sharp singlet

at 0.28 ppm, and is consistent with a square pyramidal geometry in which a mirror plane containing the imido ligand and tungsten atom bisects the N-W-N and C-W-C angles. The $^{13}C\{^1H\}$ NMR of **35** displays resonances at δ61.25 ($^1J_{W-C}$ = 73.6Hz, $^1J_{C-H}$ = 122.9Hz) and δ35.23 ($^1J_{C-H}$ = 124.3Hz) which are assigned to C_α and C_β of the metallacycle, respectively. The ^{13}C spectral parameters are similar to known tungstacyclopentane complexes reported by Chisholm[95] (C_α : δ64 ($^1J_{W-C}$ = 77 Hz); C_β : δ37) and Schrock[96] (C_α : δ76.8; C_β : δ38.6).

A single crystal of **35** suitable for an X-ray structure determination was grown from a pentane solution of **35** at -20°C. A thermal ellipsoid plot of complex **35** along with the atom-labeling scheme is given in **Figure 3.1**, while a table of selected bond lengths and angles is shown in **Table 3.I**. The coordination geometry around the W atom is that of a slightly distorted square pyramid. In this structure, the imido N occupies the axial site while the N atoms of the TMS_2pda ligand and the C atoms of the metallacyclopentane group form the basal plane. The tungsten atom resides 0.717Å above the plane defined by N(1), N(2), C(1), and C(4) (mean deviation is 0.001Å). The W-C(1) and W-C(4) bond lengths (2.182(5) Å, 2.183(5) Å, respectively) are within the range expected for W(VI)-C distances.[55,69] The $W\text{-}N_{imido}$ bond length is 1.736(4)Å and is consistent with a W-N triple bond.[53,54] The geometry about the N atoms of the $[o\text{-}(Me_3SiN)_2C_6H_4]^{2-}$ ligand is planar as is observed in silyl amines.[97] The ligand is folded about the N-N vector which causes the $SiMe_3$ groups to be displaced above the basal plane. The folding of the ligand also tilts the N coordination planes by 60 - 65° relative to the basal plane of the molecule.

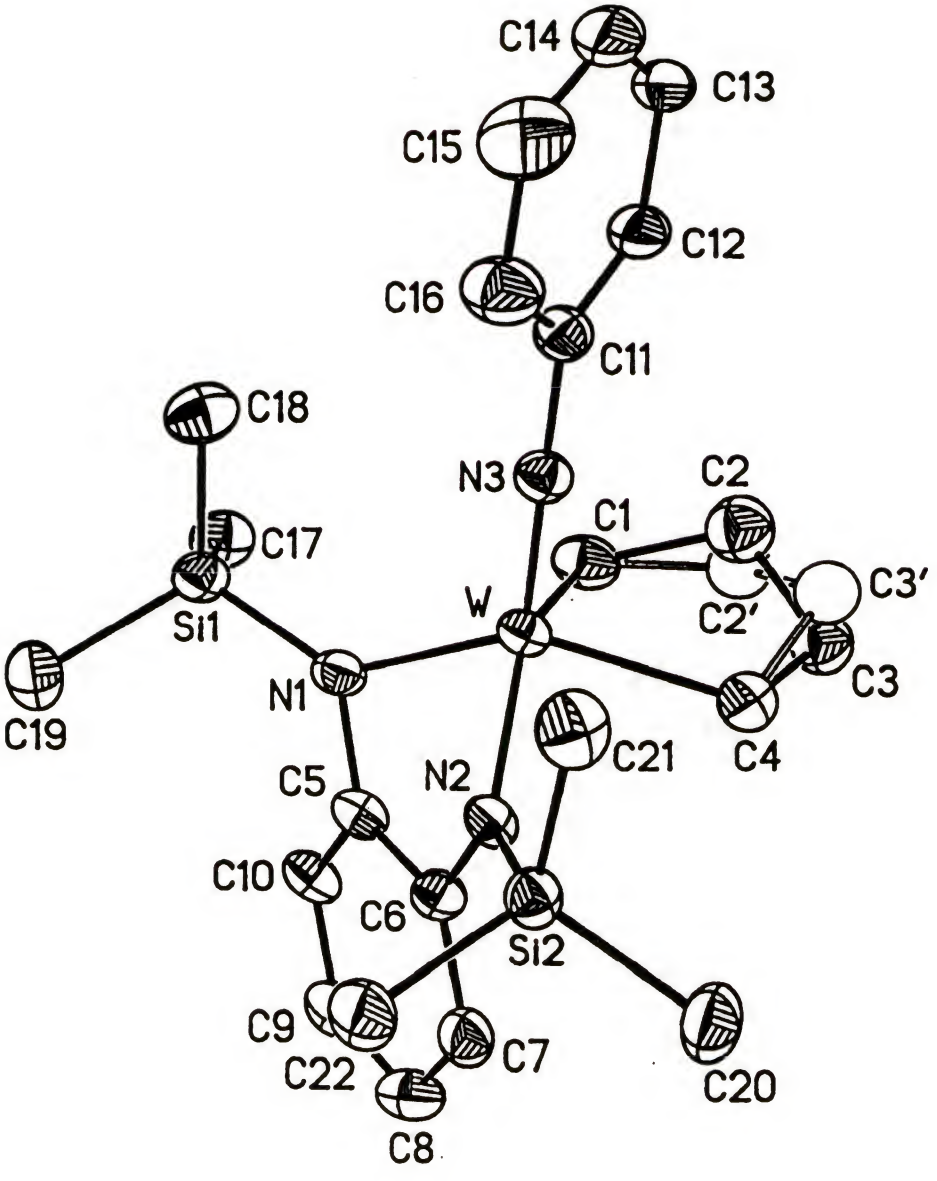

Figure 3.1. Molecular structure of W(NPh)[*o*-$(Me_3SiN)_2C_6H_4$]($CH_2CH_2CH_2CH_2$), **35**, with 50% probability ellipsoids and showing the atom numbering scheme. All hydrogen atoms are omitted for clarity. The metallacyclopentane ring is disordered by the flipping of the 5-membered ring, denoted by W-C(1)-C(2)-C(3)-C(4) and W-C(1)-C(2')-C(3')-C(4.)

Table 3.I. Selected Bond Lengths (Å) and Angles (°) for W(NPh)[*o*-$(Me_3SiN)_2C_6H_4$]($CH_2CH_2CH_2CH_2$), **35**.

W-N(1)	2.023(4)	W-C(1)	2.182(5)
W-N(2)	2.004(4)	W-C(4)	2.183(5)
W-N(3)	1.736(4)		
N(1)-W-N(2)	84.1(2)	N(2)-W-C(4)	85.5(2)
N(1)-W-N(3)	118.1(2)	N(3)-W-C(1)	99.8(2)
N(1)-W-C(1)	86.3(2)	N(3)-W-C(4)	102.0(2)
N(1)-W-C(4)	138.4(2)	C(1)-W-C(4)	76.1(2)
N(2)-W-N(3)	119.5(2)	C(11)-N(3)-W	174.0(3)
N(2)-W-C(1)	139.3(2)		

The formal electron count at the metal center could be as high as 18 e^- if both sets of nitrogen lone pairs of the [*o*-$(Me_3SiN)_2C_6H_4]^{2-}$ ligand can be donated to the metal center. Donation of both amide lone pairs is not possible since there are only three d orbitals that are of the proper symmetry to form π bonds with the ligands. Given that the d_{xz} and d_{yz} orbitals form the π bonds with the imido group, only the d_{xy} orbital is available to overlap with the N π electrons on the diamido ligand. Thus, the maximum electron count at the metal center is 16 e^-. Furthermore, the structure of **4** shows that the folding of the diamide ligand brings the p orbitals on the N atoms to within only *ca.* 25 - 30° of the xy plane, preventing efficient overlap between the d_{xy} orbital and the N lone pairs. The structural constraints imposed by the chelating nature of the [*o*-$(Me_3SiN)_2C_6H_4]^{2-}$ ligand lead us to suggest that **35** and the other square pyramidal dialkyl complexes[69] are best described as 14 e^- or at most 16 e^- compounds.

Mechanism of the Formation of Metallacyclopentane Complex

The observation that the reaction between **10** and ethylene (equation 3.3) produces neohexene and neopentane along with **35** suggests to us that the formation of **35** likely proceeds through a metathetical pathway. This is because neopentane is the product of α-H abstraction to form a neopentylidene complex and neohexene is the first product formed when a neopentylidene complex undergoes productive metathesis with ethylene. Previously,[76] we had established that upon heating complex **10**, α-H abstraction to form the base free neopentylidene complex is the predominant reaction pathway. In the presence of PMe_3, complex **34** is isolated, while in the absence of PMe_3, a reversible metallation of one of the Me_3Si groups of the *o*-$(Me_3SiN)_2C_6H_4$ ligand occurs.[76] Given that **34** is readily synthesized and isolated, and that dissociation of PMe_3 from **3** in solution is a rapid process, we examined the reaction between **34** and ethylene in order to determine whether complex **35** would form.

When **3** was allowed to react with ethylene at room temperature, an intermediate, W(CH*t*-BuCH_2CH_2)(NPh)[*o*-$(Me_3SiN)_2C_6H_4$], **36**, was observed before any neohexene is produced. The ^{1}H-NMR spectrum of **36** (**Figure 3.2**) shows five multiplet resonances at 0.39, 0.71, 2.45, 2.61, and 3.75 ppm in a 1:1:1:1:1 ratio, which account for the five ring-protons of the metallacycle. In the $^{13}C\{^1H\}$ NMR spectrum, three singlets are observed at 77.6 (J_{W-C} = 56 Hz), 38.8 (J_{W-C} = 49.4 Hz), and 25.1 ppm for the metallacycle carbons. Further investigation by 2D NMR, (^{1}H-^{1}H homonuclear and ^{13}C-^{1}H heteronuclear correlation experiments) allows us to assign all the proton and carbon resonances of **36**. The proton at 0.39 ppm is attached to C_α (77.6 ppm, *t*-butyl substituted carbon), the two multiplets at 0.71 and 2.45 ppm are assigned to the protons bonded to $C_{\alpha'}$ (38.8 ppm), and the most downfield resonances at 2.61 and 3.75 ppm are assigned to the β-protons of the metallacyclobutane ring. The observation that the β-protons appear at

the most downfield chemical shifts is consistent with similar metallacyclobutane complexes.[98]

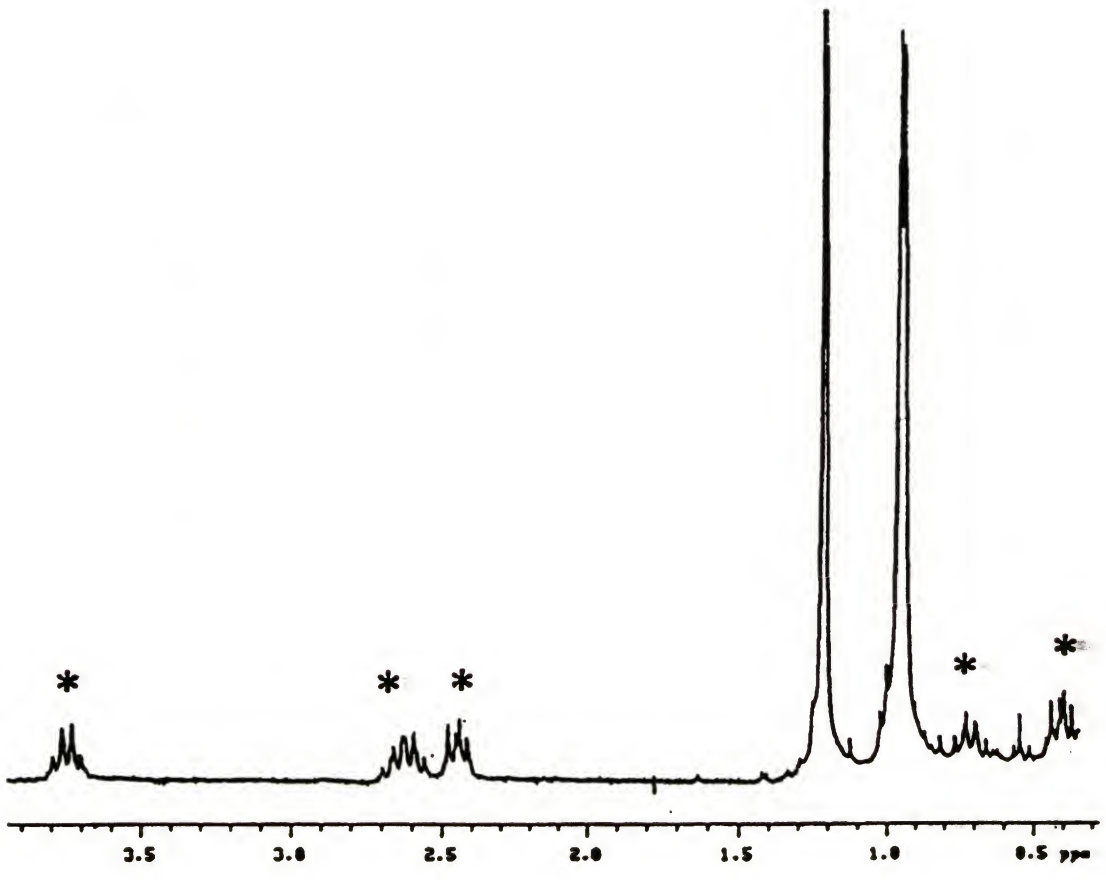

Figure 3.2. Partial ^{1}H NMR spectrum of W(NPh)[*o*--$Me_3SiN)_2C_6H_4$] ($CH^tBuCH_2CH_2$), **36**. (300 MHz, room temperature, benzene-*d6*, *'s indicate five ring protons).

Attempts to synthesize and isolate complex **36** on a preparative scale were thwarted by the instability of **36** in solution. While crude **36** can be isolated as a solid by removing the solvent and PMe_3 under reduced pressure, the ^{1}H-NMR spectrum of this material (C_6D_6 solution) reveals that **36** readily loses ethylene or neohexene to generate the metallated complex **32**, or the unsubstituted metallacyclobutane complex, **37**, respectively.

Presumably, loss of ethylene gives the base free neopentylidene complex which rapidly metallates as shown in **Scheme 3.F**, while loss of neohexene leads to **37** via an intermediate methylidene complex which is scavenged by the ethylene produced in the formation of **32**.

Scheme 3.F

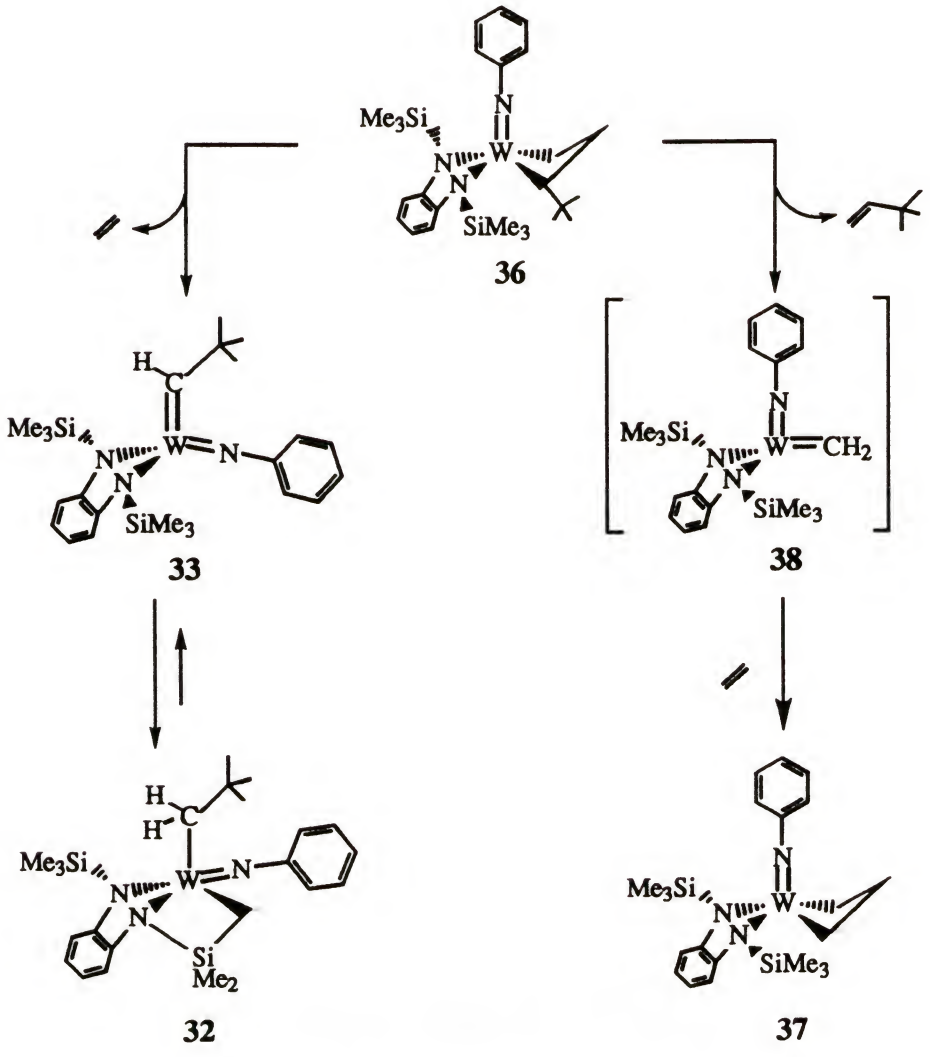

When complex **34** was allowed to react with ethylene at room temperature for four days, two products were observed in a 44:56 ratio by ^{1}H-NMR spectroscopy. One set of

peaks (44%) was found at 3.89 (m,2H$_\alpha$), 2.86 (m,1H$_\beta$), 2.90 (m,1H$_\beta$), and 2.59 (m,2H$_\alpha$) ppm, which were assigned to the metallacyclobutane complex W(NPh)[(Me$_3$SiN)$_2$C$_6$H$_4$](CH$_2$CH$_2$CH$_2$), **37**. The structure of **37** is either square pyramidal, or the compound is undergoing a rapid interconversion between square pyramidal and trigonal bipyramidal geometries (**Scheme 2.C**). This is supported by the fact that only one singlet is observed at 0.31 ppm for the trimethylsilyl groups.

The other set of peaks (56%) was observed at 1.94 (2H) and 2.17 (2H) ppm. This product was shown to be the tungsten(IV) complex W(NPh)[*o*-(Me$_3$SiN)$_2$C$_6$H$_4$](PMe$_3$)$_2$ (η^2-C$_2$H$_4$), **39**, by comparison with the spectrum of an authentic sample which was obtained from the reaction between diethyl complex, **4**, and excess PMe$_3$ (equation 4.1). We propose that the unstable methylidene complex undergoes bimolecular coupling of methylene ligands to give ethylene and a tungsten(IV) complex, which is then trapped by phosphine and ethylene to form compound **39** (**Scheme 3.G**). There is abundant evidence that methylidene complexes can decompose via formation of bis(μ-methylidene) species initially followed by coupling of the two alkylidene ligands to give 0.5 equivalent of an ethylene complex.[15a] Formation of a W(IV) intermediate either through β-H elimination followed by reductive elimination or rearrangement (**Scheme 3.D-b**) from unsubstituted metallacyclobutane ring of **37** does not occur since we see no evidence for the presence of propene in the reaction mixture. Therefore, the faster reaction is likely to be the reverse pathway, loss of ethylene from **37** to give **38**.

In the presence of excess ethylene, both **37** and **39** were converted to the more stable metallacyclopentane complex W(CH$_2$CH$_2$CH$_2$CH$_2$)(NPh)[(Me$_3$SiN)$_2$C$_6$H$_4$], **35** (>95% by NMR). The formation of complex **35** arises from the oxidative coupling of two equivalents of ethylene to the tungsten(IV) complex. The oxidative coupling of two olefins to form a metallacyclopentane complex is a well known reversible reaction as shown in **Scheme 3.H**.[99]

Scheme 3.G

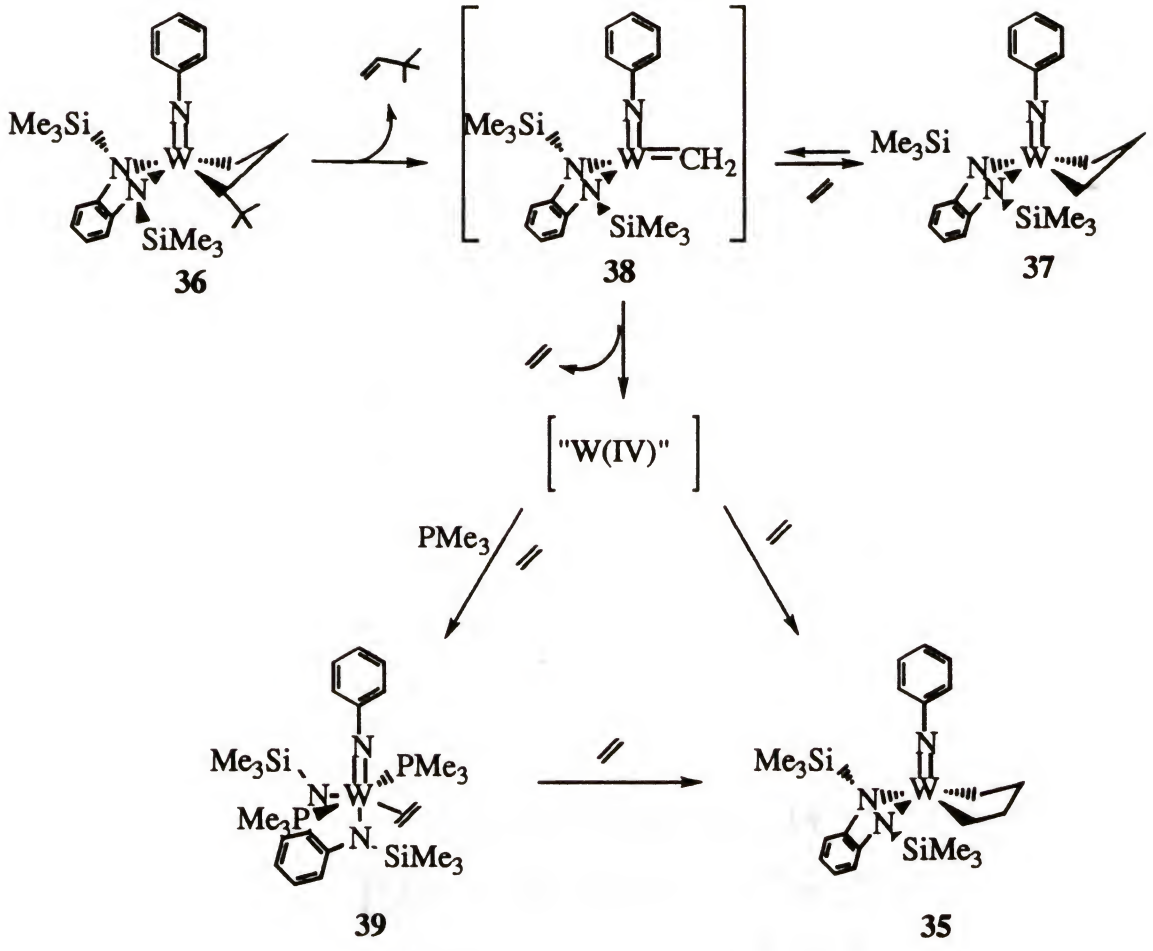

Scheme 3.H

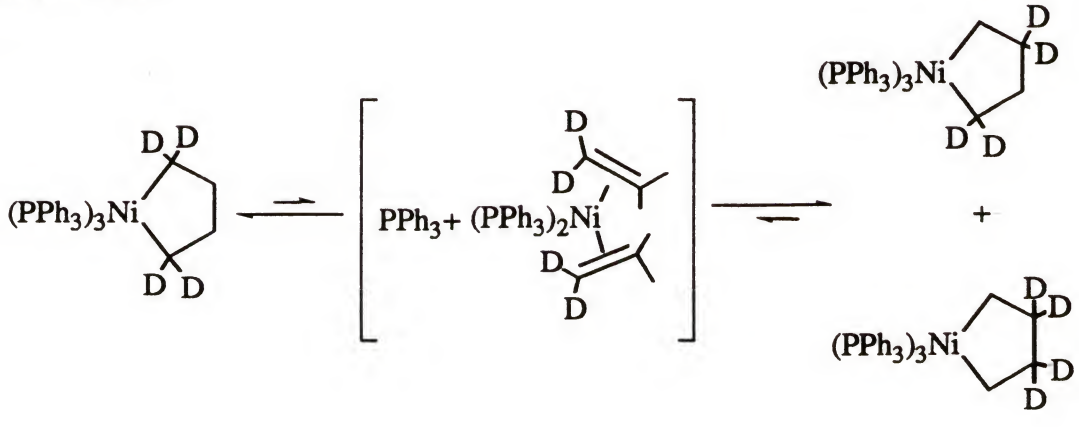

The relative concentrations of all the intermediates in the reaction of **34** with ethylene as a function of time is shown in **Figure 3.3**. In a separate experiment, complex **39** was cleanly converted to **35** within a few hours with addition of ethylene. This suggests that the formation of **35** from **32** is inevitable in the presence of ethylene.

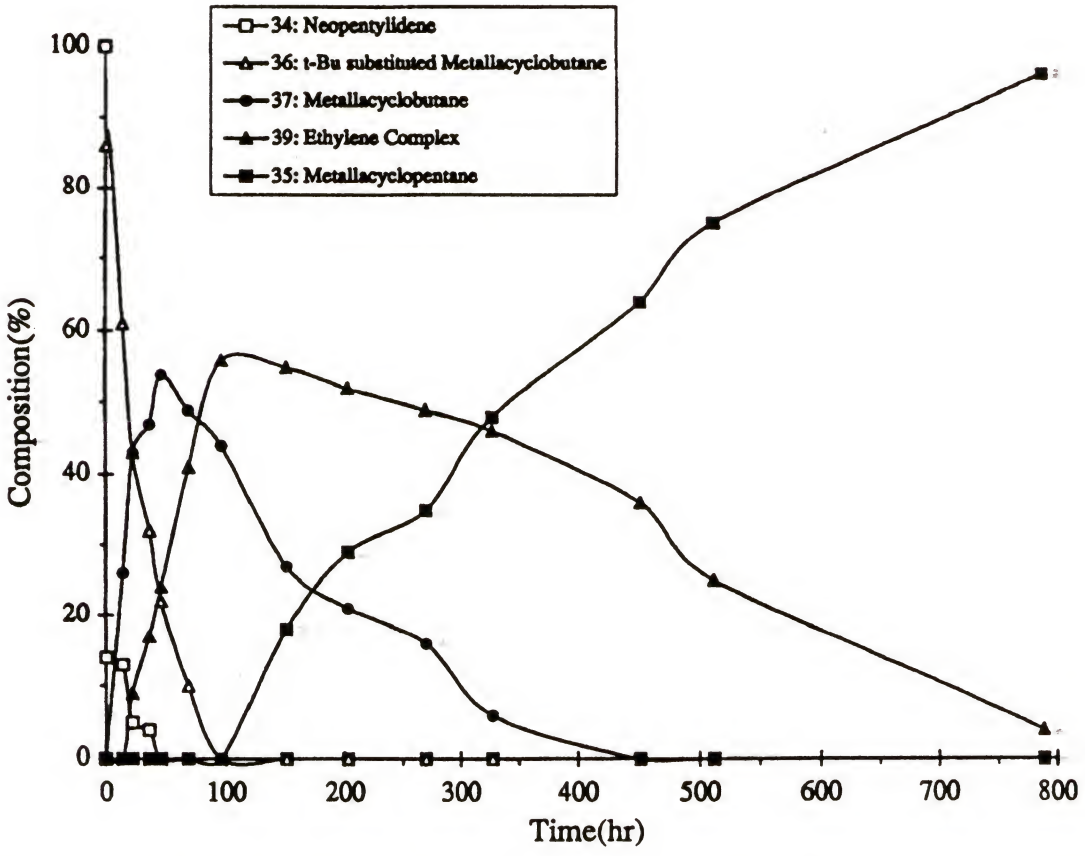

Figure 3.3. Relative amounts of **34**, **35**, **39**, **36**, and **37** as a function of time during thermolysis of **32** in the presence of ethylene.

In order to compare the reactivity of the metallacyclopentane, **35**, and the bisneopentyl, **10**, complexes, **35** was allowed to react with trimethylphosphine. No reaction was observed within a few days at room temperature. However, when the reaction was heated to 90°C, **35** slowly (60% conversion after 10 days; 91% after 30 days) converts to **39** with the loss of ethylene (equation 3.5).

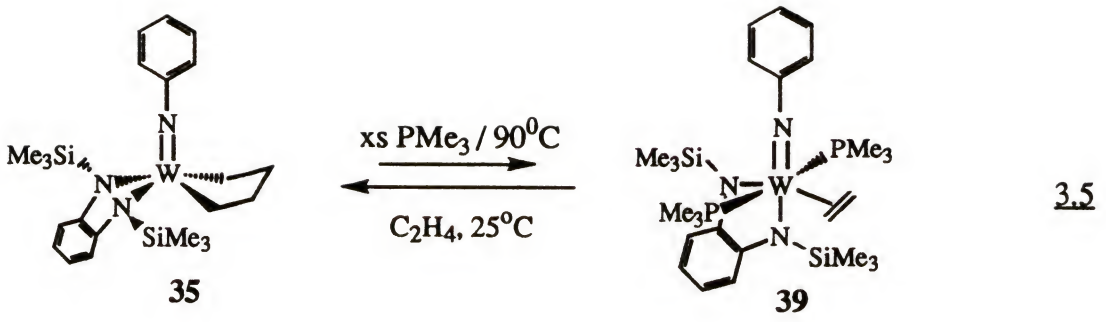

35 39 3.5

Although the bisneopentyl complex, **10** is quantitatively converted to metallacyclopentane in the presence of ethylene at 80°C, compounds **35** or **3** (Chapter 2) do not react with ethylene even at elevated temperatures. This provides further evidence that the formation of **35** from **10** proceeds through a neopentylidene intermediate.

Experiments using **34** as a metathesis catalyst for 1-pentene or 1,9-decadiene showed very little productive metathesis (36 turnovers before deactivation), but rather the formation of neohexene. Complex **35** was the only observable metal containing product. This is to be expected since the productive metathesis of terminal olefins always gives ethylene as one of the products. Thus, the ethylene that is produced reacts with **34** or other alkylidene complexes that are formed during the reaction and effectively deactivates the catalyst system by converting all of the tungsten complexes in the system to **35** which is inactive for further metathesis.

It is worthwhile to note that the formation of 1-butene was not observed when **35** is heated to its decomposition temperature (*ca.* 150°C). The formation of 1-butene from metallacyclopentanes have been reported with Ni(II),[32] Pd(II),[33] Pt(II),[34] Pt(IV),[35] Ta[36] and Ti.[37] The mechanism for the elimination of 1-butene from these complexes is believed to be more complex than simple β-hydride elimination/reductive-elimination pathways. Whitesides proposed a chain transfer process initiated by ligand-cyclometalation.[38] McLain, Sancho, and Schrock proposed two additional steps, ring contraction followed by a second β-H elimination process, between the original two steps based on their deuterium

labeling experiments on the olefin dimerization with the Cp^*Cl_2Ta(olefin) system.[100] However, it is likely that complex **35** does not undergo β-hydride elimination because of the steric and geometric constraints of the bulky, chelating, TMS_2pda ligand. Evidently these constraints make it difficult for the metallacyclopentane ring to achieve the optimal M-C-C-H dihedral angle of 0° that is necessary for β-H elimination.[12a,16,101] As a result, the reactivity of **35** is apparently limited to disruption of the metallacyclopentane structure by expulsion of ethylene and reduction of the metal center.

Conclusions

The observation that ethylene reacts with the bis neopentyl complex, **10**, at elevated temperatures to give the metallacyclopentane complex, **35**, is consistent with the proposal that this reaction actually occurs through a neopentylidene complex which is generated *in situ* during the reaction. The formation of **35** in the reaction of W(NPh)[*o*-$(Me_3SiN)_2C_6H_4$](CHCMe_3)(PMe_3), **34**, with ethylene confirms this since **34** is an effective source of base free alkylidene through the dissociation of PMe_3. The conversion of the unsubstituted metallacyclobutane complex, **37**, to the W(IV) ethylene complex appears to proceed through the methylidene complex, **38**, and probably through a W(IV) intermediate both of which are unobserved.

In related chemistry, a dimeric Mo(IV) complex has been isolated from the reaction of Mo[N(2,6-*i*$Pr_2C_6H_3$)][$OCMe_3$]$_2$(C(H)CMe_3) with ethylene.[88a] The origin of the Mo(IV) complex is proposed to be a Mo(VI) methylidene which reductively coupled giving ethylene and the observed dimeric Mo(IV) product. Changing the alkoxide ligands to $OCMe(CF_3)_2$ allows the observation of an unstable metallacyclopentane complex, Mo($CH_2CH_2CH_2CH_2$)[N(2,6-*i*$Pr_2C_6H_3$)][$OCMe(CF_3)_2$]$_2$. A similar process is possible in the present case, only the increased stability of W(VI) vs Mo(VI) facilitates the formation

and isolation of the metallacyclopentane complex, **35**, via the oxidative coupling of two molecules of ethylene. Because PMe_3 is present in the system when **3** reacts with ethylene, the W(IV) PMe_3-ethylene complex, **39**, is formed. The conversion of **39** to **35** is somewhat surprising since it involves loss of PMe_3 in favor of coordination of ethylene. However, it is clear that stability of W(VI) relative to W(IV) is the driving force for the formation of **35**.

The formation of **35** from the alkylidene, **34**, also provides an explanation for why **34** is a poor catalyst for the ADMET polymerization of terminal dienes and depolymerization of unsaturated polymers using ethylene as the olefin reactant. When terminal olefins undergo metathesis, ethylene is always produced. The presence of ethylene thereby provides a facile path for the deactivation of **34** via the formation of **35**. In a more general sense, the results presented in this dissertation suggest that formation of metallacyclopentane complexes akin to **35** are clearly a potential deactivation pathway for metathesis catalysts whenever terminal olefins are substrates because ethylene is formed in these reactions. We would expect that metallacyclopentane formation would be most likely to occur when third row transition metals are used as metathesis catalysts because of the propensity of these metals to form stable, high oxidation state complexes.

CHAPTER 4
MECHANISTIC INVESTIGATIONS OF THE DECOMPOSITION OF β-HYDROGEN CONTAINING W(VI) DIALKYL COMPLEXES

Introduction

For transition metal dialkyl complexes, the thermal decomposition often proceeds via several modes of intramolecular C-H activation,[48a,102] including α,[103] β,[104] γ,[105] or ε-hydrogen[43b] transfer. Among these pathways, the β-elimination process is the most frequently observed thermolysis pathway. Indeed, the facility of this pathway often precludes isolation of alkyl complexes with β-hydrogen atoms, especially when the complexes are coordinatively unsaturated.[12a]

We have synthesized (**Scheme 4.A**) a series of coordinatively-unsaturated tungsten(VI) dialkyl complexes containing β-hydrogen atoms (W(NPh)[*o*-$(Me_3SiN)_2C_6H_4$]R_2, R = Et(**4**), Pr(**5**), CH_2CH_2Ph(**6**), *i*-Bu(**7**)). Details of the reactivities of these complexes towards trimethylphosphine, and a mechanistic study of their β-H transfer chemistry, including kinetics, activation parameters and deuterium isotope effects will be discussed here.

Scheme 4.A

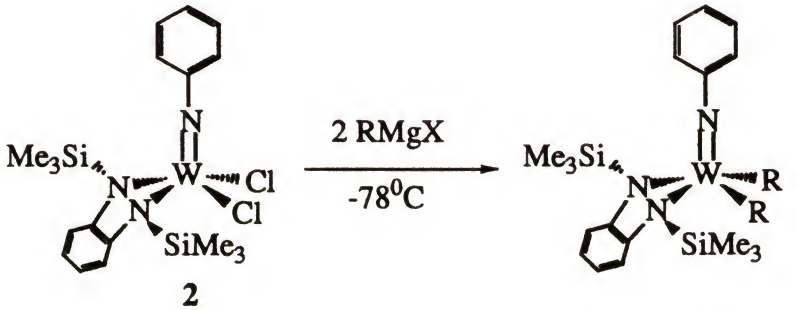

2

R = Et(**4**), *n*-Pr(**5**), CH_2CH_2Ph(**6**), CH_2CHMe_2(**7**)

Synthesis of Tungsten(IV) Olefin Complexes

It is surprising, despite their coordinative and electronic unsaturation, that these complexes, **4-7**, as well as monoalkyl complexes, W(NPh)[*o*-$(Me_3SiN)_2C_6H_4$]ClR, R=Et(**13**), CH_2CH_2Ph(**15**), are indefinitely stable at room temperature in the absence of coordinating ligands. It is also reasonable to assume that coordination of trimethylphosphine to these d^0 metal centers would be facile. Addition of PMe_3 to **13** and **15** results in an immediate color change, indicating the coordination of PMe_3. However, no PMe_3 adduct is observed for **4-7** at room temperature. At low temperature, those adducts can be observed by ^1H, ^{13}C, and ^{31}P NMR spectroscopy (Chapter 2).

In the presence of trimethylphosphine, complexes **4** and **6** are converted to the ethylene complex, **39**, and the styrene complex, **40**, quantitatively (equation 4.1). The formation of **39** proceeds much faster (<1 hour at room temperature) than the formation of **40** (>6 hours at 60^0C). Complex **5** reacts with trimethylphosphine to form the propylene complex, **41**, in low yield. The reaction between **7** and trimethylphosphine proceeds much more slowly at room temperature and decomposes at elevated temperature with the formation of isobutane and isobutylene. Although the isobutylene complexes have been isolated for Hf,[106] W,[107] and Mo,[108] we were not able to isolate the desired complex, presumably due to the poor σ-donor ability of the isobutylene substrate or the high temperature needed to get **7** to react.

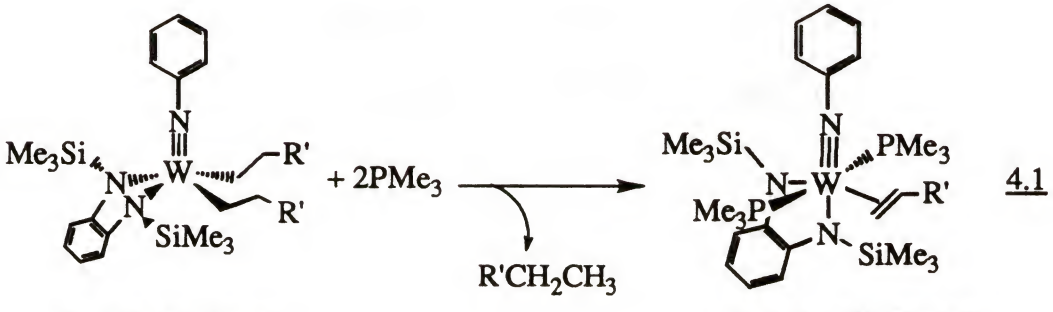

4.1

R' = H (**4**), Ph (**6**)

R' = H (**39**), Ph (**40**)

The ^{1}H NMR spectrum of **39** shows two multiplets at 1.96 and 2.19 ppm for the ethylene protons, while the two equivalent PMe_3 groups appear at 1.05 ppm. The trimethylsilyl groups are observed as two broad peaks at 0.28 and 0.61 ppm, indicating their inequivalence. The gated, coupled ^{13}C NMR spectrum reveals a triplet at 36 ppm corresponding to the ethylene carbons with $^1J_{C\text{-}H}$ = 156 Hz, indicating some "metallacyclopropane" character.[109] The significant upfield shift (C_2H_4: δ123.2) for the ethylene carbon (δ36) indicates strong back-donation from the metal. According to difference nOe experiments, the upfield ethylene multiplets (1.96 ppm) correspond to the protons lying *syn* to the imido ligand. Upon irradiation of the *ortho*-protons of the imido group, a 4.8% enhancement was observed for only the *syn* protons (1.96 ppm) of the coordinated ethylene ligand, which indicates that the rotation of the C_2H_4 unit around the W-ethylene bond is slow on the NMR time scale (**Scheme 4.B**). All of the spectroscopic data suggests that ethylene coordinates *cis* to the imido ligand, in accordance with other d^2 ethylene complexes possessing imido co-ligands reported by Schrock[110] and Nielson.[111]

Scheme 4.B

The structure of complex **39** was verified by a single crystal X-ray diffraction study. A thermal ellipsoid plot of **39** with the atom-labeling scheme is given in **Figure 4.1**, while a table of selected bond lengths and angles is shown in **Table 4.I**. The coordination geometry around the W atom is that of a slightly distorted octahedron. In this structure, the imido N and one of the amide N atoms occupy *trans* sites, while the phosphines are also *trans* with respect to each other. The W-N_{imido} bond length is 1.784(4)Å and is consistent with a W-N triple bond making **39** an 18e$^-$ complex.[53,54] The

W-N(1) and W-N(2) bond lengths (2.154(4)Å, 2.160(3)Å) are essentially the same which is surprising since this implies that the imido group does *not* exert a significant *trans* influence on the W-N(1) bond. It appears that the steric bulk of the two trimethyl phosphine ligands prevents an asymmetric approach of the amido N atoms to the W center causing an increase in the expected W-N(2) bond length.

Table 4.I. Selected Bond Lengths (Å) and Angles (°) for W(NPh)[*o*-$(Me_3SiN)_2C_6H_4$]$(PMe_3)_2(\eta^2\text{-}C_2H_4)$, **39**

W-N(1)	2.154(4)	W-P(2)	2.564(1)
W-N(2)	2.160(3)	W-C(1)	2.234(5)
W-N(3)	1.784(4)	W-C(2)	2.223(5)
W-P(1)	2.562(1)	C(1)-C(2)	1.434(6)
N(1)-W-N(2)	78.60(14)	N(3)-W-P(1)	94.40(12)
N(1)-W-N(3)	175.9(2)	N(3)-W-P(2)	89.64(12)
N(1)-W-P(1)	89.66(10)	N(3)-W-C(1)	91.2(2)
N(1)-W-P(2)	86.26(10)	N(3)-W-C(2)	89.8(2)
N(1)-W-C(1)	87.7(2)	P(1)-W-P(2)	170.27(4)
N(1)-W-C(2)	91.8(2)	P(1)-W-C(1)	113.19(13)
N(2)-W-N(3)	101.2(2)	P(1)-W-C(2)	75.92(13)
N(2)-W-P(1)	84.42(10)	P(2)-W-C(1)	75.50(13)
N(2)-W-P(2)	86.12(10)	P(2)-W-C(2)	113.00(13)
N(2)-W-C(1)	157.8(2)	C(1)-W-C(2)	37.5(2)
N(2)-W-C(2)	158.2(2)	C(21)-N-W	170.3(3)

The ethylene ligand indeed coordinates *cis* to the imido ligand. It is oriented with the C atoms in the W-P-N(2)-P plane in order to maximize back donation from the d_{xy} orbital to the ethylene π^* orbital. This also explains why the ethylene does not rotate readily about the metal-ligand bond axis, since there is no filled π orbital orthogonal to the "in-plane" orbital (d_{xy}) to assist such a rotation. The C(1)-C(2) bond length, 1.434(6)Å, is in the middle of the range of C-C bond lengths observed in other d^2 olefin complexes

(**Table 4.II**).[112] The W-C(1) and W-C(2) bond lengths of 2.234(5) and 2.223(5)Å are similar to those of other W(IV) olefin complexes that have been structurally characterized.[112c,e,f]

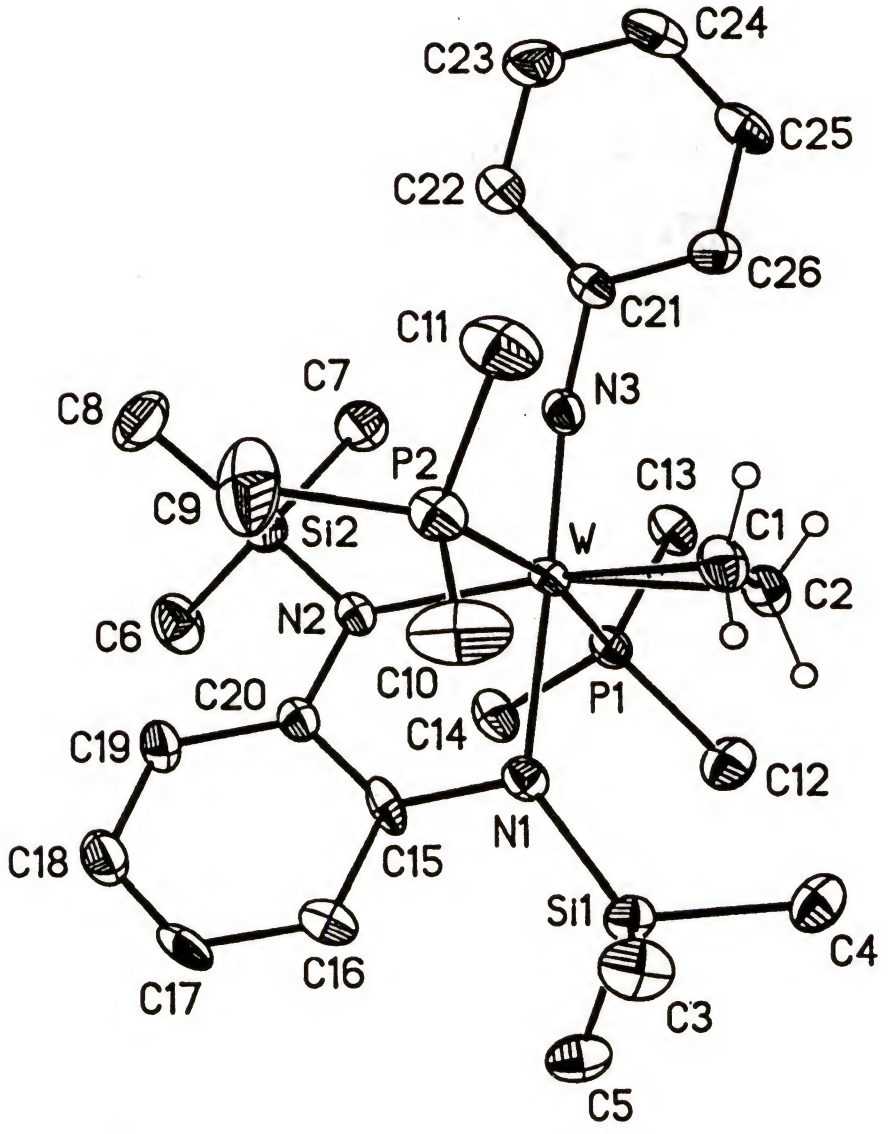

Figure 4.1. Molecular structure of W(NPh)[*o*-$(Me_3SiN)_2C_6H_4$](η^2-C_2H_4)$(PMe_3)_2$, **39**, with 50% probability ellipsoids and showing the atom numbering scheme. All hydrogen atoms, except those on the η^2-ethylene, are omitted for clarity.

Table 4.II. Structure and NMR data for early transition metal ethylene complexes and related compounds.

Compound	d(C-C) Å	Ref.
free C_2H_4	1.337(2)	
$W(OC_6H_3Ph\text{-}C_6H_4)_2(PMe_2Ph)(\eta^2\text{-}C_2H_4)$	1.39(1)	112c
$W(O)Cl_2(PMePh_2)_2(CH_2{=}CH_2)$	1.404(17)	112f
$(\eta\text{-}C_5H_5)_2Nb(C_2H_5)(CH_2{=}CH_2)$	1.406(13)	112i
$W(NPh)[o\text{-}(Me_3SiN)_2C_6H_4](PMe_3)_2(\eta^2\text{-}C_2H_4)$	1.434(6)	this work
$(\eta\text{-}C_5Me_5)_2Ti(CH_2{=}CH_2)$	1.438(5)	112g
$WCl_2(NPh)(CH_2{=}CMe_2)(PMe_3)_2$	1.45(3)	112e
$(\eta\text{-}C_5Me_5)Ta(CHCMe_3)(PMe_3)(CH_2{=}CH_2)$	1.477(4)	112h
$[Zr\{(SiMe_2)_2(\eta\text{-}C_5H_3)_2\}Et]_2(\mu\text{-}CH_2{=}CH_2)$	1.479(12)	112b
$Ta(CNN)(O\text{-}t\text{-}Bu)_2(CH_2{=}CH_2)$ $CNN = [C_6H_4(CH_2N(Me)CH_2CH_2NMe_2)\text{-}2]^-$	1.491(9)	112a

Mechanistic Studies

Whitesides[113] proposed a dissociative mechanism for the decomposition of $Pt(n\text{-}Bu)_2(PPh_3)_2$ and pointed out the necessity to increase the stability of the complex by blocking the site for β-elimination by the ligand. Reger[114] also showed that the ligand dissociation to open an coordination site is required for β-elimination in the case of $Fe(Cp)(CO)(PPh_3)R$. However, the β-H transfer chemistry of **4-7** is promoted by adding a ligand to the metal center. This behavior is clearly unexpected since it implies that β-H transfer is induced by increasing the coordination number and electron count of the

complex. To understand the role of PMe_3 and clarify the mechanism, we have undertaken kinetic studies of the reactions of **4** and **6** with PMe_3.

The kinetics of the thermal decomposition of **4** and **6** in toluene-d_8 were examined by following the appearance and disappearance of the trimethylsilyl peaks of starting materials, **4** and **6**, and products, **39** and **40** using ^1H NMR spectroscopy in the presence of excess PMe_3. The data points were obtained by plotting the absolute peak intensity with respect to time for more than three half-lives.

Activation parameters for the conversion of **4** to **39** were determined by reacting toluene-d_8 solutions (0.0486M) of **4** with PMe_3 (0.972M) in the NMR probe at temperatures between 263 and 293K (three samples at each temperature). Both the appearance of **39** and disappearance of **4** follow first-order kinetics throughout the reaction with a pseudo first order rate constant at 293K of $k = 9.61(82)\times10^{-4}$ sec^{-1} ($t_{1/2}$ = 12 min). Conversion of **4** to **39** is essentially quantitative and no ^1H NMR signals corresponding to any intermediate were observed. Activation parameters, obtained from an Eyring plot ($\Delta S^{\ddagger}$= R[(intercept) - 23.76]; $\Delta H^{\ddagger}$ = -R(slope)), for the formation of **39** from **4** are $\Delta H^{\ddagger}$ = 5.1(0.6) Kcal·mol^{-1} and $\Delta S^{\ddagger}$ = -54.9(2.0) cal·mol^{-1}·K^{-1}, which correspond to $\Delta G^{\ddagger}$ = 21.2 Kcal·mol^{-1} at 293K. The standard errors for $\Delta H^{\ddagger}$ and $\Delta S^{\ddagger}$ are calculated using 2σ.

The observation that the addition of ethylene has no effect on the rate of thermolysis as well as the large, negative entropy of activation suggests that liberation of ethylene does not occur prior to the rate-determining step in this reaction. The observed value of $\Delta S^{\ddagger}$ is a combination of the PMe_3 binding and the subsequent steps to reach the transition state. Values of $\Delta S^{\ddagger}$ between -30 and -40 cal·$mol^{-1}K^{-1}$ are often observed in purely associative substitution reactions. Thus the majority of the observed value of $\Delta S^{\ddagger}$ is accounted for in the binding of PMe_3.[115] Loss of the remaining 10 - 20 cal·$mol^{-1}K^{-1}$ is accounted for by the formation of the highly constrained transition state necessary for the proposed β-H transfer.[14] Similar values of $\Delta S^{\ddagger}$ (-10 to -20 eu) have also been observed in direct α-

abstraction reactions to form alkylidene complexes.[138] Graphs of representative first-order data and the Eyring plot are shown in **Figure 4.2.**

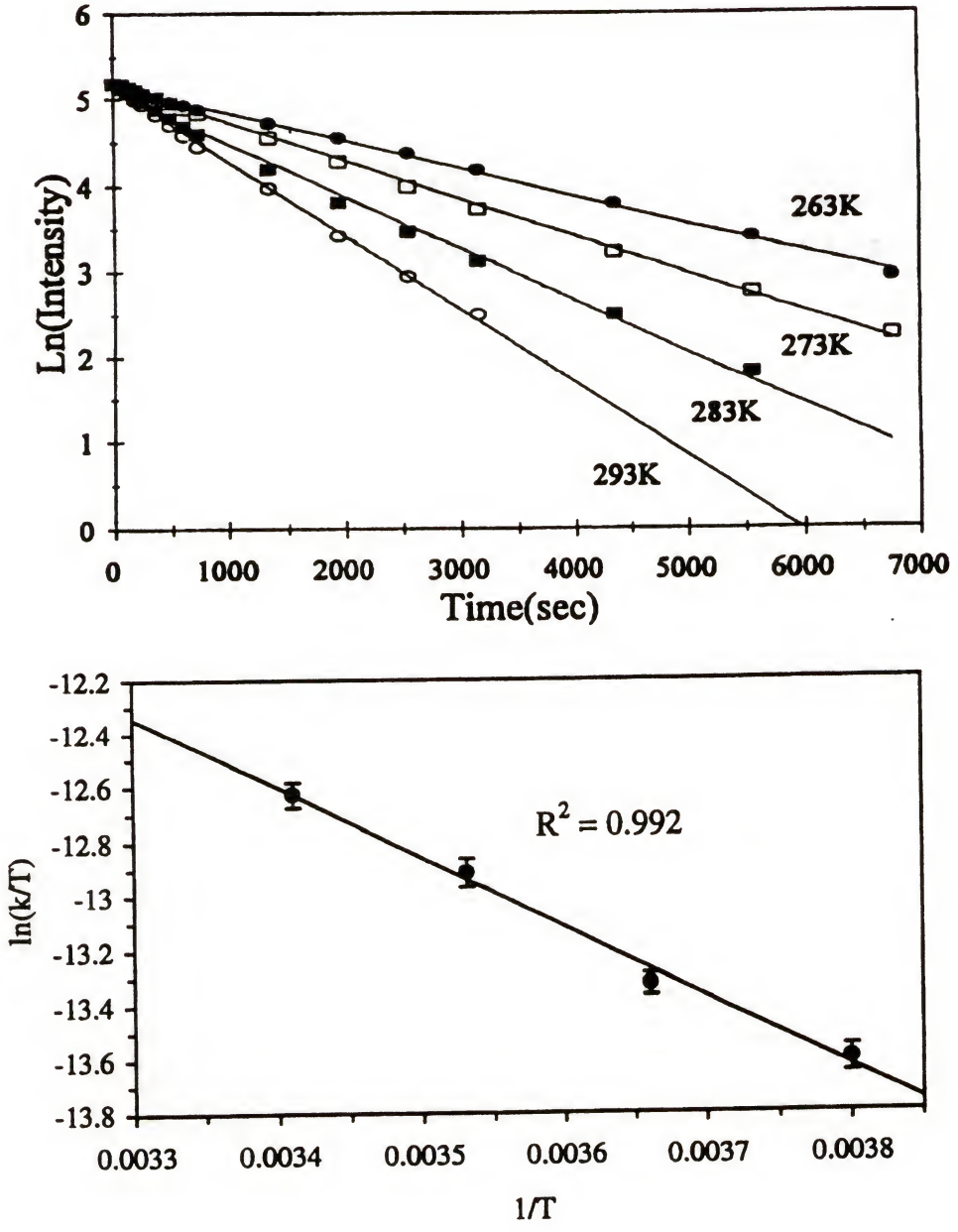

Figure 4.2. First order kinetics (top) and Eyring plot (bottom) for the formation of **39.**

The kinetics of the formation of **6** from **40** were carried out by reacting toluene-d_8 solutions (0.0309M) of **6** with PMe_3 (0.662M) over a temperature range of 333-363K (three samples at each temperature). The reaction follows first-order kinetics with a pseudo first order rate constant at 333K of $k = 6.9(4)\times10^{-5}$ sec^{-1} ($t_{1/2}$ = 167 min). Activation parameters for the formation of **40** from **6** are $\Delta H^{\ddagger}$ = 13.7(0.8) Kcal·mol^{-1} and $\Delta S^{\ddagger}$ = -36.6(2.3) cal·mol^{-1}·K^{-1}, which correspond to $\Delta G^{\ddagger}$ = 25.9 Kcal·mol^{-1} at 333K. The standard errors for $\Delta H^{\ddagger}$ and $\Delta S^{\ddagger}$ are calculated using 2σ. Graphs of representative first-order data and an Eyring plot are shown in **Figure 4.3**. The observation that the addition of styrene has no effect on the rate of thermolysis suggests that the liberation of styrene does not occur prior to the rate-determining step in this reaction. The activation parameters in the conversion of **6** to **40** are significantly different from those of **4** to **39** ($\delta\Delta H^{\ddagger}$ = 8.6 Kcal·mol^{-1} and $\delta\Delta S^{\ddagger}$ = 18.3 cal·mol^{-1}·K^{-1}), suggesting that the two reactions do not follow the similar pathways. This will be discussed in detail later. Rate constants obtained for both reactions studied are shown in **Table 4.III.**

Table 4.III. Rate Constants (average numbers of three samples at each temperature) for the Reactions of **4** and **6** with PMe_3.

[4] = 0.0486M	[PMe3] = 0.972M	[6] = 0.0309M	[PMe3] = 0.662M
T(K)	k * 10^4 sec^{-1}	T(K)	k * 10^4 sec^{-1}
293.15	9.61(82)	363.15	4.21(21)
283.15	6.98(37)	353.15	2.29(7)
273.15	4.46(18)	343.15	1.30(5)
263.15	3.26(16)	333.15	0.69(4)

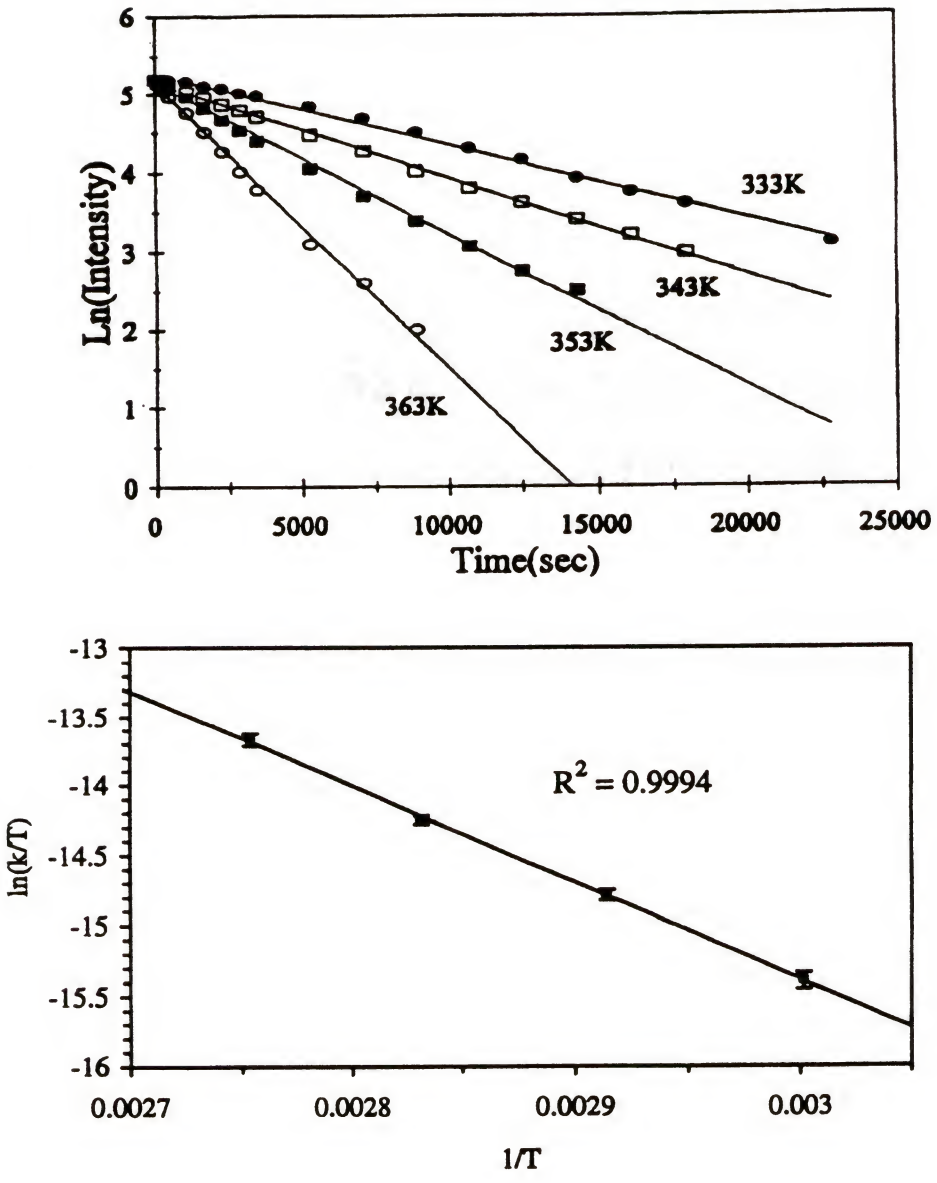

Figure 4.3. First order kinetics (top) and Eyring plot (bottom) for the formation of **40.**

Phosphine Dependence

The role of trimethylphosphine in the conversion of **4** to **39** was examined by reacting **4** (0.0243M) with 0-60 equivalents of PMe_3 (0-1.7M) at 283K. In the absence of trimethylphosphine, the diethyl complex, **4**, is stable in the solution with no decomposition observed within several hours. The rate constants were obtained through the same procedure as described above, but at different PMe_3 concentrations. The reaction is first order in PMe_3, according to the slope of 1.096 obtained from the plot of $\ln(k)$ *vs* $\ln[PMe_3]$ (**Figure 4.4**). Though saturation of the rate at high concentrations of PMe_3 is predicted, we were not able to observe such behavior even at PMe_3 concentrations of 1.7M.

The phosphine dependence for the formation of **40** from **6** was examined by reacting **6** (0.0309M) with PMe_3 over a range of 0-2M. The reaction exhibits near linear behavior at high phosphine concentrations. However, if the phosphine concentrations are less than ca. 0.6M (20 equiv.), there is no profound effect on the rate of thermolysis (**Figure 4.5**) and a rate constant of $2.1*10^{-4}$ sec^{-1} (measuring the disappearance of **6**) was observed when no PMe_3 is added. The data suggests that more than one pathway, in which one of them is phosphine independent, are involved in the reaction but excludes the possibility of two parallel pathways where one is phosphine independent and one is first order phosphine dependent, because such pathways would result in a straight line with a positive intercept. Details of the mechanism will be discussed later.

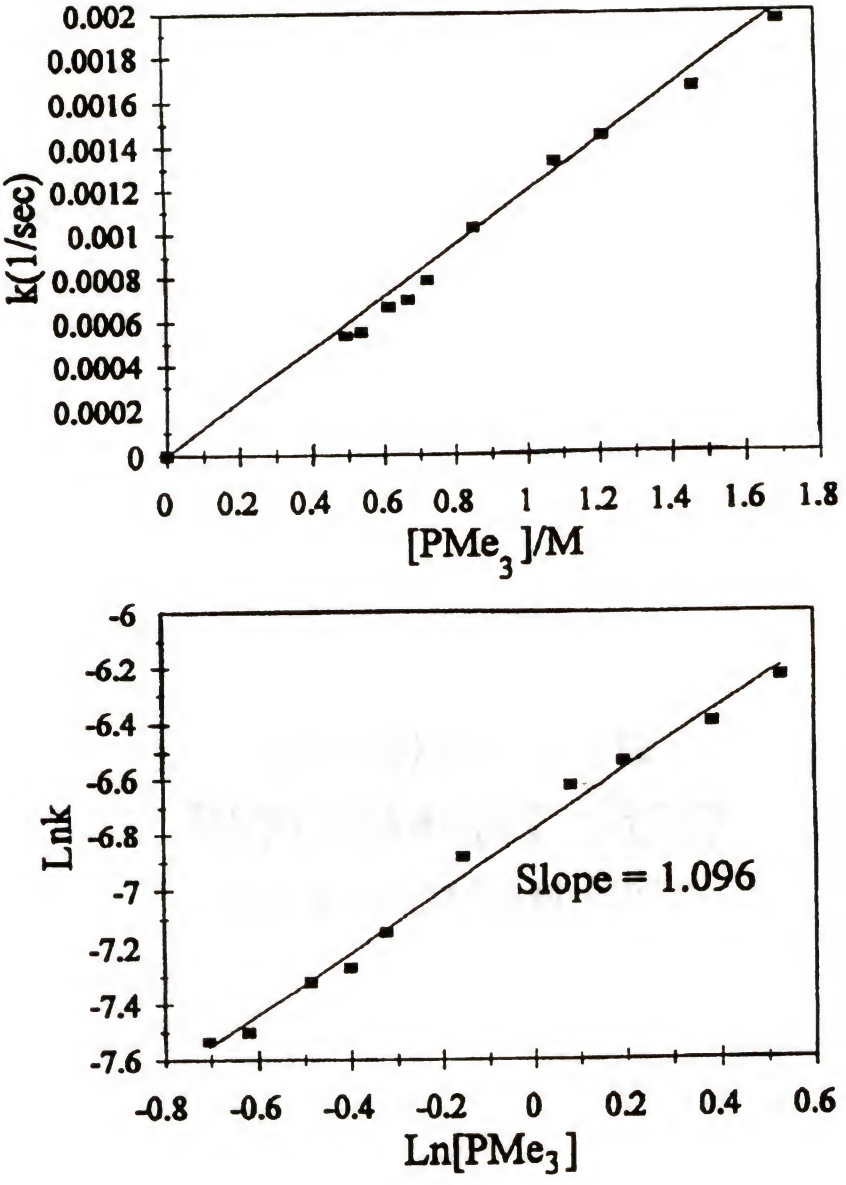

Figure 4.4. PMe_3 dependence for the reaction of **4** with PMe_3.

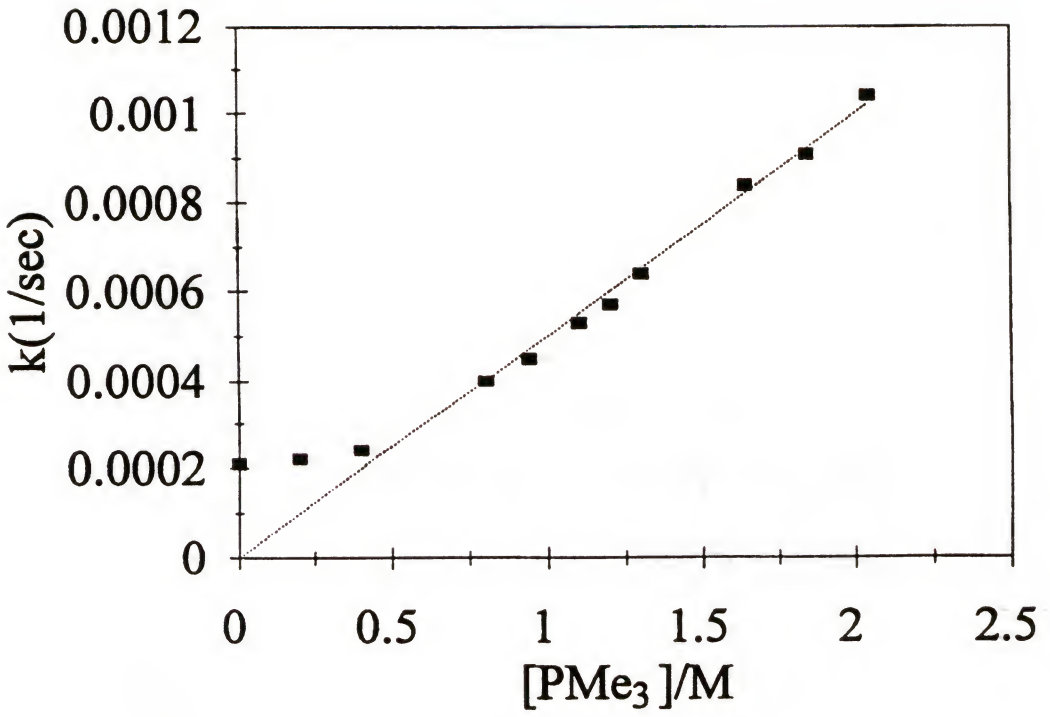

Figure 4.5. PMe_3 dependence for the reaction of **6** with PMe_3.

Deuterium Labeling Experiment

In order to establish the extent to which the β-elimination pathway, possibly responsible for the formation of olefin complexes, **39** and **40**, is reversible, the β-deuterated analogs of **4** and **6**, W(NPh)[*o*-$(Me_3SiN)_2C_6H_4$]$(CH_2CD_3)_2$, **4**-d_6 and W(NPh)[*o*-$(Me_3SiN)_2C_6H_4$]$(CH_2CD_2Ph)_2$, **6**-d_4 were prepared. The results of this study, combined with those described previously, provide a detailed picture of the reaction profiles for the formation of **39** and **40**. Complex **4**-d_6 was prepared from the deuterated Grignard reagent, CD_3CH_2MgCl, under the same conditions as described in **Scheme 2.A**. If the β-elimination pathway involves a fast equilibrium between β-H elimination and olefin insertion[117] into metal-hydride bond, scrambling of the deuterium labels[29,104a,b]

from β-carbon into α-carbon and a mixture of ethane with different isotopic composition (d_2-d_6) should be observed (**Scheme 4.C**).

Scheme 4.C. Mechanism of the H-D Scrambling in the Products of (**4** + PMe_3)

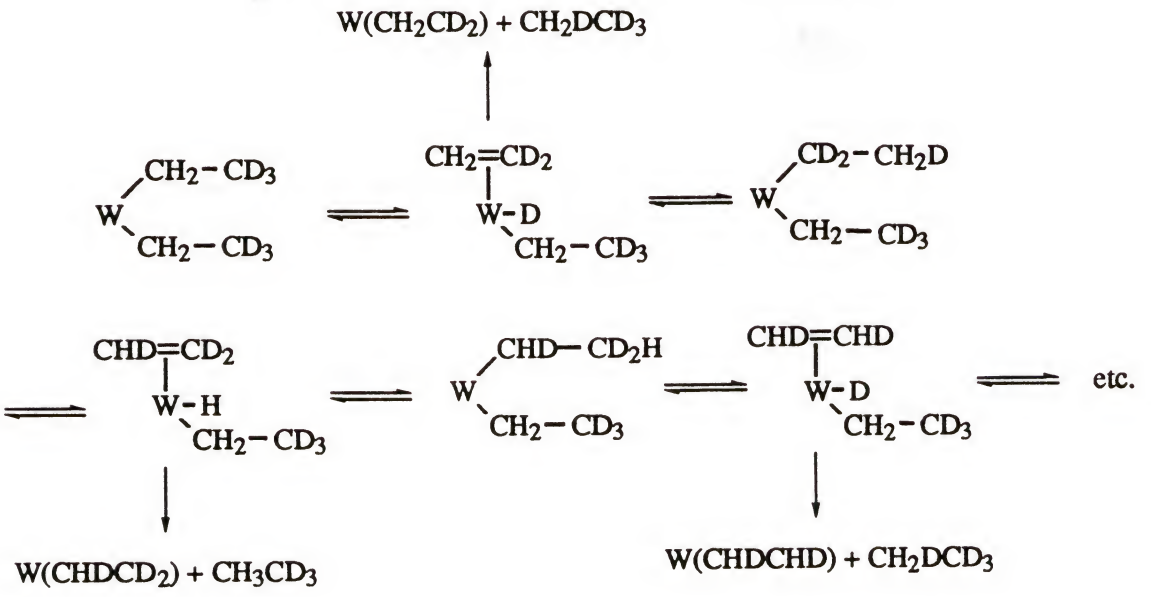

The reaction of the conversion of **4**-d_6 to **39**-d_2 was followed by ^2H NMR in toluene. In both the absence and presence of PMe_3, no scrambling of the deuterium labels among the α- and β-carbons was observed. The products of the reaction are exclusively W(NPh)[*o*-$(Me_3SiN)_2C_6H_4$](η^2-CH_2CD_2)$(PMe_3)_2$, **39**-d_2, and CH_2DCD_3. The formation of CH_2DCD_3 is supported by the observation of a mass peak at 34 m/e in EI-MS experiments. This is also observed for the product of the reaction between CD_3CH_2MgCl and D_2O. The above observations suggest an irreversible β-H abstraction process as proposed by Yamamoto.[118]

The kinetic isotope effect for the transformation of **4** to **39** was determined by reacting **4**-d_6 with trimethylphosphine under the same conditions at 293K, giving k_D = $1.57(4)\times10^{-4}$ sec^{-1}. This cooresponds to a k_H/k_D of 6.1(5), which strongly suggests a near linear transition state for the β-H transfer process. This is consistent with the direct

transfer of one β-H to the other α-carbon atom as is proposed in **Figure 1.2.** The large KIE in our system is significantly different from those compounds which decompose by β-elimination followed by reductive elimination, *eg*. $PdEt_2(PMePh_2)_2$ (KIE=1.4),[26] $CoEt_2(acac)(PMe_2Ph)_2$ (KIE=2.3),[27] $PtEt_2(PEt_3)_2$ (KIE=1.4-1.7),[28] $Cp^*_2ScCH_2CH_2Ph$ (KIE=2.0)[29] and $(CO)(PPh_3)_2IrCH_2CH_2C_6H_{13}$ (KIE=2.3).[30] Buchwald,[22] Erker,[23] Marks[24] and Schrock[25] have proposed the direct β-hydrogen abstraction process from an sp^2-hybridized carbon in the formation of alkyne/aryne complexes. Similar kinetic isotope effects have also been determined by Marks (6.5)[119] and Teuben (5.1).[120] The KIE observed in our system is also consistent with those observed for $Cp_2Zr(SCH_2Ph)(Me)$,[18a] KIE = 5.2, and $[Me_3SiNCH_2CH_2]_3NTa(Et)_2$,[18b] KIE = 5.7, in which the direct β-hydrogen abstraction was proposed to be the most-likely pathway.

The deuterated analog of **6**, $W(NPh)[o\text{-}(Me_3SiN)_2C_6H_4](CH_2CD_2Ph)_2$, **6**-$d_4$ was prepared (**Scheme 4.D**) by reaction of the dichloride precursor with the deuterated Grignard reagent,[121] $PhCD_2CH_2MgBr$, under the same conditions as mentioned earlier. The NMR spectrum of $W(NPh)[o\text{-}(Me_3SiN)_2C_6H_4](CH_2CD_2Ph)_2$, **6**-$d_4$, is shown in **Figure 4.6.**

Scheme 4.D. Synthesis of $W(NPh)[o\text{-}(Me_3SiN)_2C_6H_4](CH_2CD_2Ph)_2$, **6**-$d_4$.

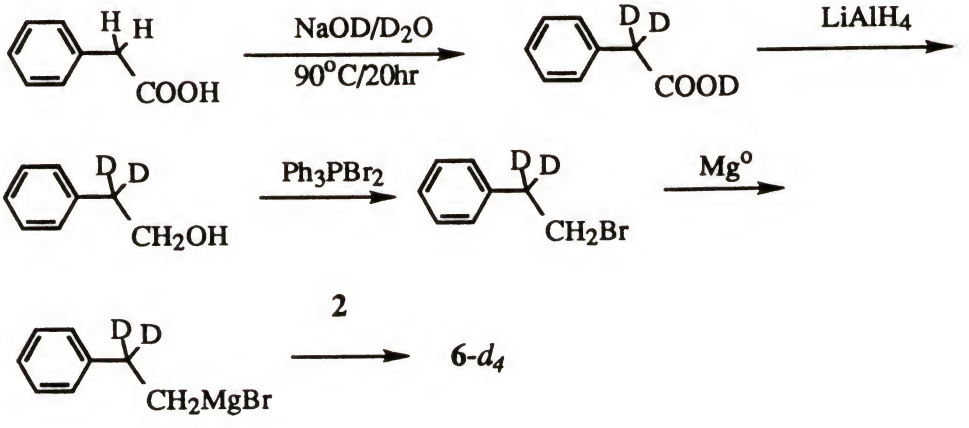

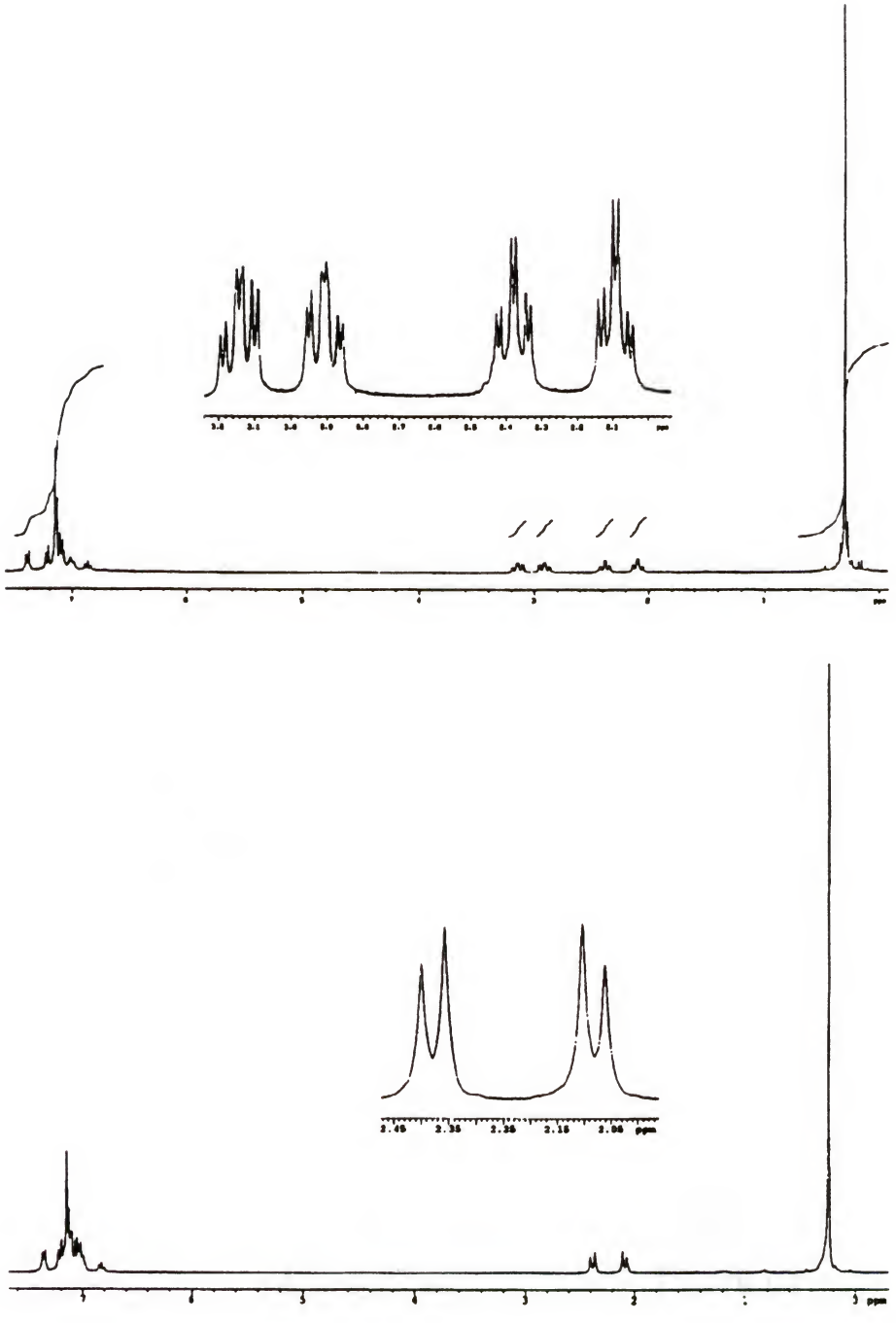

Figure 4.6. 1H NMR spectra of W(NPh)[*o*-$(Me_3SiN)_2C_6H_4$]$(CH_2CH_2Ph)_2$, **6**, (top) and W(NPh)[*o*-$(Me_3SiN)_2C_6H_4$]$(CH_2CD_2Ph)_2$, **6-*d*$_4$** .

The kinetic isotope effect for the transformation of **6** to **40** was determined by reacting **6**-d_4 (0.031M) with PMe_3 (0.8M) at 343K, giving $k_D = 0.62(4)\times10^{-4}$ sec^{-1}. This cooresponds to a k_H/k_D of 2.1(2) (2.4 when extrapolated to room temperature, assuming linear Arrhenius[46] behavior, equation 4.2. This is consistent with the data reported for the β-elimination pathway.[27-31] The unusual rate constants observed at low phosphine concentrations urged us to study the kinetic isotope effect at different PMe_3 concentrations. With 0.4M PMe_3 at 353K, a kinetic isotope effect of 3.4(3) (4.3 at room temperature) was observed, whereas 4.8(5) (6.4 at room temperature) was observed for the thermolysis of **6** in the absence of PMe_3. The difference in kinetic isotope effects at different PMe_3 concentrations (**Table 4.IV**) suggests that there is more than one pathway involved in the transformation. The large number (6.4) observed in the absence of PMe_3 is similar to that of **4** (6.1), and suggests that the β-abstraction is the dominant pathway at low PMe_3 concentrations.

$$\frac{k_H}{k_D} = \exp\left(\frac{0.1865}{T(K)}\,\upsilon_H\right) \qquad 4.2$$

Table 4.IV. KIE for the dacomposition of **6** (0.031M) under different [PMe3].

[PMe3]/M	KIE/Temperature	KIE (extrapolated to room temperature, 298K)
0	4.8(5)/353K	6.4
0.4	3.4(3)/353K	4.3
0.8	2.1(2)/343K	2.4

Mechanistic Study of the Formation of ethylene complex, **39**

In the thermolysis of dialkyl complexes which disproportionates the two alkyl groups to alkanes and alkenes, the following three pathways are conceivable: (a) A dissociative pathway which involves ligand dissociation to provide an open coordination site from which facile disproportionation of the two alkyl groups takes place; (b) A nondissociative pathway which proceeds without dissociation of ligand; and (c) An associative pathway in which the transformation is facilitated by pre-coordination of a ligand.

(a) Dissociative Pathway

$$MR_2L \xrightarrow{-L} MR_2 \longrightarrow \text{product}$$

(b) Nondissociative Pathway

$$MR_2 \longrightarrow \text{product}$$

(c) Associative Pathway

$$MR_2 + L \longrightarrow MR_2L \longrightarrow \text{product}$$

Given the experimental data described above, the mechanism in **Scheme 4.E** is proposed which accounts for all the observations. A rapid pre-equilibrium coordination of PMe_3 is proposed as the initial step for the transformation of **4** to **39** due to the first order dependence on PMe_3 and the fact that the PMe_3 adduct, W(NPh)[*o*-$(Me_3SiN)_2C_6H_4$]$(PMe_3)Et_2$, **21**, has been observed at -50°C. This adduct exists as a mixture of two isomers as determined by ^{13}C and ^{31}P NMR spectroscopy. The major isomer has *trans* ethyl groups with PMe_3 coordinated *cis* to the imido ligand. The minor isomer has the PMe_3 coordinated *trans* to the imido ligand leaving the ethyl groups mutually *cis* . We suggest that the reaction proceeds through the minor isomer of **21** in which the *cis* disposition of the ethyl groups is retained.

Scheme 4.E. Proposed Mechanism of the Formation of **39**.

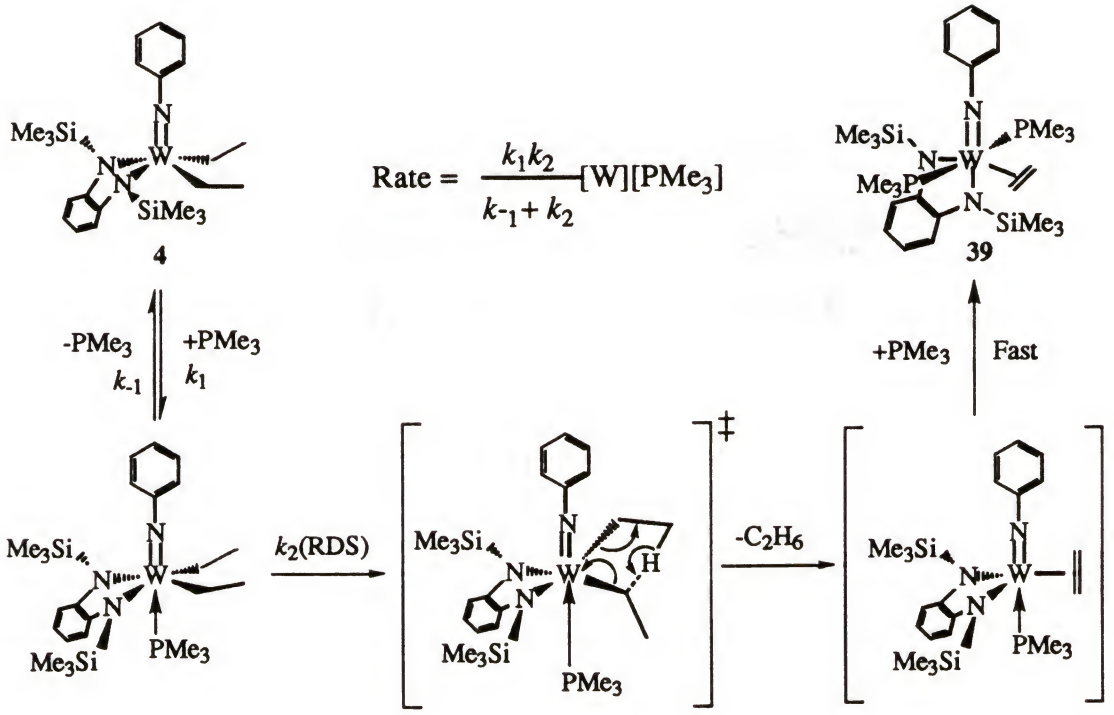

The reaction obeys first order kinetics in both W and PMe_3. No deuterium scrambling was observed both in the presence and absence of PMe_3 which excludes a β-elimination process in which there is a rapid equilibrium between an olefin-hydride complex and starting material. The observation of a large kinetic isotope effect (6.1) at 293K suggests a symmetrical linear transition state, according to Kwart's study.[148] The observed value of $\Delta S^{\ddagger}$ (-54.9 eu) is consistent with the bimolecular nature of this reaction and the highly-ordered transition state, imposed by the geometric requirements of the β-hydrogen to transfer to the α-carbon of the other ethyl group. Evidently, the increased electron density on the metal center in $W(NPh)[o\text{-}(Me_3SiN)_2C_6H_4](Et)_2(PMe_3)$ combined with the increased steric congestion induces the rapid β-H abstraction reaction.

Mechanistic Study For the Formation of styrene complex, **40**

The transformation of **6** to **40** proceeds via more complicated pathways than that of **4** based on the observations mentioned earlier. The near linear PMe_3 dependence at high concentration is similar to the previous study. However, the kinetic isotope effect observed (2.1) implies that the β-elimination pathway is more reasonable than a β-abstraction pathway which gives a k_H/k_D of 6.1 for the transformation of **4** to **39**.

In the absence of PMe_3, **42**, the product of the thermolysis of **6**, was observed, associated with the ethylbenzene being released from tungsten center. A rate constant of $2.1*10^{-4}$ sec^{-1} and large kinetic isotope effect (6.4) are observed for the thermolysis of **6**, suggesting that a similar β-abstraction pathway accounts for this reaction. The styrene complex, **42** can be isolated as a dark brown solid. Upon further addition of PMe_3 to **42**, compound **40** is formed quantitatively. Details of the properties and reactivities of compound **42** will be discussed in Chapter 5. The kinetics of the thermolysis of **6** were also performed (**Figure 4.7**) over a temperature range of 333-363K and in the absence of PMe_3. The reaction follows first-order kinetics with activation parameters being $\Delta H^{\ddagger}$ = 18.6(0.6) Kcal·mol^{-1} and $\Delta S^{\ddagger}$ = -23.3(1.6) cal·mol^{-1}·K^{-1}, which correspond to $\Delta G^{\ddagger}$ = 26.4 Kcal·mol^{-1} at 333K. The standard errors for $\Delta H^{\ddagger}$ and $\Delta S^{\ddagger}$ are calculated using 2σ. The activation parameters obtained here are similar to related studies (**Scheme 4.F**).[18]

Scheme 4.F. Synthesis of $W(NPh)[o\text{-}(Me_3SiN)_2C_6H_4](CH_2CD_2Ph)_2$, **6**-$d_4$.

(a)

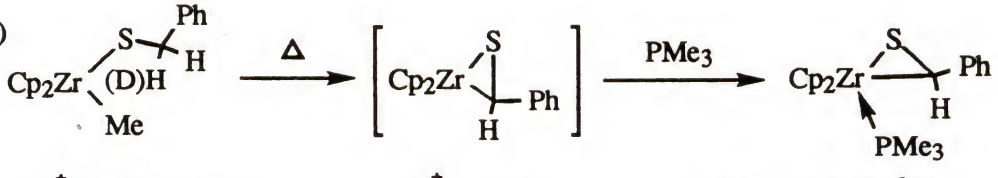

$\Delta H^{\ddagger}$ = 18.6 Kcal/mol $\Delta S^{\ddagger}$ = -20.6 e.u. k_H/k_D = 5.2 (80 °C)

(b)

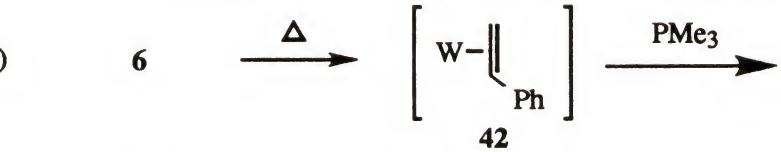

$\Delta H^{\ddagger}$ = 18.6 Kcal/mol $\Delta S^{\ddagger}$ = -23.3 e.u. k_H/k_D = 4.77 (80 °C)

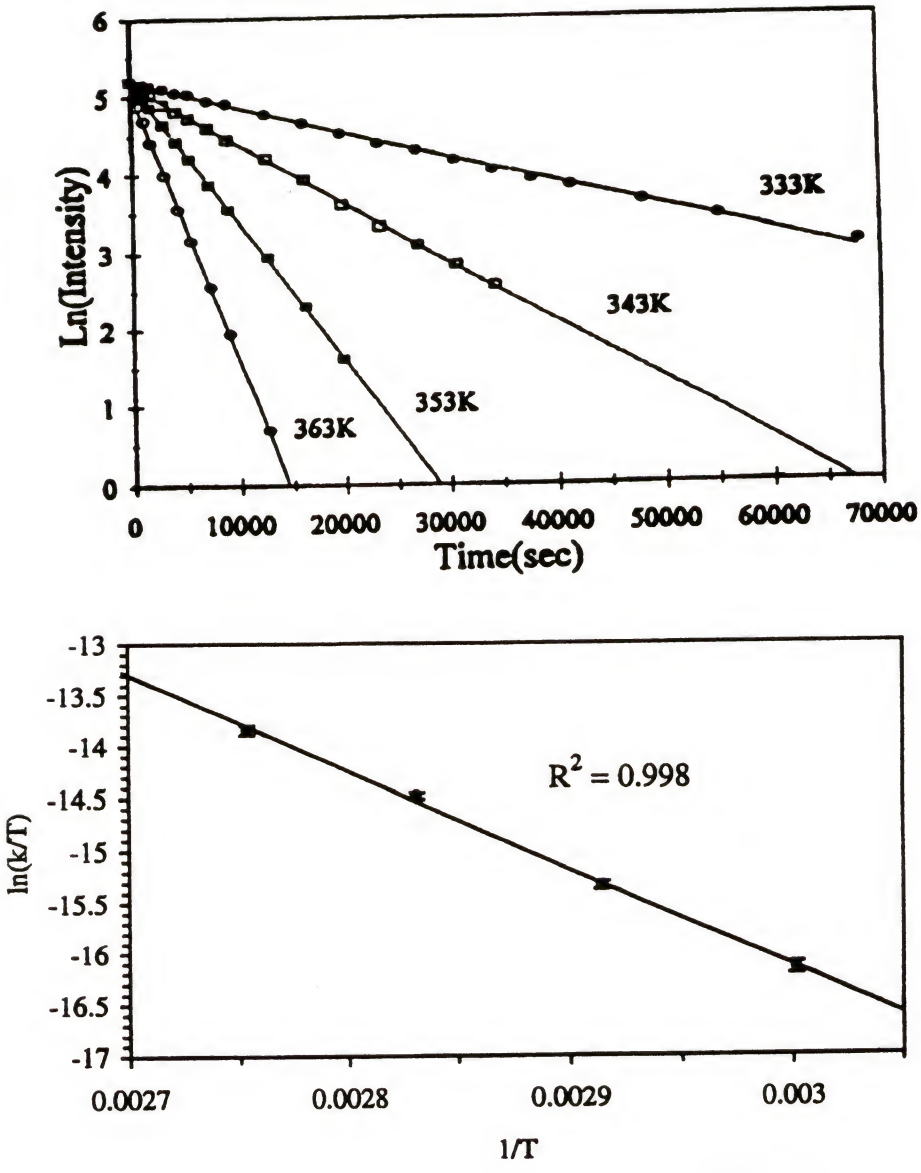

Figure 4.7. First order kinetics (top) and Eyring plot (bottom) for the thermolysis of **6**.

It should be noted that parallel pathways (one being PMe_3 independent and one being first order in PMe_3) cannot explain the non-linearity in **Figure 4.5**. The PMe_3-dependent kinetic isotope effect and the deviation from linear PMe_3 dependence at low concentrations suggest that PMe_3 plays a crucial role in determining which pathway the reaction follows. A simple mechanism consisting of phosphine association/dissociation equilibrium followed by β-H elimination can not account for the phosphine dependence observed, since it will result in a linear dependence with a positive intercept in **Figure 4.5**. Furthermore, we have established that the coordination of PMe_3 to **6** involves a geometry change in which the alkyl groups go from mutually *cis* to mutually *trans*. Although we are not certain which process happens first, isomerization or coordination, we do believe that all processes are reversible and dynamic. Therefore, we propose that all these fast equilibria are involved (**Scheme 4.G**) prior to the elimination step.

The *trans* isomer (referred to the *trans* alkyl groups) of the phosphine adduct, $W(NPh)[o\text{-}(Me_3SiN)_2C_6H_4](PMe_3)(CH_2CH_2Ph)_2$, **22**, is proposed in **Scheme 4.G** because no *cis* isomer has been observed at any temperature. Complex **22** then proceeds via a dissociative pathway to provide an open coordination site in **C**, which then decomposes by the β-elimination pathway. The lack of deuterium scrambling in the reaction (k_5 and k_{-5}) is due to the sterics of the β-phenyl ring which directs the insertion of styrene into the W-H bond in the preferred orientation to give the unscrambled product. Association/dissociation of PMe_3 and the isomerization between TBP (**C**) and SP isomers are considered to be dynamic and may happen faster than k_1 because the PMe_3 adduct can be observed at low temperature when the decomposition (k_1) does not even occur. β-H elimination from TBP isomer, **C**, affords a W(VI) intermediate, **D**. The coordination of PMe_3 to **D** forms a seven-coordinate intermediate, **E**. Reductive elimination from **E** is considered the rate limiting step in the second pathway. Reductive elimination from **D** without coordination of PMe_3 is ruled out since it will result in a linear PMe_3 dependence from the calculation of the rate equation.

Scheme 4.G. Proposed Mechanism for the Formation of **40**.

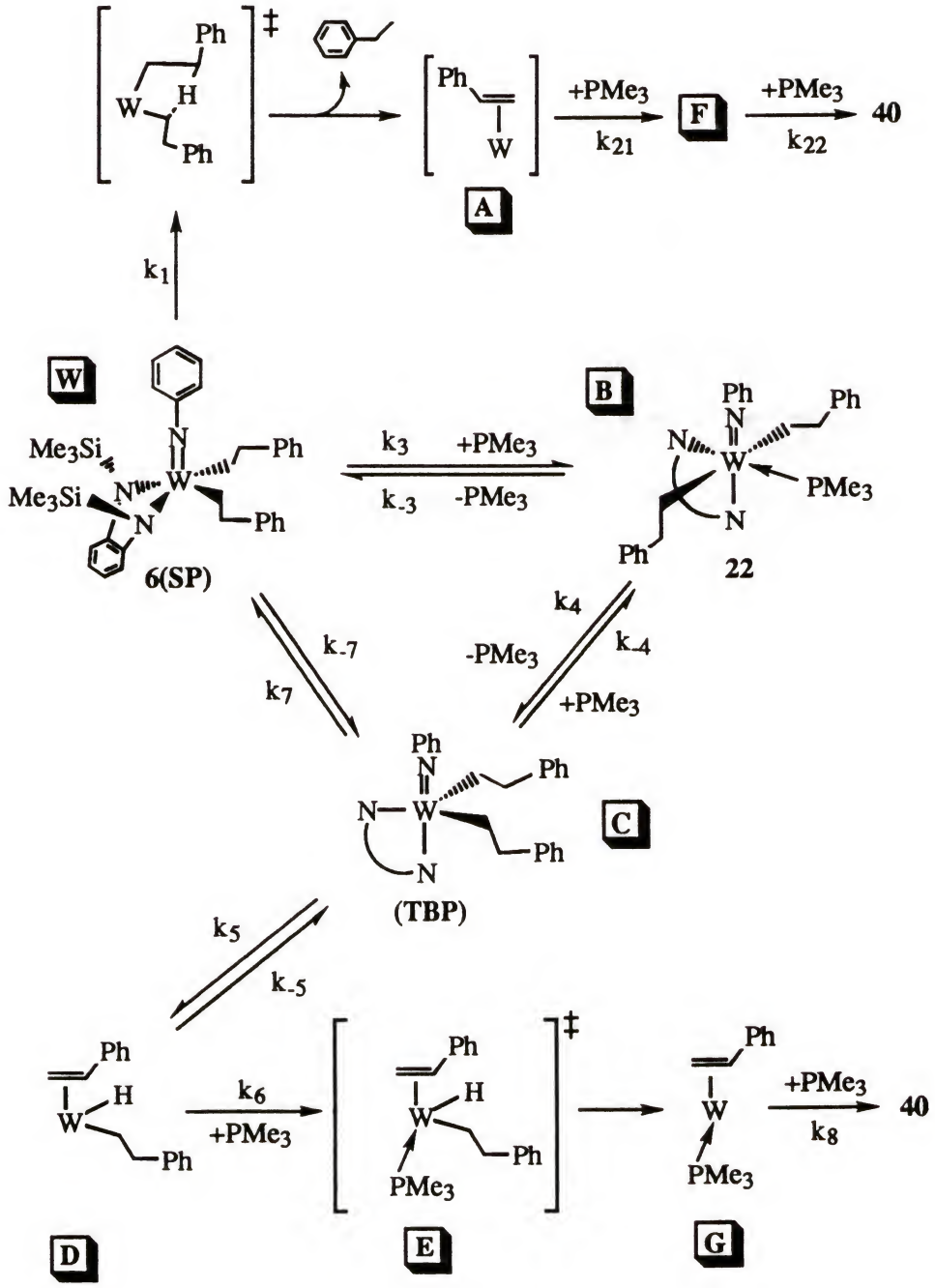

From **Scheme 4.G**, the rate of the reaction can be expressed as equation 4.3. Based on the fact that no intermediate was observed during the reaction, we are able to use the steady-state approximation for the concentration of **22**, **C**, and **D**, which gives the observed rate constant, k_{obs} (equation 4.4), as a complex dependence on rate constants and phosphine concentrations (**Scheme 4.H**).

$$\text{Rate} = \frac{-d[W]}{dt} = k_1[W] + k_3[PMe_3][W] - k_7[C] - k_{-3}[B] + k_{-7}[W] \qquad 4.3$$

Scheme 4.H. Derivation of the observed rate constant, k_{obs} for the Formation of **40**.

$$\text{Assumption}: \frac{d[B]}{dt} = \frac{d[C]}{dt} = \frac{d[D]}{dt} = 0$$

$$\Rightarrow [B]_{ss} = \frac{k_3[W][PMe_3] + k_{-4}[C][PMe_3]}{k_4 + k_{-3}}$$

$$[C]_{ss} = \frac{k_4[B] + k_{-7}[W] + k_{-5}[D]}{k_{-4}[PMe_3] + k_5 + k_7}$$

$$[D]_{ss} = \frac{k_5[C]}{k_{-5} + k_6[PMe_3]}$$

$$\Rightarrow (k_4k_{-5}+k_4k_6)[B] + k_{-5}k_{-7}[W] + k_6k_{-7}[W][PMe_3] = X[C]$$

$$X = k_{-5}k_7 + (k_{-4}k_{-5}+k_5k_6+k_6k_7)[PMe_3] + k_{-4}k_6[PMe_3]^2$$

$$[B]_{ss} = k_B[W] = [W] * \frac{(k_3X + k_{-4}k_{-5}k_{-7} + k_{-4}k_6k_{-7})[PMe_3]}{Y}$$

$$Y = (k_{-3} + k_4)X - (k_{-4}k_{-4}k_{-5}+k_4k_{-4}k_6)[PMe_3]$$

$$[C]_{ss} = k_C[W] = [W] * \frac{(k_4k_{-5} + k_4k_6)k_B + k_{-5}k_{-7} + k_6k_{-7}[PMe_3]}{X}$$

$$\text{Rate} = k_1[W] + k_3[PMe_3][W] - k_7[C] - k_{-3}[B] + k_{-7}[W]$$
$$= k_{obs}[W]$$
$$k_{obs} = (k_1 + k_7) + k_3[PMe_3] - k_{-3}\mathbf{k_B} - k_7\mathbf{k_C} \qquad 4.4$$

The complexity of the PMe_3 dependence accounts for the non-linear behavior in **Figure 4.5**. Although we are not able to measure rate constants for each step, some estimation can be made based on our results. First, we find no profound effect on the overall rate in the presence of low concentration of phosphine and the rate only doubles when large excess (*ca.* 25 equivalents) of PMe_3 is added, which indicates that rate constants for the phosphine dependent pathway are similar to those of the phosphine independent pathway (k_1= 0.00021). Second, the square pyramidal structure of **6**, obtained from single crystal X-ray study, and the inability to observe the trigonal bipyramidal isomer at any temperature suggest that the isomerization process is probably very fast or the equilibrium lies predominantly toward the SP isomer ($k_7 >> k_{-7}$). Furthermore, if the coordination of phosphines is actually much faster than all other steps, all three species, **6**, **B**, and **C**, can be considered as one species, which should result in a linear PMe_3 dependence.

Rate constants were assigned based on the above discussion, and the calculated (dotted line in **Figure 4.8**) rate constants (k_{obs} in equation 4.4) were compared with measured experimental values (points in **Figure 4.8**) . The mechanism and rate constants proposed were also examined by a kinetics simulation program, KINFIT, (Appendix C) until a set of numbers (k_1= 0.00021; k_{-3}= 0.00095; k_{-3}= 0.0015; k_4= 0.0021; k_{-4}= 0.0003; k_5= 0.005; k_{-5}= 0.01; k_6= 0.0035; k_7= 0.001; k_{-7}= 0.00001) can fit the experimental results of both the phosphine dependence of k_{obs} (**Figure 4.8**) and the reaction profile simulated (**Figure 4.9**). The KINFIT program (Appendix C) provides a reaction profile of the concentrations of all species involved in the reaction with respect to

time, which can be converted to the observed rate constant, from a set of given mechanism and rate constants for each steps.

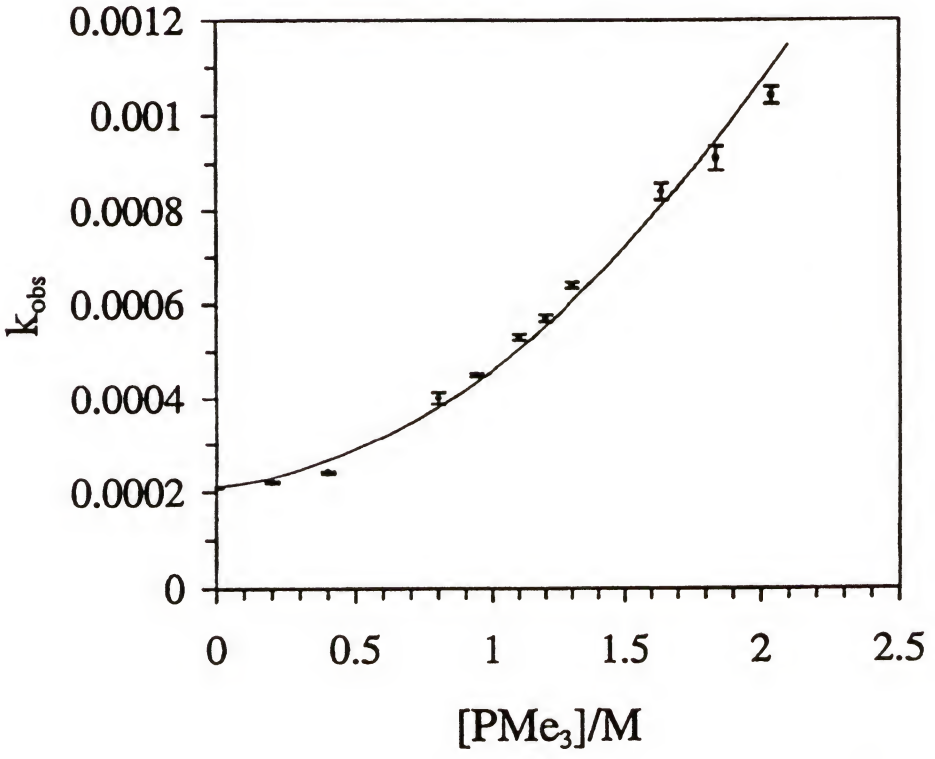

Figure 4.8. Analytical fit of the PMe_3 dependence of the observed rate constant, k_{obs}, (k_1=0.00021; k_3=0.00095; k_{-3}=0.0015; k_4=0.0021; k_{-4}=0.0003; k_5=0.005; k_{-5}=0.01; k_6=0.0035; k_7=0.001; k_{-7}=0.00001).

The result shows well behaved kinetics with the dominant species being PMe_3, **6**, **40** and ethylbenzene, which is consistent with the experimental observations. The rate constant obtained from the simulation result (k_{obs} = 0.00024(1) sec^{-1} for the consumption of **6** and k_{obs} = 0.00025(1) sec^{-1} for the formation of **40**; [PMe_3] = 0.4M) is in good agreement with the experimental data (k_{obs} = 0.00024 sec^{-1}). In the simulation results (both low and high PMe_3 concentrations), only trace amounts of intermediates are present,

which is in accord with the assumptions of steady-state approximation and k_1 and k_6 being rate limiting steps. The pre-equilibria between **6**, **B**, and **C** are supported by the noticeable amounts (4-7%) of intermediates **B** and **C** observed at the early stages of the reaction. However, due to the dynamic property of these processes, all of them show up in the ^1H NMR as an averaged peak, which is indistinguishable from the peak of **6**, causing the intermediates to be "unobservable".

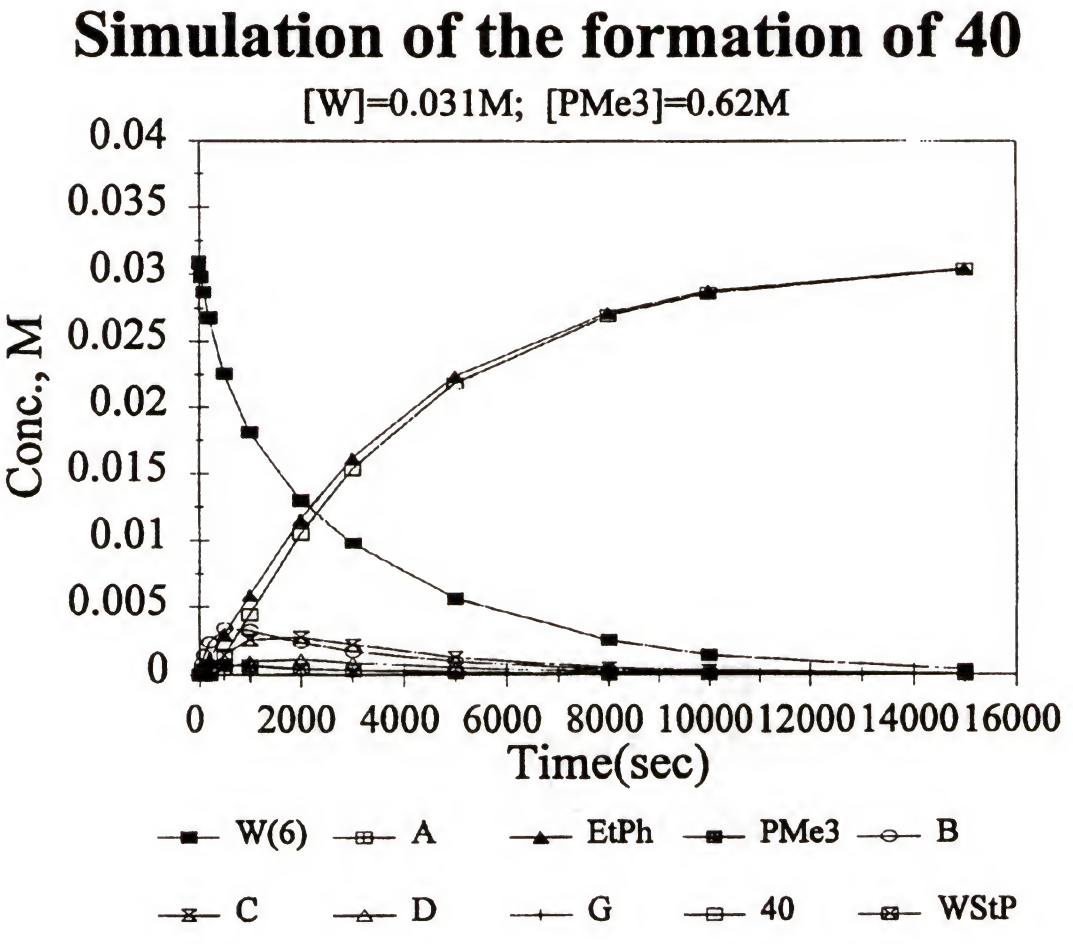

Figure 4.9. Simulation of the mechanism proposed for the formation of **40** from **6**. PMe_3 concentration (~0.6M) is out of the scale shown in this plot.

Calculation of Entropy of Activation

The large negative values of the entropy of activation observed can be explained by the bimolecular nature of the reaction and the formation of a highly ordered transition state. However, it would be more convincing if the numerical data can be obtained to balance these two factors. A statistical mechanics approach[122] to the calculation of the entropy associated with the dynamics of internal rotors has been shown to give very good agreement with a large number of experimentally obtained entropy terms. This calculation assumes free rotation along the bonds, and therefore yields maximum values for changes in entropy from freezing those free rotations, imposed by the steric requirement to achieve the transition state. If rotation is hindered, intermediate values of entropy will be obtained depending on the magnitude of the potential barrier associated with the rotation.

Internal rotational motions arise when a molecule contains groups of atoms connected by single electron-pair bonds. In our system, W-alkyl, the rotations are the rotations of the W moiety versus an alkyl group. Since the rotating groups are relatively close, it is reasonable that there should be a significant change of potential energy associated with the internal rotational coordinate. If the potential is very large in comparison with kT, it is called torsional vibration, which can be treated as a vibration case. If the potential is in the same order of magnitude as compared with kT, there are many complexities arising from the relationships between the rotation of the entire molecule and the internal rotation, which is beyond the scope of this work. If the potential change with angle of rotation is very small as compared to kT, then it can be ignored and considered as a free rotation.

The partition function for free rotation, Q_f, can be derived from the sum of all energy levels which is shown in equation 4.5, where T is the temperature (K) at which the rotation occurs, I_r is defined as the reduced moments of inertia of the internal rotor and n is

the symmetry number for the internal rotor. For example, n is 3 for a methyl or a *t*-butyl group and 2 for a phenyl group. The reduced moments of inertia are obtained using the formula shown in equation 4.6, in which I_{rot} is defined as the moment of inertia of the entire molecule, α_i is defined as the directional cosine between the i_{th} principal axis of the molecule and the bond connecting the internal rotor to the rest of the molecule, and I_i is defined as the moment of inertia of the molecule about the i_{th} principal axis. Once the partition function has been calculated, the entropy of free internal rotation can be obtained from equation 4.7, where R is the universal gas constant.

$$Q_f = \frac{2.7935}{n}(10^{38} I_r T)^{1/2} \qquad 4.5$$

$$I_r = I_{rot}\left(1 - \sum_{i=1}^{3} \frac{\alpha_i^{2} * I_{rot}}{I_i}\right) \qquad 4.6$$

$$s_f = R\,(0.5 + \ln Q_f) \qquad 4.7$$

The calculation of the moments of inertia is done on the dialkyl complexes whose structures have been solved by single crystal X-ray studies. It should be noted that the fractional atomic coordinates obtained from crystal data corresponds to the unit cell dimensions, and they need to be converted to Cartesian coordinates (x, y, z) before doing the calculation. Those coordinates are used to calculate the center of mass of the molecule and the moments of inertia of the rotors, from which the entropy associated with the free rotation of the alkyl group can be obtained (**Table 4.V**).

Table 4.V. Calculated results for the entropy of free rotation.

Compound	Rotor	$I_r(10^{38}cm^2g)$	T(K)	$Q_f (g^{1/2}T^{1/2})$	S_f (eu)
$W(CH_2CH_2Ph)_2$, **6**	W-C_α	2.82	353	88.21	9.89
	W-C_β	12.02	353	182.02	11.33
	W-C_α'	18.03	353	222.95	11.74
WEt_2, **4**	W-C_α	0.74	293	41.09	8.38
	C_α-C_β	0.04	293	3.06	3.22
WMe_2, **3**	W-C_α	0.02	293	2.36	2.70
$WiBu_2$, **7**	W-C_α	1.41	293	56.74	9.02
	C_α-C_β	1.17	293	51.84	8.84
WNp_2, **10**	W-C_α	1.29	293	54.40	8.93

The crystal lattice coordinates of **6** were used to do the calculation. In the transition state of the β-H abstraction pathway, three bonds (W-C_α, W-C_α', and C_α-C_β) will be frozen for the H-transfer process (**Scheme 4.I**), which correspond to entropy loss of 9.89, 11.74 and 11.33 respectively. The overall contribution of freezing these three free rotation gives an entropy loss of 33.96 eu. Comparing with the entropy of activation (-23.3 eu) for the thermolysis of **6** in the absence of PMe_3, the transition state proposed is justified by the calculation. The difference between the calculated and experimental entropy loss (10 eu) can be attributed to the rotational barrier arising from the repulsion between the β-phenyl and the imido phenyl groups, which is not accounted in the calculation. In the transition state of the diethyl case, **4**, the entropy loss due to the hindered-rotation is about 20 eu (calculated from the optimized structure using CAChe system), which combines with the -30 to -40 entropy loss observed[113] in purely associative substitution reactions to account for the observed value of $\Delta S^{\ddagger}$ in the formation of the ethylene complex.

Scheme 4.I. Loss of free rotational entropy in the transition state of the thermolysis of **6**.

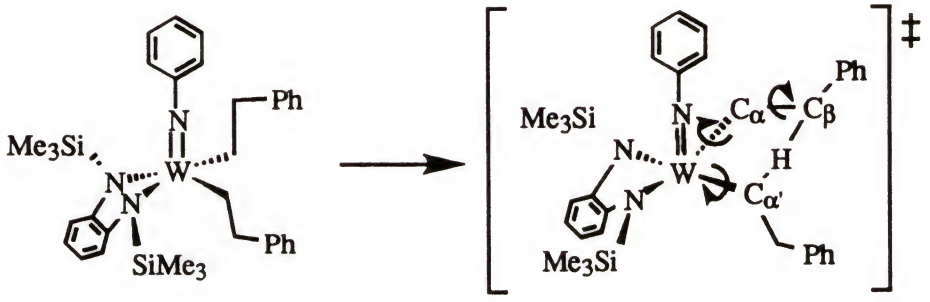

α- *v.s.* β-Abstraction Reactions

For complexes containing both α- and β-hydrogens, β-abstraction usually occurs preferentially over α-H processes.[123,124] However, it has been demonstrated that α-elimination or abstraction processes can compete with[18b] or be preferred over[19] analogous β processes in a sterically crowded environment. This accounts for the observation that alkylidene ligands can be formed in olefin metathesis reactions from alkyls that have β-hydrogens.[18b]

Several asymmetric dialkyl compounds that have been synthesized are suitable for the study of competition between α- and β-abstraction processes. Addition of trimethylphosphine to W(NPh)[$(NSiMe_3)_2C_6H_4$](CH_2CMe_3)(Et), **17**, yields exclusively β-abstraction products (**Scheme 4.J**). Reaction of W(NPh)[$(NSiMe_3)_2C_6H_4$] (CH_2CMe_3)(CH_2CHMe_2), **18**, with PMe_3 yields isobutane, isobutylene, neopentane, and three alkylidene species (δ9.61(d), **34**, 10.12(d), 10.43(d)). Isobutane and neopentylidene, **34**, are the products of an α-abstraction pathway. This observation indicates that the α-abstraction process is competing with the β-process, which yields isobutylene. Similar competion between α- and β- abstractions is also observed in the thermolysis of W(NPh)[$(NSiMe_3)_2C_6H_4$](CH_2CMe_3)(CH_2CH_2Ph), **19**, in the presence

of PMe_3, which yields neopentane, styrene complex, **40**, ethylbenzene, neopentylidene, **34**, and a new alkylidene species (δ265.34 in ^{13}C NMR). The observed competition between α- and β- abstraction is presumably due to the steric hindrance, caused by two bulky alkyl groups, for the β-abstraction pathway.

Scheme 4.J. Competition between α- and β- abstraction for asymmetric dialkyls.

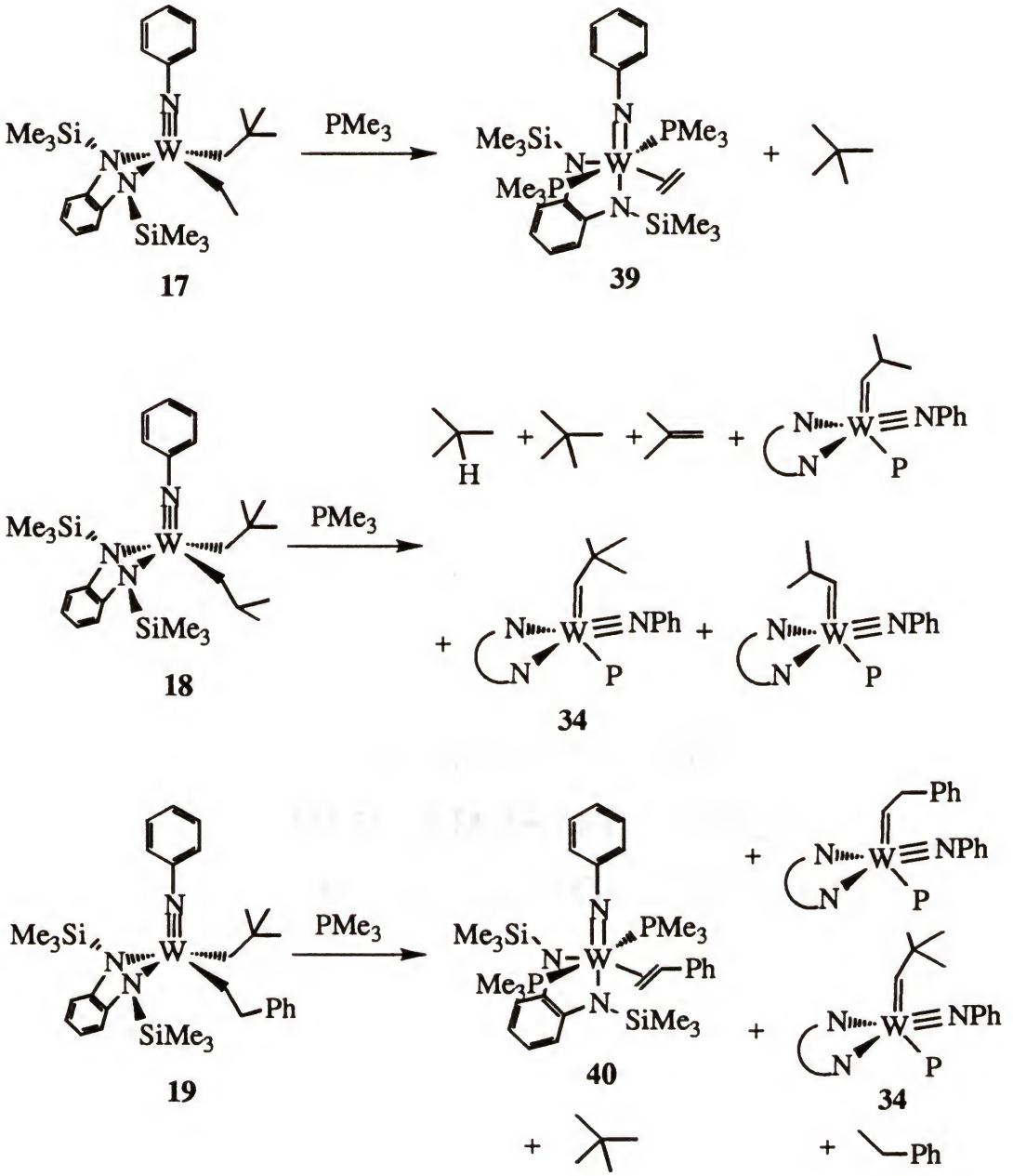

Discussion and Conclusion

We have proposed a mechanism for the formation of olefin complexes, **39** and **40**, from stable, coordinatively unsaturated W(VI) dialkyl complexes, **4** and **6**, induced by the addition of PMe_3 which accounts for all our observations. An alternative mechanism which involves transfer of the β-H atom to the imido nitrogen followed by α-abstraction of the N-H of the resultant amido group by the remaining ethyl group is also conceivable. While we have no direct evidence that excludes this pathway, we believe that such a mechanism is unlikely because of observations that we have made on the conversion of **6** to the styrene complex, **40**. The conversion of **6** to **40** occurs much more slowly ($t_{1/2}$ = 167 min at 333K) than **4** is converted to **39** ($t_{1/2}$ = 12 min at 293K). Furthermore, the data indicates that the conversion of **6** to **40** proceeds via a different mechanism (KIE = 2.3) than the conversion of **4** to **39** (KIE = 6.1). When complex **6** binds PMe_3, only the isomer with PMe_3 *cis* to the imido group and the ethyl groups *trans* to one another is observed via low temperature NMR. Apparently, this is responsible for the change in mechanism because the alkyl groups are no longer *cis* to one another. If transfer of the β-H to the imido is the mechanism that is followed, we would expect that changing the geometry of the PMe_3 adduct in this fashion would not cause such a dramatic change in the reaction rate because the alkyl groups remain *cis* to the imido group.

Our observations of a large isotope effect, negative entropy of activation, and no deuterium scrambling are all consistent with the β-H abstraction mechanism proposed for the formation of the ethylene complex, **39**, from **4**. The PMe_3 dependent KIE, non-linear PMe_3 dependence, and positive rate constant in the absence of PMe_3 all support the existence of another competing pathway in the transformation of **6** to **40**. The combination of the bimolecular nature of this reaction and the highly-ordered transition state, imposed

by the geometric requirements needed for the β-hydrogen transfer account for the large negative entropy value. Evidently, the increased electron density on the metal center combined with the increased steric congestion induces the rapid β-H abstraction reaction group.

CHAPTER 5
HYDROGENOLYSIS AND HYDROGENATION REACTIONS

Introduction

Transition metal complexes containing M-H bonds[125] are of great interest both because of their unusual reactivity in many stoichiometric reactions[126] and their potential as homogeneous catalysts for hydrogenation and other reactions of organic substrates.[127] These compounds can be synthesized in a variety of ways,[2] such as utilizing hydride reagents (e.g. *n*-Bu_3SnH and $LiBEt_3H$),[128] hydrogen transfer substrates,[129] and most importantly, oxidative addition of molecular hydrogen (equation 5.1).[130] Kubas first reported that the H-H bond can remain intact when coordinated in a metal complex,[131] which implies a close approach of the H_2 molecule to the metal center before cleavage of the H-H bond occurs (equation 5.2). The equilibrium between the dihydrogen (**A**) and dihydride (**B**) complexes are well established[132] and the properties of such dihydrogen complexes have been extensively reviewed.[133]

5.1

5.2

It is quite possible that dihydrogen complexes as such are intermediates in oxidative addition reactions of H_2 and in the hydrogenolysis of metal alkyls (equation 5.3).[134] The η^2-dihydrogen/dihydride equilibrium has direct parallels to the equilibria between η^2-alkane/alkylhydride[135] and η^2-silane/silylhydride species,[136] which are important in C-H activation and catalytic hydrosilylation. Furthermore, equation 5.2 is of direct importance to the mechanism of many homogeneous hydrogenation catalysts, including Wilkinson's catalyst,[137] $RhCl(PPh_3)_3$, where the unobserved dihydrogen ligand in a Rh(I) intermediate rapidly splits to give the dihydride intermediate responsible for the hydrogenation of many unsaturated organic substrates.

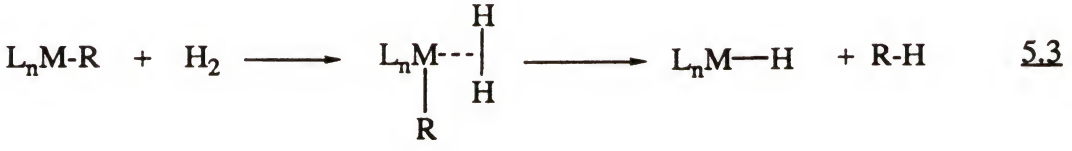

5.3

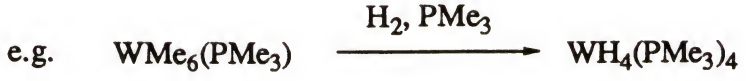

Synthesis of Hydridotungsten(VI) Complexes

We attempted to synthesize a tungsten hydride complex by hydrogenolysis of W(NPh)[*o*-$(Me_3SiN)_2C_6H_4$]Me_2, **3**. No reaction was observed for several days at 80°C. Similar reactions were also carried out by reacting W(NPh)[*o*-$(Me_3SiN)_2C_6H_4$]Et_2, **4**, and W(NPh)[*o*-$(Me_3SiN)_2C_6H_4$]$(CH_2CMe_3)_2$, **10**, with molecular hydrogen (equation 5.4). Several hydride species (presumably mono- and dihydrides) were observed by ^1H NMR. However, attempted isolations of these compounds have been unsuccessful to date.

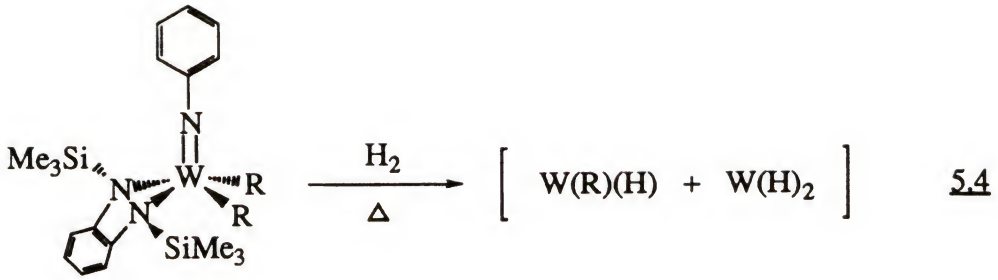

5.4

R = Et(**4**), CH_2CMe_3(**10**)

Other attempts were also made by reacting W(NPh)[*o*-$(Me_3SiN)_2C_6H_4$]Cl_2 , **2**, with hydride reagents, such as KH, $LiAlH_4$, $LiBEt_3H$, Li(O-*t*-Bu)$_3AlH$, and $NaBH_4$, and reducing **2** with Na/Hg amalgam in the presence of H_2. Mixtures of hydride species were observed for all the above reactions. Although the isolations of these species have proven difficult, the existence of the hydride species is unquestionable, as is supported by the observed (NMR, GC) isomerization of 1,9-decadiene into internal olefins by **2** in the presence of *n*-Bu_3SnH (equation 5.5).[138]

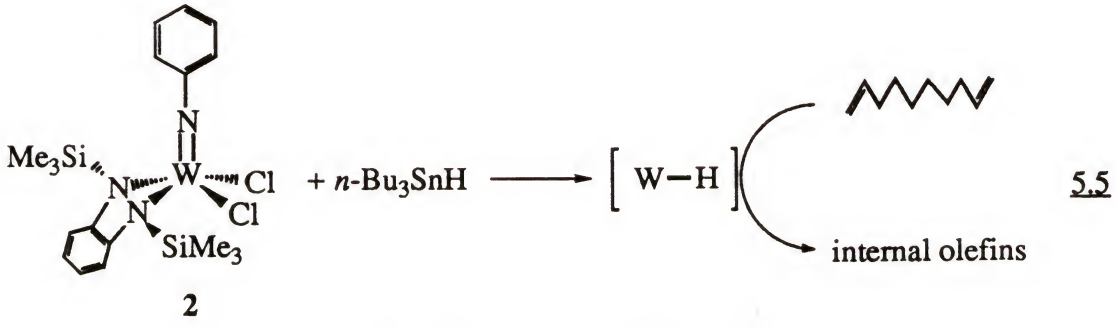

2

5.5

The hydrogenolysis (20 psi H_2) of W(NPh)[*o*-$(Me_3SiN)_2C_6H_4$]$(CH_2CH_2Ph)_2$, **6**, at room temperature does not produce any spectroscopically observable hydride species, but instead, a new tungsten(IV) arene complex W(NPh)[*o*-$(Me_3SiN)_2C_6H_4$](η^6-PhEt), **43**, (equation 5.6). The ^1H NMR spectrum (**Figure 5.1**) of **43** reveals peaks at δ4.13 (t, 1H), 4.70 (d, 2H), and 4.77 (t, 2H) for the five ring protons of the coordinated ethylbenzene, which are significantly shifted upfield from the uncoordinated ethylbenzene.

The upfield shift is characteristic for η^6-arene complexes.[139] It is generally interpreted in terms of a combination of effects, including quenching of ring current from coordination, electron-withdrawing effect of the metal moiety, magnetic anisotropy of the metal-arene bond, and partial sp^2-sp^3 rehybridization of the ring carbon atoms.[140] The ethyl group gives rise to peaks at 0.59 (t, 3H) and 1.71 (q, 2H) ppm, which are also shifted upfield from the uncoordinated ethylbenzene (δ1.06 and 2.42). A single peak at δ0.40 (18H) is assigned to the two equivalent trimethylsilyl groups. Compound **43** is an air and water sensitive, dark-brown microcrystalline solid which is indefinitely stable in the solid state or in solution if stored under an inert atmosphere. The valence electron count for complex **43** is 18 and no exchange between the ethylbenzene and other arenes (e.g. benzene, toluene) is observed.

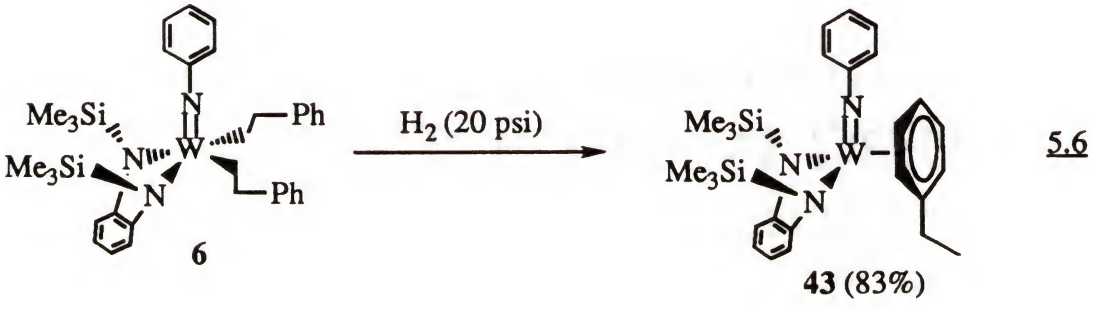

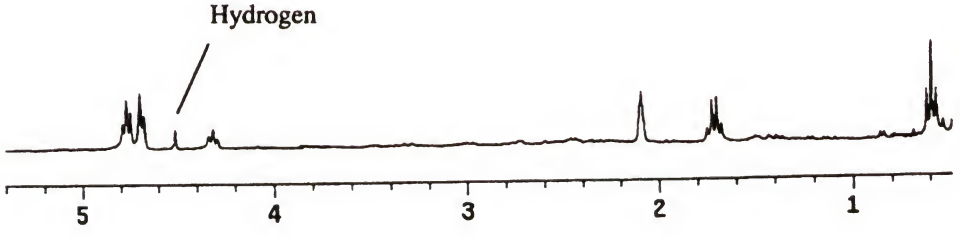

Figure 5.1. Partial ^{1}H NMR spectrum (in C_7D_8) of W(NPh)[*o*-$(Me_3SiN)_2C_6H_4$](η^6-PhEt), **43**.

When W(NPh)[*o*-$(Me_3SiN)_2C_6H_4$]$(CH_2CMe_3)_2$, **10**, was allowed to react with hydrogen in the presence of PMe_3, a seven-coordinate dihydride complex, W(NPh)[*o*-$(Me_3SiN)_2C_6H_4$]$(PMe_3)_2(H)_2$, **44**, was isolated in quantitative yield with the formation of neopentane (equation 5.7).[94] Complex **44** can also be synthesized via hydrogenolysis of diethyl, **4**, and bis-β-phenylethyl, **6**, complexes in the presence of PMe_3. Complex **44** was characterized by multinuclear NMR spectroscopy and X-ray diffraction study. In the ^{1}H-NMR, the hydrides appear at 9.26 ppm as a broad triplet. The PMe_3 group appears as a singlet at 1.04 ppm, suggesting a *trans* disposition. Two singlets at 0.79 and 0.81 ppm are assigned to the inequivalent trimethylsilyls. The ^{1}H-NMR spectrum at -50°C reveals significant changes. The PMe_3 resonance resolves into a triplet at 0.84 ppm ($^2J_{P\text{-}H}$ = 3 Hz) and the hydrides appear as a pair of doublets at 8.92 and 9.06 ppm respectively (J = 37 Hz). The $^{31}P\{^1H\}$ NMR spectrum reveals a singlet at -24.38 ppm ($^1J_{W\text{-}P}$ = 187.1 Hz) consistent with equivalent phosphine groups. These data suggest a pentagonal bipyramidal geometry (similar to complex **39** as described in Chapter 4) with the imido and one amido N occupying the axial positions. The phosphines are *trans* to each other in the equatorial plane. The preference of phosphines being *trans* is also observed in related Ta complexes.[141]

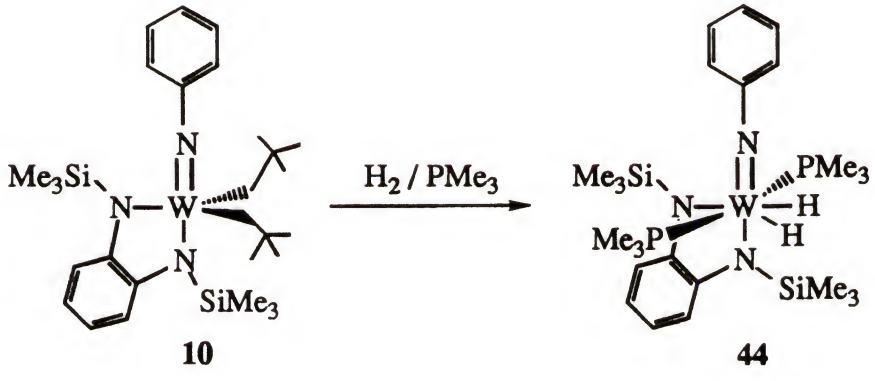

10 **44** 5.7

Although high quality single crystals of complex **44** have not yet been obtained, some data was collected to determine the approximate structure. The data confirms the

geometry about the tungsten center. Unfortunately, the hydrides could not be resolved due to scattering problems. In order to have equivalent phosphines and inequivalent hydrides, the hydrides probably lie *cis* to each other, *trans* to the amido N in the equatorial plane in an out-of-plane fashion.

In order to investigate the role of the trans phosphines and to find out whether or not *cis* phosphines are stable, a chelating phosphine, diphenylphosphinoethane (DPPE), was selected to react with **10** and hydrogen. A new hydride complex W(NPh)[*o*-$(Me_3SiN)_2C_6H_4$](dppe)$(H)_2$, **45**, was formed (equation 5.8).

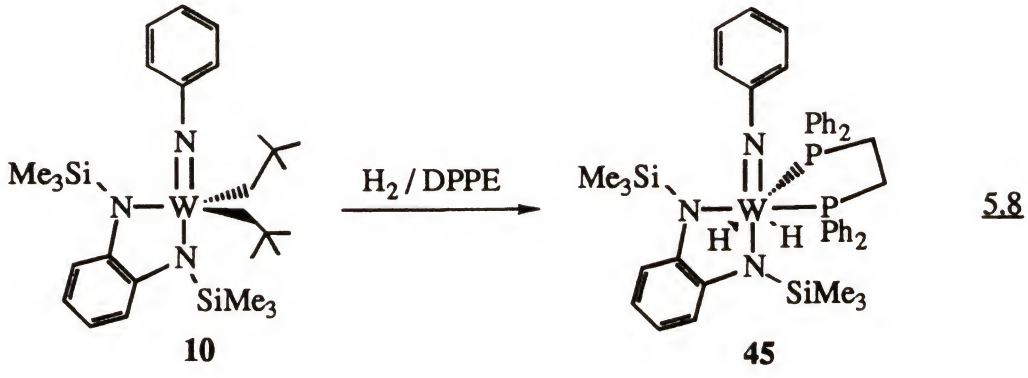

10 **45** 5.8

Compounds **44** and **45** are best described as W(VI) dihydrides rather than W(IV) dihydrogen complexes given the increased stability of W(VI) relative to W(IV). The preference is due to the stronger M-H bond for third row transition metals in which a relativistic contracted orbital improves d(M)-σ(H^-)overlap. The trend, 3d<4d<5d, in the M-H bond strength is also consistent with the observations of complexes of vanadium triad. Complex $V(H_2)Cp(CO)_3$ is a dihydrogen complex, $Ta(H)_2Cp(CO)_3$ is a dihydride, and $Nb(H_2)Cp(CO)_3$ and $Nb(H)_2Cp(CO)_3$ co-exist in equilibrium.[142]

Reactivity of W(VI) Dihydrides, 44 and 45

Transition metal hydride complexes are known to undergo a wide range of reactions such as migratory insertion of organic substrates into M-H bond (equation 5.9)[2] and hydrogenation of olefins both stoichiometrically and catalytically.[125,130] The reactions of complexes **44** and **45** with ethylene give two distinct products. The reaction of **44** with excess ethylene or styrene produced one equivalent of ethane or ethylbenzene and the tungsten(IV) olefin complexes, W(NPh)[*o*-$(Me_3SiN)_2C_6H_4$]$(PMe_3)_2(\eta^2\text{-}C_2H_4)$, **39** and W(NPh)[*o*-$(Me_3SiN)_2C_6H_4$]$(PMe_3)_2(\eta^2\text{-}C_2H_3Ph)$, **40** (equation 5.10). Complexes **39** and **40** can also be converted back to the dihydride complex, **44**, upon addition of hydrogen. The reaction of **45** with ethylene does not produce ethane, but gives the metallacyclopentane complex W(NPh)[*o*-$(Me_3SiN)_2C_6H_4$]$(CH_2CH_2CH_2CH_2)$, **35** (equation 5.11), formed by the addition of two equivalents of ethylene to the reduced metal center[143] and the removal of free DPPE from the metal center. Details of the characterization of **39** and **35** were reported in Chapter 3.

$$M\text{—}H + XY \longrightarrow M\text{—}\overset{Y}{X}\text{-}H \text{ or } M\text{—}XY\text{-}H \qquad 5.9$$

XY = CO, O_2, CO_2, RNC, Alkene, Alkyne

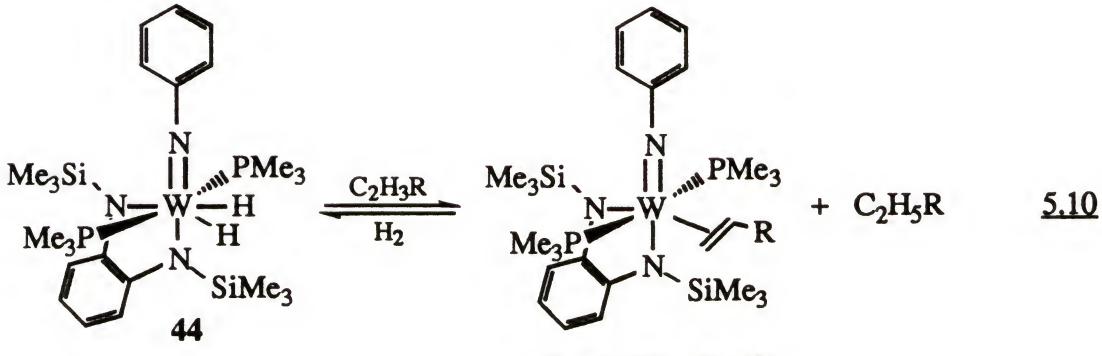

44 5.10

R = H(**39**), Ph(**40**)

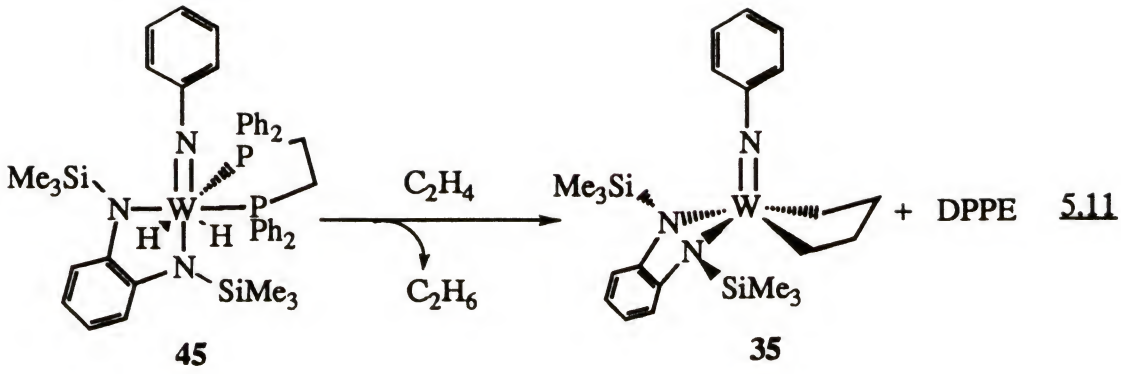

As described in Chapter 3, the ethylene complex, **39**, reacts rapidly with ethylene to give the metallacyclopentane, **35** (equation 3.5). Disproportion of **39** under thermolysis also affords 50% of **35** and another unidentified compound, presumably a highly reactive W(IV) specie, which upon further reaction with MeI yields oxidative addition product, **46** (equation 5.12). The ^{1}H NMR spectrum of compound **46** reveals two peaks at 0.17 and 0.44 ppm for the inequivalent trimethylsilyl groups and one peak at 1.32 ppm ($^{2}J_{W\text{-}H} = 6.1$ Hz) for the methyl group.

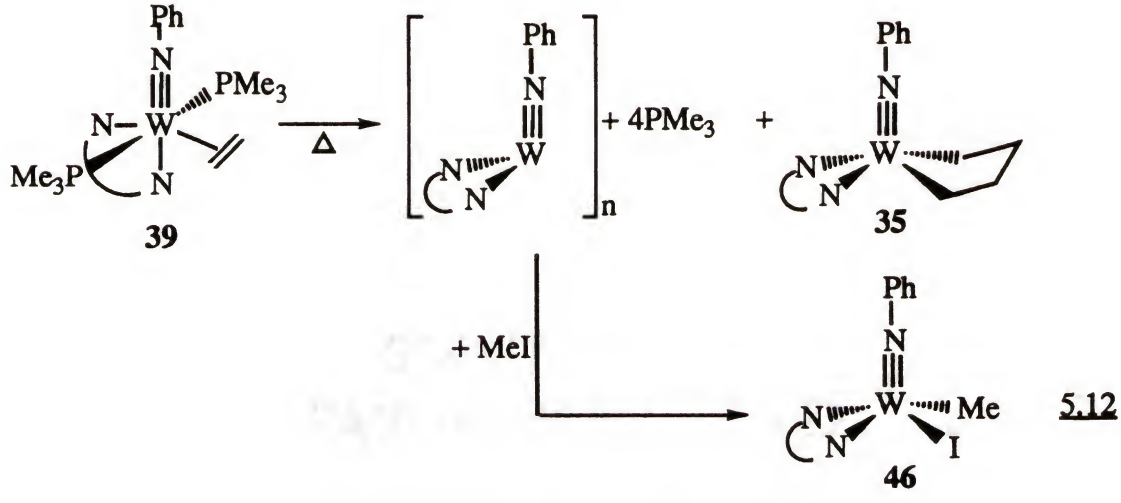

Catalytic Hydrogenation Reactions

Introduction

Catalytic hydrogenation of alkenes by transition metal compounds is a well-studied process and a wide variety of mechanisms have been proposed.[6,12a,144] For late transition metal systems, two distinct mechanisms are usually proposed based on the nature of the catalysts. For monohydride catalysts, such as $HRh(CO)(PPh_3)_3$, it involves initial ligand loss, binding and insertion of an alkene, oxidative addition of hydrogen, and reductive elimination of the alkane (**Scheme 5.A-1**).[145] For non-hydride catalysts, such as Wilkinson's catalyst,[137] $RhCl(PPh_3)_3$, hydrogenation occurs via a route consisting of ligand loss, oxidative addition of hydrogen, binding and insertion of an alkene, and reductive elimination of the alkane (**Scheme 5.A-2**). It has been shown that the oxidative addition of hydrogen can occur either before[146] or after[147] the alkene coordination.

Scheme 5.A. Mechanisms of catalytic hydrogenation of alkenes.

(1)

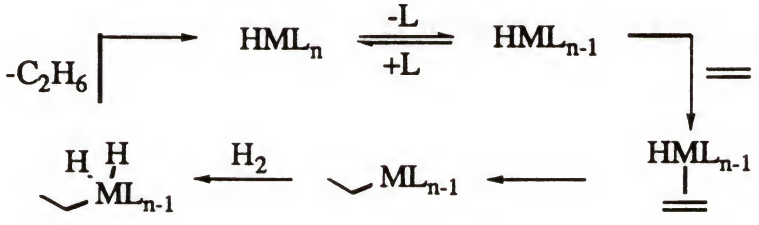

(2)

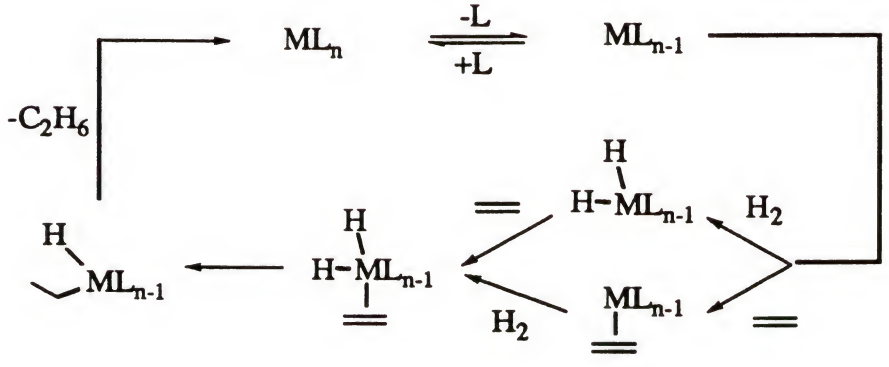

Catalytic Hydrogenation of Alkenes by 44 or 40

As shown in equation 5.10, the styrene complex, **40**, reacts with hydrogen to yield one equivalent of ethylbenzene and the dihydride complex, **44**. Complex **44** can then hydrogenate styrene and yield **40**. This reversibility provides the opportunity for both **40** and **44** being potential catalysts for catalytic hydrogenation. In the presence of hydrogen, styrene is catalytically converted to ethylbenzene, using either **40** or **44** as a catalyst (equation 5.13). The reaction is clean but slow, and only gives 33% conversion to ethylbenzene after 5 days at room temperature. The slow rate is due to the relatively strong tungsten-phosphine bond, which disfavors the dissociation of PMe_3 that is involved in the formation of active intermediate (**Scheme 5.B**).

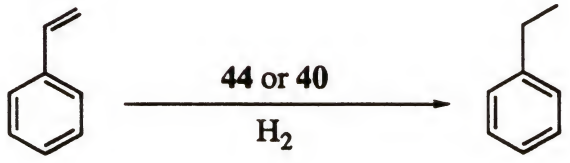

5.13

For conjugated dienes, the hydrogenation can take place stepwise to complete saturation or half-hydrogenation of dienes to monoolefins.[148] The reactivity and selectivity of diene hydrogenation is largely determined by the catalyst system used. For example, $CoBr(PPh_3)_3/BF_3{\cdot}OEt_2$ selectively reduces conjugated dienes to monoenes via 1,2-hydrogenation at the more substituted double bond.[149] Tricarbonylchromium complexes are used for 1,4-addition of H_2 to conjugated dienes.[150] Palladium chloride in DMF hydrogenates isoprene to a mixture of methylbutenes,[151] but $[Cr(C_5H_5)(CO)_3]_2$ hydrogenates isoprene with high selectivity (**Scheme 5.C**).[152]

Scheme 5.B. Mechanisms for catalytic hydrogenation of alkenes.

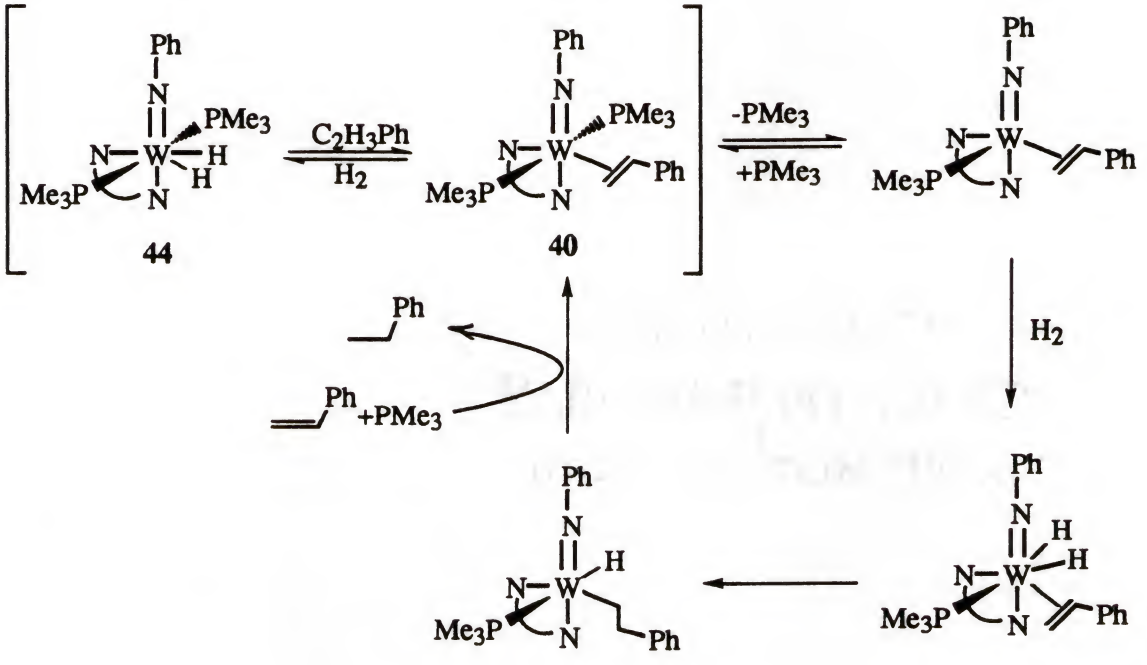

Scheme 5.C. Different Selectivities in Hydrogenation of Isoprene.

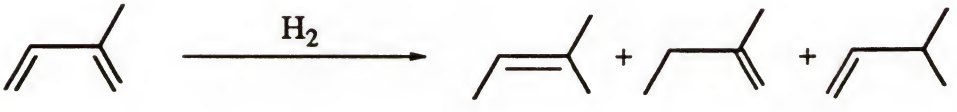

$PdCl_2$/DMF	44%	25%	29%
$[Cr(C_5H_5)(CO)_3]_2$	95%	3%	2%

Complex **44** is also active towards hydrogenation of 1,3-cyclohexadiene. Under a hydrogen atmosphere (20 psi), 1,3-cyclohexadiene was selectively hydrogenated to cyclohexene (equation 5.14). The reaction was monitored by ^1H NMR spectroscopy. The hydride peak disappers immediately upon the addition of 1,3-cyclohexadiene with the formation of a new complex which is identified as a tungsten(IV) cyclohexene complex,

47. The reaction proceeds rapidly at low conversion but slows down as the concentration of cyclohexene increases. This is because the formation of active catalyst involves the dissociation of cyclohexene from **47**, which is disfavored by the cyclohexene formed in the reaction (**Scheme 5.D**).

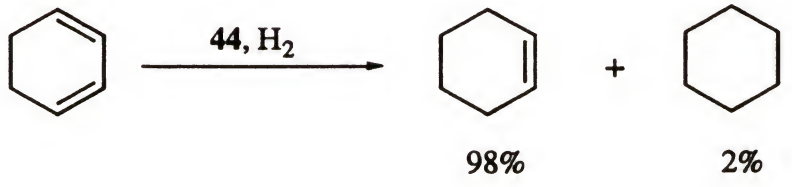

5.14

Scheme 5.D. Mechanism for Selective Hydrogenation of 1,3-cyclohexadiene.

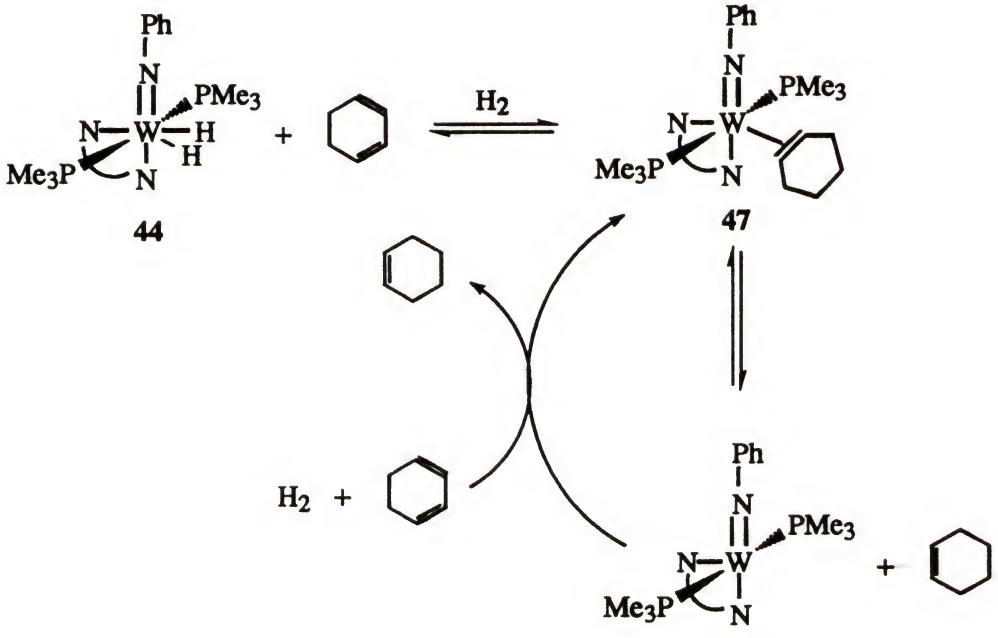

The low reactivity observed for **44** and **40** is due to their stability (both 18 e^- complexes and coordinatively saturated). The observation of no reactivity towards more sterically hindered dienes (e.g. 2,3-dimethyl-1,3-butadiene) also supports this supposition. Reducing the electron count and coordination number, through the removal of PMe_3,

should provide a more reactive catalyst system. The 14e⁻, 4-coordinate complex **42**, thermolysis product of **6** (Chapter 4), seems to fulfill this requirement.

Synthesis and Reactivity of W(NPh)[*o*-$(Me_3SiN)_2C_6H_4$](η^6-PhEt), **43**

In the presence of hydrogen, complex **42** is converted to an η^6-arene complex, W(NPh)[*o*-$(Me_3SiN)_2C_6H_4$](η^6-PhEt), **43**, quantitatively (**Scheme 5.E**). Complex **43** can also be synthesized via replacing styrene by ethylbenzene from **42** or direct thermolysis of **6** in the presence of hydrogen (equation 5.6). The formation of **43** (18 e⁻) from **42** in the presence of ethylbenzene shows that ethylbenzene is coordinated to the tungsten(IV) preferentially over styrene. Displacement of ethylbenzene by styrene (**43** to **42**) is not observed, even at elevated temperature. This preference seems to restrict the utility of **42** as a hydrogenation catalyst.

Scheme 5.E. Synthesis of Tungsten (η^6-arene) Complex, **43**.

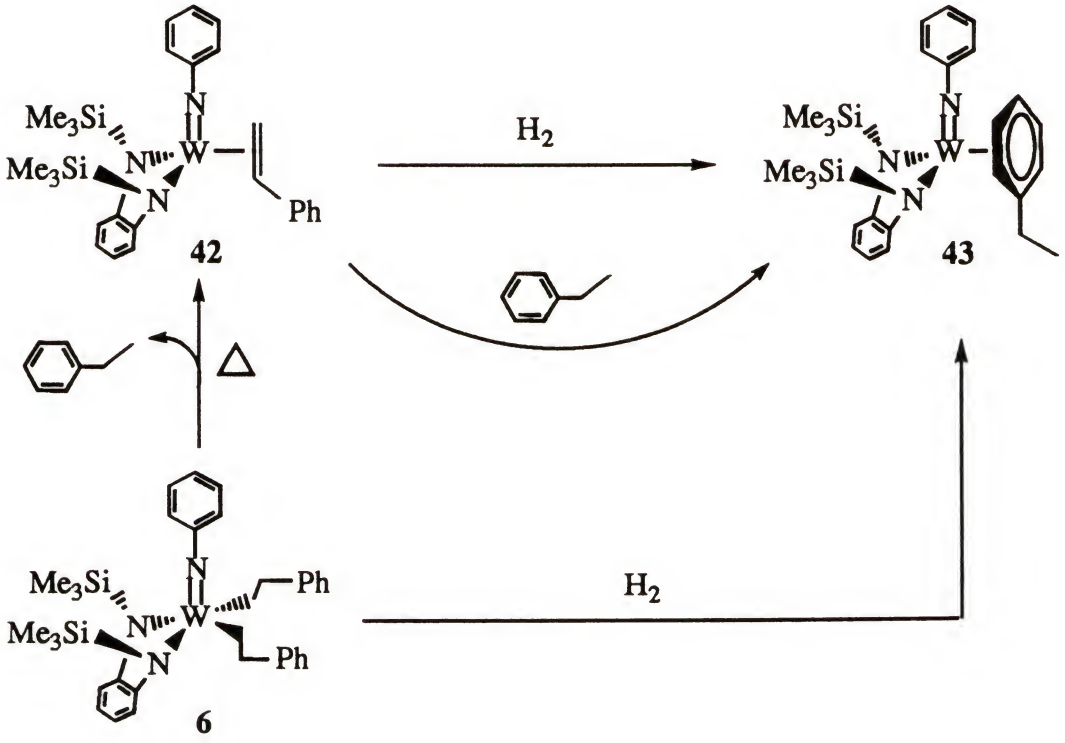

In fact, complex **43** is active towards hydrogenation of alkenes. The hydrogenation of styrene was achieved by reacting **43** with neat styrene under 1000 psi hydrogen (equation 5.15). The turnover frequency (TOF) is only 40/hr. However the catalyst remains active over a period of 2 weeks. A higher turnover number (TON) can be achieved by sequentially adding more styrene and hydrogen.

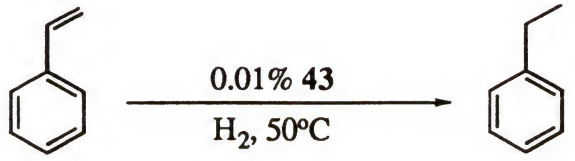

TOF = 40/hr
TON > 5000 5.15

As mentioned above, the styrene does not substitute η^6-ethylbenzene in **42**. The reactivity observed can be attributed to the displacement of ethylbenzene by hydrogen, froming a dihydride specie (**A**) by oxidative addition of hydrogen. Further coordination and insertion of styrene, followed by reductive elimination yields ethylbenzene catalytically (**Scheme 5.F**).

Scheme 5.F. Proposed Pathway for **43** Catalyzed Hydrogenation of Styrene.

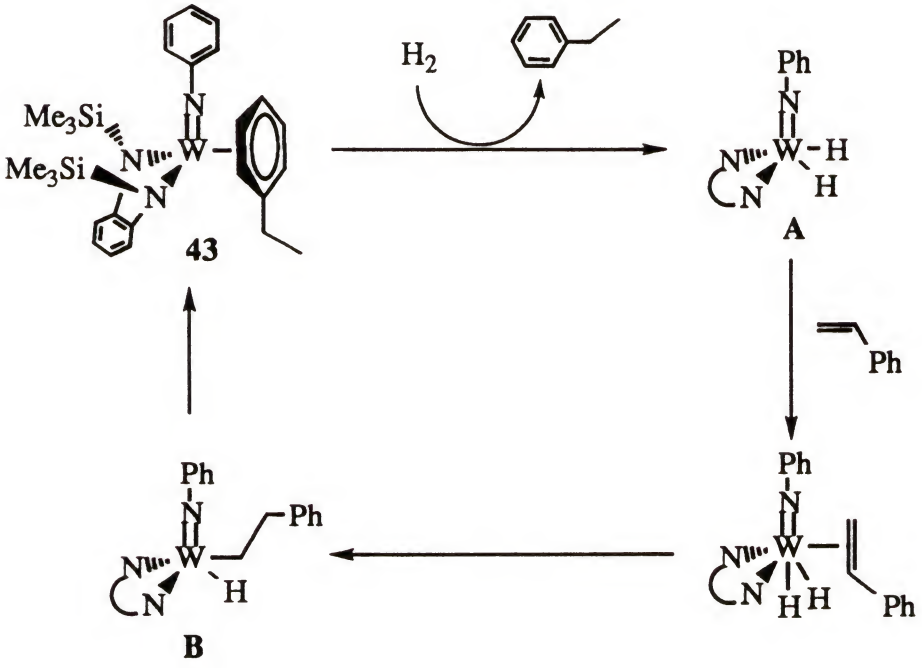

The displacement of η^6-ethylbenzene from metal center by a σ-donor ligand was also observed in the thermolysis of **6** in the presence of PMe_3 (Chapter 4). Thermolysis of **6** affords a mixture of products which can be identified as **42** and **43** via NMR spectroscopy (**Scheme 5.G**). Upon addition of PMe_3, both **42** and **43** are converted to the bisphosphine-styrene complex, **40**, quantitatively. Displacement of arene ligands by other σ-donor nucleophiles in other tungsten complexes have also been reported.[153]

Scheme 5.G. Displacement of η^6-arene by Trimethylphosphine in the Formation of **40**.

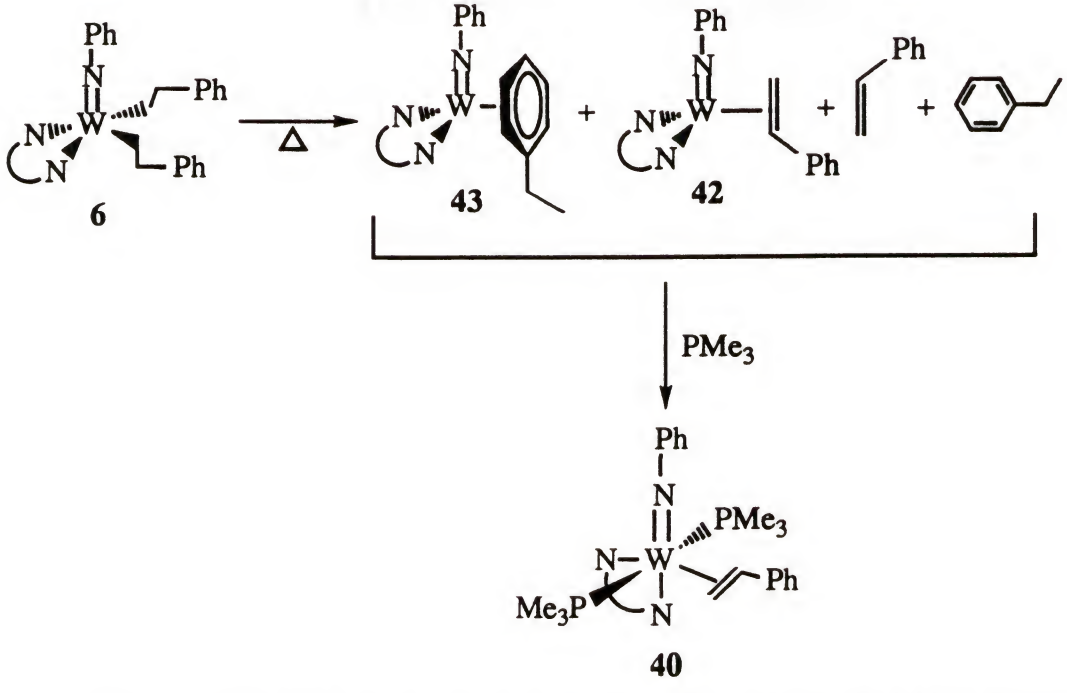

Complex **43** also shows reactivity towards hydrogenation of 2,3-dimethyl-1,3-butadiene. Upon addition of hydrogen, the diene is hydrogenated to a mixture of 2,3-dimethylbutane (major) and 2,3-dimethyl-2-butene (minor) (equation 5.16). The reactivity observed for **43**, but not **44** or **40**, is attributed to the less crowded metal environment and the absence of strong-coordinating phosphine ligands. Different selectivity has been reported, using $Cr(CO)_6$ as catalyst, for hydrogenation (1,4-addition of hydrogen) of 2,3-dimethyl-1,3-butadiene.[154]

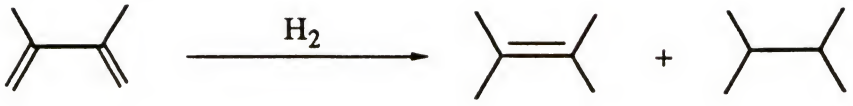

5.16

43	19%	81%
$Cr(CO)_6$	100%	0%

It is worth noting that the Mo analog of **43** exhibits much higher reactivity for hydrogenation of alkenes.[108] This can be attributed to the weaker Mo-arene bonds relative to W-arene bonds. It has been shown that the strength of metal-arene bonds, from microcalorimetric data, decreases down the series W >> Mo >> Cr.[155] Kinetic studies of the thermal arene exchange of $[M(CO)_3(\eta^6\text{-}MeC_6H_5)]$ with ^{14}C-labelled toluene also shows that the rates decreases markedly in the order of Mo >> W (10^2 : 1).[156] Details of the properties and potential utilities of these olefin and arene complexes of both tungsten and molybdenum are currently studied in our research group.

CHAPTER 6
EXPERIMENTAL PROCEDURES

Materials and Methods

All procedures were performed using standard Schlenk techniques or in a N_2-filled dry box. Diethyl ether (Et_2O), tetrahydrofuran (THF), pentane, and hexanes were distilled from sodium benzophenone ketyl; toluene was previously deolefinated by washing twice with cold H_2SO_4 followed by water and bicarbonate, and was then distilled from potassium metal; dichloromethane (CH_2Cl_2) was distilled from CaH_2. After collection, all solvents were stored under argon and over molecular sieves. Glassware was oven dried before use. All NMR solvents were degassed and stored over molecular sieves in the dry box prior to use. Complexes **21** - **25** and **28** - **32** are reported elsewhere.[51,69,71]

^1H, ^2H, ^{31}P and ^{13}C NMR spectra were measured at 300 MHz on a Varian Gemini 300 or VXR 300 spectrometer with C_6D_6 and C_7D_8 as solvents. The chemical shifts for ^1H and ^{13}C NMR are reported in parts per million downfield from tetramethylsilane ($\delta = 0$ ppm) and were referenced to residual protons of benzene and toluene in deuterated solvents. The chemical shifts for ^{31}P NMR are reported in parts per million downfield, referenced to H_3PO_4 (0 ppm). Mass spectrometry was performed by the UF Department of Chemistry Analytical Services. Elemental analyses (C,H,N) were performed by University of Florida Department of Chemistry Analytical Services or Atlantic Microlab, Inc., Norcross, GA. Chemicals used are purchased from Aldrich.

Syntheses

Preparation of [*o*-$(Me_3SiNH)_2C_6H_4$], **1**.

1,2-phenylenediamine (10.0 g, 0.092 mol) was placed in a Schlenk tube and dried under reduced pressure for 30 minutes. The solid was dissolved in Et_2O (250 mL), and the resulting solution was cooled to 0°C. $Si(CH_3)_3Cl$ (25.7 mL, 0.2 mol) was added dropwise, giving a light-pink precipitate. The mixture was stirred for 30 minutes. NEt_3 (28.3 mL, 0.2 mol) was added dropwise, and the thickened solution was stirred for 3 hours at room temperature. After the mixture was allowed to settle, the solvent was filtered off, and the remaining solid was extracted with cold pentane (0°C). The pentane and ether extracts were combined, and the solvent was removed under reduced pressure to give a pale yellow solid. Yield: 19.69 g (84.2 %). ^1H NMR (C_6D_6): δ 0.15 (s, 18H, -$SiMe_3$), 3.00 (s, 2H, -NH), 6.85 (m, 2H, aromatic), 6.95 (m, 2H, aromatic).

Preparation of W(NPh)[*o*-$(Me_3SiN)_2C_6H_4$]$(Cl)_2$, **2**.

N,N'-bis(trimethylsilyl)-*o*-phenylenediamine, **1**, (3.83 g, 15.16 mmol) was dissolved in 30 mL of Et_2O and cooled to -78°C. Two equivalents of n-BuLi (12.13 mL, 30.32 mmol, 2.5 M solution in hexanes) were then added. The reaction was warmed to room temperature and stirred for one hour. The reaction was recooled, and .95 equivalents of $W(NPh)Cl_4(OEt_2)$[50] (7.10 g, 14.4 mmol) in 20 mL of Et_2O was added. The reaction was allowed to warm to room temperature and stirred for three hours, then filtered through a celite pad, which, in turn, was rinsed with more Et_2O. Solvent was removed under reduced pressure and dried in vacuo for 3 hours. The dark red solid was washed with pentane until an orange powder remained. The powder was dried to yield 7.31 g of 1; 85.1%. ^1H NMR: 0.35 (s, 18H, -$Si(CH_3)_3$, $^2J_{Si-H}$ = 6.4Hz); 6.71 (t, 1H, *p*-NPh-H); 6.94 (m, 2H, aromatic); 7.01 (t, 2H, *m*-NPh-H); 7.14 (m, 2H, aromatic); 7.31 (d, 2H,

o-NPh-H); $^{13}C\{^1H\}$ NMR: 0.6 (-Si(CH_3)$_3$, J_{C-H} = 120.1 Hz); 122.0, 126.1, 128.1, 128.5, 128.6, 130.8 (aromatic). Anal. Calc'd for $C_{18}H_{27}N_3Cl_2Si_2W$: C, 36.25; H, 4.56; N, 7.05. Found: C, 35.91; H, 4.78; N, 6.78.

Preparation of W(NPh)[*o*-(Me_3SiN)$_2C_6H_4$](CH_3)$_2$, **3.**

W(NPh)[*o*-(Me_3SiN)$_2C_6H_4$](Cl)$_2$, **2**, (2.01g, 3.37 mmol) was dissolved in 50 ml of Et_2O and cooled to -78°C. Two equivalents of MeMgI (2.24ml, 6.74 mmol; 3.0M solution in Et_2O) were then added by a syringe. The reaction was allowed to warm to room temperature and was stirred for 1 hours, during which time a brownish-gold color appeared and salts precipitated. The solvent was then removed under reduced pressure, and the remaining brown solid was dried in vacuo for 2 hours. The solid was then extracted with pentane and filtered through a double-wrapped filter cannula until filtrate was almost clear. The solution was concentrated to about 10 ml and cooled to -78°C for two hours. The resulting golden solid was isolated by filtration and were dried under reduced pressure for 1 hour to yield 1.38 g of **3** as a yellow solid. Yield: 73.7%. ^1H NMR: 0.30 (s, 18H, -Si(CH_3)$_3$, $^2J_{Si-H}$ = 6.6Hz); 1.12 (s, 6H, -CH_3, $^2J_{W-H}$ = 6.0 Hz); 6.86 (t, 1H, *p*-NPh-H); 7.06 (m, 2H, aromatic); 7.11 (t, 2H, *m*-NPh-H); 7.32 (d, 2H, *o*-NPh-H); 7.35 (m, 2H, aromatic). $^{13}C\{^1H\}$ NMR: 1.25 (-Si(CH_3)$_3$, J_{C-H} = 119.5 Hz); 41.29 (-CH_3, J_{C-H} = 122.9 Hz, J_{W-C} = 74.1 Hz); 122.30, 124.85, 125.12, 125.79, 128.67, 131.21, 156.29 (aromatic). Anal. Calcd. for $C_{20}H_{33}N_3Si_2W$: C, 43.24; H, 5.99; N, 7.56. Found: C, 42.89; H, 5.94; N, 7.29.

W(NPh)[(*o*-Me_3SiN)$_2C_6H_4$](CH_2CH_3)$_2$, **4.**

W(NPh)[(*o*-Me_3SiN)$_2C_6H_4$](Cl)$_2$, **2**, (2.01g, 3.37 mmol) was dissolved in 50 ml of Et_2O and cooled to -78°C. Two equivalents of EtMgCl (3.37ml, 6.74 mmol; 2.0M

solution in Et_2O) were then added by a syringe. The reaction was allowed to warm to room temperature and was stirred for 1 hours, during which time a brown color appeared and salts precipitated. The solvent was then removed under reduced pressure, and the remaining brown-black oil was dried in vacuo for 3 hours. The oil was then extracted with pentane and filtered by filter cannula until filtrate was almost clear. The solvent was then removed under reduced pressure, and the remaining brown oil was dried in vacuo for 2 hours to yield 1.68 g of **4** as a thick red oil. Yield: 85.3%. ^{1}H NMR: 0.29 (s, 18H, -Si(CH_3)$_3$, $^2J_{Si-H}$ = 6.6Hz); 1.86 (t, 6H, -$CH_2\underline{C}H_3$); 1.91 (m, 2H, -$\underline{C}H_2CH_3$); 2.31 (m, 2H, -$\underline{C}H_2CH_3$); 6.86 (t, 1H, *p*-NPh-$\underline{H}$); 7.04 (m, 2H, aromatic); 7.11 (t, 2H, *m*-NPh-$\underline{H}$); 7.31 (d, 2H, *o*-NPh-$\underline{H}$); 7.37 (m, 2H, aromatic). ^{13}C{^{1}H} NMR: 1.5 (-Si(CH_3)$_3$, J_{C-H} = 119 Hz); 17.4 (-$CH_2\underline{C}H_3$, J_{C-H} = 122 Hz); 58.4 (-$\underline{C}H_2CH_3$, J_{C-H} = 120 Hz); 122.3, 123.9, 125.0, 125.6, 128.8, 135.1, 156.2 (aromatic).

W(NPh)[*o*-(Me_3SiN)$_2C_6H_4$](CH_2CD_3)$_2$, **4-*d*$_6$.**

Deuterated analog of **4** was prepared in the same way as described above. Grignard reagent, CD_3CH_2MgCl, used for alkylation reaction, was prepared from CD_3CH_2Cl (Exxon) and Mg^0 metal. ^{1}H NMR: 0.29 (s, 18H, -Si(CH_3)$_3$, $^2J_{Si-H}$ = 6.6Hz); 1.81 (m, 2H, -$\underline{C}H_2CD_3$); 2.19 (m, 2H, -$\underline{C}H_2CD_3$); 6.85 (t, 1H, *p*-NPh-$\underline{H}$); 7.03 (m, 2H, aromatic); 7.11 (t, 2H, *m*-NPh-$\underline{H}$); 7.26 (d, 2H, *o*-NPh-$\underline{H}$); 7.34 (m, 2H, aromatic).

Preparation of W(NPh)[*o*-(Me_3SiN)$_2C_6H_4$]($CH_2CH_2CH_3$)$_2$, **5.**

W(NPh)[*o*-(Me_3SiN)$_2C_6H_4$](Cl)$_2$, **2**, (1.0 g, 1.68 mmol) was dissolved in 30 mL of Et_2O and cooled to -78°C. Two equivalents of *n*-PrMgCl (1.7mL, 3.4 mmol; 2.0M solution in Et_2O) were then added by a syringe. The reaction was allowed to warm to room

temperature and was stirred for 1 hour, during which time a brown color appeared and salts precipitated. The solvent was then removed under reduced pressure, and the remaining brown-black oil was dried under reduced pressure for 3 hours. The oil was then extracted with pentane and filtered by filter cannula until filtrate was almost clear. The solvent was then removed under reduced pressure, and the remaining brown oil was dried *in vacuo* for 2 hours. Yield: 78%. ^{1}H NMR: 0.53 (s, 18H, -Si(CH_3)$_3$, $^{2}J_{Si\text{-}H}$ = 6.6Hz); 1.30 (t, 6H, -$CH_2CH_2C\underline{H}_3$); 1.92 (m, 2H, -$CH_2C\underline{H}_2CH_3$); 2.06 (dt, 2H, -$C\underline{H}_2CH_2CH_3$); 2.16 (m, 2H, -$CH_2C\underline{H}_2CH_3$); 2.33 (dt, 2H, -$C\underline{H}_2CH_2CH_3$); 7.09 (t, 1H, *p*-NPh-H); 7.27 (m, 2H, aromatic); 7.34 (t, 2H, *m*-NPh-H); 7.53 (d, 2H, *o*-NPh-H); 7.57 (m, 2H, aromatic). ^{13}C{^{1}H} NMR: 1.49 (-Si(CH_3)$_3$, $J_{C\text{-}H}$ = 119.3 Hz); 21.79 (-$CH_2CH_2\underline{C}H_3$, $J_{C\text{-}H}$ = 121.4 Hz); 26.70 (-$CH_2\underline{C}H_2CH_3$, $J_{C\text{-}H}$ = 132.2 Hz); 69.29 (-$\underline{C}H_2CH_2CH_3$, $J_{C\text{-}H}$ = 113.1 Hz); 122.36, 124.08, 125.04, 125.77, 128.64, 134.48, 156.42 (aromatic).

Preparation of W(NPh)[*o*-$(Me_3SiN)_2C_6H_4$]$(CH_2CH_2Ph)_2$, **6.**

W(NPh)[*o*-$(Me_3SiN)_2C_6H_4$]$(Cl)_2$, **2**, (2.0 g, 3.36 mmol) was dissolved in 50 mL of Et_2O and cooled to -78°C. Two equivalents of $PhCH_2CH_2MgCl$ (3.4 mL, 3.4 mmol; 2.0M solution in Et_2O) were then added by a syringe. The reaction was allowed to warm to room temperature and was stirred for 2 hours, during which time a brown color appeared and salts precipitated. The solvent was then removed under reduced pressure, and the remaining brown-orange solid was dried *in vacuo* for 3 hours. The solid was then extracted with pentane and filtered by filter cannula until the filtrate was almost clear. The solution was concentrated to about 10 mL and cooled to -78°C for three hours. The resulting orange solid was isolated by filtration and were dried under reduced pressure for 1 hour to yield 1.68 g of **6** as a orange crystalline solid. Yield: 68.2%. ^{1}H NMR: 0.30 (s, 18H, -Si(CH_3)$_3$); 2.09 (dt, 2H, -$C\underline{H}_2CH_2Ph$); 2.38 (dt, 2H, -$C\underline{H}_2CH_2Ph$); 2.91 (dt, 2H, -$CH_2C\underline{H}_2Ph$); 3.14 (dt, 2H, -$CH_2C\underline{H}_2Ph$); 6.86 (t, 1H, *p*-NPh-H); 6.99 (m, 5H,

aromatic); 7.02 (m, 2H, aromatic); 7.08 (t, 2H, *m*-NPh-H); 7.15 (m, 5H, aromatic); 7.22 (d, 2H, *o*-NPh-H); 7.39 (m, 2H, aromatic). $^{13}C\{^{1}H\}$ NMR: 1.48 (-Si$(CH_3)_3$, J_{C-H} = 118.3 Hz); 39.65 (-CH_2CH_2Ph, J_{C-H} = 123.4 Hz); 65.61 (-CH_2CH_2Ph, J_{C-H} = 119.2 Hz, J_{W-C} = 77.2 Hz); 122.83, 125.01, 125.20, 125.43, 125.58, 128.14, 128.48, 128.62, 132.95, 149.20, 156.22 (aromatic). Anal. Calcd. for $C_{34}H_{45}N_3Si_2W$: C, 55.50; H, 6.17; N, 5.71. Found: C, 55.23; H, 6.09; N, 5.75.

W(NPh)[*o*-$(Me_3SiN)_2C_6H_4$]$(CH_2CD_2Ph)_2$, **6-*d*$_4$.**

Deuterated analog of **6** was prepared in the same way as described above using Grignard reagent, $PhCD_2CH_2MgBr$, prepared from $PhCD_2CH_2Br$ and Mg^0. $PhCD_2CH_2Br$ was synthesized from $PhCD_2CH_2OH$ and PPh_3Br_2 in CH_2Cl_2. 2-Phenylethanol-2,2-*d*$_2$, $PhCD_2CH_2OH$, was prepared following the literature preparation method described in reference 147. NMR analysis showed >98% deuteration at the benzylic position. ^{1}H NMR: 0.25 (s, 18H, -Si$(CH_3)_3$); 2.08 (d, 2H, -CH_2CD_2Ph, $^{2}J_{H-H}$ = 12.6Hz); 2.38 (d, 2H, -CH_2CD_2Ph, $^{2}J_{H-H}$ = 12.9Hz); 6.78 - 7.42 (19H, aromatic). $^{13}C\{^{1}H\}$ NMR: 1.45 (s, -Si$(CH_3)_3$, J_{C-H} = 120.7 Hz); 38.93 (-CH_2CD_2Ph); 65.57 (-CH_2CD_2Ph, J_{C-H} = 122.3 Hz, J_{W-C} = 76.3 Hz); 122.86, 124.94, 125.22, 125.49, 125.64, 125.94, 128.54, 128.67, 133.04, 149.22, 156.30 (aromatic).

Preparation of W(NPh)[*o*-$(Me_3SiN)_2C_6H_4$]$(CH_2CH(CH_3)_2)_2$, **7.**

W(NPh)[*o*-$(Me_3SiN)_2C_6H_4$]$(Cl)_2$, **2**, (1.2 g, 2.01mmol) was dissolved in 50 mL of Et_2O and cooled to -78°C. Two equivalents of *i*-BuMgCl (2.01mL, 4.02mmol; 2.0M solution in Et_2O) were then added by a syringe. The reaction was allowed to warm to room temperature and was stirred for 1 hour, during which time a brown color appeared and salts precipitated. The solvent was then removed under reduced pressure, and the

remaining brown-black oil was dried *in vacuo* for 3 hours. The oil was then extracted with pentane and filtered by filter cannula until filtrate was almost clear. The solution was concentrated to about 10 mL and cooled to -78°C for three hours. The resulting golden-brown solid was isolated by filtration and was dried under reduced pressure for 1 hour to yield 0.78 g of **7** as a brown crystalline solid. Yield: 63.7%. ^{1}H NMR: 0.33 (s, 18H, -Si(CH_3)$_3$); 0.93 (d, 6H, -CH_2CH($\underline{CH_3}$)$_2$); 1.10 (d, 6H, -CH_2CH($\underline{CH_3}$)$_2$); 1.72 (m, 2H, -$C\underline{H_2}$CH(CH_3)$_2$); 1.94 (m, 2H, -$C\underline{H_2}$CH(CH_3)$_2$); 2.55 (m, 2H, -$CH_2C\underline{H}$(CH_3)$_2$); 6.84 (t, 1H, *p*-NPh-$\underline{H}$); 7.01 (m, 2H, aromatic); 7.12 (t, 2H, *m*-NPh-$\underline{H}$); 7.31 (d, 2H, *o*-NPh-$\underline{H}$); 7.36 (m, 2H, aromatic). ^{13}C{^{1}H} NMR: 2.20 (-Si(CH_3)$_3$, J_{C-H} = 119.3 Hz); 27.33 (-CH_2CH($\underline{CH_3}$)$_2$, J_{C-H} = 125.8 Hz); 29.15 (-CH_2CH($\underline{CH_3}$)$_2$, J_{C-H} = 126.5 Hz); 33.73 (-$CH_2\underline{C}$H(CH_3)$_2$, J_{C-H} = 127.2 Hz); 80.01 (-$\underline{C}H_2$CH(CH_3)$_2$); 121.79, 123.60, 125.46, 126.65, 128.62, 133.12, 155.97 (aromatic). Anal. Calcd. for $C_{26}H_{45}N_3Si_2W$: C, 48.82; H, 7.09; N, 6.57. Found: C, 48.54; H, 7.11; N, 6.50.

Preparation of W(NPh)[*o*-(Me_3SiN)$_2C_6H_4$](Ph)$_2$, **8.**

W(NPh)[*o*-(Me_3SiN)$_2C_6H_4$](Cl)$_2$, **2**, (1.0 g, 1.68 mmol) was dissolved in 50 mL of Et_2O and cooled to -78°C. Two equivalents of PhMgCl (1.12 mL, 3.36 mmol; 3.0M solution in Et_2O) were then added by a syringe. The reaction was allowed to warm to room temperature and was stirred for 2 hours, during which time a brown color appeared and salts precipitated. The solvent was then removed under reduced pressure, and the remaining brown-orange solid was dried in vacuo for 3 hours. The solid was then extracted with pentane and filtered by filter cannula until filtrate was almost clear. The solution was concentrated to about 10 mL and cooled to -78°C for three hours. The resulting orange solid was isolated by filtration and were dried under reduced pressure for 1 hour to yield 0.77 g of **8** as a purple crystalline solid. Yield: 67.6%. ^{1}H NMR: 0.12 (s,

18H, -Si(CH_3)$_3$); 6.80-7.66 (19 H overlapping aromatic protons). Anal. Calcd. for $C_{30}H_{37}N_3Si_2W$: C, 53.02; H, 5.49; N, 6.18. Found: C, 52.83; H, 5.44; N, 6.13.

Preparation of W(NPh)[*o*-(Me_3SiN)$_2C_6H_4$](CH_2Ph)$_2$, **9.**

W(NPh)[*o*-(Me_3SiN)$_2C_6H_4$](Cl)$_2$, **2**, (2.02 g, 3.39 mmol) was dissolved in 50 mL of Et_2O and cooled to -78 °C. Two equivalents of $ClMgCH_2Ph$ (6.77 mL, 6.77 mmol, 1.0 M soln. in Et_2O) were then added. The reaction was allowed to warm to room temperature after 15 minutes. After 30 minutes, solvent was removed under reduced pressure. The solid was extracted with pentane until clear and filtered through a double-wrapped filter cannula. The solution was concentrated to 10 mL and cooled to -78 °C to give 1.47 grams of **9** as a dark solid. Yield: 61.3%. ^{1}H NMR: 0.09 (s, 18H, -Si(CH_3)$_3$); 2.78 (s, 4H, -CH_2Ph); 6.81-7.37 (aromatic). $^{13}C\{^1H\}$ NMR: 2.10 (-Si(CH_3)$_3$); 66.33 (-$\underline{C}H_2$Ph); 123.49, 123.78, 125.65, 126.20, 126.51, 127.68, 128.04, 128.42, 128.61, 128.97, 154.20 (aromatic). Anal. Calc'd for $C_{32}H_{41}N_3Si_2W$: C, 54.31; H, 5.84; N, 5.94. Found: C, 53.98; H, 5.61; N, 5.69.

Preparation of W(NPh)[*o*-(Me_3SiN)$_2C_6H_4$]($CH_2C(CH_3)_3$)$_2$, **10.**

W(NPh)[*o*-(Me_3SiN)$_2C_6H_4$](Cl)$_2$, **2**, (2.78g, 4.66 mmol), was dissolved in 50 mL of Et_2O and cooled to -78°C. Two equivalents of $ClMgCH_2C(CH_3)_3$ (7.37 mL, 9.32 mmol, 1.27 M soln in Et_2O) were then added. The reaction was allowed to warm to room temperature after 30 minutes. After one hour, solvent was removed under reduced pressure. The solid was extracted with pentane until clear and filtered through a double-wrapped filter cannula. The solution was concentrated to a total volume of about 10 mL and cooled in a -78°C cold bath to yield 2.19 g dark crystals of **10.** Yield: 70.1%. ^{1}H NMR: 0.54 (s, 18H, -Si(CH_3)$_3$, $^2J_{Si\text{-}H}$ = 6.2Hz); 1.00 (s, 18H, -$CH_2C(\underline{CH_3})_3$); 2.13 (d,

2H, -C$\underline{H_2}$C$(CH_3)_3$, $^2J_{W\text{-}H}$ = 11.2 Hz); 2.29 (d, 2H, -C$\underline{H_2}$C$(CH_3)_3$, $^2J_{W\text{-}H}$ = 11.2 Hz); 6.83 (t, 1H, *p*-NPh-$\underline{H}$); 6.86 (m, 2H, aromatic); 7.19 (t, 2H, *m*-NPh-$\underline{H}$); 7.25 (m, 2H, aromatic); 7.59 (d, 2H, *o*-NPh-$\underline{H}$); . $^{13}C\{^1H\}$ NMR: 4.41 (-Si$(CH_3)_3$); 34.8 2(-$CH_2C(\underline{C}H_3)_3$); 38.33 (-$CH_2\underline{C}(CH_3)_3$); 90.81 (-$\underline{C}H_2C(CH_3)_3$, $^1J_{C\text{-}H}$ = 123.3 Hz); 118.91, 119.32, 126.01, 128.45, 129.22, 144.19, 155.78 (aromatic). Anal. Calc'd for $C_{28}H_{47}N_3Si_2W$: C, 50.52; H, 7.12; N, 6.31. Found: C, 50.36; H, 7.04; N, 6.14.

Prepararion of W(NPh)[*o*-$(Me_3SiN)_2C_6H_4$]$(CH_2C(CH_3)_2Ph)_2$, **11**.

W(NPh)[*o*-$(Me_3SiN)_2C_6H_4$]$(Cl)_2$, **2**, (2.04 g, 3.42 mmol) was dissolved in 50 mL of Et_2O and cooled to -78 °C. Two equivalents of $ClMgCH_2C(CH_3)_2Ph$ (6.55 mL, 6.84 mmol, 1.045 M soln in Et_2O) were then added. The reaction was allowed to warm to room temperature after 30 minutes. After one hour, solvent was removed under reduced pressure. The solid was extracted with pentane until clear and filtered through a double-wrapped filter cannula. The solution was concentrated to a total volume of about 15 mL and cooled in an -78 °C cold bath to yield 2.21 g of **11** as a light brown solid. Yield: 82.4%. ^1H NMR: 0.42 (s, 18H, -Si$(CH_3)_3$); 1.37 (s, 6H, -$CH_2C(\underline{CH_3})_2Ph$); 1.38 (s, 6H, -$CH_2C(\underline{CH_3})_2Ph$); 1.95 (s, 2H, -C$\underline{H_2}C(CH_3)_2Ph$); 2.94 (s, 2H, -C$\underline{H_2}C(CH_3)_2Ph$); 2.13 (d, 2H, -C$\underline{H_2}C(CH_3)_3$, $^2J_{W\text{-}H}$ = 11.2 Hz); 2.29 (d, 2H, -C$\underline{H_2}$C$(CH_3)_3$, $^2J_{W\text{-}H}$ = 11.2 Hz); 6.83 (t, 1H, aromatic), 6.94 (t, 2H, aromatic), 6.97 (m, 2H, aromatic), 7.01 (t, 4H, aromatic), 7.06 (t, 2H, aromatic), 7.18 (d, 4H, aromatic), 7.19 (d, 2H, aromatic), 7.30 (m, 2H, aromatic). $^{13}C\{^1H\}$ NMR: 4.11 (-Si$(CH_3)_3$); 32.51 (-$CH_2C(\underline{C}H_3)_2Ph$); 35.87 (-$CH_2C(\underline{C}H_3)_2Ph$); 44.2 (-$CH_2\underline{C}(CH_3)_2Ph$); 93.1 (-$\underline{C}H_2C(CH_3)_2Ph$, $^1J_{C\text{-}H}$ = 126.3 Hz); 119.41, 119.82, 125.51, 125.59, 126.12, 128.23, 128.38, 129.23, 143.78, 153.44, 155.21 (aromatic). Anal. Calc'd for $C_{38}H_{45}N_3Si_2W$: C, 58.23; H, 5.79; N, 5.36. Found: C, 57.95; H, 5.58; N, 5.29.

Prepararion of W(NPh)[*o*-$(Me_3SiN)_2C_6H_4$]$(CH_2Si(CH_3)_3)_2$, **12.**

W(NPh)[*o*-$(Me_3SiN)_2C_6H_4$]$(Cl)_2$, **2**, (2.0g, 3.35 mmol), was dissolved in 50 mL of Et_2O and cooled to -78°C. Two equivalents of $ClMgCH_2Si(CH_3)_3$ (5.23 mL, 6.70 mmol, 1.28 M soln in Et_2O) were then added. The reaction was allowed to warm to room temperature after 30 minutes. After one hour, solvent was removed under reduced pressure. The solid was extracted with pentane until clear and filtered through a double-wrapped filter cannula. The solution was concentrated to a total volume of about 10 mL and cooled in a -78°C cold bath to yield 1.98 g red crystals of **12.** Yield: 84.2%. ^1H NMR: 0.01 (s, 18H, $-CH_2Si(\underline{CH_3})_3$); 0.49 (s, 18H, $-NSi(CH_3)_3$); 1.32 (d, 2H, $-\underline{CH_2}Si(CH_3)_3$); 1.96 (d, 2H, $-\underline{CH_2}Si(CH_3)_3$); 6.85 (t, 1H, *p*-NPh-H); 6.91 (m, 2H, aromatic); 7.19 (t, 2H, *m*-NPh-H); 7.23 (m, 2H, aromatic); 7.52 (d, 2H, *o*-NPh-H); . $^{13}C\{^1H\}$ NMR: 2.93 ($-CH_2Si(\underline{C}H_3)_3$); 3.96 ($-NSi(\underline{C}H_3)_3$, $^1J_{Si-C}$ = 56.8 Hz); 63.64 ($-\underline{C}H_2Si(CH_3)_3$); 119.91, 126.37, 127.92, 128.51, 128.58, 142.55, 155.59 (aromatic). Anal. Calc'd for $C_{28}H_{47}N_3Si_2W$: C, 44.62; H, 7.06; N, 6.00. Found: C, 44.63; H, 7.02; N, 6.10.

W(NPh)[(*o*-$Me_3SiN)_2C_6H_4$]$(CH_2CH_3)Cl$, **13.**

W(NPh)[(*o*-$Me_3SiN)_2C_6H_4$]$(Cl)_2$, **2**, (0.7 g, 1.17 mmol) was dissolved in 20 ml of Et_2O and cooled to -78°C. One equivalents of EtMgCl (5.87 ml, 1.17 mmol; 2.0M solution in Et_2O) were then added by a syringe. The reaction was allowed to warm to room temperature and was stirred for 1 hours, during which time a brown color appeared and salts precipitated. The solvent was then removed under reduced pressure, and the remaining brown-black oil was dried in vacuo for 3 hours. The oil was then extracted with pentane and filtered by filter cannula until filtrate was almost clear. The solvent was then removed under reduced pressure, and the remaining brown solid was dried in vacuo for 2 hours to yield 0.31 g of **13** as a thick red oil. Yield: 45.1%. ^1H NMR: 0.24 (s, 9H,

-Si(CH_3)$_3$); 0.43 (s, 9H, -Si(CH_3)$_3$); 1.62 (t, 3H, -$CH_2C\underline{H}_3$, J = 7.5 Hz); 2.14 (dq, 1H, -$C\underline{H}_2CH_3$, J = 13.7(d); 7.6(q) Hz); 2.49 (dq, 1H, -$C\underline{H}_2CH_3$, J = 13.7(d); 7.6(q) Hz); 6.76 (t, 1H, *p*-NPh-H); 6.98 (m, 2H, aromatic); 7.07 (t, 2H, *m*-NPh-H); 7.26 (m, 2H, aromatic); 7.30 (d, 2H, *o*-NPh-H). Anal. Calcd. for $C_{20}H_{32}N_3ClSi_2W$: C, 40.72; H, 5.47; N, 7.12. Found: C, 40.81; H, 5.52; N, 7.12.

Preparation of W(NPh)[*o*-(Me_3SiN)$_2C_6H_4$](CH_2CH_2Ph)Cl , **14.**

W(NPh)[*o*-(Me_3SiN)$_2C_6H_4$](Cl)$_2$, **2**, (0.5 g, 0.84 mmol) was dissolved in 20 mL of Et_2O and cooled to -78°C. One equivalents of $PhCH_2CH_2MgCl$ (0.42 mL, 0.84 mmol; 2.0M solution in Et_2O) were then added by a syringe. The reaction was allowed to warm to room temperature and was stirred for 1 hours, during which time a brown color appeared and salts precipitated. The solvent was then removed under reduced pressure, and the remaining brown-orange solid was dried *in vacuo* for 3 hours. The solid was then extracted with cold pentane (0°C) and filtered by filter cannula until the filtrate was almost clear. The solution was concentrated to about 3 mL and cooled to -78°C for one hour. The resulting orange solid was isolated by filtration and were dried under reduced pressure for 1 hour to yield 0.37 g of **14** as a orange crystalline solid. Yield: 65.5%. ^{1}H NMR: 0.26 (s, 9H, -Si(CH_3)$_3$); 0.44 (s, 9H, -Si(CH_3)$_3$); 2.19 (dt, 1H, -$C\underline{H}_2CH_2Ph$, J = 4.5(d); 12.3(t) Hz); 2.58 (dt, 1H, -$C\underline{H}_2CH_2Ph$, J = 4.5(d); 12.3(t) Hz); 2.76 (dt, 1H, -$CH_2C\underline{H}_2Ph$, J = 4.5(d); 12.3(t) Hz); 2.93 (dt, 1H, -$CH_2C\underline{H}_2Ph$, J = 4.5(d); 12.3(t) Hz); 6.77 (t, 1H, *p*-NPh-H); 6.94 - 7.33 (m, 9H, aromatic). $^{13}C\{^1H\}$ NMR: 0.77 (-Si(CH_3)$_3$, $J_{C\text{-}H}$ = 119.4 Hz); 1.56 (-Si(CH_3)$_3$, $J_{C\text{-}H}$ = 119.8 Hz); 38.48 (-$CH_2\underline{C}H_2Ph$, $J_{C\text{-}H}$ = 123.6 Hz); 62.29 (-$\underline{C}H_2CH_2Ph$, $J_{C\text{-}H}$ = 124.8 Hz, $J_{W\text{-}C}$ = 83.8 Hz); 121.37, 122.14, 124.05, 125.55, 126.03, 126.98, 127.35, 128.25, 128.31, 128.49, 132.36, 135.84, 148.36, 155.64 (aromatic). Anal. Calcd. for $C_{26}H_{36}N_3ClSi_2W$: C, 46.89; H, 5.45; N, 6.31. Found: C, 46.55; H, 5.22; N, 6.11.

Preparation of W(NPh)[*o*-$(Me_3SiN)_2C_6H_4$]($CH_2C(CH_3)_3$)Cl, **15.**

W(NPh)[*o*-$(Me_3SiN)_2C_6H_4$]$(Cl)_2$, **2**, (2.0g, 3.35 mmol), was dissolved in 50 mL of Et_2O and cooled to -78°C. One equivalents of $ClMgCH_2C(CH_3)_3$ (2.65 mL, 3.35 mmol, 1.27 M soln in Et_2O) were then added. The reaction was allowed to warm to room temperature after 15 minutes. After stirring at room temperature for 45 minutes, solvent was removed under reduced pressure. The solid was extracted with pentane until clear and filtered through a double-wrapped filter cannula. The solution was concentrated to a total volume of about 10 mL and cooled in a -78°C cold bath to yield 1.41 g brown-red crystals of **15.** Yield: 66.2 %. ^{1}H NMR: 0.24 (s, 9H, $-Si(CH_3)_3$); 0.43 (s, 9H, $-Si(CH_3)_3$); 1.23 (s, 9H, $-CH_2C(\underline{CH_3})_3$); 1.93(d, 1H, $-C\underline{H_2}C(CH_3)_3$, J = 12.3 Hz, $^2J_{W-H}$ = 9.6 Hz); 2.08 (d, 1H, $-C\underline{H_2}C(CH_3)_3$, J = 12.3 Hz, $^2J_{W-H}$ = 8.4 Hz); 6.75 (t, 1H, *p*-NPh-H); 6.98 (m, 2H, aromatic); 7.10 (t, 2H, *m*-NPh-H); 7.21 (m, 2H, aromatic); 7.41 (d, 2H, *o*-NPh-H); . $^{13}C\{^1H\}$ NMR: 1.26 ($-Si(CH_3)_3$); 2.08 ($-Si(CH_3)_3$); 35.13 ($-CH_2C(\underline{C}H_3)_3$); 36.11 ($-CH_2\underline{C}(CH_3)_3$); 80.15 ($-\underline{C}H_2C(CH_3)_3$, $^1J_{C-H}$ = 121.2 Hz); 121.7, 122.3, 123.6, 126.1, 127.2, 1128.6, 132.0, 136.9, 155.9 (aromatic). Anal. Calc'd for $C_{23}H_{38}N_3ClSi_2W$: C, 43.71; H, 6.06; N, 6.65. Found: C, 43.38; H, 5.81; N, 6.09.

W(NPh)[*o*-$(Me_3SiN)_2C_6H_4$][η^2-(^{t}Bu)NC$CH_2CH_2Ph]_2$, **26.**

^{t}BuNC (0.16 mL, 1.37 mmol) was added via syringe to a 20 mL orange pentane solution of [W(NPh)[*o*-$(Me_3SiN)_2C_6H_4$]$(CH_2CH_2Ph)_2$, **6** (0.5 g, 0.68 mmol). The resulting green solution was stirred for 1 hour at room temperature. Subsequent concentration and cooling to -78°C for 1 hour resulted in a green solid, which was isolated by filtration and dried under reduced pressure for one hour to yield 0.42 g green crystals of **26.** Yield: 68.4 %. ^{1}H NMR: 0.33 (s, 9H, $-Si(CH_3)_3$); 0.82 (s, 9H, $-Si(CH_3)_3$); 1.46

(s, 18H, -C(CH_3)$_3$); 2.89 (dt, 1H, -CH_2CH_2Ph, J = 5.7(d); 13.2(t) Hz); 3.47 (dt, 1H, -CH_2CH_2Ph, J = 5.7(d); 13.2(t) Hz); 3.83 (dt, 1H, -CH_2CH_2Ph, J = 5.7(d); 13.2(t) Hz); 4.10 (dt, 1H, -CH_2CH_2Ph, J = 5.7(d); 13.2(t) Hz); 6.76 - 7.49 (m, 19H, aromatic). $^{13}C\{^1H\}$ NMR: 4.35 (-Si(CH_3)$_3$, J_{C-H} = 116.0 Hz); 5.72 (-Si(CH_3)$_3$, J_{C-H} = 117.8 Hz); 30.19 (-C(CH_3)$_3$); 33.35 (-C(CH_3)$_3$); 38.71 (-CH_2CH_2Ph); 61.01 (-CH_2CH_2Ph); 116.17, 116.36, 118.36, 125.23, 126.24, 126.84, 128.47, 129.03, 140.50, 150.29, 153.01, 156.06 (aromatic); 211.48 ((^{t}Bu)NCCH$_2$CH$_2$Ph). Anal. Calc'd for $C_{44}H_{63}N_5Si_2W$: C, 58.59; H, 7.04; N, 7.76. Found: C, 58.38; H, 7.08; N, 7.64.

W(NPh)[*o*-(Me_3SiN)$_2C_6H_4$][(^{t}Bu)NC(CH_2CH_2Ph)=C(CH_2CH_2Ph)N(^{t}Bu)] , **27.**

A 10 mL toluene solution of **26** (0.3 g, 0.33 mmol) in a round-bottom ampule was heated to 80°C for 3 days. The resulting red-orange solution was concentrated and cooled to -78°C for 1 hour. The resulting red solid was isolated via filtration and dried under reduced pressure for 1 hour to yield 0.18 g orange crystals of **27.** Yield: 60%. ^1H NMR: 0.47 (s, 18H, -Si(CH_3)$_3$); 1.33 (s, 18H, -C(CH_3)$_3$); 2.34 (m, 2H, -CH_2CH_2Ph); 2.75 (m, 2H, -CH_2CH_2Ph); 2.77 (m, 4H, -CH_2CH_2Ph); 6.52 - 7.28 (m, 19H, aromatic). $^{13}C\{^1H\}$ NMR: 4.38 (-Si(CH_3)$_3$, J_{C-H} = 117.9 Hz); 32.59 (-C(CH_3)$_3$, J_{C-H} = 126.0 Hz); 33.00 (-CH_2CH_2Ph); 35.52 (-CH_2CH_2Ph); 60.25 (-C(CH_3)$_3$); 118.86, 119.27, 126.17, 126.41, 126.59, 128.97, 142.79, 152.56, 156.74 (aromatic). Anal. Calc'd for $C_{44}H_{63}N_5Si_2W$: C, 58.59; H, 7.04; N, 7.76. Found: C, 58.38; H, 7.08; N, 7.64.

Preparation of W(NPh)[*o*-(Me_3SiN)$_2C_6H_4$](CHCMe_3)(PMe_3), **34.**

In a 200 mL glass tube fitted with a teflon Young's joint, W(NPh)[*o*-(Me_3SiN)$_2C_6H_4$] (CH_2CMe_3)$_2$, **10**, (1.25 g, 1.87 mmol) was dissolved in 25 mL of toluene. Five equivalents of PMe_3 (.968 mL, 9.35 mmol) were then added and the tube

was sealed. The reaction was then heated to 80 °C for 24 hours. The solution was transferred to a round-bottom Schlenk were solvent was removed under reduced pressure. The brown oil was extracted with pentane and the volume of the filtrate was concentrated to about 15 mL. The solution was cooled to -10 °C to yield 0.83 g of **34** as orange crystals. Yield: 66.0%. ^{1}H NMR: 0.38 (s, 9H, -Si(CH_3)$_3$); 0.41 (s, 9H, -Si'(CH_3)$_3$); 0.98 (d, 9H, -P$\underline{Me_3}$, $^{2}J_{W\text{-}C}$ = 9 Hz); 1.39 (s, 9H, -C$\underline{Me_3}$); 6.68-7.13 (m, 9H, aromatic). ^{13}C{^{1}H} NMR: 3.41 (-Si(CH_3)$_3$); 4.11 (-Si'(CH_3)$_3$); 16.22 (d, -P$\underline{Me_3}$); 34.93 (-C$\underline{Me_3}$); 45.04 (-$\underline{C}Me_3$); 117.61, 119.32, 122.44, 123.56, 124.71, 128.71, 148.13 (aromatic); 277.4 1(-$\underline{C}$HCMe3, $^{1}J_{C\text{-}H}$ = 110 Hz). Anal. Calc'd for $C_{26}H_{46}N_3PSi_2W$: C, 46.49; H, 6.90; N, 6.26. Found: C, 46.23; H, 6.81; N, 6.05.

Preparation of W($CH_2CH_2CH_2CH_2$)(NPh)[*o*-(Me_3SiN)$_2C_6H_4$], **35.**

W(NPh)[*o*-(Me_3SiN)$_2C_6H_4$](Cl)$_2$, **2**, (1.05g, 1.76 mmol) was dissolved in 50 mL of Et_2O and cooled to -78°C. One equivalent of $BrMgCH_2CH_2CH_2CH_2MgBr$ (1.75mL, 1.76 mmol; 0.99M solution in Et_2O, prepared from $BrCH_2CH_2CH_2CH_2Br$ and Mg^0 metal) was then added by a syringe. The reaction was allowed to warm to room temperature after one hour and was stirred for another two hours. The solvent was removed under reduced pressure and the resulting solid was dried *in vacuo* for three hours. The solid was then extracted with cold pentane (-78°C) and filtered through a double-wrapped filter cannula until the filtrate was almost clear. The solution was concentrated to about 10 mL and cooled to -78°C for two hours. The resulting golden solid was isolated by filtration and were dried under reduced pressure for 1 hour to yield 0.77 g of **35** as a brown solid. Yield: 75.2%. ^{1}H NMR: 0.28 (s, 18H, -Si(CH_3)$_3$); 1.54 (m, 2H, α-CH); 2.42 (m, 2H, β-CH); 2.91 (m, 2H, β-CH'); 2.93 (m, 2H, α-CH'); 6.86-7.44 (m, 9H, aromatic). ^{13}C{^{1}H} and ^{13}C NMR: 1.08 (-Si(CH_3)$_3$, $^{2}J_{Si\text{-}H}$ = 6.6Hz, $J_{C\text{-}H}$ = 119.1Hz); 35.23 (β-C, $J_{C\text{-}H}$ = 124.3Hz); 61.25 (α-C, $J_{W\text{-}C}$ = 73.6Hz, $J_{C\text{-}H}$ = 122.9Hz). Anal.

Calcd. for $C_{22}H_{35}N_3Si_2W$: C, 45.43; H, 6.07; N, 7.23. Found: C, 45.19; H, 5.97; N, 7.03.

Preparation of W(NPh)[*o*-$(Me_3SiN)_2C_6H_4$](CH_2-*t*-$BuCH_2CH_2$), **36.**

W(NPh)[*o*-$(Me_3SiN)_2C_6H_4$]($CHCMe_3$)(PMe_3) , **34** (1 g, 1.49 mmol) was dissolved in 50 mL of hexane and allowed to reacte with 16 psi of ethylene in the presence of excess neohexene at room temperature for 30 minutes. The solvent was removed under reduced pressure and the resulting solid was dried in vacuo for one hour. The solid was then extracted with pentane and filtered by cannula. The solution was concentrated to about 10 mL and cooled to -78°C for one hour. The resulting golden solid was isolated by filtration and were dried under reduced pressure for 1 hour to yield red orangre solid at 54% yield. ^{1}H NMR: 0.24 (s, 9H, -Si$(CH_3)_3$); 0.26 (s, 9H, -Si'$(CH_3)_3$); 0.39 (m, 1H, -C<u>H</u>^{t}$BuCH_2CH_2$); 0.71 (m, 1H, -CH^t$BuCH_2C$<u>H$_2$</u>); 1.21 (s, 9H, *t*-Bu); 2.45 (m, 1H, -CH^t$BuCH_2C$<u>H$_2$</u>); 2.61 (m, 1H, -CH^tBuC<u>H$_2$</u>CH_2); 3.75 (m, 1H, -CH^tBuC<u>H$_2$</u>CH_2); 6.82-7.44 (m, 9H, aromatic). ^{13}C{^{1}H} NMR: 1.35 (s, -Si$(CH_3)_3$); 1.54 (s, -Si'$(CH_3)_3$); 25.07 (-CH^tBuC<u>H$_2$</u>CH_2); 38.80 (-CH^t$BuCH_2C$<u>H$_2$</u>, $^1J_{W\text{-}C}$ = 49.4Hz); 77.58 (-<u>C</u>H^t$BuCH_2CH_2$, $J_{W\text{-}C}$ = 56.1 Hz).

Preparation of W(NPh)[*o*-$(Me_3SiN)_2C_6H_4$](η^2-C_2H_4)(PMe_3)$_2$, **39.**

In a glass tube with a Teflon Young's joint, W(NPh)[*o*-$(Me_3SiN)_2C_6H_4$]$(CH_2CH_3)_2$, **4** (1.35 g, 2.32 mmol) was dissolved in 50 mL of pentane. Five equivalents of PMe_3 (1.19 mL, 11.56 mmol) were added by a syringe, then the flask was sealed. The reaction was stirred at room temperature for 4 hours, during which time the brown solution turned purple and purple crystals precipitated. The mixture was transferred to a Schlenck tube and purple crystals were isolated. The mother liquors

were reduced in volume under reduced pressure and cooled to -78°C to give more solid. Total yield: 1.44g, 88.3%. ^{1}H NMR: 0.31 (s, 9H, -Si(CH_3)$_3$); 0.60 (s, 9H, -Si'(CH_3)$_3$); 1.03 (s, 18H, -P$\underline{Me_3}$); 1.91 (m, C_2H_4); 2.09 (m, C_2H_4); 6.61-7.42 (aromatic). ^{13}C{^{1}H} NMR: 2.67 (-Si(CH_3)$_3$); 6.34 (-Si'(CH_3)$_3$); 15.78 (s, -P$\underline{Me_3}$); 38.13 (s, $\underline{C_2H_4}$, J_{C-H} = 156.2Hz); 122.23, 123.13, 124.28, 125.51, 127.23, 128.91, 129.23, 129.78, 158.23 (aromatic); Anal. Calcd. for $C_{26}H_{49}N_3Si_2P_2W$: C, 44.25; H, 7.00; N, 5.95. Found: C, 43.91; H, 6.79; N, 5.78.

W(NPh)[(*o*-$Me_3SiN)_2C_6H_4$](η^2-CH_2=CHPh)(PMe_3)$_2$, **40.**

In a glass tube with a Rotoflo joint, W(NPh)[(*o*-$Me_3SiN)_2C_6H_4$](CH_2CH_2Ph)$_2$, **6** (0.8 g, 1.09 mmol) was dissolved in 50 mL of pentane. Five equivalents of PMe_3 (0.56 ml, 5.45 mmol) were added by a syringe, then the flask was sealed. The reaction was heated to 80°C and was stirred for 8 hours, during which time the solution changed color from brown to purple. The solvent was then removed under reduced pressure and the remaining brown-purple oil was dried overnight. The oil was then redissolved in minimum amount of pentane and cooled to -78°C for 2 hours. The resulting brown-purple solid was isolated by filtration and were dried under reduced pressure for 1 hour to yield 0.48 g of **40**. Yield: 56.3%. ^{1}H NMR: 0.41 (s, 18H, -Si(CH_3)$_3$); 0.86 (s, 18H, -P$\underline{Me_3}$); 2.62 (m, -C$\underline{H_2}$CHPh); 2.80 (m, -C$\underline{H_2}$CHPh); 3.87 (t, -CH_2C$\underline{H}$Ph); 6.41-7.24 (aromatic). Anal. Calcd. for $C_{32}H_{53}N_3Si_2P_2W$: C, 49.16; H, 6.83; N, 5.38. Found: C, 48.80; H, 6.71; N, 5.22.

W(NPh)[(*o*-$Me_3SiN)_2C_6H_4$](η^2-CH_2=$CHCH_3$)(PMe_3)$_2$, **41.**

41 can be observed in the reaction of **5** with PMe_3. ^{1}H NMR: 0.44 (br,s, 18H, -Si(CH_3)$_3$); 1.02 (s, 18H, -PMe_3); 1.62 (dd, 1H, -CH_2CHCH_3); 2.39 (dd, 1H, -CH_2CHCH_3); 2.55 (d, 3H, -CH_2CHCH_3); 2.85 (m, 1H, -CH_2CHCH_3); 6.42-7.58 (aromatic).

W(NPh)[*o*-$(Me_3SiN)_2C_6H_4$]$(H)_2(PMe_3)_2$, **44**

Method 1:

In a glass tube with a Teflon Young's joint, W(NPh)[*o*-$(Me_3SiN)_2C_6H_4$]$(CH_2C(CH_3)_3)_2$, **10** (1.66 g, 2.48 mmol), was dissolved in 25 mL of hexanes. PMe_3 (0.64 mL, 6.20 mmol) was added via syringe. The solution was then placed in liquid nitrogen while a vacuum was applied. Once the solution was frozen solid under vacuum, the flask was sealed. The neck of the flask was then purged with hydrogen gas and the H_2 hose was wired securely to the flask. The flask was opened until the H_2 reached a pressure of 10 PSI. The flask was then resealed and the H_2 line removed. The reaction was then allowed to warm to room temperature. After four hours of stirring, the color of the solution changed from brown to magenta, and magenta crystals precipitated from solution. The remaining solution was transferred to a Schlenk tube and cooled to -10 °C to give additional magenta crystals. The mother liquors were concentrated and cooled to give an additional yield. Total Yield of **44**: 1.48 g (87.8%). ^1H NMR: 0.79 (s, 9H, -$Si(CH_3)_3$); 0.81 (s, 9H, -$Si'(CH_3)_3$); 1.04 (s, 18H, -P$\underline{Me_3}$); 6.80-7.45 (m, 9H, aromatic); 9.26 (t, 2H, W-H). $^{13}C\{^1H\}$ NMR: 4.92 ($Si(CH_3)_3$); 6.43 (-$Si'(CH_3)_3$); 15.99 (s, -P$\underline{Me_3}$); 115.21, 116.53, 118.17, 119.20, 123.31, 126.71, 128.68, 151.13 (aromatic). ^{31}P NMR: -24.46 (s, $^1J_{W\text{-}P}$ = 188 Hz). Anal Calcd for $C_{24}H_{47}N_3P_2Si_2W$: C, 42.41; H, 6.97; N, 6.18. Found: C, 42.18; H, 6.79; N, 6.03.

Method 2:

W(NPh)[*o*-$(Me_3SiN)_2C_6H_4$](CHCMe$_3$)(PMe$_3$), **34**, (50 mg, 0.07 mmol) was dissolved in C_6D_6 in an NMR tube fitted with a teflon Young's joint. One equivalent of PMe$_3$ (7 mL, 0.07 mmol) was added via a microliter syringe. The NMR tube was then fitted with a Schlenk adapter, frozen in liquid nitrogen, and placed under vacuum. The tube was then sealed while frozen, under vacuum. Hydrogen gas was then purged through the Schlenk adapter for five minutes. The teflon seal was opened to allow the H_2 to fill the vacuum in the NMR tube. The NMR tube was charged with about 15 PSI of H_2. Over a period of less than 2 hours, complete conversion of **34** to **44** was observed by ^{1}H NMR.

W(NPh)[*o*-$(Me_3SiN)_2C_6H_4$]$(H)_2$(DPPE), **45**

In a glass tube with a Teflon Young's joint, W(NPh)[*o*-$(Me_3SiN)_2C_6H_4$]$(CH_2C(CH_3)_3)_2$, **10**, (0.65 g, 0.98 mmol) and DPPE (0.39 g, 0.98 mmol) were dissolved in 30 mL of hexanes. The solution was then placed in liquid nitrogen while a vacuum was applied. H_2 gas was introduced as described for **44**. The reaction was then allowed to warm to room temperature. After eight hours of stirring, the color of the solution had changed from brown to purple. Purple solid had also precipitated from solution. The solution was transferred to a Schlenk tube, concentrated to 10 mL, and cooled to -10 °C to give additional purple solid. Total Yield: 0.71 g (78.2%). ^{1}H NMR: 0.49 (s, 18H, -Si$(CH_3)_3$); 2.23 (m, 2H, PC$\underline{H_2}$C$\underline{H_2}$P); 2.42 (m, 2H, PC$\underline{H_2}$C$\underline{H_2}$P); 6.72-7.69 (aromatic); 10.33 (d, 1H, W-H); 10.62 (d, 1H, W-H). ^{31}P NMR: 30.43 (d, $^2J_{P\text{-}P}$ = 83 Hz); -12.70 (d, $^2J_{P\text{-}P}$ = 83 Hz). Anal. Calcd. for $C_{44}H_{53}N_3Si_2P_2W$: C, 57.08; H, 5.77; N, 4.54. Found: C, 57.33; H, 5.84; N, 4.54.

Kinetics Study

Sealable NMR tube samples were prepared by dissolving **6** and **6**-d_4 (ca. 10mg) in 0.44 ml of toluene-d_8 solution. Concentration of **4** and **4**-d_6 samples was obtained from a known concentration of $(\eta^5\text{-}C_5H_5)_2Fe$ as internal standard. The samples were sealed and stored at -196°C immediately after adding desired amount of PMe_3. The NMR probe was equilibrated to the desired temperature and the sample was thawed and well shaken prior to loading into the probe. Approximately 18 spectra were recorded at increasing intervals (more points for early stage of reaction) over the duration more than 3 half-lives. Absolute peak intensities of the trimethylsilyl peaks for both starting material and product were recorded for each spectrum. The observed rate constants were obtained from the slope of the plots of Ln(Intensity) *vs* time. Three samples were performed at each temperature and the rate constants reported were the average of all three runs. Activation parameters were obtained by measuring rate constants at four different temperatures. A plot of Ln(k/T)*vs* 1/T (T, temperature in Kelvin) results in a line with a slope of $-\Delta H^{\ddagger}/R$ and an intercept of $[(\Delta S^{\ddagger}/R)+23.76]$. Reported errors in the rate constants represent the standard deviation from the least squares fit of the experimental data. Reported errors in the activation parameters are obtained from all experimental data (12 points in the Eyring plot), using 2σ. Procedure of using the Gemini 300 NMR spectrometer for kinetic study is shown in **Scheme 6.A.**

Scheme 6.A. Peocedure for kinetic study using Gemini 300 NMR spectrometer.

Spectrometer

JEXP4 * only experiment 4 has enough memory to run the array experiments
SETUP(H,SOLVENT)
LK & SHIMI * as usual
START * run a simple proton first to prevent "ADC OVERFLOW"
GAIN=Y
PAD(1)=0,600,600,600,.....600
* This command is to set the Pre-Acquisition Delay as the time interval (in second) you desire between the end of the previous acquisition and the beginning of the following acquisition. The example shown above is to run the first experiment as you start (0 second delay) and then run the others every 600 seconds. You can run as many as 18 FIDs. ("VALUE OUT OF NORMAL RANGE" will appear when you set up for a long period of time. Neglect the message!)
AI * Absolute Intensity: The relative intensity of each spectrum will not change when you adjust the peak intensity, which gives you a reliable kinetic analysis.
START
SAVE * All spectra will be saved as one file. To look at each spectrum: use the command **WFT(N)** , N is the index of the spectrum (1,2,3,....).

Sparc Station

* transfer the file, load, WFT, phase, set reference... as usual.
* expand the region and select the peaks (TH) that you want to analyze.

WFT DSSH FULL DS APH
* Fourier transform each FID, display all spectra, then display the full size spectrum. (DSSH: display all spectra horizontally. DSSA: display stacked spectra. To print those spectra: PL(first, last); e.g. PL(1,18))
DLL FP * Display chemical shift and intensity of each peak then flip page.
KIND or **KINI**
* Kinetic analysis for peak decreasing (KIND) or increasing (KINI) will give you the information of intensity change wwith respect to time for each peak. You can click on FLIP to see the result on the text window.
PRINTON DLL KIND TEXT
* Print the information of chemical shifts(DLL), kinetic analysis result(KIND), and others(TEXT) to a text file.
PRINTOFF * Print the text file to the printer.
* You can also use command "**EXPL**" to see the plot (intensity *vs* time).

Phosphine Dependence

Sealable NMR tube samples were prepared and experiments were carried out as described above. To determine the dependence of the PMe_3 concentration on the observed rate constants, a series of experiments were carried out with **4** and **6** with various concentrations of PMe_3. Plotting the observed rate constants obtained from these experiments *vs* the concentration of added PMe_3 gave a line in the case of **4** and **6** (at high concentration). The order of PMe_3 (**4**) was determined from the slope (1.096) of the plot of Lnk *vs* Ln[PMe3].

Hydrogenation Reaction

In a sealable NMR tube, the desired catalyst was dissolved in C_6D_6 and excess olefins were added. The solution was then placed in isopropanol/dry ice bath (-78^{0}C) while a vacuum was applied. Once the solution was frozen solid under vacuum, the tube was sealed. The adapter of the tube was then purged with hydrogen for 30 seconds and connected securely to the tube. The tube was opened until the H_2 reached a pressure of 20 PSI. The tube was then resealed and the H_2 line removed. The reaction was then allowed to warm to room temperature. The reaction was monitored by ^{1}H NMR spectroscopy and the turnover number was determined by the relative integrals of the catalyst, olefins, and the hydrogenated products.

The hydrogenation of styrene, using **43**, was performed inside a high pressure reactor. The mixture of styrene and catalytic amount of **43** were sealed in the reactor (dry box) and hydrogen was added via a high pressure tube until the H_2 reached a pressure of 1000 PSI. Values of TOF and TON were obtained from the relative ratio of styrene and

ethylbenzene via ^1H NMR spectroscopy. Internal standard (ferrocene) was also used to determine the correct turnover numbers.

Crystallographic Studies

X-ray data collection and structure refinement for compounds **3**, **10** and **21**.

Data for **3**, **10** and **21**were collected at 173 K on a Siemens SMART PLATFORM equipped with a CCD area detector and a graphite monochromator utilizing MoK_α radiation (λ= 0.71073 Å). Cell parameters were refined using the entire data set. A hemisphere of data (1321 frames) was collected for each crystal using the ω-scan method (0.3° frame width). The first 50 frames were remeasured at the end of data collection to monitor instrument and crystal stability (maximum correction on I was < 1 %). Psi scan absorption corrections were applied based on the entire data set. The structures of **3**, **10** and **21** were solved by the Direct Methods in *SHELXTL5*,[157] and refined using full-matrix least squares. The non-H atoms were treated anisotropically, whereas the hydrogen atoms were calculated in ideal positions and were riding on their respective carbon atoms. 244, 307 and 151 parameters were refined in the final cycle of refinement for **3**, **10** and **21**, respectively, using 4572, 5881 and 3057 reflections for **3**, **10** and **21**, respectively, with $I > 2\sigma(I)$ to yield R_1 and wR_2 of 2.47, 2.72 and 5.97 and 7.12, 5.71 and 2.61, for **3**, **10** and **21**, respectively. Refinement of **3**, **10** and **21** was done using F^2. The final atomic coordinates for the non-hydrogen atoms of **3**, **10** and **21** are given in **Tables A1.1-A1.5, A4.1-A4.5, A6.1-A6.5** of Appendix A.

X-ray data collection and structure refinement for compounds **35** and **39.**

Data for both compounds were collected at 173 K on a Siemens CCD SMART PLATFORM equipped with a CCD area detector and a graphite monochromator utilizing MoK_α radiation ($\lambda = 0.71073$ Å). Cell parameters were refined using 8192 and 8173 reflections for **39** and **35**, respectively. A hemisphere of data (1381 frames) was collected using the ω-scan method (0.3° frame width). The first 50 frames were remeasured at the end of data collection to monitor instrument and crystal stability (maximum correction on I was < 1 %). Absorption corrections were applied based on the psi scan using the entire data set for **39**, and based on measured crystal faces for **35**.

Both structures were solved by the Direct Methods in *SHELXTL*, and refined using full-matrix least squares on F^2. The non-H atoms were refined with anisotropic thermal parameters except for the disordered C atoms. All of the H atoms were included in the final cycle of refinement and were riding on the atoms to which they are bonded. The ethylene ligand in **35** was found to be disordered in the 2 and 3 positions. Two partial $-CH_2CH_2-$ were refined with isotropic thermal parameters and their occupation factors refined depentenly to 0.54(2) for one, and consequently 0.46(2) for the other. The final atomic coordinates for the non-hydrogen atoms of **35** and **39** are given in **Tables A7.1-A9.5** of Appendix A.

X-ray data collection and structure refinement for compound **6.**

Data were collected at 173 K on a Siemens SMART PLATFORM equipped with A CCD area detector and a graphite monochromator utilizing MoK_αradiation ($\lambda = 0.71073$ Å). Cell parameters were refined using up to 8192 reflections. A hemisphere of data (1381 frames) was collected using the ω-scan method (0.3° frame width). The first 50 frames were remeasured at the end of data collection to monitor instrument and crystal

stability (maximum correction on I was < 1 %). Psi scan absorption corrections were applied based on the entire data set.

The structure was solved by the Direct Methods in *SHELXTL5*, and refined using full-matrix least squares. The non-H atoms were treated anisotropically, whereas the hydrogen atoms were calculated in ideal positions and were riding on their respective carbon atoms. 362 parameters were refined in the final cycle of refinement using 5292 reflections with $I > 2\sigma(I)$ to yield R_1 and wR_2 of 3.4 and 7.29% , respectively. Refinement was done using F^2. The final atomic coordinates for the non-hydrogen atoms of **6** are given in **Tables A2.1-A2.5** of Appendix A.

X-ray data collection and structure refinement for compound **7.**

Data for compound **7** were collected at 173 K on a Siemens SMART PLATFORM equipped with A CCD area detector and a graphite monochromator utilizing Mo K_α radiation ($\lambda = 0.71073$ Å). Cell parameters were refined using up to 9856 reflections for **7**. A hemisphere of data (1381 frames) was collected using the ω-scan method (0.3^0 frame width). The first 50 frames were remeasured at the end of data collection to monitor instrument and crystal stability (maximum correction on I was < 1 %). Psi scan absorption corrections were applied based on the entire data set.

Both structures were solved by the Direct Methods in *SHELXTL5*, and refined using full-matrix least squares. The non-H atoms were treated anisotropically, whereas the hydrogen atoms were calculated in ideal positions and were riding on their respective carbon atoms. 470 parameters were refined **7** in the final cycle of refinement using 6252 reflections with $I > 2\sigma(I)$ to yield R_1 and wR_2 of 1.65 and 3.94%, respectively. Refinement was done using F^2. The final atomic coordinates for the non-hydrogen atoms of **7** are given in **Tables A3.1-A3.5** of Appendix A.

APPENDIX A
TABLES OF CRYSTALLOGRAPHIC DATA

Crystallographic Data for W(NPh)[*o*-$(Me_3SiN)_2C_6H_4$]$(CH_3)_2$, **3.**

Table A1.1: Crystallographic Data

Empirical formula	$C_{20}\ H_{33}\ N_3\ Si_2\ W$
Formula weight	555.52
Temperature	173(2) K
Wavelength	0.71073 Å
Crystal system	Monoclinic
Space group	P2(1)/n
Unit cell dimensions	a = 10.3545(2) Å $\alpha = 90°$
	b = 17.9669(1) Å $\beta = 103.826(1)°$
	c = 13.3168(1) Å $\gamma = 90°$
Volume, Z	2405.65(5) $Å^3$, 4
Density (calculated)	1.534 Mg/m^3
Absorption coefficient	4.910 mm^{-1}
F(000)	1104
Crystal size	0.29 x 0.24 x 0.15 mm
Theta range for data collection	3.15° to 27.38°
Limiting indices	$-5 \le h \le 13$, $-7 \le k \le 22$, $-17 \le l \le 16$
Reflections collected	8305
Independent reflections	4830 [R(int) = 0.0232]
Refinement method	Full-matrix least-squares on F^2
Data / restraints / parameters	4830 / 0 / 244
Goodness-of-fit on F^2	1.164
Final R indices [I>2sigma(I)]	$R_1 = 0.0247$, $wR_2 = 0.0597$
R indices (all data)	$R_1 = 0.0267$, $wR_2 = 0.0613$
Extinction coefficient	0.0020(2)
Largest diff. peak and hole	0.768 and -1.190 e.$Å^{-3}$

$R_1 = \hat{A}(||F_o| - |F_c||) / \hat{A}|F_o|$

$wR_2 = [\hat{A}[w(F_o^2 - F_c^2)^2] / \hat{A}[w(F_o^2)^2]]^{1/2}$

$S = [\hat{A}[w(F_o^2 - F_c^2)^2] / (n-p)]^{1/2}$

$w = 1/[s^2(F_o^2)+(0.0370*p)^2+0.31*p]$, $p = [\max(F_o^2,0)+ 2* F_c^2]/3$

Table A1.2. Atomic coordinates (x 10^4) and equivalent isotropic displacement parameters (A^2 x 10^3) for **3**. U(eq) is defined as one third of the trace of the orthogonalized Uij tensor.

Atom	x	y	z	U(eq)
W	8179(1)	2164(1)	1863(1)	27(1)
Si(1)	8354(1)	1568(1)	-575(1)	31(1)
Si(2)	7168(1)	4012(1)	1687(1)	34(1)
N(1)	8828(3)	2094(2)	562(2)	29(1)
N(2)	8202(3)	3258(2)	1569(2)	29(1)
N(3)	6657(3)	1756(2)	1863(2)	35(1)
C(1)	9579(4)	1269(2)	2417(3)	43(1)
C(2)	8826(5)	2482(3)	3482(3)	45(1)
C(3)	7806(5)	4522(2)	2921(3)	46(1)
C(4)	7070(5)	4638(3)	560(3)	52(1)
C(5)	5508(4)	3609(3)	1633(4)	56(1)
C(6)	6925(5)	981(2)	-455(3)	47(1)
C(7)	9724(5)	945(3)	-756(4)	54(1)
C(8)	7893(5)	2248(2)	-1648(3)	51(1)
C(9)	9740(4)	2682(2)	720(2)	28(1)
C(10)	10938(4)	2697(2)	393(3)	33(1)
C(11)	11753(4)	3313(2)	578(3)	35(1)
C(12)	11422(4)	3927(2)	1100(3)	35(1)
C(13)	10263(3)	3928(2)	1452(3)	30(1)
C(14)	9400(3)	3314(2)	1262(2)	26(1)
C(15)	5490(3)	1445(2)	2015(3)	30(1)
C(16)	4348(4)	1388(3)	1217(3)	48(1)
C(17)	3211(4)	1066(3)	1424(4)	57(1)
C(18)	3204(4)	808(2)	2392(4)	50(1)
C(19)	4323(4)	878(2)	3174(3)	43(1)
C(20)	5466(4)	1188(2)	2993(3)	35(1)

Table A1.3. Bond lengths (Å) and angles [°] for **3**.

W-N(3)	1.738(3)
W-N(2)	2.006(3)
W-N(1)	2.007(3)
W-C(1)	2.173(4)
W-C(2)	2.176(4)
Si(1)-N(1)	1.752(3)
Si(1)-C(8)	1.853(4)
Si(1)-C(6)	1.855(4)
Si(1)-C(7)	1.868(4)
Si(2)-N(2)	1.757(3)
Si(2)-C(5)	1.851(4)
Si(2)-C(4)	1.858(4)
Si(2)-C(3)	1.860(4)
N(1)-C(9)	1.399(5)
N(2)-C(14)	1.399(4)
N(3)-C(15)	1.389(4)
C(1)-H(1A)	0.96
C(1)-H(1B)	0.96
C(1)-H(1C)	0.96
C(2)-H(2A)	0.96
C(2)-H(2B)	0.96
C(2)-H(2C)	0.96
C(3)-H(3A)	0.96
C(3)-H(3B)	0.96
C(3)-H(3C)	0.96
C(4)-H(4A)	0.96
C(4)-H(4B)	0.96
C(4)-H(4C)	0.96
C(5)-H(5A)	0.96
C(5)-H(5B)	0.96
C(5)-H(5C)	0.96
C(6)-H(6A)	0.96
C(6)-H(6B)	0.96
C(6)-H(6C)	0.96
C(7)-H(7A)	0.96
C(7)-H(7B)	0.96
C(7)-H(7C)	0.96
C(8)-H(8A)	0.96
C(8)-H(8B)	0.96
C(8)-H(8C)	0.96
C(9)-C(10)	1.411(5)
C(9)-C(14)	1.434(5)
C(10)-C(11)	1.377(5)
C(10)-H(10A)	0.93
C(11)-C(12)	1.390(5)
C(11)-H(11A)	0.93
C(12)-C(13)	1.389(5)
C(12)-H(12A)	0.93
C(13)-C(14)	1.404(5)

C(13)-H(13A)	0.93
C(15)-C(20)	1.387(5)
C(15)-C(16)	1.392(5)
C(16)-C(17)	1.398(6)
C(16)-H(16A)	0.93
C(17)-C(18)	1.372(7)
C(17)-H(17A)	0.93
C(18)-C(19)	1.366(7)
C(18)-H(18A)	0.93
C(19)-C(20)	1.380(5)
C(19)-H(19A)	0.93
C(20)-H(20A)	0.93

N(3)-W-N(2)	117.81(13)
N(3)-W-N(1)	117.64(13)
N(2)-W-N(1)	82.55(11)
N(3)-W-C(1)	102.7(2)
N(2)-W-C(1)	138.87(14)
N(1)-W-C(1)	84.98(14)
N(3)-W-C(2)	100.2(2)
N(2)-W-C(2)	85.5(2)
N(1)-W-C(2)	141.7(2)
C(1)-W-C(2)	80.5(2)
N(1)-Si(1)-C(8)	106.2(2)
N(1)-Si(1)-C(6)	107.3(2)
C(8)-Si(1)-C(6)	112.2(2)
N(1)-Si(1)-C(7)	111.7(2)
C(8)-Si(1)-C(7)	111.1(2)
C(6)-Si(1)-C(7)	108.4(2)
N(2)-Si(2)-C(5)	106.0(2)
N(2)-Si(2)-C(4)	108.1(2)
C(5)-Si(2)-C(4)	109.6(2)
N(2)-Si(2)-C(3)	111.3(2)
C(5)-Si(2)-C(3)	111.0(2)
C(4)-Si(2)-C(3)	110.7(2)
C(9)-N(1)-Si(1)	125.2(2)
C(9)-N(1)-W	100.1(2)
Si(1)-N(1)-W	134.2(2)
C(14)-N(2)-Si(2)	124.9(2)
C(14)-N(2)-W	100.4(2)
Si(2)-N(2)-W	134.6(2)
C(15)-N(3)-W	171.7(3)
W-C(1)-H(1A)	109.47(11)
W-C(1)-H(1B)	109.47(11)
H(1A)-C(1)-H(1B)	109.5
W-C(1)-H(1C)	109.47(11)
H(1A)-C(1)-H(1C)	109.5
H(1B)-C(1)-H(1C)	109.5
W-C(2)-H(2A)	109.47(12)
W-C(2)-H(2B)	109.47(12)
H(2A)-C(2)-H(2B)	109.5
W-C(2)-H(2C)	109.47(13)
H(2A)-C(2)-H(2C)	109.5
H(2B)-C(2)-H(2C)	109.5

Si(2)-C(3)-H(3A)	109.47(14)
Si(2)-C(3)-H(3B)	109.47(14)
H(3A)-C(3)-H(3B)	109.5
Si(2)-C(3)-H(3C)	109.47(14)
H(3A)-C(3)-H(3C)	109.5
H(3B)-C(3)-H(3C)	109.5
Si(2)-C(4)-H(4A)	109.5(2)
Si(2)-C(4)-H(4B)	109.5(2)
H(4A)-C(4)-H(4B)	109.5
Si(2)-C(4)-H(4C)	109.5(2)
H(4A)-C(4)-H(4C)	109.5
H(4B)-C(4)-H(4C)	109.5
Si(2)-C(5)-H(5A)	109.5(2)
Si(2)-C(5)-H(5B)	109.5(2)
H(5A)-C(5)-H(5B)	109.5
Si(2)-C(5)-H(5C)	109.5(2)
H(5A)-C(5)-H(5C)	109.5
H(5B)-C(5)-H(5C)	109.5
Si(1)-C(6)-H(6A)	109.47(14)
Si(1)-C(6)-H(6B)	109.47(13)
H(6A)-C(6)-H(6B)	109.5
Si(1)-C(6)-H(6C)	109.5(2)
H(6A)-C(6)-H(6C)	109.5
H(6B)-C(6)-H(6C)	109.5
Si(1)-C(7)-H(7A)	109.5(2)
Si(1)-C(7)-H(7B)	109.5(2)
H(7A)-C(7)-H(7B)	109.5
Si(1)-C(7)-H(7C)	109.5(2)
H(7A)-C(7)-H(7C)	109.5
H(7B)-C(7)-H(7C)	109.5
Si(1)-C(8)-H(8A)	109.5(2)
Si(1)-C(8)-H(8B)	109.5(2)
H(8A)-C(8)-H(8B)	109.5
Si(1)-C(8)-H(8C)	109.47(13)
H(8A)-C(8)-H(8C)	109.5
H(8B)-C(8)-H(8C)	109.5
N(1)-C(9)-C(10)	125.5(3)
N(1)-C(9)-C(14)	115.8(3)
C(10)-C(9)-C(14)	118.7(3)
C(11)-C(10)-C(9)	120.5(3)
C(11)-C(10)-H(10A)	119.8(2)
C(9)-C(10)-H(10A)	119.8(2)
C(10)-C(11)-C(12)	120.9(3)
C(10)-C(11)-H(11A)	119.6(2)
C(12)-C(11)-H(11A)	119.6(2)
C(13)-C(12)-C(11)	120.4(3)
C(13)-C(12)-H(12A)	119.8(2)
C(11)-C(12)-H(12A)	119.8(2)
C(12)-C(13)-C(14)	120.1(3)
C(12)-C(13)-H(13A)	119.9(2)
C(14)-C(13)-H(13A)	119.9(2)
N(2)-C(14)-C(13)	125.1(3)
N(2)-C(14)-C(9)	115.6(3)
C(13)-C(14)-C(9)	119.4(3)

C(20)-C(15)-N(3)	118.8(3)
C(20)-C(15)-C(16)	119.3(3)
N(3)-C(15)-C(16)	121.8(3)
C(15)-C(16)-C(17)	118.8(4)
C(15)-C(16)-H(16A)	120.6(2)
C(17)-C(16)-H(16A)	120.6(3)
C(18)-C(17)-C(16)	121.3(4)
C(18)-C(17)-H(17A)	119.4(3)
C(16)-C(17)-H(17A)	119.4(3)
C(19)-C(18)-C(17)	119.4(4)
C(19)-C(18)-H(18A)	120.3(2)
C(17)-C(18)-H(18A)	120.3(3)
C(18)-C(19)-C(20)	120.7(4)
C(18)-C(19)-H(19A)	119.7(2)
C(20)-C(19)-H(19A)	119.7(3)
C(19)-C(20)-C(15)	120.5(4)
C(19)-C(20)-H(20A)	119.8(3)
C(15)-C(20)-H(20A)	119.8(2)

Table A1.4. Anisotropic displacement parameters ($A^2 \times 10^3$) for **3**. The anisotropic displacement factor exponent takes the form: $-2\ p^2\ [\ h^2\ a^{*2}\ U11 + ... + 2\ h\ k\ a^*\ b^*\ U12\ ]$

Atom	U11	U22	U33	U23	U13	U12
W	27(1)	31(1)	23(1)	-1(1)	8(1)	-6(1)
Si(1)	41(1)	28(1)	26(1)	-3(1)	8(1)	-2(1)
Si(2)	31(1)	37(1)	37(1)	-5(1)	11(1)	1(1)
N(1)	30(2)	31(2)	28(1)	-1(1)	8(1)	-3(1)
N(2)	28(1)	32(2)	29(1)	-3(1)	10(1)	-5(1)
N(3)	36(2)	39(2)	31(2)	3(1)	12(1)	-6(1)
C(1)	40(2)	43(2)	44(2)	7(2)	6(2)	-1(2)
C(2)	51(2)	57(3)	28(2)	0(2)	9(2)	-5(2)
C(3)	53(3)	42(2)	48(2)	-14(2)	21(2)	0(2)
C(4)	51(3)	51(3)	51(2)	6(2)	5(2)	9(2)
C(5)	31(2)	68(3)	74(3)	-15(3)	22(2)	-4(2)
C(6)	56(3)	39(2)	45(2)	-9(2)	9(2)	-16(2)
C(7)	58(3)	48(2)	59(3)	-23(2)	19(2)	5(2)
C(8)	68(3)	45(2)	31(2)	4(2)	-5(2)	-9(2)
C(9)	34(2)	28(2)	21(2)	1(1)	7(1)	-3(1)
C(10)	34(2)	38(2)	29(2)	-3(1)	13(2)	-1(2)
C(11)	29(2)	49(2)	28(2)	2(2)	10(1)	-3(2)
C(12)	34(2)	40(2)	31(2)	3(2)	7(2)	-7(2)
C(13)	31(2)	33(2)	27(2)	2(1)	6(1)	-3(1)
C(14)	27(2)	28(2)	24(1)	1(1)	8(1)	-1(1)
C(15)	29(2)	26(2)	38(2)	0(1)	12(1)	-1(1)
C(16)	41(2)	53(3)	47(2)	13(2)	2(2)	-8(2)
C(17)	29(2)	47(2)	86(3)	8(2)	-3(2)	-7(2)
C(18)	35(2)	32(2)	92(3)	3(2)	31(2)	-2(2)
C(19)	49(2)	32(2)	58(2)	2(2)	32(2)	-1(2)
C(20)	34(2)	34(2)	38(2)	-4(2)	14(2)	-1(2)

Table A1.5. Hydrogen coordinates (x 10^4) and isotropic displacement parameters (A^4 x 10^4) for **3**.

Atom	x	y	z	U(eq)
H(1A)	10471(4)	1455(5)	2524(23)	64
H(1B)	9445(21)	876(8)	1915(11)	64
H(1C)	9442(21)	1081(12)	3058(12)	64
H(2A)	9673(15)	2728(16)	3598(6)	68
H(2B)	8907(31)	2046(3)	3908(3)	68
H(2C)	8185(16)	2814(14)	3655(7)	68
H(3A)	8682(14)	4708(16)	2944(12)	69
H(3B)	7840(31)	4191(5)	3492(3)	69
H(3C)	7224(18)	4931(11)	2963(12)	69
H(4A)	7948(6)	4804(15)	548(15)	78
H(4B)	6525(28)	5060(10)	618(14)	78
H(4C)	6689(31)	4373(6)	-66(4)	78
H(5A)	5203(16)	3344(17)	993(13)	84
H(5B)	4893(9)	4001(3)	1676(28)	84
H(5C)	5566(8)	3272(15)	2202(16)	84
H(6A)	7179(11)	676(13)	152(14)	70
H(6B)	6663(21)	669(13)	-1055(12)	70
H(6C)	6193(12)	1294(2)	-401(25)	70
H(7A)	10093(24)	685(15)	-123(9)	81
H(7B)	10405(17)	1237(3)	-946(27)	81
H(7C)	9377(9)	591(13)	-1294(19)	81
H(8A)	8675(7)	2506(14)	-1727(18)	76
H(8B)	7269(27)	2600(12)	-1495(13)	76
H(8C)	7496(32)	1990(3)	-2278(6)	76
H(10A)	11180(4)	2289(2)	49(3)	39
H(11A)	12535(4)	3318(2)	350(3)	42
H(12A)	11980(4)	4340(2)	1214(3)	42
H(13A)	10058(3)	4337(2)	1814(3)	36
H(16A)	4342(4)	1562(3)	558(3)	58
H(17A)	2444(4)	1026(3)	895(4)	68
H(18A)	2444(4)	588(2)	2515(4)	60
H(19A)	4315(4)	715(2)	3835(3)	52
H(20A)	6225(4)	1224(2)	3530(3)	41

Crystallographic Data for W(NPh)[*o*-$(Me_3SiN)_2C_6H_4$]$(CH_2CH_2Ph)_2$, **6.**

Table A2.1: Crystallographic Data

Empirical formula	$C_{34}\ H_{45}\ N_3\ Si_2\ W$
Formula weight	735.76
Temperature	173(2) K
Wavelength	0.71073 Å
Crystal system	Triclinic
Space group	P-1
Unit cell dimensions	a = 10.0571(1) Å α = 93.043(1)°
	b = 10.1133(2) Å β = 99.667(1)°
	c = 19.1479(4) Å γ = 112.048(1)°
Volume, Z	1765.06(5) $Å^3$, 2
Density (calculated)	1.384 Mg/m^3
Absorption coefficient	3.365 mm^{-1}
F(000)	744
Crystal size	0.28 x 0.25 x 0.21 mm
Theta range for data collection	1.09 to 26.88°
Limiting indices	-12≤h≤ 8, -10≤k≤ 12, -23≤l≤ 23
Reflections collected	9322
Independent reflections	6519 [R(int) = 0.0370]
Absorption correction	Psi Scan
Minimum & maximum Transmission	0.448, 0.603
Refinement method	Full-matrix least-squares on F^2
Data / restraints / parameters	6519 / 0 / 362
Goodness-of-fit on F^2	0.921
Final R indices [I>2sigma(I)]	R_1 = 0.0340, wR_2 = 0.0729 [5292]
R indices (all data)	R_1 = 0.0445, wR_2 = 0.0766
Extinction coefficient	0.0018(2)
Largest diff. peak and hole	1.013 and -0.928 $e.A^{-3}$

$R_1 = \hat{A}(||F_o| - |F_c||) / \hat{A}|F_o|$

$wR_2 = [\hat{A}[w(F_o^2 - F_c^2)^2] / \hat{A}[w(F_o^2)^2]]^{1/2}$

$S = [\hat{A}[w(F_o^2 - F_c^2)^2] / (n-p)]^{1/2}$

$w= 1/[s^2(F_o^2)+(0.0370*p)^2+0.31*p]$, $p = [\max(F_o^2,0)+ 2* F_c^2]/3$

Table A2.2. Atomic coordinates (x 10^4) and equivalent isotropic displacement parameters (A^2 x 10^3) for **6**. U(eq) is defined as one third of the trace of the orthogonalized Uij tensor.

Atom	x	y	z	U(eq)
W	-44(1)	-3261(1)	-2260(1)	40(1)
Si1	-2939(2)	-2985(2)	-1580(1)	55(1)
Si2	617(2)	-6007(2)	-1466(1)	53(1)
N1	-2094(4)	-3749(4)	-2120(2)	44(1)
N2	-418(4)	-5249(4)	-2008(2)	42(1)
N3	1315(4)	-1779(4)	-1727(2)	44(1)
C1	1314(5)	-3682(5)	-2953(3)	53(1)
C2	566(6)	-4886(6)	-3561(3)	55(1)
C3	1530(6)	-4921(6)	-4083(3)	54(1)
C4	1781(7)	-3975(7)	-4570(3)	76(2)
C5	2639(8)	-3976(8)	-5063(4)	91(2)
C6	3203(7)	-4994(11)	-5078(4)	93(3)
C7	2950(9)	-5978(9)	-4609(4)	99(3)
C8	2148(7)	-5912(7)	-4097(3)	78(2)
C9	-701(6)	-2341(6)	-3192(3)	57(1)
C10	-1185(9)	-1158(7)	-3077(3)	89(2)
C11	-1739(8)	-665(7)	-3764(3)	71(2)
C12	-3214(9)	-1255(7)	-4110(4)	84(2)
C13	-3704(8)	-843(7)	-4735(4)	87(2)
C14	-2733(9)	161(8)	-5049(4)	96(2)
C15	-1258(9)	757(9)	-4723(5)	113(3)
C16	-804(8)	330(8)	-4084(4)	98(2)
C17	-2755(5)	-5188(5)	-2465(2)	45(1)
C18	-1852(5)	-5999(5)	-2408(2)	43(1)
C19	-2410(6)	-7403(5)	-2761(3)	56(1)
C20	-3830(6)	-8001(6)	-3141(3)	63(2)
C21	-4718(6)	-7237(6)	-3191(3)	67(2)
C22	-4198(6)	-5845(6)	-2863(3)	60(1)
C23	-3747(8)	-4316(7)	-987(4)	87(2)
C24	-4410(8)	-2519(8)	-2094(4)	98(2)
C25	-1478(7)	-1334(6)	-1062(4)	83(2)
C26	-585(8)	-7171(8)	-909(4)	98(2)
C27	1394(8)	-7049(7)	-1989(4)	90(2)
C28	2150(6)	-4475(6)	-895(3)	69(2)
C29	2537(5)	-586(5)	-1367(2)	43(1)
C30	2775(6)	-235(6)	-635(3)	66(2)
C31	3989(7)	949(7)	-292(3)	80(2)
C32	4962(6)	1779(6)	-664(3)	71(2)
C33	4730(6)	1421(6)	-1387(3)	72(2)
C34	3526(6)	252(6)	-1744(3)	60(2)

Table A2.3. Bond lengths (Å) and angles [°] for **6**.

W-N3	1.728(4)
W-N1	2.000(4)
W-N2	2.003(4)
W-C9	2.175(5)
W-C1	2.189(5)
W-C17	2.637(4)
Si1-N1	1.758(4)
Si1-C23	1.847(6)
Si1-C25	1.850(6)
Si1-C24	1.862(7)
Si2-N2	1.753(4)
Si2-C28	1.852(5)
Si2-C27	1.870(6)
Si2-C26	1.865(6)
N1-C17	1.421(6)
N2-C18	1.410(6)
N3-C29	1.399(5)
C1-C2	1.507(7)
C1-H1A	0.97
C1-H1B	0.97
C2-C3	1.514(7)
C2-H2A	0.97
C2-H2B	0.97
C3-C4	1.357(8)
C3-C8	1.364(8)
C4-C5	1.381(9)
C4-H4A	0.93
C5-C6	1.350(10)
C5-H5A	0.93
C6-C7	1.358(10)
C6-H6A	0.93
C7-C8	1.384(8)
C7-H7A	0.93
C8-H8A	0.93
C9-C10	1.470(8)
C9-H9A	0.97
C9-H9B	0.97
C10-C11	1.525(9)
C10-H10A	0.97
C10-H10B	0.97
C11-C16	1.348(8)
C11-C12	1.399(9)
C12-C13	1.362(9)
C12-H12A	0.93
C13-C14	1.365(9)
C13-H13A	0.93
C14-C15	1.390(10)
C14-H14A	0.93
C15-C16	1.382(9)

C15-H15A	0.93
C16-H16A	0.93
C17-C22	1.408(7)
C17-C18	1.430(7)
C18-C19	1.400(6)
C19-C20	1.374(7)
C19-H19A	0.93
C20-C21	1.379(8)
C20-H20A	0.93
C21-C22	1.376(7)
C21-H21A	0.93
C22-H22A	0.93
C23-H23A	0.96
C23-H23B	0.96
C23-H23C	0.96
C24-H24A	0.96
C24-H24B	0.96
C24-H24C	0.96
C25-H25A	0.96
C25-H25B	0.96
C25-H25C	0.96
C26-H26A	0.96
C26-H26B	0.96
C26-H26C	0.96
C27-H27A	0.96
C27-H27B	0.96
C27-H27C	0.96
C28-H28A	0.96
C28-H28B	0.96
C28-H28C	0.96
C29-C34	1.379(6)
C29-C30	1.385(6)
C30-C31	1.380(7)
C30-H30A	0.93
C31-C32	1.359(8)
C31-H31A	0.93
C32-C33	1.371(8)
C32-H32A	0.93
C33-C34	1.376(7)
C33-H33A	0.93
C34-H34A	0.93

N3-W-N1	117.1(2)
N3-W-N2	120.7(2)
N1-W-N2	82.9(2)
N3-W-C9	102.6(2)
N1-W-C9	85.1(2)
N2-W-C9	135.8(2)
N3-W-C1	97.2(2)
N1-W-C1	145.0(2)
N2-W-C1	85.4(2)
C9-W-C1	80.6(2)
N3-W-C17	146.9(2)
N1-W-C17	32.11(14)

N2-W-C17	60.2(2)
C9-W-C17	88.7(2)
C1-W-C17	115.4(2)
N1-Si1-C23	107.2(2)
N1-Si1-C25	106.5(2)
C23-Si1-C25	111.3(3)
N1-Si1-C24	113.7(3)
C23-Si1-C24	108.8(3)
C25-Si1-C24	109.4(3)
N2-Si2-C28	105.9(2)
N2-Si2-C27	112.9(2)
C28-Si2-C27	108.6(3)
N2-Si2-C26	107.7(3)
C28-Si2-C26	110.6(3)
C27-Si2-C26	111.1(3)
C17-N1-Si1	123.7(3)
C17-N1-W	99.4(3)
Si1-N1-W	135.3(2)
C18-N2-Si2	125.6(3)
C18-N2-W	100.3(3)
Si2-N2-W	134.1(2)
C29-N3-W	171.8(3)
C2-C1-W	117.6(3)
C2-C1-H1A	107.9(3)
W-C1-H1A	107.91(14)
C2-C1-H1B	107.9(3)
W-C1-H1B	107.91(14)
H1A-C1-H1B	107.2
C1-C2-C3	113.5(4)
C1-C2-H2A	108.9(3)
C3-C2-H2A	108.9(3)
C1-C2-H2B	108.9(3)
C3-C2-H2B	108.9(3)
H2A-C2-H2B	107.7
C4-C3-C8	117.6(6)
C4-C3-C2	120.5(5)
C8-C3-C2	121.9(5)
C3-C4-C5	122.6(7)
C3-C4-H4A	118.7(4)
C5-C4-H4A	118.7(5)
C6-C5-C4	118.7(7)
C6-C5-H5A	120.7(5)
C4-C5-H5A	120.7(5)
C5-C6-C7	120.4(7)
C5-C6-H6A	119.8(5)
C7-C6-H6A	119.8(5)
C6-C7-C8	119.9(7)
C6-C7-H7A	120.0(5)
C8-C7-H7A	120.0(4)
C3-C8-C7	120.7(6)
C3-C8-H8A	119.6(4)
C7-C8-H8A	119.6(4)
C10-C9-W	117.7(4)
C10-C9-H9A	107.9(4)

W-C9-H9A	107.9(2)
C10-C9-H9B	107.9(4)
W-C9-H9B	107.9(2)
H9A-C9-H9B	107.2
C9-C10-C11	113.9(5)
C9-C10-H10A	108.8(4)
C11-C10-H10A	108.8(4)
C9-C10-H10B	108.8(4)
C11-C10-H10B	108.8(4)
H10A-C10-H10B	107.7
C16-C11-C12	116.8(6)
C16-C11-C10	120.8(7)
C12-C11-C10	122.3(6)
C13-C12-C11	122.4(7)
C13-C12-H12A	118.8(5)
C11-C12-H12A	118.8(4)
C12-C13-C14	119.7(7)
C12-C13-H13A	120.2(5)
C14-C13-H13A	120.2(5)
C13-C14-C15	119.4(7)
C13-C14-H14A	120.3(5)
C15-C14-H14A	120.3(5)
C16-C15-C14	119.3(7)
C16-C15-H15A	120.3(5)
C14-C15-H15A	120.3(5)
C11-C16-C15	122.4(7)
C11-C16-H16A	118.8(4)
C15-C16-H16A	118.8(5)
C22-C17-N1	125.1(5)
C22-C17-C18	118.5(4)
N1-C17-C18	116.4(4)
C22-C17-W	151.8(4)
N1-C17-W	48.5(2)
C18-C17-W	74.8(3)
C19-C18-N2	125.8(5)
C19-C18-C17	119.5(4)
N2-C18-C17	114.7(4)
C20-C19-C18	119.8(5)
C20-C19-H19A	120.1(3)
C18-C19-H19A	120.1(3)
C19-C20-C21	121.3(5)
C19-C20-H20A	119.3(3)
C21-C20-H20A	119.3(3)
C22-C21-C20	120.5(5)
C22-C21-H21A	119.7(3)
C20-C21-H21A	119.7(3)
C21-C22-C17	120.4(5)
C21-C22-H22A	119.8(3)
C17-C22-H22A	119.8(3)
Si1-C23-H23A	109.5(2)
Si1-C23-H23B	109.5(2)
H23A-C23-H23B	109.5
Si1-C23-H23C	109.5(2)
H23A-C23-H23C	109.5

H23B-C23-H23C	109.5
Si1-C24-H24A	109.5(2)
Si1-C24-H24B	109.5(2)
H24A-C24-H24B	109.5
Si1-C24-H24C	109.5(2)
H24A-C24-H24C	109.5
H24B-C24-H24C	109.5
Si1-C25-H25A	109.5(2)
Si1-C25-H25B	109.5(2)
H25A-C25-H25B	109.5
Si1-C25-H25C	109.5(2)
H25A-C25-H25C	109.5
H25B-C25-H25C	109.5
Si2-C26-H26A	109.5(2)
Si2-C26-H26B	109.5(2)
H26A-C26-H26B	109.5
Si2-C26-H26C	109.5(2)
H26A-C26-H26C	109.5
H26B-C26-H26C	109.5
Si2-C27-H27A	109.5(2)
Si2-C27-H27B	109.5(2)
H27A-C27-H27B	109.5
Si2-C27-H27C	109.5(2)
H27A-C27-H27C	109.5
H27B-C27-H27C	109.5
Si2-C28-H28A	109.5(2)
Si2-C28-H28B	109.5(2)
H28A-C28-H28B	109.5
Si2-C28-H28C	109.5(2)
H28A-C28-H28C	109.5
H28B-C28-H28C	109.5
C34-C29-C30	119.4(4)
C34-C29-N3	119.7(4)
C30-C29-N3	120.9(4)
C31-C30-C29	119.8(5)
C31-C30-H30A	120.1(3)
C29-C30-H30A	120.1(3)
C32-C31-C30	120.9(5)
C32-C31-H31A	119.6(3)
C30-C31-H31A	119.6(3)
C31-C32-C33	119.1(5)
C31-C32-H32A	120.4(3)
C33-C32-H32A	120.4(3)
C32-C33-C34	121.3(5)
C32-C33-H33A	119.4(3)
C34-C33-H33A	119.4(3)
C33-C34-C29	119.5(5)
C33-C34-H34A	120.2(3)
C29-C34-H34A	120.2(3)

Table A2.4. Anisotropic displacement parameters ($A^2 \times 10^3$) for **6**. The anisotropic displacement factor exponent takes the form: $-2\ p^2\ [\ h^2\ a^{*2}\ U11 + ... + 2\ h\ k\ a^*\ b^*\ U12\ ]$

Atom	U11	U22	U33	U23	U13	U12
W	36(1)	34(1)	43(1)	-4(1)	5(1)	10(1)
Si1	51(1)	46(1)	71(1)	3(1)	21(1)	20(1)
Si2	54(1)	48(1)	54(1)	3(1)	4(1)	22(1)
N1	41(2)	37(2)	52(2)	-1(2)	8(2)	13(2)
N2	40(2)	39(2)	41(2)	-6(2)	1(2)	12(2)
N3	42(2)	36(2)	48(2)	-2(2)	12(2)	8(2)
C1	47(3)	49(3)	58(3)	-1(3)	12(3)	14(3)
C2	48(3)	57(3)	57(3)	-4(3)	10(3)	19(3)
C3	54(3)	51(3)	51(3)	-5(3)	12(3)	16(3)
C4	90(5)	67(4)	79(4)	17(4)	31(4)	31(4)
C5	76(5)	98(6)	71(4)	11(4)	22(4)	1(4)
C6	61(4)	169(8)	51(4)	-7(5)	11(3)	50(5)
C7	120(6)	143(7)	78(5)	5(5)	30(5)	96(6)
C8	101(5)	83(5)	73(4)	23(4)	33(4)	54(4)
C9	59(3)	55(3)	59(3)	5(3)	10(3)	24(3)
C10	133(7)	73(5)	73(4)	16(4)	19(4)	55(5)
C11	94(5)	52(4)	76(4)	16(3)	25(4)	34(4)
C12	98(6)	59(4)	107(6)	18(4)	37(5)	37(4)
C13	85(5)	57(4)	118(6)	13(4)	7(5)	31(4)
C14	108(6)	81(5)	92(5)	18(4)	-11(5)	43(5)
C15	91(6)	115(7)	130(7)	71(6)	19(5)	32(5)
C16	81(5)	92(6)	108(6)	43(5)	0(4)	25(4)
C17	42(3)	39(3)	45(3)	-1(2)	12(2)	7(2)
C18	40(3)	38(3)	45(3)	2(2)	12(2)	9(2)
C19	52(3)	41(3)	64(3)	-13(3)	1(3)	13(3)
C20	64(4)	44(3)	60(3)	-13(3)	3(3)	5(3)
C21	52(3)	56(4)	63(3)	-12(3)	-15(3)	3(3)
C22	44(3)	62(4)	67(4)	0(3)	1(3)	20(3)
C23	104(5)	70(4)	107(5)	23(4)	59(5)	38(4)
C24	96(5)	119(6)	109(6)	8(5)	21(4)	76(5)
C25	79(5)	61(4)	105(5)	-21(4)	38(4)	21(3)
C26	114(6)	87(5)	102(5)	48(5)	32(5)	38(5)
C27	96(5)	87(5)	96(5)	-17(4)	-15(4)	63(4)
C28	69(4)	65(4)	62(3)	1(3)	-12(3)	26(3)
C29	42(3)	33(3)	45(3)	-6(2)	4(2)	8(2)
C30	61(4)	64(4)	53(3)	-7(3)	19(3)	1(3)
C31	81(5)	75(4)	57(4)	-21(3)	7(3)	7(4)
C32	59(4)	44(3)	76(4)	-9(3)	1(3)	-10(3)
C33	60(4)	58(4)	76(4)	7(3)	22(3)	-6(3)
C34	60(4)	54(3)	51(3)	-2(3)	10(3)	7(3)

Table A2.5. Hydrogen coordinates (x 10^4) and isotropic displacement parameters (A^4 x 10^4) for **6**.

Atom	x	y	z	U(eq)
H1A	1789(5)	-2805(5)	-3153(3)	64
H1B	2079(5)	-3886(5)	-2656(3)	64
H2A	-303(6)	-4786(6)	-3815(3)	66
H2B	253(6)	-5796(6)	-3367(3)	66
H4A	1359(7)	-3299(7)	-4573(3)	92
H5A	2824(8)	-3290(8)	-5378(4)	109
H6A	3769(7)	-5021(11)	-5412(4)	112
H7A	3315(9)	-6695(9)	-4632(4)	119
H8A	2029(7)	-6551(7)	-3758(3)	93
H9A	120(6)	-1997(6)	-3432(3)	69
H9B	-1490(6)	-3109(6)	-3517(3)	69
H10A	-373(9)	-347(7)	-2789(3)	107
H10B	-1961(9)	-1465(7)	-2808(3)	107
H12A	-3883(9)	-1954(7)	-3907(4)	101
H13A	-4694(8)	-1243(7)	-4946(4)	104
H14A	-3056(9)	444(8)	-5477(4)	115
H15A	-584(9)	1437(9)	-4932(5)	135
H16A	183(8)	743(8)	-3866(4)	117
H19A	-1822(6)	-7929(5)	-2739(3)	67
H20A	-4198(6)	-8939(6)	-3368(3)	75
H21A	-5677(6)	-7667(6)	-3449(3)	80
H22A	-4803(6)	-5336(6)	-2906(3)	72
H23A	-4501(8)	-5159(7)	-1269(4)	131
H23B	-4160(8)	-3908(7)	-661(4)	131
H23C	-2999(8)	-4574(7)	-723(4)	131
H24A	-4003(8)	-1829(8)	-2405(4)	147
H24B	-4830(8)	-2116(8)	-1769(4)	147
H24C	-5157(8)	-3370(8)	-2373(4)	147
H25A	-1078(7)	-664(6)	-1383(4)	124
H25B	-717(7)	-1573(6)	-798(4)	124
H25C	-1880(7)	-910(6)	-737(4)	124
H26A	-1372(8)	-7959(8)	-1213(4)	148
H26B	-980(8)	-6616(8)	-650(4)	148
H26C	-22(8)	-7538(8)	-578(4)	148
H27A	610(8)	-7847(7)	-2288(4)	136
H27B	1989(8)	-7400(7)	-1668(4)	136
H27C	1983(8)	-6436(7)	-2282(4)	136
H28A	1766(6)	-3930(6)	-624(3)	103
H28B	2738(6)	-3871(6)	-1191(3)	103
H28C	2742(6)	-4832(6)	-576(3)	103
H30A	2118(6)	-795(6)	-375(3)	79
H31A	4144(7)	1181(7)	199(3)	96
H32A	5774(6)	2580(6)	-430(3)	85
H33A	5400(6)	1980(6)	-1642(3)	87
H34A	3380(6)	28(6)	-2236(3)	72

Crystallographic Data for W(NPh)[*o*-$(Me_3SiN)_2C_6H_4$]$(CH_2CH(CH_3)_2)_2$, 7.

Table A3.1: Crystallographic Data

Empirical formula	$C_{26}H_{45}N_3Si_2W$
Formula weight	639.68
Temperature	173(2) K
Wavelength	0.71073 Å
Crystal system	Triclinic
Space group	P-1
Unit cell dimensions	a = 9.5617(2) Å α = 92.220(1)°
	b = 10.1808(3) Å β = 103.419(1)°
	c = 17.2475(4) Å γ = 110.999(1)°
Volume, Z	1510.87(6) $Å^3$, 2
Density (calculated)	1.406 Mg/m^3
Absorption coefficient	3.919 mm^{-1}
F(000)	648
Crystal size	0.28 x 0.27 x 0.19 mm
Theta range for data collection	2.16 to 27.50°
Limiting indices	$-12 \le h \le 11$, $-11 \le k \le 13$, $-22 \le l \le 20$
Reflections collected	9856
Independent reflections	6643 [R(int) = 0.0154]
Absorption correction	Semi-empirical from psi-scans
Max. and min. transmission	0.790 and 0.628
Refinement method	Full-matrix least-squares on F^2
Data / restraints / parameters	6643 / 0 / 470
Goodness-of-fit on F^2	1.069
Final R indices [I>2sigma(I)]	$R1 = 0.0165$, $wR_2 = 0.0394$ [6252]
R indices (all data)	$R1 = 0.0184$, $wR_2 = 0.0399$
Extinction coefficient	0.00028(14)
Largest diff. peak and hole	0.590 and -0.411 $e.Å^{-3}$

$R_1 = \hat{A}(||F_o| - |F_c||) / \hat{A}|F_o|$

$wR_2 = [\hat{A}[w(F_o^2 - F_c^2)^2] / \hat{A}[w(F_o^2)^2]]^{1/2}$

$S = [\hat{A}[w(F_o^2 - F_c^2)^2] / (n-p)]^{1/2}$

$w= 1/[s^2(F_o^2)+(0.0370*p)^2+0.31*p]$, $p = [\max(F_o^2,0)+ 2* F_c^2]/3$

Table A3.2. Atomic coordinates (x 10^4) and equivalent isotropic displacement parameters (A^2 x 10^3) for **7**. U(eq) is defined as one third of the trace of the orthogonalized Uij tensor.

Atom	x	y	z	U(eq)
W	3169(1)	1417(1)	2606(1)	20(1)
Si1	-111(1)	1831(1)	1504(1)	28(1)
Si2	3037(1)	-1947(1)	2042(1)	34(1)
N1	4340(2)	2423(2)	2039(1)	26(1)
N2	890(2)	1023(2)	2182(1)	24(1)
N3	2368(2)	-727(2)	2413(1)	25(1)
C1	3181(3)	3099(2)	3434(1)	30(1)
C2	2014(3)	2757(3)	3953(2)	36(1)
C3	2214(4)	1708(4)	4538(2)	50(1)
C4	2130(5)	4116(4)	4419(2)	60(1)
C5	4898(3)	1160(2)	3610(1)	29(1)
C6	6262(3)	2338(3)	4193(1)	32(1)
C7	7342(4)	3333(4)	3783(2)	53(1)
C8	7181(5)	1720(5)	4817(3)	72(1)
C9	5175(2)	3273(2)	1558(1)	24(1)
C10	5164(3)	2701(3)	809(2)	36(1)
C11	5983(3)	3577(3)	338(2)	46(1)
C12	6821(3)	4999(3)	604(2)	46(1)
C13	6836(3)	5562(3)	1343(2)	40(1)
C14	6013(3)	4710(2)	1822(2)	31(1)
C15	207(2)	-159(2)	2544(1)	26(1)
C16	-1151(3)	-445(3)	2804(1)	33(1)
C17	-1685(3)	-1616(3)	3190(2)	41(1)
C18	-891(3)	-2526(3)	3321(2)	40(1)
C19	437(3)	-2288(3)	3071(2)	34(1)
C20	1017(2)	-1102(2)	2678(1)	26(1)
C21	-855(4)	2973(4)	2020(2)	50(1)
C22	-1733(4)	413(4)	765(2)	50(1)
C23	1269(3)	2951(3)	975(2)	37(1)
C24	1395(4)	-3214(4)	1237(3)	59(1)
C25	3778(5)	-2900(4)	2840(3)	64(1)
C26	4645(3)	-943(3)	1611(2)	43(1)

Table A3.3. Bond lengths (Å) and angles [°] for **7**.

W-N1	1.738(2)
W-N2	2.013(2)
W-N3	2.023(2)
W-C1	2.182(2)
W-C5	2.195(2)
Si1-N2	1.755(2)
Si1-C23	1.853(3)
Si1-C22	1.857(3)
Si1-C21	1.859(3)
Si2-N3	1.748(2)
Si2-C26	1.850(3)
Si2-C24	1.859(4)
Si2-C25	1.866(4)
N1-C9	1.393(3)
N2-C15	1.397(3)
N3-C20	1.400(3)
C1-C2	1.542(3)
C1-H1A	1.01(3)
C1-H1B	1.00(3)
C2-C3	1.528(4)
C2-C4	1.529(4)
C2-H2	0.96(3)
C3-H3B	0.96(3)
C3-H3C	0.99(4)
C4-H4A	0.92(3)
C4-H4B	1.06(4)
C4-H4C	0.93(4)
C5-C6	1.526(3)
C5-H5A	0.99(3)
C5-H5B	0.91(3)
C6-C7	1.495(4)
C6-C8	1.528(4)
C6-H6	0.90(3)
C7-H7A	1.00(3)
C7-H7B	0.89(3)
C7-H7C	0.91(4)
C8-H8A	1.04(4)
C8-H8B	1.04(5)
C8-H8C	0.92(5)
C9-C14	1.389(3)
C9-C10	1.392(3)
C10-C11	1.385(4)
C10-H10	0.96(3)
C11-C12	1.377(4)
C11-H11	0.96(4)
C12-C13	1.372(4)
C12-H12	0.98(3)
C13-C14	1.387(3)
C13-H13	0.89(3)

C14-H14	0.91(3)
C15-C16	1.407(3)
C15-C20	1.429(3)
C16-C17	1.382(4)
C16-H16	0.92(2)
C17-C18	1.388(4)
C17-H17	0.87(3)
C18-C19	1.378(4)
C18-H18	0.89(3)
C19-C20	1.407(3)
C19-H19	0.98(3)
C21-H21A	0.88(4)
C21-H21B	0.90(4)
C21-H21C	0.94(4)
C22-H22A	0.92(4)
C22-H22B	1.01(5)
C22-H22C	0.95(5)
C23-H23A	0.95(3)
C23-H23B	0.88(3)
C23-H23C	0.97(4)
C24-H24A	0.88(4)
C24-H24B	0.87(4)
C24-H24C	0.87(4)
C25-H25A	0.87(4)
C25-H25B	0.90(4)
C25-H25C	0.98(6)
C26-H26A	0.94(4)
C26-H26B	1.00(4)
C26-H26C	0.98(4)

N1-W-N2	114.77(8)
N1-W-N3	120.17(8)
N2-W-N3	81.43(7)
N1-W-C1	100.35(8)
N2-W-C1	85.09(8)
N3-W-C1	139.31(8)
N1-W-C5	101.54(9)
N2-W-C5	143.55(8)
N3-W-C5	83.13(8)
C1-W-C5	85.47(9)
N2-Si1-C23	107.53(10)
N2-Si1-C22	108.26(13)
C23-Si1-C22	109.45(14)
N2-Si1-C21	112.22(12)
C23-Si1-C21	108.7(2)
C22-Si1-C21	110.6(2)
N3-Si2-C26	107.40(11)
N3-Si2-C24	107.13(14)
C26-Si2-C24	109.9(2)
N3-Si2-C25	112.7(2)
C26-Si2-C25	108.6(2)
C24-Si2-C25	111.0(2)
C9-N1-W	174.9(2)
C15-N2-Si1	125.7(2)

C15-N2-W	102.24(13)
Si1-N2-W	132.05(9)
C20-N3-Si2	124.30(14)
C20-N3-W	101.61(12)
Si2-N3-W	134.08(10)
C2-C1-W	120.0(2)
C2-C1-H1A	107.0(14)
W-C1-H1A	104.6(14)
C2-C1-H1B	111(2)
W-C1-H1B	109(2)
H1A-C1-H1B	104(2)
C3-C2-C4	109.5(3)
C3-C2-C1	113.3(2)
C4-C2-C1	110.6(2)
C3-C2-H2	105.0(14)
C4-C2-H2	109.3(14)
C1-C2-H2	108.9(14)
C2-C3-H3A	107(2)
C2-C3-H3B	109(2)
H3A-C3-H3B	104(3)
C2-C3-H3C	110(2)
H3A-C3-H3C	113(3)
H3B-C3-H3C	114(3)
C2-C4-H4A	112(2)
C2-C4-H4B	111(2)
H4A-C4-H4B	106(3)
C2-C4-H4C	114(2)
H4A-C4-H4C	102(3)
H4B-C4-H4C	110(3)
C6-C5-W	127.0(2)
C6-C5-H5A	107(2)
W-C5-H5A	99(2)
C6-C5-H5B	109(2)
W-C5-H5B	104(2)
H5A-C5-H5B	110(2)
C7-C6-C5	113.2(2)
C7-C6-C8	109.2(3)
C5-C6-C8	111.0(2)
C7-C6-H6	111(2)
C5-C6-H6	106(2)
C8-C6-H6	106(2)
C6-C7-H7A	111(2)
C6-C7-H7B	111(2)
H7A-C7-H7B	108(3)
C6-C7-H7C	109(2)
H7A-C7-H7C	115(3)
H7B-C7-H7C	103(3)
C6-C8-H8A	114(2)
C6-C8-H8B	112(3)
H8A-C8-H8B	113(3)
C6-C8-H8C	110(3)
H8A-C8-H8C	103(4)
H8B-C8-H8C	104(4)
C14-C9-C10	119.5(2)

C14-C9-N1	119.8(2)
C10-C9-N1	120.7(2)
C11-C10-C9	119.4(2)
C11-C10-H10	123(2)
C9-C10-H10	118(2)
C12-C11-C10	121.0(2)
C12-C11-H11	123(2)
C10-C11-H11	116(2)
C13-C12-C11	119.6(2)
C13-C12-H12	119(2)
C11-C12-H12	121(2)
C12-C13-C14	120.5(3)
C12-C13-H13	119(2)
C14-C13-H13	121(2)
C13-C14-C9	120.0(2)
C13-C14-H14	119(2)
C9-C14-H14	121(2)
N2-C15-C16	125.2(2)
N2-C15-C20	115.5(2)
C16-C15-C20	119.2(2)
C17-C16-C15	120.3(2)
C17-C16-H16	120(2)
C15-C16-H16	120(2)
C16-C17-C18	120.3(2)
C16-C17-H17	115(2)
C18-C17-H17	125(2)
C19-C18-C17	121.1(2)
C19-C18-H18	118(2)
C17-C18-H18	121(2)
C18-C19-C20	120.1(2)
C18-C19-H19	122(2)
C20-C19-H19	118(2)
N3-C20-C19	125.6(2)
N3-C20-C15	115.5(2)
C19-C20-C15	119.0(2)
Si1-C21-H21A	111(2)
Si1-C21-H21B	113(3)
H21A-C21-H21B	104(3)
Si1-C21-H21C	110(2)
H21A-C21-H21C	112(3)
H21B-C21-H21C	105(3)
Si1-C22-H22A	114(2)
Si1-C22-H22B	118(3)
H22A-C22-H22B	95(3)
Si1-C22-H22C	109(3)
H22A-C22-H22C	109(3)
H22B-C22-H22C	111(4)
Si1-C23-H23A	112(2)
Si1-C23-H23B	110(2)
H23A-C23-H23B	110(3)
Si1-C23-H23C	103(2)
H23A-C23-H23C	109(3)
H23B-C23-H23C	113(3)
Si2-C24-H24A	103(2)

Si2-C24-H24B	111(3)
H24A-C24-H24B	113(3)
Si2-C24-H24C	109(3)
H24A-C24-H24C	113(4)
H24B-C24-H24C	107(4)
Si2-C25-H25A	114(3)
Si2-C25-H25B	112(3)
H25A-C25-H25B	103(4)
Si2-C25-H25C	112(3)
H25A-C25-H25C	102(4)
H25B-C25-H25C	113(4)
Si2-C26-H26A	117(2)
Si2-C26-H26B	118(2)
H26A-C26-H26B	96(3)
Si2-C26-H26C	116(2)
H26A-C26-H26C	103(3)
H26B-C26-H26C	105(3)

Symmetry transformations used to generate equivalent atoms:

Table A3.4. Anisotropic displacement parameters ($A^2 \times 10^3$) for **7**. The anisotropic displacement factor exponent takes the form: $-2\,p^2\,[\,h^2\,a^{*2}\,U11 + ... + 2\,h\,k\,a^*\,b^*\,U12\,]$

Atom	U11	U22	U33	U23	U13	U12
W	21(1)	18(1)	22(1)	4(1)	7(1)	5(1)
Si1	27(1)	35(1)	27(1)	9(1)	9(1)	15(1)
Si2	29(1)	21(1)	51(1)	2(1)	11(1)	10(1)
N1	25(1)	24(1)	25(1)	4(1)	7(1)	7(1)
N2	23(1)	23(1)	25(1)	5(1)	8(1)	7(1)
N3	23(1)	18(1)	31(1)	3(1)	6(1)	5(1)
C1	37(1)	22(1)	31(1)	0(1)	12(1)	11(1)
C2	42(1)	37(1)	31(1)	-2(1)	14(1)	14(1)
C3	59(2)	64(2)	35(2)	13(1)	23(1)	24(2)
C4	73(2)	51(2)	61(2)	-13(2)	30(2)	23(2)
C5	30(1)	25(1)	28(1)	7(1)	3(1)	7(1)
C6	33(1)	35(1)	26(1)	5(1)	5(1)	10(1)
C7	40(2)	57(2)	35(2)	4(1)	2(1)	-7(1)
C8	61(2)	69(2)	52(2)	21(2)	-21(2)	7(2)
C9	21(1)	29(1)	24(1)	9(1)	8(1)	9(1)
C10	37(1)	38(1)	29(1)	1(1)	11(1)	9(1)
C11	48(2)	65(2)	29(1)	7(1)	18(1)	19(1)
C12	35(1)	60(2)	40(2)	27(1)	16(1)	9(1)
C13	36(1)	31(1)	45(2)	15(1)	9(1)	2(1)
C14	33(1)	28(1)	30(1)	7(1)	9(1)	8(1)
C15	25(1)	25(1)	23(1)	3(1)	6(1)	6(1)
C16	26(1)	41(1)	33(1)	7(1)	11(1)	9(1)
C17	31(1)	50(2)	35(1)	8(1)	16(1)	4(1)
C18	38(1)	36(1)	33(1)	13(1)	10(1)	-3(1)
C19	36(1)	27(1)	32(1)	7(1)	5(1)	5(1)
C20	26(1)	24(1)	23(1)	1(1)	3(1)	5(1)
C21	61(2)	64(2)	50(2)	20(2)	23(2)	46(2)
C22	38(2)	57(2)	40(2)	7(1)	1(1)	5(1)
C23	39(1)	41(1)	39(1)	19(1)	15(1)	18(1)
C24	48(2)	39(2)	79(3)	-21(2)	19(2)	4(2)
C25	58(2)	52(2)	104(3)	40(2)	29(2)	37(2)
C26	37(1)	37(1)	60(2)	-1(1)	21(1)	16(1)

Table A3.5. Hydrogen coordinates (x 10^4) and isotropic displacement parameters (A^4 x 10^4) for **7**.

Atom	x	y	z	U(eq)
H1A	2970(3)	3810(3)	3077(15)	32(6)
H1B	4260(3)	3620(3)	3774(16)	39(7)
H2	960(3)	2280(2)	3600(14)	23(6)
H3A	3230(3)	2160(3)	4898(17)	36(7)
H3B	1530(4)	1620(3)	4880(2)	61(9)
H3C	2060(4)	800(4)	4240(2)	64(10)
H4A	1930(4)	4750(3)	4085(18)	42(8)
H4B	3260(4)	4650(4)	4800(2)	61(10)
H4C	1400(4)	3980(4)	4710(2)	64(10)
H5A	5340(3)	630(3)	3308(15)	31(6)
H5B	4320(4)	570(3)	3900(2)	60(9)
H6	5850(3)	2800(3)	4469(17)	41(7)
H7A	8250(4)	4060(3)	4187(19)	50(8)
H7B	7710(3)	2870(3)	3487(18)	36(8)
H7C	6790(5)	3690(4)	3410(2)	78(12)
H8A	8100(5)	2490(4)	5240(2)	78(11)
H8B	6460(5)	940(5)	5080(3)	105(15)
H8C	7670(6)	1260(6)	4570(3)	120(2)
H10	4580(3)	1710(3)	642(16)	35(7)
H11	5900(4)	3140(4)	-180(2)	73(11)
H12	7350(4)	5630(3)	259(19)	57(9)
H13	7350(4)	6490(4)	1500(19)	54(9)
H14	6020(3)	5110(3)	2308(18)	41(8)
H16	-1690(3)	150(3)	2711(14)	25(6)
H17	-2490(3)	-1680(3)	3364(17)	40(7)
H18	-1220(4)	-3270(3)	3577(18)	47(8)
H19	1040(3)	-2900(3)	3186(16)	39(7)
H21A	-1270(4)	3440(4)	1680(2)	69(11)
H21B	-1630(5)	2480(4)	2230(2)	86(13)
H21C	-60(5)	3580(4)	2460(2)	74(12)
H22A	-2370(4)	-280(4)	990(2)	68(11)
H22B	-1460(5)	-260(5)	440(3)	103(15)
H22C	-2330(5)	830(5)	420(3)	95(14)
H23A	2120(4)	3700(3)	1331(18)	49(8)
H23B	1620(4)	2420(4)	720(2)	57(10)
H23C	640(4)	3350(4)	610(2)	70(10)
H24A	710(4)	-3640(4)	1490(2)	64(11)
H24B	1690(5)	-3800(4)	990(2)	83(13)
H24C	1070(5)	-2740(4)	880(3)	87(16)
H25A	4390(5)	-2350(4)	3280(2)	70(13)
H25B	4370(5)	-3320(4)	2690(2)	82(12)
H25C	2940(7)	-3540(6)	3040(3)	134(19)
H26A	5400(4)	-100(4)	1920(2)	59(9)
H26B	4400(4)	-500(4)	1120(2)	67(11)
H26C	5270(5)	-1460(4)	1490(2)	77(11)

Crystallographic Data for W(NPh)[*o*-$(Me_3SiN)_2C_6H_4$]$(CH_2C(CH_3)_3)_2$, **10.**

Table A4.1: Crystallographic Data

Empirical formula	$C_{28}H_{49}N_3Si_2W$
Formula weight	667.73
Temperature	173(2) K
Wavelength	0.71073 Å
Crystal system	Monoclinic
Space group	P2(1)/n
Unit cell dimensions	a = 10.6992(4) Å $\alpha = 90°$
	b = 18.3144(7) Å $\beta = 92.042(1)°$
	c = 16.0726(6) Å $\gamma = 90°$
Volume, Z	3147.4(2) $Å^3$, 4
Density (calculated)	1.409 Mg/m^3
Absorption coefficient	3.766 mm^{-1}
F(000)	1360
Crystal size	29 x 24 x 15 mm
Theta range for data collection	3.31° to 27.43°
Limiting indices	$-13 \le h \le 8$, $-22 \le k \le 15$, $-20 \le l \le 20$
Reflections collected	13346
Independent reflections	6279 [R(int) = 0.0370]
Absorption correction	Integration
Max. and min. transmission	0.8591 and 0.3916
Refinement method	Full-matrix least-squares on F^2
Data / restraints / parameters	6274 / 0 / 307
Goodness-of-fit on F^2	1.124
Final R indices [I>2sigma(I)]	$R_1 = 0.0261$, $wR_2 = 0.0571$
R indices (all data)	$R_1 = 0.0294$, $wR_2 = 0.0600$
Largest diff. peak and hole	0.787 and -1.203 $e.Å^{-3}$

$R_1 = \hat{A}(||F_o| - |F_c||) / \hat{A}|F_o|$

$wR_2 = [\hat{A}[w(F_o^2 - F_c^2)^2] / \hat{A}[w(F_o^2)^2]]^{1/2}$

$S = [\hat{A}[w(F_o^2 - F_c^2)^2] / (n-p)]^{1/2}$

$w = 1/[s^2(F_o^2)+(0.0370*p)^2+0.31*p]$, $p = [\max(F_o^2,0)+ 2* F_c^2]/3$

Table A4.2. Atomic coordinates (x 10^4) and equivalent isotropic displacement parameters (A^2 x 10^3) for **10**. U(eq) is defined as one third of the trace of the orthogonalized Uij tensor.

Atom	x	y	z	U(eq)
W	4278(1)	2175(1)	2733(1)	17(1)
Si(1)	1245(1)	2897(1)	2441(1)	30(1)
Si(2)	5725(1)	1179(1)	1300(1)	26(1)
N(1)	5723(3)	1977(2)	3262(2)	22(1)
N(2)	2429(3)	2268(2)	2202(2)	23(1)
N(3)	4354(2)	1462(2)	1809(2)	20(1)
C(1)	4728(3)	3234(2)	2274(2)	22(1)
C(2)	5628(3)	3792(2)	2704(2)	27(1)
C(3)	6985(3)	3539(2)	2663(3)	33(1)
C(4)	5290(4)	3911(2)	3609(2)	33(1)
C(5)	5483(4)	4522(2)	2236(3)	43(1)
C(6)	3353(3)	2016(2)	3895(2)	23(1)
C(7)	3028(3)	1235(2)	4199(2)	29(1)
C(8)	4205(4)	776(2)	4364(3)	40(1)
C(9)	2358(5)	1319(3)	5025(3)	47(1)
C(10)	2161(4)	834(2)	3576(3)	42(1)
C(11)	6709(3)	1780(2)	3809(2)	21(1)
C(12)	7335(4)	1112(2)	3722(2)	32(1)
C(13)	8283(4)	915(2)	4286(3)	36(1)
C(14)	8624(3)	1366(2)	4946(2)	32(1)
C(15)	8014(3)	2024(2)	5042(2)	31(1)
C(16)	7068(3)	2234(2)	4472(2)	26(1)
C(17)	2153(3)	1684(2)	1668(2)	24(1)
C(18)	951(4)	1488(2)	1346(2)	33(1)
C(19)	788(4)	876(2)	849(3)	41(1)
C(20)	1790(4)	440(2)	666(3)	40(1)
C(21)	2982(4)	615(2)	980(2)	33(1)
C(22)	3167(3)	1239(2)	1469(2)	24(1)
C(23)	520(4)	3318(3)	1475(3)	52(1)
C(24)	1(4)	2472(3)	3077(3)	44(1)
C(25)	1881(4)	3688(2)	3064(3)	38(1)
C(26)	5445(4)	1290(3)	154(3)	45(1)
C(27)	6123(4)	215(2)	1573(3)	43(1)
C(28)	7102(4)	1761(2)	1550(3)	35(1)

Table A4.3. Bond lengths (Å) and angles [°] for **10**.

W-N(1)	1.775(3)
W-N(3)	1.981(3)
W-N(2)	2.133(3)
W-C(1)	2.135(3)
W-C(6)	2.165(3)
Si(1)-N(2)	1.764(3)
Si(1)-C(24)	1.875(4)
Si(1)-C(25)	1.876(4)
Si(1)-C(23)	1.876(4)
Si(2)-N(3)	1.783(3)
Si(2)-C(28)	1.850(4)
Si(2)-C(26)	1.865(4)
Si(2)-C(27)	1.867(4)
N(1)-C(11)	1.396(4)
N(2)-C(17)	1.395(4)
N(3)-C(22)	1.424(4)
C(1)-C(2)	1.550(5)
C(1)-H(1A)	0.97
C(1)-H(1B)	0.97
C(2)-C(3)	1.527(5)
C(2)-C(4)	1.528(5)
C(2)-C(5)	1.538(5)
C(3)-H(3A)	0.96
C(3)-H(3B)	0.96
C(3)-H(3C)	0.96
C(4)-H(4A)	0.96
C(4)-H(4B)	0.96
C(4)-H(4C)	0.96
C(5)-H(5A)	0.96
C(5)-H(5B)	0.96
C(5)-H(5C)	0.96
C(6)-C(7)	1.554(5)
C(6)-H(6A)	0.97
C(6)-H(6B)	0.97
C(7)-C(10)	1.528(5)
C(7)-C(8)	1.530(5)
C(7)-C(9)	1.539(5)
C(8)-H(8A)	0.96
C(8)-H(8B)	0.96
C(8)-H(8C)	0.96
C(9)-H(9A)	0.96
C(9)-H(9B)	0.96
C(9)-H(9C)	0.96
C(10)-H(10A)	0.96
C(10)-H(10B)	0.96
C(10)-H(10C)	0.96
C(11)-C(16)	1.395(5)
C(11)-C(12)	1.404(5)
C(12)-C(13)	1.384(5)

C(12)-H(12A)	0.93
C(13)-C(14)	1.383(6)
C(13)-H(13A)	0.93
C(14)-C(15)	1.382(5)
C(14)-H(14A)	0.93
C(15)-C(16)	1.394(5)
C(15)-H(15A)	0.93
C(16)-H(16A)	0.93
C(17)-C(22)	1.404(5)
C(17)-C(18)	1.415(5)
C(18)-C(19)	1.384(6)
C(18)-H(18A)	0.93
C(19)-C(20)	1.378(7)
C(19)-H(19A)	0.93
C(20)-C(21)	1.393(6)
C(20)-H(20A)	0.93
C(21)-C(22)	1.397(5)
C(21)-H(21A)	0.93
C(23)-H(23A)	0.96
C(23)-H(23B)	0.96
C(23)-H(23C)	0.96
C(24)-H(24A)	0.96
C(24)-H(24B)	0.96
C(24)-H(24C)	0.96
C(25)-H(25A)	0.96
C(25)-H(25B)	0.96
C(25)-H(25C)	0.96
C(26)-H(26A)	0.96
C(26)-H(26B)	0.96
C(26)-H(26C)	0.96
C(27)-H(27A)	0.96
C(27)-H(27B)	0.96
C(27)-H(27C)	0.96
C(28)-H(28A)	0.96
C(28)-H(28B)	0.96
C(28)-H(28C)	0.96

N(1)-W-N(3)	99.58(12)
N(1)-W-N(2)	170.89(12)
N(3)-W-N(2)	79.35(11)
N(1)-W-C(1)	98.47(13)
N(3)-W-C(1)	108.93(12)
N(2)-W-C(1)	90.40(12)
N(1)-W-C(6)	88.62(13)
N(3)-W-C(6)	126.15(12)
N(2)-W-C(6)	84.83(12)
C(1)-W-C(6)	122.40(13)
N(2)-Si(1)-C(24)	112.1(2)
N(2)-Si(1)-C(25)	111.7(2)
C(24)-Si(1)-C(25)	106.3(2)
N(2)-Si(1)-C(23)	111.5(2)
C(24)-Si(1)-C(23)	109.9(2)
C(25)-Si(1)-C(23)	104.8(2)
N(3)-Si(2)-C(28)	113.3(2)

N(3)-Si(2)-C(26)	108.4(2)
C(28)-Si(2)-C(26)	104.5(2)
N(3)-Si(2)-C(27)	110.6(2)
C(28)-Si(2)-C(27)	108.7(2)
C(26)-Si(2)-C(27)	111.2(2)
C(11)-N(1)-W	168.5(2)
C(17)-N(2)-Si(1)	119.7(2)
C(17)-N(2)-W	111.0(2)
Si(1)-N(2)-W	128.9(2)
C(22)-N(3)-Si(2)	118.5(2)
C(22)-N(3)-W	114.7(2)
Si(2)-N(3)-W	126.3(2)
C(2)-C(1)-W	126.2(2)
C(2)-C(1)-H(1A)	105.8(2)
W-C(1)-H(1A)	105.78(9)
C(2)-C(1)-H(1B)	105.8(2)
W-C(1)-H(1B)	105.78(9)
H(1A)-C(1)-H(1B)	106.2
C(3)-C(2)-C(4)	110.0(3)
C(3)-C(2)-C(5)	108.8(3)
C(4)-C(2)-C(5)	108.6(3)
C(3)-C(2)-C(1)	110.9(3)
C(4)-C(2)-C(1)	110.7(3)
C(5)-C(2)-C(1)	107.8(3)
C(2)-C(3)-H(3A)	109.5(2)
C(2)-C(3)-H(3B)	109.5(2)
H(3A)-C(3)-H(3B)	109.5
C(2)-C(3)-H(3C)	109.5(2)
H(3A)-C(3)-H(3C)	109.5
H(3B)-C(3)-H(3C)	109.5
C(2)-C(4)-H(4A)	109.5(2)
C(2)-C(4)-H(4B)	109.5(2)
H(4A)-C(4)-H(4B)	109.5
C(2)-C(4)-H(4C)	109.5(2)
H(4A)-C(4)-H(4C)	109.5
H(4B)-C(4)-H(4C)	109.5
C(2)-C(5)-H(5A)	109.5(2)
C(2)-C(5)-H(5B)	109.5(2)
H(5A)-C(5)-H(5B)	109.5
C(2)-C(5)-H(5C)	109.5(2)
H(5A)-C(5)-H(5C)	109.5
H(5B)-C(5)-H(5C)	109.5
C(7)-C(6)-W	120.6(2)
C(7)-C(6)-H(6A)	107.2(2)
W-C(6)-H(6A)	107.17(9)
C(7)-C(6)-H(6B)	107.2(2)
W-C(6)-H(6B)	107.17(9)
H(6A)-C(6)-H(6B)	106.8
C(10)-C(7)-C(8)	109.0(4)
C(10)-C(7)-C(9)	108.8(3)
C(8)-C(7)-C(9)	108.2(3)
C(10)-C(7)-C(6)	111.9(3)
C(8)-C(7)-C(6)	111.6(3)
C(9)-C(7)-C(6)	107.2(3)

C(7)-C(8)-H(8A)	109.5(2)
C(7)-C(8)-H(8B)	109.5(2)
H(8A)-C(8)-H(8B)	109.5
C(7)-C(8)-H(8C)	109.5(2)
H(8A)-C(8)-H(8C)	109.5
H(8B)-C(8)-H(8C)	109.5
C(7)-C(9)-H(9A)	109.5(2)
C(7)-C(9)-H(9B)	109.5(2)
H(9A)-C(9)-H(9B)	109.5
C(7)-C(9)-H(9C)	109.5(2)
H(9A)-C(9)-H(9C)	109.5
H(9B)-C(9)-H(9C)	109.5
C(7)-C(10)-H(10A)	109.5(2)
C(7)-C(10)-H(10B)	109.5(2)
H(10A)-C(10)-H(10B)	109.5
C(7)-C(10)-H(10C)	109.5(2)
H(10A)-C(10)-H(10C)	109.5
H(10B)-C(10)-H(10C)	109.5
C(16)-C(11)-N(1)	120.6(3)
C(16)-C(11)-C(12)	118.4(3)
N(1)-C(11)-C(12)	121.0(3)
C(13)-C(12)-C(11)	120.2(3)
C(13)-C(12)-H(12A)	119.9(2)
C(11)-C(12)-H(12A)	119.9(2)
C(14)-C(13)-C(12)	120.9(4)
C(14)-C(13)-H(13A)	119.5(2)
C(12)-C(13)-H(13A)	119.5(2)
C(15)-C(14)-C(13)	119.6(3)
C(15)-C(14)-H(14A)	120.2(2)
C(13)-C(14)-H(14A)	120.2(2)
C(14)-C(15)-C(16)	120.1(3)
C(14)-C(15)-H(15A)	120.0(2)
C(16)-C(15)-H(15A)	120.0(2)
C(15)-C(16)-C(11)	120.8(3)
C(15)-C(16)-H(16A)	119.6(2)
C(11)-C(16)-H(16A)	119.6(2)
N(2)-C(17)-C(22)	115.9(3)
N(2)-C(17)-C(18)	126.1(3)
C(22)-C(17)-C(18)	117.9(3)
C(19)-C(18)-C(17)	120.7(4)
C(19)-C(18)-H(18A)	119.6(2)
C(17)-C(18)-H(18A)	119.6(2)
C(20)-C(19)-C(18)	120.7(4)
C(20)-C(19)-H(19A)	119.7(2)
C(18)-C(19)-H(19A)	119.7(2)
C(19)-C(20)-C(21)	119.9(4)
C(19)-C(20)-H(20A)	120.1(2)
C(21)-C(20)-H(20A)	120.1(3)
C(20)-C(21)-C(22)	120.2(4)
C(20)-C(21)-H(21A)	119.9(3)
C(22)-C(21)-H(21A)	119.9(2)
C(21)-C(22)-C(17)	120.6(3)
C(21)-C(22)-N(3)	123.9(3)
C(17)-C(22)-N(3)	115.6(3)

Si(1)-C(23)-H(23A)	109.5(2)
Si(1)-C(23)-H(23B)	109.5(2)
H(23A)-C(23)-H(23B)	109.5
Si(1)-C(23)-H(23C)	109.5(2)
H(23A)-C(23)-H(23C)	109.5
H(23B)-C(23)-H(23C)	109.5
Si(1)-C(24)-H(24A)	109.5(2)
Si(1)-C(24)-H(24B)	109.5(2)
H(24A)-C(24)-H(24B)	109.5
Si(1)-C(24)-H(24C)	109.47(14)
H(24A)-C(24)-H(24C)	109.5
H(24B)-C(24)-H(24C)	109.5
Si(1)-C(25)-H(25A)	109.47(13)
Si(1)-C(25)-H(25B)	109.47(14)
H(25A)-C(25)-H(25B)	109.5
Si(1)-C(25)-H(25C)	109.47(12)
H(25A)-C(25)-H(25C)	109.5
H(25B)-C(25)-H(25C)	109.5
Si(2)-C(26)-H(26A)	109.5(2)
Si(2)-C(26)-H(26B)	109.5(2)
H(26A)-C(26)-H(26B)	109.5
Si(2)-C(26)-H(26C)	109.5(2)
H(26A)-C(26)-H(26C)	109.5
H(26B)-C(26)-H(26C)	109.5
Si(2)-C(27)-H(27A)	109.47(14)
Si(2)-C(27)-H(27B)	109.47(14)
H(27A)-C(27)-H(27B)	109.5
Si(2)-C(27)-H(27C)	109.5(2)
H(27A)-C(27)-H(27C)	109.5
H(27B)-C(27)-H(27C)	109.5
Si(2)-C(28)-H(28A)	109.47(13)
Si(2)-C(28)-H(28B)	109.47(14)
H(28A)-C(28)-H(28B)	109.5
Si(2)-C(28)-H(28C)	109.47(12)
H(28A)-C(28)-H(28C)	109.5
H(28B)-C(28)-H(28C)	109.5

Table A4.4. Anisotropic displacement parameters ($A^2 \times 10^3$) for **10**. The anisotropic displacement factor exponent takes the form: $-2\,p^2\,[\,h^2\,a^{*2}\,U11 + ... + 2\,h\,k\,a^*\,b^*\,U12\,]$

Atom	U11	U22	U33	U23	U13	U12
W	15(1)	19(1)	16(1)	0(1)	-2(1)	-1(1)
Si(1)	19(1)	44(1)	26(1)	2(1)	0(1)	8(1)
Si(2)	26(1)	26(1)	25(1)	-6(1)	0(1)	4(1)
N(1)	22(1)	19(1)	23(1)	1(1)	-1(1)	-3(1)
N(2)	16(1)	31(2)	21(1)	0(1)	-4(1)	-1(1)
N(3)	18(1)	23(1)	20(1)	-3(1)	-4(1)	-2(1)
C(1)	25(2)	23(2)	18(2)	1(1)	1(1)	-3(1)
C(2)	28(2)	20(2)	31(2)	1(1)	-5(2)	-3(1)
C(3)	25(2)	30(2)	43(2)	-3(2)	-1(2)	-8(2)
C(4)	37(2)	30(2)	32(2)	-10(2)	-4(2)	6(2)
C(5)	50(3)	24(2)	52(3)	7(2)	-15(2)	-8(2)
C(6)	23(2)	31(2)	16(2)	1(1)	1(1)	-3(1)
C(7)	26(2)	39(2)	23(2)	8(2)	-2(1)	-8(2)
C(8)	34(2)	35(2)	49(3)	16(2)	-5(2)	-2(2)
C(9)	48(3)	62(3)	31(2)	11(2)	6(2)	-15(2)
C(10)	49(3)	40(2)	36(2)	9(2)	-12(2)	-18(2)
C(11)	15(2)	26(2)	21(2)	1(1)	-3(1)	-1(1)
C(12)	31(2)	31(2)	32(2)	-10(2)	-9(2)	8(2)
C(13)	35(2)	35(2)	39(2)	-2(2)	-6(2)	15(2)
C(14)	24(2)	44(2)	28(2)	2(2)	-6(2)	4(2)
C(15)	25(2)	42(2)	24(2)	-3(2)	-8(1)	0(2)
C(16)	23(2)	29(2)	26(2)	-6(1)	-4(1)	4(1)
C(17)	24(2)	32(2)	16(2)	7(1)	-2(1)	-8(1)
C(18)	23(2)	46(2)	29(2)	5(2)	-6(1)	-4(2)
C(19)	34(2)	53(3)	34(2)	5(2)	-12(2)	-22(2)
C(20)	52(3)	35(2)	32(2)	-3(2)	-13(2)	-16(2)
C(21)	38(2)	30(2)	30(2)	0(2)	-6(2)	-8(2)
C(22)	27(2)	26(2)	20(2)	3(1)	-4(1)	-6(1)
C(23)	41(3)	72(3)	41(2)	10(2)	-6(2)	27(2)
C(24)	18(2)	71(3)	43(2)	0(2)	4(2)	3(2)
C(25)	32(2)	40(2)	43(2)	-5(2)	8(2)	10(2)
C(26)	48(3)	58(3)	29(2)	-5(2)	5(2)	2(2)
C(27)	43(2)	30(2)	55(3)	-9(2)	-10(2)	9(2)
C(28)	25(2)	43(2)	37(2)	-9(2)	9(2)	-4(2)

Table A4.5. Hydrogen coordinates (x 10^4) and isotropic displacement parameters (A^4 x 10^4) for **10**.

Atom	x	y	z	U(eq)
H(1A)	5045(3)	3156(2)	1723(2)	26
H(1B)	3936(3)	3486(2)	2193(2)	26
H(3A)	7190(3)	3465(2)	2092(3)	49
H(3B)	7089(3)	3089(2)	2963(3)	49
H(3C)	7528(3)	3903(2)	2907(3)	49
H(4A)	4436(4)	4070(2)	3630(2)	49
H(4B)	5829(4)	4276(2)	3856(2)	49
H(4C)	5391(4)	3462(2)	3911(2)	49
H(5A)	4632(4)	4686(2)	2258(3)	64
H(5B)	5696(4)	4456(2)	1666(3)	64
H(5C)	6028(4)	4879(2)	2492(3)	64
H(6A)	3874(3)	2241(2)	4329(2)	28
H(6B)	2578(3)	2290(2)	3859(2)	28
H(8A)	4755(4)	1024(2)	4755(3)	60
H(8B)	4624(4)	704(2)	3851(3)	60
H(8C)	3976(4)	311(2)	4588(3)	60
H(9A)	2896(5)	1571(3)	5421(3)	70
H(9B)	2158(5)	846(3)	5238(3)	70
H(9C)	1603(5)	1595(3)	4931(3)	70
H(10A)	1420(4)	1120(2)	3470(3)	63
H(10B)	1935(4)	369(2)	3802(3)	63
H(10C)	2582(4)	762(2)	3065(3)	63
H(12A)	7111(4)	801(2)	3284(2)	38
H(13A)	8697(4)	474(2)	4220(3)	44
H(14A)	9259(3)	1227(2)	5323(2)	39
H(15A)	8234(3)	2327(2)	5488(2)	37
H(16A)	6673(3)	2681(2)	4535(2)	31
H(18A)	263(4)	1773(2)	1470(2)	39
H(19A)	-6(4)	759(2)	636(3)	49
H(20A)	1670(4)	29(2)	333(3)	48
H(21A)	3656(4)	315(2)	865(2)	40
H(23A)	1162(4)	3534(3)	1153(3)	77
H(23B)	-66(4)	3687(3)	1627(3)	77
H(23C)	93(4)	2948(3)	1151(3)	77
H(24A)	-356(4)	2062(3)	2782(3)	66
H(24B)	-640(4)	2826(3)	3173(3)	66
H(24C)	362(4)	2312(3)	3600(3)	66
H(25A)	2526(4)	3925(2)	2763(3)	58
H(25B)	2224(4)	3515(2)	3588(3)	58
H(25C)	1221(4)	4029(2)	3160(3)	58
H(26A)	4736(4)	1001(3)	-25(3)	67
H(26B)	6170(4)	1131(3)	-130(3)	67
H(26C)	5284(4)	1794(3)	29(3)	67
H(27A)	5415(4)	-93(2)	1446(3)	64
H(27B)	6340(4)	182(2)	2157(3)	64

H(27C)	6820(4)	58(2)	1257(3)	64
H(28A)	7306(4)	1732(2)	2136(3)	52
H(28B)	6914(4)	2257(2)	1402(3)	52
H(28C)	7800(4)	1594(2)	1243(3)	52

Crystallographic Data for W(NPh)[*o*-$(Me_3SiN)_2C_6H_4$]$(CH_2C(CH_3)_3)Cl$, **15.**

Table A5.1: Crystallographic Data

Identification code	sw06
Empirical formula	C_{23} H_{38} Cl N_3 Si_2 W
Formula weight	632.04
Temperature	173(2) K
Wavelength	0.71073 Å
Crystal system	Triclinic
Space group	P-1
Unit cell dimensions	a = 9.35310(10) Å α = 96.705(1)°
	b = 11.2640(2) Å β = 93.814(1)°
	c = 14.1166(2) Å γ = 111.296(1)°
Volume, Z	1366.63(3) $Å^3$, 2
Density (calculated)	1.536 Mg/m^3
Absorption coefficient	4.426 mm^{-1}
F(000)	632
Crystal size	0.09 x 0.10 x 0.23 mm
Theta range for data collection	1.46° to 27.49°
Limiting indices	$-12 \le h \le 11$, $-14 \le k \le 15$, $-11 \le l \le 19$
Reflections collected	8884
Independent reflections	6107 [R(int) = 0.0487]
Absorption correction	Integration
Refinement method	Full-matrix least-squares on F^2
Data / restraints / parameters	6069 / 0 / 272
Goodness-of-fit on F^2	1.083
Final R indices [I>2sigma(I)]	R_1 = 0.0339, wR_2 = 0.0850
R indices (all data)	R_1 = 0.0376, wR_2 = 0.0913
Extinction coefficient	0.0021(4)
Largest diff. peak and hole	0.997 and -1.461 e.$Å^{-3}$

$R_1 = \hat{A}(||F_o| - |F_c||) / \hat{A}|F_o|$

$wR_2 = [\hat{A}[w(F_o^2 - F_c^2)^2] / \hat{A}[w(F_o^2)^2]]^{1/2}$

$S = [\hat{A}[w(F_o^2 - F_c^2)^2] / (n-p)]^{1/2}$

$w = 1/[s^2(F_o^2)+(0.0370*p)^2+0.31*p]$, $p = [\max(F_o^2,0)+ 2* F_c^2]/3$

Table A5.2. Atomic coordinates (x 10^4) and equivalent isotropic displacement parameters (A^2 x 10^3) for **15**. U(eq) is defined as one third of the trace of the orthogonalized Uij tensor.

Atom	x	y	z	U(eq)
W	4307(1)	3137(1)	2355(1)	21(1)
Cl	6426(2)	3169(1)	1448(1)	40(1)
Si(1)	901(1)	2537(1)	3413(1)	25(1)
Si(2)	6712(2)	6319(1)	2355(1)	29(1)
N(1)	2379(4)	3321(3)	2695(3)	22(1)
N(2)	4915(4)	5012(3)	2222(3)	23(1)
N(3)	4890(4)	2516(4)	3317(3)	26(1)
C(1)	5683(5)	2318(5)	4112(3)	27(1)
C(2)	6043(6)	1228(5)	4084(4)	35(1)
C(3)	6857(7)	1030(6)	4873(5)	47(1)
C(4)	7265(7)	1904(7)	5703(4)	50(2)
C(5)	6910(7)	2983(7)	5754(4)	49(2)
C(6)	6110(6)	3210(5)	4960(4)	35(1)
C(7)	2155(5)	4179(4)	2104(3)	23(1)
C(8)	716(5)	4213(5)	1770(3)	29(1)
C(9)	652(6)	5113(5)	1205(4)	34(1)
C(10)	2004(7)	5963(5)	931(4)	38(1)
C(11)	3405(6)	5939(4)	1221(3)	29(1)
C(12)	3530(5)	5071(4)	1836(3)	23(1)
C(13)	1697(7)	1749(6)	4279(4)	39(1)
C(14)	-799(6)	1303(5)	2618(4)	38(1)
C(15)	293(6)	3755(5)	4088(4)	32(1)
C(16)	8075(7)	5956(6)	3185(5)	45(1)
C(17)	7459(7)	6588(6)	1170(4)	43(1)
C(18)	6471(8)	7806(5)	2928(5)	47(1)
C(19)	2907(6)	1539(5)	1246(3)	28(1)
C(20)	2778(6)	127(5)	1190(4)	34(1)
C(21)	1843(9)	-608(6)	228(5)	54(2)
C(22)	1956(9)	-489(6)	2007(5)	52(2)
C(23)	4358(7)	9(6)	1238(4)	42(1)

Table A5.3. Bond lengths (Å) and angles [°] for **15**.

W-N(3)	1.741(4)
W-N(1)	1.973(4)
W-N(2)	2.013(4)
W-C(19)	2.182(5)
W-Cl	2.4216(11)
Si(1)-N(1)	1.796(4)
Si(1)-C(13)	1.856(5)
Si(1)-C(15)	1.857(5)
Si(1)-C(14)	1.874(5)
Si(2)-N(2)	1.768(4)
Si(2)-C(16)	1.860(6)
Si(2)-C(18)	1.869(6)
Si(2)-C(17)	1.870(6)
N(1)-C(7)	1.410(5)
N(2)-C(12)	1.399(6)
N(3)-C(1)	1.388(6)
C(1)-C(2)	1.383(7)
C(1)-C(6)	1.402(7)
C(2)-C(3)	1.393(7)
C(2)-H(2A)	0.93
C(3)-C(4)	1.373(10)
C(3)-H(3A)	0.93
C(4)-C(5)	1.366(10)
C(4)-H(4A)	0.93
C(5)-C(6)	1.405(8)
C(5)-H(5A)	0.93
C(6)-H(6A)	0.93
C(7)-C(8)	1.411(6)
C(7)-C(12)	1.422(6)
C(8)-C(9)	1.377(7)
C(8)-H(8A)	0.93
C(9)-C(10)	1.392(8)
C(9)-H(9A)	0.93
C(10)-C(11)	1.358(7)
C(10)-H(10A)	0.93
C(11)-C(12)	1.410(6)
C(11)-H(11A)	0.93
C(13)-H(13A)	0.96
C(13)-H(13B)	0.96
C(13)-H(13C)	0.96
C(14)-H(14A)	0.96
C(14)-H(14B)	0.96
C(14)-H(14C)	0.96
C(15)-H(15A)	0.96
C(15)-H(15B)	0.96
C(15)-H(15C)	0.96
C(16)-H(16A)	0.96
C(16)-H(16B)	0.96
C(16)-H(16C)	0.96

C(17)-H(17A)	0.96
C(17)-H(17B)	0.96
C(17)-H(17C)	0.96
C(18)-H(18A)	0.96
C(18)-H(18B)	0.96
C(18)-H(18C)	0.96
C(19)-C(20)	1.543(6)
C(19)-H(19A)	0.97
C(19)-H(19B)	0.97
C(20)-C(22)	1.524(8)
C(20)-C(23)	1.528(8)
C(20)-C(21)	1.532(7)
C(21)-H(21A)	0.96
C(21)-H(21B)	0.96
C(21)-H(21C)	0.96
C(22)-H(22A)	0.96
C(22)-H(22B)	0.96
C(22)-H(22C)	0.96
C(23)-H(23A)	0.96
C(23)-H(23B)	0.96
C(23)-H(23C)	0.96

N(3)-W-N(1)	103.9(2)
N(3)-W-N(2)	126.6(2)
N(1)-W-N(2)	82.6(2)
N(3)-W-C(19)	108.8(2)
N(1)-W-C(19)	88.0(2)
N(2)-W-C(19)	124.5(2)
N(3)-W-Cl	95.88(12)
N(1)-W-Cl	160.21(11)
N(2)-W-Cl	86.42(11)
C(19)-W-Cl	84.69(14)
N(1)-Si(1)-C(13)	108.9(2)
N(1)-Si(1)-C(15)	109.4(2)
C(13)-Si(1)-C(15)	109.1(2)
N(1)-Si(1)-C(14)	109.7(2)
C(13)-Si(1)-C(14)	110.0(3)
C(15)-Si(1)-C(14)	109.7(2)
N(2)-Si(2)-C(16)	107.5(2)
N(2)-Si(2)-C(18)	108.9(2)
C(16)-Si(2)-C(18)	108.0(3)
N(2)-Si(2)-C(17)	111.5(2)
C(16)-Si(2)-C(17)	111.3(3)
C(18)-Si(2)-C(17)	109.5(3)
C(7)-N(1)-Si(1)	119.7(3)
C(7)-N(1)-W	104.6(3)
Si(1)-N(1)-W	135.1(2)
C(12)-N(2)-Si(2)	123.4(3)
C(12)-N(2)-W	102.9(3)
Si(2)-N(2)-W	133.2(2)
C(1)-N(3)-W	165.1(4)
C(2)-C(1)-N(3)	120.4(4)
C(2)-C(1)-C(6)	119.0(5)
N(3)-C(1)-C(6)	120.6(4)

C(1)-C(2)-C(3)	120.8(6)
C(1)-C(2)-H(2A)	119.6(3)
C(3)-C(2)-H(2A)	119.6(4)
C(4)-C(3)-C(2)	119.8(6)
C(4)-C(3)-H(3A)	120.1(4)
C(2)-C(3)-H(3A)	120.1(4)
C(5)-C(4)-C(3)	120.6(5)
C(5)-C(4)-H(4A)	119.7(4)
C(3)-C(4)-H(4A)	119.7(4)
C(4)-C(5)-C(6)	120.5(6)
C(4)-C(5)-H(5A)	119.8(4)
C(6)-C(5)-H(5A)	119.8(4)
C(1)-C(6)-C(5)	119.3(5)
C(1)-C(6)-H(6A)	120.4(3)
C(5)-C(6)-H(6A)	120.4(4)
N(1)-C(7)-C(8)	125.7(4)
N(1)-C(7)-C(12)	115.0(4)
C(8)-C(7)-C(12)	119.2(4)
C(9)-C(8)-C(7)	120.2(4)
C(9)-C(8)-H(8A)	119.9(3)
C(7)-C(8)-H(8A)	119.9(3)
C(8)-C(9)-C(10)	120.1(5)
C(8)-C(9)-H(9A)	120.0(3)
C(10)-C(9)-H(9A)	120.0(3)
C(11)-C(10)-C(9)	121.3(5)
C(11)-C(10)-H(10A)	119.4(3)
C(9)-C(10)-H(10A)	119.4(3)
C(10)-C(11)-C(12)	120.5(5)
C(10)-C(11)-H(11A)	119.7(3)
C(12)-C(11)-H(11A)	119.7(3)
N(2)-C(12)-C(11)	125.4(4)
N(2)-C(12)-C(7)	116.0(4)
C(11)-C(12)-C(7)	118.7(4)
Si(1)-C(13)-H(13A)	109.5(2)
Si(1)-C(13)-H(13B)	109.5(2)
H(13A)-C(13)-H(13B)	109.5
Si(1)-C(13)-H(13C)	109.5(2)
H(13A)-C(13)-H(13C)	109.5
H(13B)-C(13)-H(13C)	109.5
Si(1)-C(14)-H(14A)	109.5(2)
Si(1)-C(14)-H(14B)	109.5(2)
H(14A)-C(14)-H(14B)	109.5
Si(1)-C(14)-H(14C)	109.5(2)
H(14A)-C(14)-H(14C)	109.5
H(14B)-C(14)-H(14C)	109.5
Si(1)-C(15)-H(15A)	109.5(2)
Si(1)-C(15)-H(15B)	109.5(2)
H(15A)-C(15)-H(15B)	109.5
Si(1)-C(15)-H(15C)	109.5(2)
H(15A)-C(15)-H(15C)	109.5
H(15B)-C(15)-H(15C)	109.5
Si(2)-C(16)-H(16A)	109.5(2)
Si(2)-C(16)-H(16B)	109.5(2)
H(16A)-C(16)-H(16B)	109.5

Si(2)-C(16)-H(16C)	109.5(2)
H(16A)-C(16)-H(16C)	109.5
H(16B)-C(16)-H(16C)	109.5
Si(2)-C(17)-H(17A)	109.5(2)
Si(2)-C(17)-H(17B)	109.5(2)
H(17A)-C(17)-H(17B)	109.5
Si(2)-C(17)-H(17C)	109.5(2)
H(17A)-C(17)-H(17C)	109.5
H(17B)-C(17)-H(17C)	109.5
Si(2)-C(18)-H(18A)	109.5(2)
Si(2)-C(18)-H(18B)	109.5(2)
H(18A)-C(18)-H(18B)	109.5
Si(2)-C(18)-H(18C)	109.5(2)
H(18A)-C(18)-H(18C)	109.5
H(18B)-C(18)-H(18C)	109.5
C(20)-C(19)-W	126.1(3)
C(20)-C(19)-H(19A)	105.8(3)
W-C(19)-H(19A)	105.80(13)
C(20)-C(19)-H(19B)	105.8(3)
W-C(19)-H(19B)	105.80(13)
H(19A)-C(19)-H(19B)	106.2
C(22)-C(20)-C(23)	107.9(5)
C(22)-C(20)-C(21)	109.3(5)
C(23)-C(20)-C(21)	108.7(5)
C(22)-C(20)-C(19)	111.0(4)
C(23)-C(20)-C(19)	112.3(4)
C(21)-C(20)-C(19)	107.6(4)
C(20)-C(21)-H(21A)	109.5(4)
C(20)-C(21)-H(21B)	109.5(3)
H(21A)-C(21)-H(21B)	109.5
C(20)-C(21)-H(21C)	109.5(3)
H(21A)-C(21)-H(21C)	109.5
H(21B)-C(21)-H(21C)	109.5
C(20)-C(22)-H(22A)	109.5(4)
C(20)-C(22)-H(22B)	109.5(3)
H(22A)-C(22)-H(22B)	109.5
C(20)-C(22)-H(22C)	109.5(3)
H(22A)-C(22)-H(22C)	109.5
H(22B)-C(22)-H(22C)	109.5
C(20)-C(23)-H(23A)	109.5(3)
C(20)-C(23)-H(23B)	109.5(3)
H(23A)-C(23)-H(23B)	109.5
C(20)-C(23)-H(23C)	109.5(3)
H(23A)-C(23)-H(23C)	109.5
H(23B)-C(23)-H(23C)	109.5

Table A5.4. Anisotropic displacement parameters ($A^2 \times 10^3$) for **15**. The anisotropic displacement factor exponent takes the form: $-2\pi^2 [h^2 a^{*2} U11 + ... + 2 h k a^* b^* U12]$

Atom	U11	U22	U33	U23	U13	U12
W	21(1)	20(1)	23(1)	6(1)	4(1)	9(1)
Cl	37(1)	39(1)	52(1)	13(1)	26(1)	19(1)
Si(1)	24(1)	24(1)	26(1)	6(1)	6(1)	7(1)
Si(2)	24(1)	26(1)	36(1)	9(1)	6(1)	5(1)
N(1)	23(2)	22(2)	23(2)	3(1)	3(1)	8(1)
N(2)	18(2)	19(2)	32(2)	9(1)	5(1)	3(1)
N(3)	21(2)	31(2)	31(2)	7(2)	5(2)	15(2)
C(1)	21(2)	31(2)	26(2)	11(2)	3(2)	6(2)
C(2)	32(2)	35(3)	40(3)	14(2)	4(2)	12(2)
C(3)	40(3)	52(3)	54(3)	31(3)	4(3)	18(3)
C(4)	36(3)	68(4)	40(3)	33(3)	-1(2)	6(3)
C(5)	37(3)	66(4)	27(3)	10(3)	2(2)	1(3)
C(6)	33(3)	39(3)	31(2)	5(2)	5(2)	10(2)
C(7)	24(2)	22(2)	23(2)	2(2)	0(2)	11(2)
C(8)	23(2)	36(2)	32(2)	6(2)	4(2)	15(2)
C(9)	31(2)	41(3)	34(2)	7(2)	-2(2)	18(2)
C(10)	51(3)	29(2)	37(3)	10(2)	0(2)	20(2)
C(11)	32(2)	21(2)	33(2)	8(2)	3(2)	10(2)
C(12)	27(2)	24(2)	22(2)	3(2)	2(2)	13(2)
C(13)	43(3)	42(3)	37(3)	16(2)	15(2)	19(2)
C(14)	28(2)	31(3)	46(3)	3(2)	4(2)	4(2)
C(15)	31(2)	35(3)	31(2)	5(2)	11(2)	13(2)
C(16)	31(3)	47(3)	51(3)	12(3)	-5(2)	8(2)
C(17)	39(3)	43(3)	48(3)	19(2)	16(2)	12(2)
C(18)	48(3)	29(3)	58(4)	4(2)	13(3)	6(2)
C(19)	36(2)	28(2)	23(2)	0(2)	-2(2)	17(2)
C(20)	42(3)	29(2)	33(2)	2(2)	1(2)	17(2)
C(21)	69(4)	36(3)	52(3)	-13(3)	-24(3)	26(3)
C(22)	72(4)	30(3)	56(4)	13(3)	14(3)	17(3)
C(23)	51(3)	38(3)	42(3)	-4(2)	-3(2)	28(3)

Table A5.5. Hydrogen coordinates (x 10^4) and isotropic displacement parameters (A^4 x 10^4) for **15**.

Atom	x	y	z	U(eq)
H(2A)	5738(6)	619(5)	3530(4)	42
H(3A)	7122(7)	308(6)	4839(5)	56
H(4A)	7789(7)	1762(7)	6234(4)	60
H(5A)	7199(7)	3571(7)	6319(4)	58
H(6A)	5867(6)	3943(5)	4997(4)	43
H(8A)	-192(5)	3625(5)	1933(3)	35
H(9A)	-295(6)	5153(5)	1005(4)	41
H(10A)	1947(7)	6559(5)	541(4)	45
H(11A)	4290(6)	6499(4)	1014(3)	34
H(13A)	2013(7)	1118(6)	3933(4)	58
H(13B)	918(7)	1335(6)	4671(4)	58
H(13C)	2571(7)	2386(6)	4679(4)	58
H(14A)	-1203(6)	1719(5)	2173(4)	56
H(14B)	-1585(6)	884(5)	3004(4)	56
H(14C)	-481(6)	676(5)	2270(4)	56
H(15A)	-119(6)	4166(5)	3644(4)	48
H(15B)	1169(6)	4391(5)	4489(4)	48
H(15C)	-484(6)	3339(5)	4481(4)	48
H(16A)	8217(7)	5193(6)	2904(5)	67
H(16B)	7661(7)	5819(6)	3784(5)	67
H(16C)	9052(7)	6668(6)	3294(5)	67
H(17A)	6734(7)	6773(6)	757(4)	64
H(17B)	7593(7)	5827(6)	879(4)	64
H(17C)	8433(7)	7302(6)	1265(4)	64
H(18A)	5770(8)	8012(5)	2511(5)	71
H(18B)	7456(8)	8509(5)	3038(5)	71
H(18C)	6065(8)	7660(5)	3529(5)	71
H(19A)	1859(6)	1513(5)	1246(3)	34
H(19B)	3238(6)	1801(5)	641(3)	34
H(21A)	2359(9)	-222(6)	-288(5)	81
H(21B)	832(9)	-572(6)	200(5)	81
H(21C)	1753(9)	-1491(6)	169(5)	81
H(22A)	958(9)	-426(6)	1992(5)	78
H(22B)	2557(9)	-48(6)	2610(5)	78
H(22C)	1834(9)	-1379(6)	1935(5)	78
H(23A)	4900(7)	392(6)	729(4)	62
H(23B)	4222(7)	-884(6)	1171(4)	62
H(23C)	4945(7)	447(6)	1846(4)	62

Crystallographic Data for W(NPh)[*o*-$(Me_3SiN)_2C_6H_4$]$(CH_3)_2(PMe_3)$, **21.**

Table A6.1: Crystallographic Data

Identification code	wangt
Empirical formula	$C_{23}\ H_{42}\ N_3\ P\ Si_2\ W$
Formula weight	631.60
Temperature	173(2) K
Wavelength	0.71073 Å
Crystal system	Monoclinic
Space group	C2/m
Unit cell dimensions	a = 13.5336(1) Å α = 90°
	b = 14.4291(1) Å β = 110.365(1)°
	c = 15.3785(1) Å γ = 90°
Volume, Z	2815.37(3) $Å^3$, 4
Density (calculated)	1.490 Mg/m^3
Absorption coefficient	4.259 mm^{-1}
F(000)	1272
Crystal size	0.16 x 0.15 x 0.04 mm
Theta range for data collection	3.93° to 27.44°
Limiting indices	$-17\le h\le 17$, $-18\le k\le 17$, $-19\le l\le 10$
Reflections collected	7731
Independent reflections	3130 [R(int) = 0.0574]
Refinement method	Full-matrix least-squares on F^2
Data / restraints / parameters	3129 / 0 / 151
Goodness-of-fit on F^2	1.091
Final R indices [I>2sigma(I)]	R_1 = 0.0272, wR_2 = 0.0712
R indices (all data)	R_1 = 0.0280, wR_2 = 0.0724
Largest diff. peak and hole	1.037 and -1.642 $e.Å^{-3}$

$R_1 = \hat{A}(||F_o| - |F_c||) / \hat{A}|F_o|$

$wR_2 = [\hat{A}[w(F_o^2 - F_c^2)^2] / \hat{A}[w(F_o^2)^2]]^{1/2}$

$S = [\hat{A}[w(F_o^2 - F_c^2)^2] / (n-p)]^{1/2}$

$w= 1/[s^2(F_o^2)+(0.0370*p)^2+0.31*p]$, $p = [\max(F_o^2,0)+ 2* F_c^2]/3$

Table A6.2. Atomic coordinates (x 10^4) and equivalent isotropic displacement parameters (A^2 x 10^3) for **21**. U(eq) is defined as one third of the trace of the orthogonalized Uij tensor.

Atom	x	y	z	U(eq)
W	4041(1)	0	2172(1)	21(1)
P	2483(1)	0	485(1)	28(1)
Si	3363(1)	-2029(1)	3007(1)	23(1)
N(1)	5314(3)	0	3016(3)	26(1)
N(2)	3057(2)	-895(2)	2537(2)	19(1)
C(1)	6357(3)	0	3590(3)	23(1)
C(2)	6641(4)	0	4555(3)	31(1)
C(3)	7683(4)	0	5119(3)	36(1)
C(4)	8474(4)	0	4739(4)	36(1)
C(5)	8204(4)	0	3785(4)	34(1)
C(6)	7156(3)	0	3201(3)	27(1)
C(7)	2091(2)	-498(2)	2448(2)	20(1)
C(8)	1155(2)	-964(2)	2383(2)	24(1)
C(9)	257(2)	-483(3)	2336(2)	29(1)
C(10)	2815(3)	-2266(3)	3940(2)	33(1)
C(11)	2820(3)	-2890(2)	2043(3)	35(1)
C(12)	4815(3)	-2174(3)	3563(3)	37(1)
C(13)	1586(3)	-990(4)	205(3)	46(1)
C(14)	2952(5)	0	-500(3)	39(1)
C(15)	4480(3)	-1133(3)	1402(3)	34(1)

Table A6.3. Bond lengths (Å) and angles [°] for **21**.

W-N(1)	1.760(4)
W-N(2)	2.067(2)
W-N(2)#1	2.067(2)
W-C(15)	2.218(3)
W-C(15)#1	2.218(3)
W-P	2.7148(12)
P-C(13)#1	1.827(4)
P-C(13)	1.827(4)
P-C(14)	1.834(5)
Si-N(2)	1.779(3)
Si-C(12)	1.861(4)
Si-C(10)	1.863(4)
Si-C(11)	1.877(4)
N(1)-C(1)	1.380(6)
N(2)-C(7)	1.390(4)
C(1)-C(2)	1.399(7)
C(1)-C(6)	1.406(6)
C(2)-C(3)	1.374(7)
C(2)-H(2)	0.93
C(3)-C(4)	1.387(8)
C(3)-H(3)	0.93
C(4)-C(5)	1.383(8)
C(4)-H(4)	0.93
C(5)-C(6)	1.391(7)
C(5)-H(5)	0.93
C(6)-H(6)	0.93
C(7)-C(8)	1.406(4)
C(7)-C(7)#1	1.437(6)
C(8)-C(9)	1.379(5)
C(8)-H(8)	0.93
C(9)-C(9)#1	1.394(8)
C(10)-H(10A)	0.96
C(10)-H(10B)	0.96
C(10)-H(10C)	0.96
C(11)-H(11A)	0.96
C(11)-H(11B)	0.96
C(11)-H(11C)	0.96
C(12)-H(12A)	0.96
C(12)-H(12B)	0.96
C(12)-H(12C)	0.96
C(13)-H(13A)	0.96
C(13)-H(13B)	0.96
C(13)-H(13C)	0.96
C(14)-H(14A)	0.96
C(14)-H(14B)	0.96
C(15)-H(15A)	0.96
C(15)-H(15B)	0.96
C(15)-H(15C)	0.96

N(1)-W-N(2)	110.99(12)
N(1)-W-N(2)#1	110.99(12)
N(2)-W-N(2)#1	77.30(14)
N(1)-W-C(15)	91.03(13)
N(2)-W-C(15)	90.13(12)
N(2)#1-W-C(15)	157.34(12)
N(1)-W-C(15)#1	91.03(13)
N(2)-W-C(15)#1	157.34(12)
N(2)#1-W-C(15)#1	90.13(12)
C(15)-W-C(15)#1	94.9(2)
N(1)-W-P	160.04(13)
N(2)-W-P	84.28(7)
N(2)#1-W-P	84.28(7)
C(15)-W-P	75.67(10)
C(15)#1-W-P	75.67(10)
C(13)#1-P-C(13)	102.9(3)
C(13)#1-P-C(14)	101.4(2)
C(13)-P-C(14)	101.4(2)
C(13)#1-P-W	117.17(13)
C(13)-P-W	117.17(13)
C(14)-P-W	114.4(2)
N(2)-Si-C(12)	110.4(2)
N(2)-Si-C(10)	112.5(2)
C(12)-Si-C(10)	105.3(2)
N(2)-Si-C(11)	108.47(14)
C(12)-Si-C(11)	110.5(2)
C(10)-Si-C(11)	109.6(2)
C(1)-N(1)-W	173.1(4)
C(7)-N(2)-Si	119.8(2)
C(7)-N(2)-W	112.9(2)
Si-N(2)-W	127.16(13)
N(1)-C(1)-C(2)	121.4(4)
N(1)-C(1)-C(6)	119.6(4)
C(2)-C(1)-C(6)	118.9(4)
C(3)-C(2)-C(1)	120.8(5)
C(3)-C(2)-H(2)	119.6(3)
C(1)-C(2)-H(2)	119.6(3)
C(2)-C(3)-C(4)	120.4(5)
C(2)-C(3)-H(3)	119.8(3)
C(4)-C(3)-H(3)	119.8(3)
C(5)-C(4)-C(3)	119.4(4)
C(5)-C(4)-H(4)	120.3(3)
C(3)-C(4)-H(4)	120.3(3)
C(4)-C(5)-C(6)	121.2(5)
C(4)-C(5)-H(5)	119.4(3)
C(6)-C(5)-H(5)	119.4(3)
C(5)-C(6)-C(1)	119.2(4)
C(5)-C(6)-H(6)	120.4(3)
C(1)-C(6)-H(6)	120.4(3)
N(2)-C(7)-C(8)	127.1(3)
N(2)-C(7)-C(7)#1	114.3(2)
C(8)-C(7)-C(7)#1	118.5(2)
C(9)-C(8)-C(7)	121.3(3)
C(9)-C(8)-H(8)	119.4(2)

C(7)-C(8)-H(8)	119.4(2)
C(8)-C(9)-C(9)#1	120.2(2)
Si-C(10)-H(10A)	109.47(11)
Si-C(10)-H(10B)	109.47(12)
H(10A)-C(10)-H(10B)	109.5
Si-C(10)-H(10C)	109.47(12)
H(10A)-C(10)-H(10C)	109.5
H(10B)-C(10)-H(10C)	109.5
Si-C(11)-H(11A)	109.47(12)
Si-C(11)-H(11B)	109.47(12)
H(11A)-C(11)-H(11B)	109.5
Si-C(11)-H(11C)	109.47(12)
H(11A)-C(11)-H(11C)	109.5
H(11B)-C(11)-H(11C)	109.5
Si-C(12)-H(12A)	109.47(12)
Si-C(12)-H(12B)	109.47(12)
H(12A)-C(12)-H(12B)	109.5
Si-C(12)-H(12C)	109.47(13)
H(12A)-C(12)-H(12C)	109.5
H(12B)-C(12)-H(12C)	109.5
P-C(13)-H(13A)	109.5(2)
P-C(13)-H(13B)	109.47(13)
H(13A)-C(13)-H(13B)	109.5
P-C(13)-H(13C)	109.5(2)
H(13A)-C(13)-H(13C)	109.5
H(13B)-C(13)-H(13C)	109.5
P-C(14)-H(14A)	109.6(2)
P-C(14)-H(14B)	109.43(9)
H(14A)-C(14)-H(14B)	109.5
W-C(15)-H(15A)	109.47(10)
W-C(15)-H(15B)	109.47(10)
H(15A)-C(15)-H(15B)	109.5
W-C(15)-H(15C)	109.47(10)
H(15A)-C(15)-H(15C)	109.5
H(15B)-C(15)-H(15C)	109.5

Symmetry transformations used to generate equivalent atoms:
#1 x,-y,z

Table A6.4. Anisotropic displacement parameters ($A^2 \times 10^3$) for **21**. The anisotropic displacement factor exponent takes the form: $-2\ p^2\ [\ h^2\ a^{*2}\ U11 + ... + 2\ h\ k\ a^*\ b^*\ U12\ ]$

Atom	U11	U22	U33	U23	U13	U12
W	14(1)	27(1)	21(1)	0	6(1)	0
P	27(1)	40(1)	19(1)	0	8(1)	0
Si	22(1)	22(1)	24(1)	0(1)	6(1)	2(1)
N(1)	19(2)	30(2)	30(2)	0	9(2)	0
N(2)	14(1)	23(1)	20(1)	-1(1)	6(1)	0(1)
C(1)	18(2)	23(2)	25(2)	0	4(2)	0
C(2)	29(2)	42(3)	25(2)	0	12(2)	0
C(3)	34(3)	47(3)	22(2)	0	3(2)	0
C(4)	20(2)	45(3)	35(3)	0	-2(2)	0
C(5)	21(2)	46(3)	42(3)	0	19(2)	0
C(6)	19(2)	34(2)	24(2)	0	4(2)	0
C(7)	16(1)	25(2)	17(1)	0(1)	6(1)	0(1)
C(8)	21(1)	28(2)	22(1)	-2(1)	7(1)	-4(1)
C(9)	18(1)	40(2)	29(2)	0(1)	8(1)	-5(1)
C(10)	35(2)	33(2)	31(2)	7(1)	12(1)	2(1)
C(11)	43(2)	25(2)	35(2)	-3(1)	12(2)	-1(2)
C(12)	26(2)	38(2)	43(2)	10(2)	7(1)	8(2)
C(13)	42(2)	68(3)	22(2)	-3(2)	2(1)	-22(2)
C(14)	48(3)	51(3)	19(2)	0	15(2)	0
C(15)	35(2)	39(2)	33(2)	-4(1)	18(1)	6(2)

Table A6.5. Hydrogen coordinates (x 10^4) and isotropic displacement parameters (A^4 x 10^4) for **21**.

Atom	x	y	z	U(eq)
H(2)	6119(4)	0	4819(3)	38
H(3)	7859(4)	0	5760(3)	43
H(4)	9178(4)	0	5121(4)	44
H(5)	8734(4)	0	3530(4)	41
H(6)	6985(3)	0	2560(3)	32
H(8)	1141(2)	-1608(2)	2371(2)	29
H(9)	9631(2)	-815(3)	2305(2)	35
H(10A)	2062(3)	-2202(3)	3696(2)	49
H(10B)	3104(3)	-1833(3)	4438(2)	49
H(10C)	2995(3)	-2885(3)	4169(2)	49
H(11A)	2071(3)	-2807(2)	1763(3)	52
H(11B)	2966(3)	-3507(2)	2288(3)	52
H(11C)	3143(3)	-2797(2)	1585(3)	52
H(12A)	5147(3)	-2060(3)	3114(3)	55
H(12B)	4968(3)	-2794(3)	3797(3)	55
H(12C)	5077(3)	-1742(3)	4066(3)	55
H(13A)	1986(3)	-1555(4)	330(3)	69
H(13B)	1154(3)	-968(4)	-440(3)	69
H(13C)	1145(3)	-968(4)	577(3)	69
H(14A)	2359(5)	0	-1070(3)	58
H(14B)	3371(5)	543	-472(3)	58
H(15A)	3885(3)	-1288(3)	862(3)	51
H(15B)	4692(3)	-1668(3)	1794(3)	51
H(15C)	5053(3)	-933(3)	1215(3)	51

Crystallographic Data for $W(CH_2CH_2CH_2CH_2)(NPh)[o\text{-}(Me_3SiN)_2C_6H_4]$. **35** (P2(1)/n).

Table A7.1: Crystallographic Data

Empirical formula	$C_{22}H_{35}N_3Si_2W$
Formula weight	581.56
Temperature	173(2) K
Wavelength	0.71073 Å
Crystal system	Monoclinic
Space group	P2(1)/n
Unit cell dimensions	a = 10.3249(1) Å $\alpha = 90°$
	b = 18.1030(2) Å $\beta = 103.210(1)°$
	c = 13.8308(2) Å $\gamma = 90°$
Volume, Z	2516.73(5) A^3, 4
Density (calculated)	1.535 Mg/m^3
Absorption coefficient	4.697 mm^{-1}
F(000)	1160
Crystal size	0.45 x 0.34 x 0.06 mm
Theta range for data collection	1.88° to 27.49°
Limiting indices	$-12\leq h\leq 12$, $0\leq k\leq 23$, $0\leq l\leq 17$
Reflections collected	12840
Independent reflections	5197 [R(int) = 0.0622]
Absorption correction	Integration
Max. and min. transmission	0.6866 and 0.2147
Refinement method	Full-matrix least-squares on F^2
Data / restraints / parameters	5144 / 7 / 253
Goodness-of-fit on F^2	1.059
Final R indices [I>2sigma(I)]	$R_1 = 0.0349$, $wR_2 = 0.0811$
R indices (all data)	$R_1 = 0.0445$, $wR_2 = 0.0902$
Extinction coefficient	0.00099(14)
Largest diff. peak and hole	0.922 and -1.382 $e.Å^{-3}$

$R_1 = \hat{A}(||F_o| - |F_c||) / \hat{A}|F_o|$

$wR_2 = [\hat{A}[w(F_o^2 - F_c^2)^2] / \hat{A}[w(F_o^2)^2]]^{1/2}$

$S = [\hat{A}[w(F_o^2 - F_c^2)^2] / (n-p)]^{1/2}$

$w = 1/[s^2(F_o^2)+(0.0370*p)^2+0.31*p]$, $p = [\max(F_o^2,0)+ 2* F_c^2]/3$

Table A7.2. Atomic coordinates (x 10^4) and equivalent isotropic displacement parameters (A^2 x 10^3) for **35**. U(eq) is defined as one third of the trace of the orthogonalized Uij tensor.

Atom	x	y	z	U(eq)
W	11812(1)	2183(1)	8431(1)	30(1)
Si(1)	12737(1)	4015(1)	8320(1)	37(1)
Si(2)	11604(1)	1598(1)	10776(1)	36(1)
N(1)	11780(4)	3293(2)	8585(3)	33(1)
N(2)	11254(4)	2177(2)	9727(3)	32(1)
N(3)	13301(4)	1768(2)	8352(3)	34(1)
C(1)	10952(6)	2374(3)	6858(4)	47(1)
C(2)	10562(18)	1640(6)	6313(10)	57(5)
C(3)	9771(14)	1191(8)	6902(5)	47(4)
C(2')	10128(14)	1733(5)	6306(8)	51(4)
C(3')	10366(16)	1043(6)	6943(5)	51(3)
C(4)	10397(6)	1278(3)	8014(4)	45(1)
C(5)	10602(5)	3341(3)	8934(3)	34(1)
C(6)	10315(5)	2752(3)	9543(3)	33(1)
C(7)	9119(5)	2775(3)	9852(4)	38(1)
C(8)	8274(5)	3371(4)	9644(4)	46(1)
C(9)	8562(5)	3949(3)	9068(4)	44(1)
C(10)	9691(5)	3937(3)	8701(4)	40(1)
C(11)	14460(5)	1446(3)	8181(4)	35(1)
C(12)	14503(5)	1230(3)	7237(4)	43(1)
C(13)	15640(6)	903(3)	7040(5)	49(1)
C(14)	16738(6)	802(3)	7797(6)	58(2)
C(15)	16702(6)	1028(4)	8738(6)	70(2)
C(16)	15579(6)	1351(4)	8940(5)	56(2)
C(17)	11982(6)	4449(3)	7095(4)	49(1)
C(18)	14374(6)	3605(3)	8274(4)	50(1)
C(19)	12899(6)	4690(3)	9354(4)	49(1)
C(20)	10217(6)	934(3)	10769(4)	50(1)
C(21)	13120(6)	1077(3)	10699(4)	50(1)
C(22)	11891(6)	2189(3)	11900(4)	44(1)

Table A7.3. Bond lengths (Å) and angles [°] for **35**.

W-N(3)	1.736(4)
W-N(2)	2.004(4)
W-N(1)	2.023(4)
W-C(1)	2.182(5)
W-C(4)	2.183(5)
W-C(5)	2.616(5)
W-C(6)	2.627(5)
Si(1)-N(1)	1.727(4)
Si(1)-C(18)	1.860(6)
Si(1)-C(19)	1.860(5)
Si(1)-C(17)	1.869(5)
Si(2)-N(2)	1.758(4)
Si(2)-C(21)	1.851(6)
Si(2)-C(22)	1.856(5)
Si(2)-C(20)	1.868(6)
N(1)-C(5)	1.411(6)
N(2)-C(6)	1.406(6)
N(3)-C(11)	1.399(6)
C(1)-C(2')	1.534(6)
C(1)-C(2)	1.534(6)
C(2)-C(3)	1.516(10)
C(3)-C(4)	1.534(6)
C(2')-C(3')	1.516(10)
C(3')-C(4)	1.534(6)
C(5)-C(10)	1.419(7)
C(5)-C(6)	1.431(7)
C(6)-C(7)	1.396(7)
C(7)-C(8)	1.376(8)
C(8)-C(9)	1.388(8)
C(9)-C(10)	1.374(7)
C(11)-C(12)	1.374(7)
C(11)-C(16)	1.383(7)
C(12)-C(13)	1.395(7)
C(13)-C(14)	1.369(9)
C(14)-C(15)	1.373(10)
C(15)-C(16)	1.384(8)
N(3)-W-N(2)	119.5(2)
N(3)-W-N(1)	118.1(2)
N(2)-W-N(1)	84.1(2)
N(3)-W-C(1)	99.8(2)
N(2)-W-C(1)	139.3(2)
N(1)-W-C(1)	86.3(2)
N(3)-W-C(4)	102.0(2)
N(2)-W-C(4)	85.5(2)
N(1)-W-C(4)	138.4(2)
C(1)-W-C(4)	76.1(2)
N(3)-W-C(5)	147.8(2)
N(2)-W-C(5)	60.9(2)

N(1)-W-C(5)	32.3(2)
C(1)-W-C(5)	91.6(2)
C(4)-W-C(5)	109.9(2)
N(3)-W-C(6)	148.6(2)
N(2)-W-C(6)	31.9(2)
N(1)-W-C(6)	61.49(14)
C(1)-W-C(6)	111.2(2)
C(4)-W-C(6)	90.1(2)
C(5)-W-C(6)	31.69(14)
N(1)-Si(1)-C(18)	105.9(2)
N(1)-Si(1)-C(19)	106.8(2)
C(18)-Si(1)-C(19)	111.5(3)
N(1)-Si(1)-C(17)	111.7(2)
C(18)-Si(1)-C(17)	109.3(3)
C(19)-Si(1)-C(17)	111.5(3)
N(2)-Si(2)-C(21)	105.9(2)
N(2)-Si(2)-C(22)	108.1(2)
C(21)-Si(2)-C(22)	111.6(3)
N(2)-Si(2)-C(20)	111.5(2)
C(21)-Si(2)-C(20)	109.2(3)
C(22)-Si(2)-C(20)	110.5(3)
C(5)-N(1)-Si(1)	127.3(4)
C(5)-N(1)-W	97.7(3)
Si(1)-N(1)-W	134.9(2)
C(6)-N(2)-Si(2)	126.5(3)
C(6)-N(2)-W	99.3(3)
Si(2)-N(2)-W	133.9(2)
C(11)-N(3)-W	174.0(3)
C(2')-C(1)-W	115.4(5)
C(2)-C(1)-W	110.7(7)
C(3)-C(2)-C(1)	108.3(8)
C(2)-C(3)-C(4)	109.2(9)
C(3')-C(2')-C(1)	109.7(7)
C(2')-C(3')-C(4)	107.3(8)
C(3')-C(4)-W	109.2(6)
C(3)-C(4)-W	116.4(5)
N(1)-C(5)-C(10)	123.2(4)
N(1)-C(5)-C(6)	117.7(4)
C(10)-C(5)-C(6)	119.0(4)
N(1)-C(5)-W	50.0(2)
C(10)-C(5)-W	151.8(3)
C(6)-C(5)-W	74.6(3)
C(7)-C(6)-N(2)	126.0(4)
C(7)-C(6)-C(5)	118.3(4)
N(2)-C(6)-C(5)	115.6(4)
C(7)-C(6)-W	150.5(4)
N(2)-C(6)-W	48.9(2)
C(5)-C(6)-W	73.7(3)
C(8)-C(7)-C(6)	121.5(5)
C(7)-C(8)-C(9)	120.1(5)
C(10)-C(9)-C(8)	120.8(5)
C(9)-C(10)-C(5)	120.1(5)
C(12)-C(11)-C(16)	118.9(5)
C(12)-C(11)-N(3)	119.7(4)

C(16)-C(11)-N(3)	121.4(5)
C(11)-C(12)-C(13)	121.2(5)
C(14)-C(13)-C(12)	119.6(6)
C(13)-C(14)-C(15)	119.2(5)
C(14)-C(15)-C(16)	121.6(6)
C(11)-C(16)-C(15)	119.5(6)

Table A7.4. Anisotropic displacement parameters ($A^2 \times 10^3$) for **35**. The anisotropic displacement factor exponent takes the form: $-2\pi^2 [h^2 a^{*2} U11 + ... + 2 h k a^* b^* U12]$

Atom	U11	U22	U33	U23	U13	U12
W	32(1)	30(1)	30(1)	-1(1)	10(1)	4(1)
Si(1)	41(1)	36(1)	35(1)	4(1)	12(1)	1(1)
Si(2)	45(1)	29(1)	34(1)	3(1)	9(1)	-2(1)
N(1)	32(2)	40(2)	28(2)	-4(2)	11(2)	1(2)
N(2)	39(2)	30(2)	28(2)	-3(2)	10(2)	2(2)
N(3)	35(2)	33(2)	34(2)	2(2)	10(2)	3(2)
C(1)	48(3)	60(4)	32(3)	-2(2)	9(2)	5(3)
C(4)	45(3)	46(3)	45(3)	-8(2)	14(2)	-5(2)
C(5)	38(2)	38(3)	27(2)	-2(2)	9(2)	7(2)
C(6)	37(3)	37(3)	25(2)	2(2)	7(2)	1(2)
C(7)	43(3)	39(3)	32(2)	-2(2)	9(2)	-2(2)
C(8)	34(3)	70(4)	35(3)	-3(3)	11(2)	5(3)
C(9)	43(3)	47(3)	41(3)	-4(2)	10(2)	14(2)
C(10)	47(3)	36(3)	36(2)	-4(2)	12(2)	11(2)
C(11)	33(2)	29(2)	44(3)	2(2)	12(2)	5(2)
C(12)	39(3)	37(3)	56(3)	0(2)	19(2)	3(2)
C(13)	51(3)	34(3)	72(4)	-3(3)	36(3)	-2(2)
C(14)	40(3)	42(3)	96(5)	-4(3)	27(3)	6(3)
C(15)	33(3)	83(5)	87(5)	5(4)	-3(3)	17(3)
C(16)	44(3)	71(4)	53(3)	-4(3)	10(3)	9(3)
C(17)	55(3)	47(3)	47(3)	11(3)	16(3)	4(3)
C(18)	46(3)	55(3)	52(3)	12(3)	18(3)	2(3)
C(19)	59(3)	41(3)	45(3)	-4(2)	8(3)	-7(3)
C(20)	60(4)	38(3)	52(3)	0(2)	13(3)	-13(3)
C(21)	58(3)	42(3)	48(3)	9(3)	9(3)	4(3)
C(22)	51(3)	49(3)	30(2)	-1(2)	7(2)	-2(2)

Table A7.5. Hydrogen coordinates (x 10^4) and isotropic displacement parameters (A^4 x 10^4) for **35**.

Atom	x	y	z	U(eq)
H(1A)	11586(6)	2627(3)	6567(4)	56
H(1B)	10179(6)	2682(3)	6787(4)	56
H(1C)	11660(6)	2482(3)	6535(4)	56
H(1D)	10392(6)	2803(3)	6798(4)	56
H(2A)	10030(18)	1733(6)	5650(10)	69
H(2B)	11354(18)	1372(6)	6255(10)	69
H(3A)	9775(14)	674(8)	6715(5)	57
H(3B)	8856(14)	1360(8)	6758(5)	57
H(2'A)	9191(14)	1860(5)	6160(8)	61
H(2'B)	10381(14)	1643(5)	5683(8)	61
H(3'A)	11204(16)	816(6)	6906(5)	61
H(3'B)	9657(16)	688(6)	6714(5)	61
H(4C)	9527(6)	1435(3)	8066(4)	54
H(4D)	10659(6)	868(3)	8456(4)	54
H(4A)	9693(6)	1345(3)	8355(4)	54
H(4B)	10841(6)	825(3)	8250(4)	54
H(7A)	8889(5)	2378(3)	10206(4)	46
H(8A)	7508(5)	3386(4)	9891(4)	55
H(9A)	7983(5)	4349(3)	8929(4)	52
H(10A)	9859(5)	4321(3)	8299(4)	47
H(12A)	13762(5)	1302(3)	6719(4)	51
H(13A)	15651(6)	755(3)	6398(5)	59
H(14A)	17500(6)	583(3)	7675(6)	69
H(15A)	17451(6)	962(4)	9251(6)	84
H(16A)	15577(6)	1503(4)	9582(5)	67
H(17A)	11137(6)	4661(3)	7117(4)	73
H(17B)	11859(6)	4080(3)	6583(4)	73
H(17C)	12562(6)	4829(3)	6956(4)	73
H(18A)	14257(6)	3259(3)	7735(4)	75
H(18B)	14737(6)	3354(3)	8888(4)	75
H(18C)	14971(6)	3989(3)	8177(4)	75
H(19A)	12040(6)	4892(3)	9358(4)	73
H(19B)	13487(6)	5082(3)	9264(4)	73
H(19C)	13253(6)	4446(3)	9975(4)	73
H(20A)	9429(6)	1202(3)	10809(4)	75
H(20B)	10460(6)	607(3)	11328(4)	75
H(20D)	10050(6)	651(3)	10166(4)	75
H(21A)	12939(6)	777(3)	10110(4)	75
H(21D)	13383(6)	766(3)	11273(4)	75
H(21B)	13825(6)	1417(3)	10672(4)	75
H(22D)	11088(6)	2451(3)	11918(4)	66
H(22A)	12587(6)	2537(3)	11882(4)	66
H(22B)	12146(6)	1886(3)	12482(4)	66

Crystallographic Data for $W(CH_2CH_2CH_2CH_2)(NPh)[o\text{-}(Me_3SiN)_2C_6H_4]$. **35.** ($P\bar{1}$)

Table A8.1: Crystallographic Data

Empirical formula	$C_{22}\ H_{35}\ N_3\ Si_2\ W$
Formula weight	581.56
Temperature	173 K
Wavelength	0.71073 Å
Crystal system	Triclinic
Space group	$P\bar{1}$
Unit cell dimensions	a = 9.2118(1) Å α = 104.471(1)°
	b = 12.0569(2) Å β = 97.954(1)°
	c = 12.0845(2) Å γ = 102.247(1)°
Volume, Z	1243.77(3) $Å^3$, 2
Density (calculated)	1.553 Mg/m^3
Absorption coefficient	4.752 mm^{-1}
F(000)	580
Crystal size	0.16 x 0.19 x 0.23 mm
Theta range for data collection	1.78 to 26.92°
Limiting indices	$-11 \le h \le 11$, $-15 \le k \le 9$, $-15 \le l \le 14$
Reflections collected	8213
Independent reflections	4600 [R(int) = 0.0230]
Absorption correction	None
Refinement method	Full-matrix least-squares on F^2
Data / restraints / parameters	4600 / 7 / 273
Goodness-of-fit on F^2	1.049
Final R indices [I>2sigma(I)]	R_1 = 0.0243, wR_2 = 0.0560 [4204]
R indices (all data)	R_1 = 0.0293, wR_2 = 0.0585
Extinction coefficient	0.0010(2)
Largest diff. peak and hole	0.951 and -0.776 $e.Å^{-3}$

$R_1 = \hat{A}(||F_o| - |F_c||) / \hat{A}|F_o|$

$wR_2 = [\hat{A}[w(F_o^2 - F_c^2)^2] / \hat{A}[w(F_o^2)^2]]^{1/2}$

$S = [\hat{A}[w(F_o^2 - F_c^2)^2] / (n-p)]^{1/2}$

$w = 1/[s^2(F_o^2)+(0.0370*p)^2+0.31*p]$, $p = [\max(F_o^2,0)+ 2* F_c^2]/3$

Table A8.2. Atomic coordinates (x 10^4) and equivalent isotropic displacement parameters (A^2 x 10^3) for **35**. U(eq) is defined as one third of the trace of the orthogonalized Uij tensor.

Atom	x	y	z	U(eq)
W	1906(1)	6994(1)	7971(1)	27(1)
Si1	-1806(1)	5883(1)	8047(1)	35(1)
Si2	2858(1)	8419(1)	5936(1)	34(1)
N1	-276(4)	6972(3)	7932(3)	30(1)
N2	1808(4)	8106(3)	6984(3)	30(1)
N3	2267(4)	5638(3)	7369(3)	32(1)
C1	2030(4)	6996(4)	9784(3)	39(1)
C2	3695(7)	7165(9)	10357(12)	49(3)
C3	4591(13)	8268(9)	10165(4)	43(3)
C2'	3555(9)	7640(3)	10639(11)	63(7)
C3'	4713(17)	7690(2)	9883(13)	48(5)
C4	4156(5)	8138(4)	8852(3)	39(1)
C5	-238(4)	8156(4)	8017(3)	31(1)
C6	883(4)	8761(3)	7510(3)	32(1)
C7	957(5)	9958(4)	7563(4)	42(1)
C8	-56(6)	10513(4)	8056(4)	51(1)
C9	-1147(6)	9923(4)	8540(4)	51(1)
C10	-1228(5)	8771(4)	8539(4)	42(1)
C11	2430(4)	4516(3)	6871(3)	29(1)
C12	3125(5)	3929(4)	7549(4)	37(1)
C13	3297(5)	2812(4)	7052(4)	44(1)
C14	2797(5)	2274(4)	5874(4)	44(1)
C15	2092(5)	2836(4)	5195(4)	44(1)
C16	1901(5)	3953(4)	5681(4)	36(1)
C17	-2160(6)	6169(5)	9569(4)	54(1)
C18	-1265(5)	4455(4)	7660(4)	44(1)
C19	-3520(5)	5851(5)	7027(4)	48(1)
C20	4557(5)	9700(4)	6603(4)	50(1)
C21	3517(5)	7079(4)	5358(4)	45(1)
C22	1634(5)	8716(4)	4747(4)	44(1)

Table A8.3. Bond lengths (Å) and angles [°] for **35**.

W-N3	1.736(3)
W-N1	1.998(3)
W-N2	2.013(3)
W-C1	2.177(4)
W-C4	2.185(4)
Si1-N1	1.758(3)
Si1-C19	1.851(4)
Si1-C18	1.859(5)
Si1-C17	1.873(4)
Si2-N2	1.762(3)
Si2-C21	1.855(4)
Si2-C22	1.856(4)
Si2-C20	1.867(5)
N1-C5	1.398(5)
N2-C6	1.392(5)
N3-C11	1.385(5)
C1-C2'	1.541(5)
C1-C2	1.541(5)
C1-H1A	0.9600
C1-H1B	0.9600
C1-H1C	0.9600
C1-H1D	0.9600
C2-C3	1.499(9)
C2-H2A	0.9700
C2-H2B	0.9700
C3-C4	1.541(5)
C3-H3A	0.9700
C3-H3B	0.9700
C2'-C3'	1.499(9)
C2'-H2'A	0.9700
C2'-H2'B	0.9700
C3'-C4	1.541(5)
C3'-H3'A	0.9700
C3'-H3'B	0.9700
C4-H4A	0.9600
C4-H4B	0.9600
C4-H4C	0.9600
C4-H4D	0.9600
C5-C10	1.412(5)
C5-C6	1.433(5)
C6-C7	1.415(6)
C7-C8	1.376(6)
C7-H7A	0.9300
C8-C9	1.387(7)
C8-H8A	0.9300
C9-C10	1.374(6)
C9-H9A	0.9300
C10-H10A	0.9300
C11-C12	1.386(5)

C11-C16	1.394(5)
C12-C13	1.383(6)
C12-H12A	0.9300
C13-C14	1.375(6)
C13-H13A	0.9300
C14-C15	1.368(6)
C14-H14A	0.9300
C15-C16	1.387(6)
C15-H15A	0.9300
C16-H16A	0.9300
C17-H17A	0.9600
C17-H17B	0.9600
C17-H17C	0.9600
C18-H18A	0.9600
C18-H18B	0.9600
C18-H18C	0.9600
C19-H19A	0.9600
C19-H19B	0.9600
C19-H19C	0.9600
C20-H20A	0.9600
C20-H20B	0.9600
C20-H20C	0.9600
C21-H21A	0.9600
C21-H21B	0.9600
C21-H21C	0.9600
C22-H22A	0.9600
C22-H22B	0.9600
C22-H22C	0.9600

N3-W-N1	115.8(2)
N3-W-N2	118.68(13)
N1-W-N2	83.57(12)
N3-W-C1	100.9(2)
N1-W-C1	86.17(13)
N2-W-C1	139.7(2)
N3-W-C4	103.3(2)
N1-W-C4	139.5(2)
N2-W-C4	86.87(14)
C1-W-C4	76.2(2)
N1-Si1-C19	108.6(2)
N1-Si1-C18	106.4(2)
C19-Si1-C18	111.6(2)
N1-Si1-C17	112.0(2)
C19-Si1-C17	110.0(2)
C18-Si1-C17	108.2(2)
N2-Si2-C21	106.0(2)
N2-Si2-C22	110.1(2)
C21-Si2-C22	110.4(2)
N2-Si2-C20	111.7(2)
C21-Si2-C20	108.4(2)
C22-Si2-C20	110.3(2)
C5-N1-Si1	126.7(3)
C5-N1-W	101.2(2)
Si1-N1-W	131.1(2)

C6-N2-Si2	126.8(3)
C6-N2-W	100.8(2)
Si2-N2-W	131.4(2)
C11-N3-W	175.4(3)
C2'-C1-C2	23.8(8)
C2'-C1-W	117.3(8)
C2-C1-W	109.1(6)
C2'-C1-H1A	122.0
C2-C1-H1A	110.1
W-C1-H1A	109.7
C2'-C1-H1B	86.1
C2-C1-H1B	109.7
W-C1-H1B	109.9
H1A-C1-H1B	108.2
C2'-C1-H1C	106.4
C2-C1-H1C	89.4
W-C1-H1C	108.0
H1A-C1-H1C	23.6
H1B-C1-H1C	128.1
C2'-C1-H1D	109.2
C2-C1-H1D	131.4
W-C1-H1D	108.2
H1A-C1-H1D	84.8
H1B-C1-H1D	26.5
H1C-C1-H1D	107.3
C3-C2-C1	106.6(6)
C3-C2-H2A	110.4
C1-C2-H2A	110.4
C3-C2-H2B	110.4
C1-C2-H2B	110.4
H2A-C2-H2B	108.6
C2-C3-C4	106.5(8)
C2-C3-H3A	110.4
C4-C3-H3A	110.4
C2-C3-H3B	110.4
C4-C3-H3B	110.4
H3A-C3-H3B	108.6
C3'-C2'-C1	105.0(10)
C3'-C2'-H2'A	110.7
C1-C2'-H2'A	110.7
C3'-C2'-H2'B	110.8
C1-C2'-H2'B	110.8
H2'A-C2'-H2'B	108.8
C2'-C3'-C4	109.7(14)
C2'-C3'-H3'A	109.7
C4-C3'-H3'A	109.7
C2'-C3'-H3'B	109.7
C4-C3'-H3'B	109.7
H3'A-C3'-H3'B	108.2
C3-C4-C3'	27.4(6)
C3-C4-W	115.4(4)
C3'-C4-W	107.6(8)
C3-C4-H4A	108.6
C3'-C4-H4A	133.7

W-C4-H4A	108.4
C3-C4-H4B	108.4
C3'-C4-H4B	87.7
W-C4-H4B	108.4
H4A-C4-H4B	107.4
C3-C4-H4C	83.3
C3'-C4-H4C	110.5
W-C4-H4C	109.9
H4A-C4-H4C	28.3
H4B-C4-H4C	129.3
C3-C4-H4D	125.3
C3'-C4-H4D	110.5
W-C4-H4D	110.0
H4A-C4-H4D	83.1
H4B-C4-H4D	25.5
H4C-C4-H4D	108.3
N1-C5-C10	124.9(4)
N1-C5-C6	116.2(3)
C10-C5-C6	118.9(4)
N2-C6-C7	125.1(4)
N2-C6-C5	116.5(3)
C7-C6-C5	118.4(4)
C8-C7-C6	120.6(4)
C8-C7-H7A	119.7
C6-C7-H7A	119.7
C7-C8-C9	120.9(4)
C7-C8-H8A	119.6
C9-C8-H8A	119.6
C10-C9-C8	120.4(4)
C10-C9-H9A	119.8
C8-C9-H9A	119.8
C9-C10-C5	120.8(4)
C9-C10-H10A	119.6
C5-C10-H10A	119.6
N3-C11-C12	120.5(3)
N3-C11-C16	121.0(3)
C12-C11-C16	118.6(4)
C13-C12-C11	120.5(4)
C13-C12-H12A	119.7
C11-C12-H12A	119.7
C14-C13-C12	120.4(4)
C14-C13-H13A	119.8
C12-C13-H13A	119.8
C15-C14-C13	119.7(4)
C15-C14-H14A	120.1
C13-C14-H14A	120.1
C14-C15-C16	120.6(4)
C14-C15-H15A	119.7
C16-C15-H15A	119.7
C15-C16-C11	120.1(4)
C15-C16-H16A	119.9
C11-C16-H16A	119.9
Si1-C17-H17A	109.5
Si1-C17-H17B	109.5

H17A-C17-H17B	109.5
Si1-C17-H17C	109.5
H17A-C17-H17C	109.5
H17B-C17-H17C	109.5
Si1-C18-H18A	109.5
Si1-C18-H18B	109.5
H18A-C18-H18B	109.5
Si1-C18-H18C	109.5
H18A-C18-H18C	109.5
H18B-C18-H18C	109.5
Si1-C19-H19A	109.5
Si1-C19-H19B	109.5
H19A-C19-H19B	109.5
Si1-C19-H19C	109.5
H19A-C19-H19C	109.5
H19B-C19-H19C	109.5
Si2-C20-H20A	109.5
Si2-C20-H20B	109.5
H20A-C20-H20B	109.5
Si2-C20-H20C	109.5
H20A-C20-H20C	109.5
H20B-C20-H20C	109.5
Si2-C21-H21A	109.5
Si2-C21-H21B	109.5
H21A-C21-H21B	109.5
Si2-C21-H21C	109.5
H21A-C21-H21C	109.5
H21B-C21-H21C	109.5
Si2-C22-H22A	109.5
Si2-C22-H22B	109.5
H22A-C22-H22B	109.5
Si2-C22-H22C	109.5
H22A-C22-H22C	109.5
H22B-C22-H22C	109.5

Table A8.4. Anisotropic displacement parameters ($A^2 \times 10^3$) for **35**. The anisotropic displacement factor exponent takes the form: $-2\ p^2\ [\ h^2\ a^{*2}\ U11 + ... + 2\ h\ k\ a^*\ b^*\ U12\ ]$

Atom	U11	U22	U33	U23	U13	U12
W	27(1)	27(1)	27(1)	9(1)	5(1)	8(1)
Si1	32(1)	42(1)	34(1)	15(1)	11(1)	8(1)
Si2	31(1)	37(1)	32(1)	14(1)	5(1)	4(1)
N1	31(2)	33(2)	28(2)	12(1)	6(1)	11(1)
N2	28(2)	30(2)	33(2)	12(1)	7(1)	7(1)
N3	32(2)	33(2)	34(2)	13(2)	8(1)	11(2)
C1	38(2)	48(3)	31(2)	14(2)	4(2)	6(2)
C2	53(6)	56(7)	28(6)	17(5)	-7(4)	-3(4)
C3	34(5)	46(6)	35(5)	3(4)	-9(4)	2(4)
C2'	49(9)	78(16)	33(9)	-4(8)	-13(7)	-6(8)
C3'	32(7)	70(13)	35(7)	11(8)	-9(6)	14(8)
C4	35(2)	36(2)	39(2)	12(2)	2(2)	2(2)
C5	31(2)	37(2)	26(2)	10(2)	3(2)	11(2)
C6	35(2)	34(2)	27(2)	11(2)	1(2)	11(2)
C7	49(3)	35(2)	41(2)	12(2)	3(2)	10(2)
C8	67(3)	36(3)	51(3)	11(2)	3(2)	22(2)
C9	60(3)	48(3)	52(3)	7(2)	14(2)	34(3)
C10	40(2)	48(3)	41(2)	10(2)	10(2)	20(2)
C11	28(2)	29(2)	31(2)	10(2)	10(2)	6(2)
C12	45(3)	34(2)	31(2)	10(2)	3(2)	9(2)
C13	42(3)	34(2)	57(3)	17(2)	3(2)	13(2)
C14	48(3)	26(2)	57(3)	9(2)	19(2)	8(2)
C15	57(3)	36(2)	32(2)	3(2)	12(2)	0(2)
C16	39(2)	36(2)	35(2)	14(2)	3(2)	8(2)
C17	63(3)	59(3)	51(3)	25(2)	29(3)	14(3)
C18	41(3)	41(3)	45(3)	15(2)	7(2)	1(2)
C19	27(2)	66(3)	54(3)	21(3)	10(2)	11(2)
C20	44(3)	56(3)	51(3)	27(2)	6(2)	-1(2)
C21	48(3)	56(3)	40(2)	20(2)	17(2)	18(2)
C22	43(3)	47(3)	44(3)	25(2)	6(2)	5(2)

Table A8.5. Hydrogen coordinates (x 10^4) and isotropic displacement parameters (A^4 x 10^4) for **35**.

Atom	x	y	z	U(eq)
H1A	1417	6260	9820	47
H1B	1651	7628	10196	47
H1C	1811	6187	9804	47
H1D	1246	7327	10068	47
H2A	3790	7248	11185	59
H2B	4057	6488	10002	59
H3A	5669	8351	10391	51
H3B	4344	8961	10623	51
H2'A	3540	8426	11074	75
H2'B	3771	7196	11185	75
H3'A	4877	6915	9591	57
H3'B	5669	8229	10338	57
H4A	4212	8911	8754	46
H4B	4894	7831	8470	46
H4C	4100	8944	9126	46
H4D	4837	8104	8318	46
H7A	1697	10374	7261	50
H8A	-9	11293	8066	61
H9A	-1828	10309	8866	62
H10A	-1945	8393	8887	51
H12A	3478	4288	8346	44
H13A	3754	2422	7517	53
H14A	2937	1531	5540	52
H15A	1737	2466	4400	53
H16A	1420	4328	5212	44
H17A	-1266	6185	10093	82
H17B	-2991	5551	9599	82
H17C	-2403	6919	9796	82
H18A	-375	4502	8205	65
H18B	-1060	4299	6887	65
H18C	-2082	3826	7690	65
H19A	-3767	6600	7251	72
H19B	-4353	5232	7052	72
H19C	-3329	5705	6249	72
H20A	5180	9537	7216	76
H20B	4235	10400	6917	76
H20C	5128	9822	6017	76
H21A	4147	6935	5982	67
H21B	4089	7198	4772	67
H21C	2657	6408	5021	67
H22A	1301	9411	5058	66
H22B	768	8050	4409	66
H22C	2199	8840	4159	66

Crystallographic Data for W(NPh)[*o*-$(Me_3SiN)_2C_6H_4$](η^2-C_2H_4)$(PMe_3)_2$, **39.**

Table A9.1: Crystallographic Data

Empirical formula	$C_{26}H_{49}N_3P_2Si_2W$. $1/2C_7H_8$
Formula weight	751.72
Temperature	173(2) K
Wavelength	0.71073 Å
Crystal system	Orthorhombic
Space group	Pbcn
Unit cell dimensions	a = 36.2551(8) Å $\alpha = 90°$
	b = 13.5914(4) Å $\beta = 90°$
	c = 13.9794(4) Å $\gamma = 90°$
Volume, Z	6888.5(3) $Å^3$, 8
Density (calculated)	1.450 Mg/m^3
Absorption coefficient	3.539 mm^{-1}
F(000)	3064
Crystal size	0.44 x 0.38 x 0.10 mm
Theta range for data collection	1.60° to 27.50°
Limiting indices	$-24 \le h \le 50$, $-11 \le k \le 18$, $-19 \le l \le 7$
Reflections collected	27782
Independent reflections	7881 [R(int) = 0.0334]
Refinement method	Full-matrix least-squares on F^2
Data / restraints / parameters	7784 / 0 / 341
Goodness-of-fit on F^2	1.200
Final R indices [I>2sigma(I)]	$R_1 = 0.0380$, $wR_2 = 0.0827$
R indices (all data)	$R_1 = 0.0441$, $wR_2 = 0.0909$
Extinction coefficient	0.00019(4)
Largest diff. peak and hole	1.186 and -2.322 $e.Å^{-3}$

$R_1 = \hat{A}(||F_o| - |F_c||) / \hat{A}|F_o|$

$wR_2 = [\hat{A}[w(F_o^2 - F_c^2)^2] / \hat{A}[w(F_o^2)^2]]^{1/2}$

$S = [\hat{A}[w(F_o^2 - F_c^2)^2] / (n-p)]^{1/2}$

$w = 1/[s^2(F_o^2)+(0.0370*p)^2+0.31*p]$, $p = [\max(F_o^2,0)+ 2* F_c^2]/3$

Table A9.2. Atomic coordinates (x 10^4) and equivalent isotropic displacement parameters (A^2 x 10^3) for **39**. U(eq) is defined as one third of the trace of the orthogonalized Uij tensor.

Atom	x	y	z	U(eq)
W	1510(1)	7639(1)	2032(1)	17(1)
P(1)	1683(1)	9434(1)	2366(1)	21(1)
P(2)	1282(1)	5959(1)	1445(1)	27(1)
Si(1)	2316(1)	7603(1)	469(1)	23(1)
Si(2)	705(1)	8840(1)	1219(1)	25(1)
N(1)	1842(1)	7673(3)	755(3)	20(1)
N(2)	1129(1)	8264(3)	1011(2)	19(1)
N(3)	1223(1)	7527(3)	3063(3)	21(1)
C(1)	1914(1)	6563(3)	2634(4)	28(1)
C(2)	2007(1)	7534(3)	2958(3)	27(1)
C(3)	2457(2)	6359(4)	-13(4)	36(1)
C(4)	2672(1)	7726(4)	1440(4)	36(1)
C(5)	2429(2)	8638(3)	-369(4)	32(1)
C(6)	621(2)	9914(4)	392(4)	38(1)
C(7)	655(1)	9332(4)	2462(3)	31(1)
C(8)	298(2)	8000(5)	1076(4)	43(1)
C(9)	865(2)	5894(5)	740(6)	61(2)
C(10)	1595(2)	5228(4)	719(5)	53(2)
C(11)	1171(2)	5111(4)	2413(4)	44(1)
C(12)	2168(1)	9797(3)	2333(4)	30(1)
C(13)	1557(1)	9837(3)	3565(3)	27(1)
C(14)	1506(2)	10363(4)	1547(3)	30(1)
C(15)	1602(1)	7702(3)	-49(3)	20(1)
C(16)	1715(2)	7416(3)	-988(3)	26(1)
C(17)	1472(2)	7446(4)	-1765(3)	28(1)
C(18)	1118(2)	7766(4)	-1628(3)	31(1)
C(19)	999(1)	8063(4)	-718(3)	26(1)
C(20)	1236(1)	8030(3)	76(3)	19(1)
C(21)	1049(1)	7339(3)	3913(3)	23(1)
C(22)	686(1)	6982(4)	3948(3)	30(1)
C(23)	519(2)	6777(4)	4818(4)	37(1)
C(24)	706(2)	6932(4)	5670(4)	35(1)
C(25)	1064(2)	7289(4)	5639(3)	34(1)
C(26)	1237(2)	7493(4)	4779(3)	29(1)
C(27)	0	4993(8)	7500	68(3)
C(28)	-191(2)	5508(6)	6816(6)	59(2)
C(29)	-192(2)	6511(5)	6809(4)	48(2)
C(30)	0	7043(6)	7500	45(2)
C(31)	0	8149(8)	7500	87(4)

Table A9.3. Bond lengths (Å) and angles [°] for **39**.

W-N(3)	1.784(4)
W-N(1)	2.154(4)
W-N(2)	2.160(3)
W-C(2)	2.223(5)
W-C(1)	2.234(5)
W-P(1)	2.562(1)
W-P(2)	2.564(1)
P(1)-C(13)	1.821(4)
P(1)-C(14)	1.822(5)
P(1)-C(12)	1.828(5)
P(2)-C(9)	1.804(7)
P(2)-C(10)	1.818(6)
P(2)-C(11)	1.822(5)
Si(1)-N(1)	1.766(4)
Si(1)-C(5)	1.875(5)
Si(1)-C(4)	1.881(6)
Si(1)-C(3)	1.891(5)
Si(2)-N(2)	1.747(4)
Si(2)-C(7)	1.871(5)
Si(2)-C(8)	1.876(5)
Si(2)-C(6)	1.887(5)
N(1)-C(15)	1.423(5)
N(2)-C(20)	1.401(5)
N(3)-C(21)	1.370(6)
C(1)-C(2)	1.434(6)
C(1)-H(1A)	0.97
C(1)-H(1B)	0.97
C(2)-H(2A)	0.97
C(2)-H(2B)	0.97
C(3)-H(3A)	0.96
C(3)-H(3B)	0.96
C(3)-H(3C)	0.96
C(4)-H(4A)	0.96
C(4)-H(4B)	0.96
C(4)-H(4C)	0.96
C(5)-H(5A)	0.96
C(5)-H(5B)	0.96
C(5)-H(5C)	0.96
C(6)-H(6A)	0.96
C(6)-H(6B)	0.96
C(6)-H(6C)	0.96
C(7)-H(7A)	0.96
C(7)-H(7B)	0.96
C(7)-H(7C)	0.96
C(8)-H(8A)	0.96
C(8)-H(8B)	0.96
C(8)-H(8C)	0.96
C(9)-H(9A)	0.96
C(9)-H(9B)	0.96

C(9)-H(9C)	0.96
C(10)-H(10A)	0.96
C(10)-H(10B)	0.96
C(10)-H(10C)	0.96
C(11)-H(11A)	0.96
C(11)-H(11B)	0.96
C(11)-H(11C)	0.96
C(12)-H(12A)	0.96
C(12)-H(12B)	0.96
C(12)-H(12C)	0.96
C(13)-H(13A)	0.96
C(13)-H(13B)	0.96
C(13)-H(13C)	0.96
C(14)-H(14A)	0.96
C(14)-H(14B)	0.96
C(14)-H(14C)	0.96
C(15)-C(20)	1.409(6)
C(15)-C(16)	1.430(6)
C(16)-C(17)	1.399(7)
C(16)-H(16A)	0.93
C(17)-C(18)	1.368(7)
C(17)-H(17A)	0.93
C(18)-C(19)	1.402(7)
C(18)-H(18A)	0.93
C(19)-C(20)	1.406(6)
C(19)-H(19A)	0.93
C(21)-C(22)	1.404(7)
C(21)-C(26)	1.405(7)
C(22)-C(23)	1.387(7)
C(22)-H(22A)	0.93
C(23)-C(24)	1.389(8)
C(23)-H(23A)	0.93
C(24)-C(25)	1.384(8)
C(24)-H(24A)	0.93
C(25)-C(26)	1.384(7)
C(25)-H(25A)	0.93
C(26)-H(26A)	0.93
C(27)-C(28)#1	1.372(10)
C(27)-C(28)	1.372(10)
C(27)-H(27A)	0.945(11)
C(28)-C(29)	1.363(10)
C(28)-H(28A)	0.93
C(29)-C(30)	1.393(8)
C(29)-H(29A)	0.93
C(30)-C(29)#1	1.393(8)
C(30)-C(31)	1.503(14)
C(31)-H(31A)	0.96
C(31)-H(31B)	0.96
C(31)-H(31C)	0.96
N(3)-W-N(1)	175.9(2)
N(3)-W-N(2)	101.2(2)
N(1)-W-N(2)	78.60(14)
N(3)-W-C(2)	89.8(2)

N(1)-W-C(2)	91.8(2)
N(2)-W-C(2)	158.2(2)
N(3)-W-C(1)	91.2(2)
N(1)-W-C(1)	87.7(2)
N(2)-W-C(1)	157.8(2)
C(2)-W-C(1)	37.5(2)
N(3)-W-P(1)	94.40(12)
N(1)-W-P(1)	89.66(10)
N(2)-W-P(1)	84.42(10)
C(2)-W-P(1)	75.92(12)
C(1)-W-P(1)	113.19(13)
N(3)-W-P(2)	89.64(12)
N(1)-W-P(2)	86.26(10)
N(2)-W-P(2)	86.12(10)
C(2)-W-P(2)	113.00(13)
C(1)-W-P(2)	75.50(13)
P(1)-W-P(2)	170.27(4)
C(13)-P(1)-C(14)	106.3(2)
C(13)-P(1)-C(12)	100.6(2)
C(14)-P(1)-C(12)	97.8(2)
C(13)-P(1)-W	113.1(2)
C(14)-P(1)-W	117.3(2)
C(12)-P(1)-W	119.2(2)
C(9)-P(2)-C(10)	101.0(4)
C(9)-P(2)-C(11)	101.0(3)
C(10)-P(2)-C(11)	101.9(3)
C(9)-P(2)-W	119.2(2)
C(10)-P(2)-W	117.6(2)
C(11)-P(2)-W	113.4(2)
N(1)-Si(1)-C(5)	108.3(2)
N(1)-Si(1)-C(4)	119.9(2)
C(5)-Si(1)-C(4)	103.6(3)
N(1)-Si(1)-C(3)	113.0(2)
C(5)-Si(1)-C(3)	112.9(2)
C(4)-Si(1)-C(3)	98.7(3)
N(2)-Si(2)-C(7)	113.6(2)
N(2)-Si(2)-C(8)	113.6(2)
C(7)-Si(2)-C(8)	103.9(3)
N(2)-Si(2)-C(6)	112.8(2)
C(7)-Si(2)-C(6)	106.1(2)
C(8)-Si(2)-C(6)	106.1(3)
C(15)-N(1)-Si(1)	114.8(3)
C(15)-N(1)-W	108.2(3)
Si(1)-N(1)-W	136.9(2)
C(20)-N(2)-Si(2)	120.0(3)
C(20)-N(2)-W	110.5(3)
Si(2)-N(2)-W	128.9(2)
C(21)-N(3)-W	170.3(3)
C(2)-C(1)-W	70.8(3)
C(2)-C(1)-H(1A)	116.5(3)
W-C(1)-H(1A)	116.53(13)
C(2)-C(1)-H(1B)	116.6(3)
W-C(1)-H(1B)	116.54(13)
H(1A)-C(1)-H(1B)	113.5

C(1)-C(2)-W	71.7(3)
C(1)-C(2)-H(2A)	116.4(3)
W-C(2)-H(2A)	116.42(13)
C(1)-C(2)-H(2B)	116.4(3)
W-C(2)-H(2B)	116.43(13)
H(2A)-C(2)-H(2B)	113.4
Si(1)-C(3)-H(3A)	109.5(2)
Si(1)-C(3)-H(3B)	109.5(2)
H(3A)-C(3)-H(3B)	109.5
Si(1)-C(3)-H(3C)	109.5(2)
H(3A)-C(3)-H(3C)	109.5
H(3B)-C(3)-H(3C)	109.5
Si(1)-C(4)-H(4A)	109.5(2)
Si(1)-C(4)-H(4B)	109.5(2)
H(4A)-C(4)-H(4B)	109.5
Si(1)-C(4)-H(4C)	109.5(2)
H(4A)-C(4)-H(4C)	109.5
H(4B)-C(4)-H(4C)	109.5
Si(1)-C(5)-H(5A)	109.5(2)
Si(1)-C(5)-H(5B)	109.5(2)
H(5A)-C(5)-H(5B)	109.5
Si(1)-C(5)-H(5C)	109.5(2)
H(5A)-C(5)-H(5C)	109.5
H(5B)-C(5)-H(5C)	109.5
Si(2)-C(6)-H(6A)	109.5(2)
Si(2)-C(6)-H(6B)	109.5(2)
H(6A)-C(6)-H(6B)	109.5
Si(2)-C(6)-H(6C)	109.5(2)
H(6A)-C(6)-H(6C)	109.5
H(6B)-C(6)-H(6C)	109.5
Si(2)-C(7)-H(7A)	109.5(2)
Si(2)-C(7)-H(7B)	109.5(2)
H(7A)-C(7)-H(7B)	109.5
Si(2)-C(7)-H(7C)	109.5(2)
H(7A)-C(7)-H(7C)	109.5
H(7B)-C(7)-H(7C)	109.5
Si(2)-C(8)-H(8A)	109.5(2)
Si(2)-C(8)-H(8B)	109.5(2)
H(8A)-C(8)-H(8B)	109.5
Si(2)-C(8)-H(8C)	109.5(2)
H(8A)-C(8)-H(8C)	109.5
H(8B)-C(8)-H(8C)	109.5
P(2)-C(9)-H(9A)	109.5(3)
P(2)-C(9)-H(9B)	109.5(2)
H(9A)-C(9)-H(9B)	109.5
P(2)-C(9)-H(9C)	109.5(3)
H(9A)-C(9)-H(9C)	109.5
H(9B)-C(9)-H(9C)	109.5
P(2)-C(10)-H(10A)	109.5(2)
P(2)-C(10)-H(10B)	109.5(2)
H(10A)-C(10)-H(10B)	109.5
P(2)-C(10)-H(10C)	109.5(2)
H(10A)-C(10)-H(10C)	109.5
H(10B)-C(10)-H(10C)	109.5

P(2)-C(11)-H(11A)	109.5(2)
P(2)-C(11)-H(11B)	109.5(2)
H(11A)-C(11)-H(11B)	109.5
P(2)-C(11)-H(11C)	109.5(2)
H(11A)-C(11)-H(11C)	109.5
H(11B)-C(11)-H(11C)	109.5
P(1)-C(12)-H(12A)	109.5(2)
P(1)-C(12)-H(12B)	109.5(2)
H(12A)-C(12)-H(12B)	109.5
P(1)-C(12)-H(12C)	109.5(2)
H(12A)-C(12)-H(12C)	109.5
H(12B)-C(12)-H(12C)	109.5
P(1)-C(13)-H(13A)	109.5(2)
P(1)-C(13)-H(13B)	109.5(2)
H(13A)-C(13)-H(13B)	109.5
P(1)-C(13)-H(13C)	109.5(2)
H(13A)-C(13)-H(13C)	109.5
H(13B)-C(13)-H(13C)	109.5
P(1)-C(14)-H(14A)	109.5(2)
P(1)-C(14)-H(14B)	109.5(2)
H(14A)-C(14)-H(14B)	109.5
P(1)-C(14)-H(14C)	109.5(2)
H(14A)-C(14)-H(14C)	109.5
H(14B)-C(14)-H(14C)	109.5
C(20)-C(15)-N(1)	119.2(4)
C(20)-C(15)-C(16)	118.0(4)
N(1)-C(15)-C(16)	122.8(4)
C(17)-C(16)-C(15)	121.5(4)
C(17)-C(16)-H(16A)	119.2(3)
C(15)-C(16)-H(16A)	119.2(3)
C(18)-C(17)-C(16)	119.5(4)
C(18)-C(17)-H(17A)	120.2(3)
C(16)-C(17)-H(17A)	120.2(3)
C(17)-C(18)-C(19)	120.4(5)
C(17)-C(18)-H(18A)	119.8(3)
C(19)-C(18)-H(18A)	119.8(3)
C(18)-C(19)-C(20)	121.2(5)
C(18)-C(19)-H(19A)	119.4(3)
C(20)-C(19)-H(19A)	119.4(3)
N(2)-C(20)-C(19)	124.0(4)
N(2)-C(20)-C(15)	116.7(4)
C(19)-C(20)-C(15)	119.2(4)
N(3)-C(21)-C(22)	121.8(4)
N(3)-C(21)-C(26)	119.8(4)
C(22)-C(21)-C(26)	118.4(4)
C(23)-C(22)-C(21)	120.6(5)
C(23)-C(22)-H(22A)	119.7(3)
C(21)-C(22)-H(22A)	119.7(3)
C(22)-C(23)-C(24)	120.5(5)
C(22)-C(23)-H(23A)	119.7(3)
C(24)-C(23)-H(23A)	119.7(3)
C(25)-C(24)-C(23)	119.0(5)
C(25)-C(24)-H(24A)	120.5(3)
C(23)-C(24)-H(24A)	120.5(3)

C(26)-C(25)-C(24)	121.4(5)
C(26)-C(25)-H(25A)	119.3(3)
C(24)-C(25)-H(25A)	119.3(3)
C(25)-C(26)-C(21)	120.0(5)
C(25)-C(26)-H(26A)	120.0(3)
C(21)-C(26)-H(26A)	120.0(3)
C(28)#1-C(27)-C(28)	118.7(10)
C(28)#1-C(27)-H(27A)	120.6(5)
C(28)-C(27)-H(27A)	120.6(5)
C(29)-C(28)-C(27)	121.1(7)
C(29)-C(28)-H(28A)	119.5(4)
C(27)-C(28)-H(28A)	119.4(5)
C(28)-C(29)-C(30)	120.9(7)
C(28)-C(29)-H(29A)	119.5(4)
C(30)-C(29)-H(29A)	119.7(4)
C(29)-C(30)-C(29)#1	117.4(9)
C(29)-C(30)-C(31)	121.3(4)
C(29)#1-C(30)-C(31)	121.3(4)
C(30)-C(31)-H(31A)	109.471(2)
C(30)-C(31)-H(31B)	109.471(4)
H(31A)-C(31)-H(31B)	109.5
C(30)-C(31)-H(31C)	109.471(2)
H(31A)-C(31)-H(31C)	109.5
H(31B)-C(31)-H(31C)	109.5

Symmetry transformations used to generate equivalent atoms:
#1 -x,y,-z+3/2

Table A9.4. Anisotropic displacement parameters ($A^2 \times 10^3$) for **39**. The anisotropic displacement factor exponent takes the form: $-2\,p^2\,[\,h^2\,a^{*2}\,U11 + ... + 2\,h\,k\,a^*\,b^*\,U12\,]$

Atom	U11	U22	U33	U23	U13	U12
W	22(1)	16(1)	13(1)	0(1)	0(1)	-1(1)
P(1)	26(1)	18(1)	17(1)	-1(1)	0(1)	-1(1)
P(2)	38(1)	18(1)	27(1)	0(1)	0(1)	-5(1)
Si(1)	23(1)	21(1)	25(1)	1(1)	4(1)	5(1)
Si(2)	23(1)	30(1)	22(1)	-1(1)	0(1)	2(1)
N(1)	23(2)	20(2)	17(2)	-1(1)	2(1)	4(1)
N(2)	22(2)	21(2)	15(2)	0(1)	-2(1)	0(1)
N(3)	24(2)	21(2)	18(2)	0(1)	-3(2)	-2(1)
C(1)	33(2)	22(2)	29(2)	6(2)	-6(2)	3(2)
C(2)	28(2)	30(2)	23(2)	4(2)	-5(2)	1(2)
C(3)	46(3)	24(2)	40(3)	3(2)	12(2)	13(2)
C(4)	23(2)	46(3)	40(3)	0(2)	1(2)	8(2)
C(5)	33(3)	23(2)	40(3)	1(2)	13(2)	1(2)
C(6)	39(3)	42(3)	32(3)	2(2)	-6(2)	15(2)
C(7)	28(2)	37(3)	29(2)	-1(2)	4(2)	10(2)
C(8)	24(2)	55(3)	49(3)	-9(3)	0(2)	-11(2)
C(9)	71(5)	34(3)	77(5)	5(3)	-37(4)	-19(3)
C(10)	73(5)	24(3)	61(4)	-14(3)	31(3)	-12(3)
C(11)	67(4)	27(3)	38(3)	3(2)	5(3)	-13(3)
C(12)	30(2)	23(2)	38(3)	1(2)	0(2)	-8(2)
C(13)	39(3)	22(2)	19(2)	-6(2)	-2(2)	2(2)
C(14)	40(3)	25(2)	25(2)	4(2)	-6(2)	0(2)
C(15)	34(2)	11(2)	13(2)	-3(1)	-9(2)	0(2)
C(16)	34(3)	27(2)	19(2)	0(2)	5(2)	1(2)
C(17)	41(3)	33(2)	10(2)	-3(2)	3(2)	-3(2)
C(18)	35(3)	36(3)	21(2)	1(2)	-5(2)	-7(2)
C(19)	27(2)	33(2)	19(2)	-1(2)	-7(2)	-5(2)
C(20)	22(2)	19(2)	17(2)	0(2)	-2(2)	-1(2)
C(21)	30(2)	21(2)	17(2)	3(2)	0(2)	0(2)
C(22)	29(2)	37(3)	25(2)	8(2)	-2(2)	-2(2)
C(23)	27(3)	45(3)	39(3)	12(2)	10(2)	8(2)
C(24)	46(3)	34(3)	25(2)	10(2)	12(2)	12(2)
C(25)	48(3)	42(3)	12(2)	1(2)	1(2)	0(2)
C(26)	28(2)	33(2)	25(2)	2(2)	4(2)	-5(2)
C(27)	58(6)	41(5)	106(9)	0	19(7)	0
C(28)	40(4)	67(5)	70(5)	-20(4)	11(3)	-8(3)
C(29)	31(3)	71(4)	41(3)	10(3)	8(2)	3(3)
C(30)	36(4)	41(4)	58(5)	0	18(4)	0
C(31)	78(8)	47(6)	134(12)	0	34(9)	0

Table A9.5. Hydrogen coordinates (x 10^4) and isotropic displacement parameters (A^4 x 10^4) for **39**.

Atom	x	y	z	U(eq)
H(1A)	1821(1)	6111(3)	3113(4)	34
H(1B)	2083(1)	6261(3)	2184(4)	34
H(2A)	2232(1)	7815(3)	2704(3)	32
H(2B)	1970(1)	7665(3)	3633(3)	32
H(3A)	2394(2)	5858(4)	442(4)	55
H(3B)	2719(2)	6351(4)	-122(4)	55
H(3C)	2331(2)	6236(4)	-605(4)	55
H(4A)	2635(1)	7219(4)	1909(4)	54
H(4B)	2649(1)	8359(4)	1740(4)	54
H(4C)	2914(1)	7664(4)	1168(4)	54
H(5A)	2259(2)	8633(3)	-895(4)	48
H(5B)	2676(2)	8558(3)	-606(4)	48
H(5C)	2410(2)	9253(3)	-35(4)	48
H(6A)	643(2)	9701(4)	-260(4)	57
H(6B)	798(2)	10421(4)	518(4)	57
H(6C)	377(2)	10167(4)	498(4)	57
H(7A)	855(1)	9774(4)	2597(3)	47
H(7B)	660(1)	8796(4)	2910(3)	47
H(7C)	425(1)	9676(4)	2517(3)	47
H(8A)	303(2)	7711(5)	450(4)	64
H(8B)	75(2)	8369(5)	1156(4)	64
H(8C)	310(2)	7490(5)	1550(4)	64
H(9A)	673(2)	6259(5)	1051(6)	91
H(9B)	791(2)	5219(5)	675(6)	91
H(9C)	911(2)	6168(5)	118(6)	91
H(10A)	1832(2)	5203(4)	1021(5)	79
H(10B)	1618(2)	5522(4)	98(5)	79
H(10C)	1499(2)	4573(4)	654(5)	79
H(11A)	1375(2)	5078(4)	2850(4)	66
H(11B)	1124(2)	4469(4)	2154(4)	66
H(11C)	956(2)	5339(4)	2745(4)	66
H(12A)	2272(1)	9623(3)	1725(4)	46
H(12B)	2300(1)	9463(3)	2833(4)	46
H(12C)	2188(1)	10495(3)	2425(4)	46
H(13A)	1645(1)	9368(3)	4025(3)	40
H(13B)	1293(1)	9888(3)	3611(3)	40
H(13C)	1666(1)	10467(3)	3690(3)	40
H(14A)	1566(2)	10182(4)	902(3)	45
H(14B)	1615(2)	10988(4)	1694(3)	45
H(14C)	1243(2)	10408(4)	1614(3)	45
H(16A)	1956(2)	7205(3)	-1086(3)	32
H(17A)	1550(2)	7251(4)	-2369(3)	33
H(18A)	955(2)	7787(4)	-2142(3)	37
H(19A)	758(1)	8286(4)	-639(3)	31
H(22A)	556(1)	6881(4)	3382(3)	36
H(23A)	279(2)	6534(4)	4830(4)	44

H(24A)	594(2)	6798(4)	6253(4)	42
H(25A)	1190(2)	7395(4)	6209(3)	41
H(26A)	1477(2)	7732(4)	4775(3)	35
H(27A)	0	4298	7500	102
H(28A)	-321(2)	5167(6)	6349(6)	71
H(29A)	-323(2)	6844(5)	6337(4)	57
H(31A)	146	8385(8)	8025	130
H(31B)	-248	8385(8)	7565	130
H(31C)	102	8385(8)	6910	130

APPENDIX B
TABLES OF KINETICS STUDIES

Table B.1. Substrate Dependence for the Formation of Ethylene Complex, **39.**

Ethylene Dependence :([W] = 24.3 mM ; [PMe_3] = 0.494M)

T(K)	k(sec^{-1}) : w/o C_2H_4	k(sec^{-1}) : w/ C_2H_4
293.15	0.001095	0.001035
283.15	0.000756	0.000822

Phosphine Depencence :([W] = 24.3 mM ; T = 283.15K)

[PMe_3] / M	k(sec^{-1})	Ln k	Ln [PMe_3]
0.494	0.000536	-7.532	-0.706
0.538	0.000553	-7.501	-0.621
0.614	0.000664	-7.318	-0.487
0.669	0.000696	-7.270	-0.402
0.724	0.000788	-7.146	-0.323
0.856	0.001028	-6.880	-0.156
1.086	0.001331	-6.622	0.083
1.218	0.001447	-6.538	0.197
1.470	0.001664	-6.399	0.385
1.700	0.001961	-6.234	0.531

* Plot of k vs [PMe_3] : Linear with Y-intercept = 0; (Y = -0.000068 + 0.001211X)

* Plot of Lnk vs Ln [PMe_3] : Linear with Slope = 1.10 $\pm$ 0.04

* Reaction is 0th order in ethylene and 1st order in PMe_3

Table B.2. Phosphine Depencence for the Formation of Styrene Complex, **40.**

[W] = 0.031 M

$[PMe_3]$ / M	$k_{exp}(sec^{-1})*10^4$	$k_{cal}(sec^{-1})*10^4$ (using equation 4.4)
0	2.1(013)	2.10
0.10		2.18
0.20	2.2(025)	2.30
0.30		2.46
0.40	2.4(023)	2.66
0.50		2.89
0.60		3.16
0.70		3.46
0.80	4.0(13)	3.80
0.85		3.98
0.94	4.5(042)	4.34
1.04		4.77
1.10	5.3(064)	5.05
1.15		5.27
1.20	5.7(073)	5.53
1.25		5.77
1.30	6.4(064)	6.06
1.40		6.61
1.50		7.20
1.64	8.4(18)	8.10
1.70		8.47
1.84	9.1(25)	9.46
1.90		9.90
2.04	10.4(17)	10.99
2.10		11.47

Table B.3. Kinetic Analysis for the Formation of Ethylene Complex, **39.**

T(K)	k(run#1)*10^4	k(run#2)*10^4	k(run#3)*10^4	k(ave)*10^4
293.15	9.48(14)	10.04(12)	9.30(56)	9.61(82)
283.15	7.86(14)	6.51(12)	6.58(11)	6.98(37)
273.15	4.39(4)	4.21(6)	4.78(8)	4.46(18)
263.15	3.14(4)	3.25(3)	3.40(9)	3.26(16)

[W] = 48.6 mM ; [PMe_3] = 972 mM

k : [k(reactant) + k(product)] / 2 ; k(ave) : [k(run#1) + k(run#2) + k(run#3)] / 3

Eyring Plot Analysis : $\Delta S^{\ddagger}$ = -54.9 ± 2.0 cal/mol.K; $\Delta H^{\ddagger}$ = 5.1 ± 0.6 Kcal/mol
R squared = 0.992

Table B.4. Kinetic Analysis for the Formation of Styrene Complex, **40.**

T(K)	k(run#1)*10^4	k(run#2)*10^4	k(run#3)*10^4	k(ave)*10^4
363.15	4.18(3)	4.29(9)	4.15(9)	4.21(21)
353.15	2.33(2)	2.30(2)	2.24(3)	2.29(7)
343.15	1.25(1)	1.29(2)	1.37(2)	1.30(5)
333.15	0.75(1)	0.59(2)	0.73(1)	0.69(4)

[W] = 30.9 mM ; [PMe_3] = 662 mM

k : [k(reactant) + k(product)] / 2 ; k(ave) : [k(run#1) + k(run#2) + k(run#3)] / 3

Eyring Plot Analysis : $\Delta S^{\ddagger}$ = -36.7 ± 2.3 cal/mol.K; $\Delta H^{\ddagger}$ = 13.7 ± 0.8 Kcal/mol
R squared = 0.9994

APPENDIX C
INPUT FOR KINFIT SIMULATION PROGRAM

Table C.1. Input for KINFIT Simulation Program.

Simulation for the decomposition of **6**

1110

1,6=a+ethylbenzene, 0.00021 [reactant(s)=product(s),rate constant]

2,6+pme3=b,0.00075

3,b=6+pme3,0.0000001

4,6=c,0.00001

5,c=6,0.0001

6,b=c+pme3,0.0001

7,c+p=b,0.0005

8,c=d,0.0016

9,d=c,0.02

10,d+pme3=g+ethylbenzene,0.00056

11,g+p=product,0.1

12,a+pme3=f,0.1

13,f+p=product,0.1

END

6,0.031 [reactant, initial concentration of 6]

pme3,0.4 [reactant, initial concentration of PMe_3]

END

1.0e-30,1.0e-33,1500,0.00345 [reaction time intervals]

10,50,100,200,500,1000,2000,3000,4000,5000,10000,15000

APPENDIX D
SCHEMATIC SUMMARY OF THE REACTIVITIES OF TUNGSTEN(VI) DIALKYL COMPLEXES

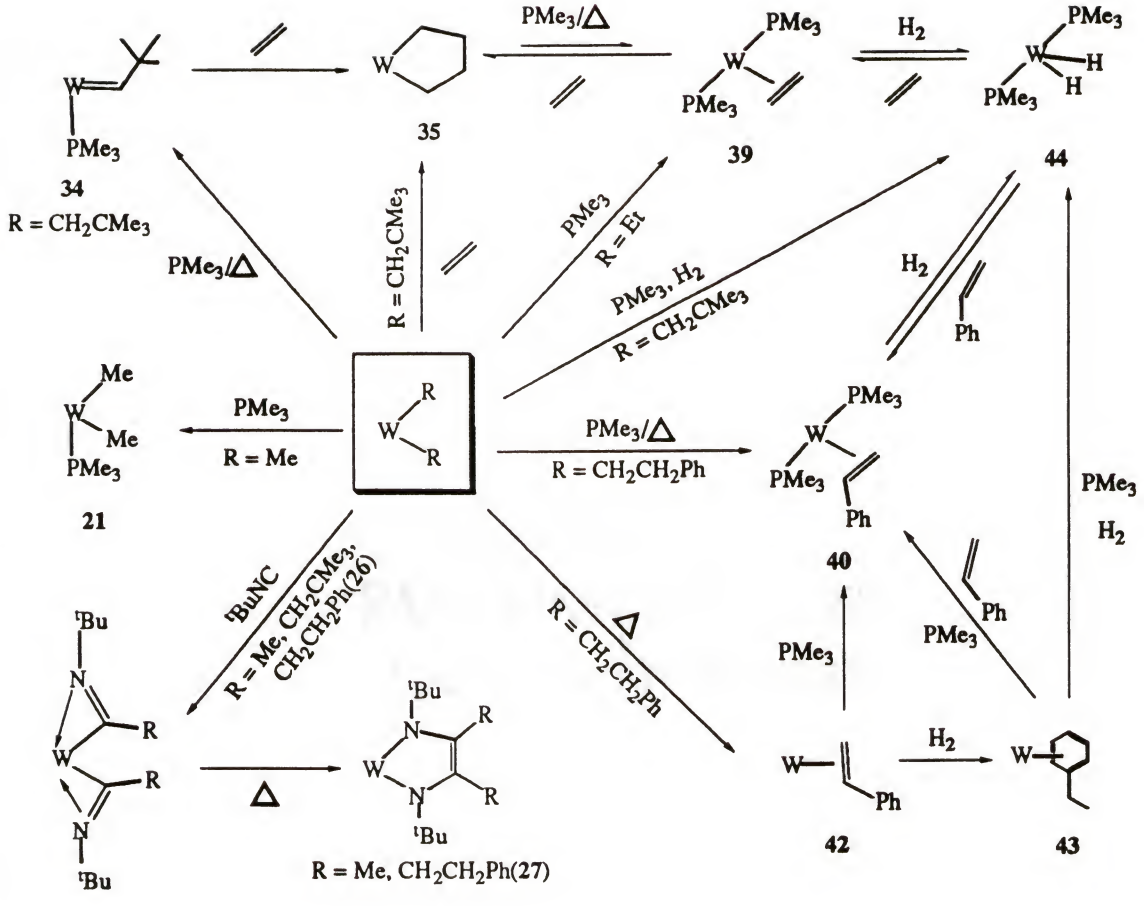

Figure D.1. Summary of the reactivities of tungsten(VI) dialkyl complexes (W = W(NPh)[*o*-$(Me_3SiN)_2C_6H_4$]).

LIST OF REFERENCES

1. Gates, B. C. *Catalytic Chemistry*, Wiley, New York, 1992.

2. Cotton, F. A.; Wilkinson, G. *Advanced Inorganic Chemistry*, Wiley, New York, 1988.

3. (a) Ivin, K. J. *Olefin Metathesis and Metathesis Polymerization*; Academic Press: San Diago, 1997. (b)*Comprehensive Coordination Chemistry*, Wilkinson, G.; Gillard, R.; McCleverty, J. A. Eds.; Pergamon Press: New York, 1987.

4. (a) Anderson, R. B.; Kobel, H.; Ralek, M. *The Fischer-Tropsch Synthesis*, Academic press, New York, 1984. (b)Herrmann, W. A. *Angew. Chem. Intl. Ed. Engl.* **1982**, *21*, 117.

5. (a) Ungvary, F. *Coord. Chem. Rev.* **1997**, *160*, 129. (b) Antolovic, D.; Davidson, E. R. *J. Am. Chem. Soc.,* **1987**, *109*, 5828.

6. (a) James, B. R. *Homogeneous Hydrogenation*, Wiley, New York, 1973. (b) Rylander, P. N. *Catalytic Hydrogenation in Organic Synthesis*, Academic Press, New York, 1979.

7. Cotton, F. A. Chem. Rev. **1955**, *55*, 551.

8. (a) Green, M. L. H. *Organometallic Compounds*, Vol.II, Methuen, London, 1968. (b) Parshall, G. W.; Mrowca, J. J. *Adv. Organomet. Chem.* **1968**, *7*, 157.

9. Schafer, W.; Thiele, K. H. *Z. Anog. Allg. Chem.* **1971**, *381*, 205.

10. (a) Theopold, K. H. *J. Chem. Soc., Chem. Commun.,* **1986,** 1491 (b) Abrahamson, H. B. *Organometallics* , **1984**, *3*, 1379. (c) Bochmann, M.; Wilkinson, G.; Young, G. B. *J. Chem. Soc., Dalton Trans.* **1980,** 1879. (d) Roberts, R. M. G. *J. Organomet. Chem.,* **1973**, *63*, 159. (e) Bower, B. K.; Tennent, H. G. *J. Am. Chem. Soc.,* **1972**, *94*, 2512.

11. (a) Atwood, J. L. *J. Chem. Soc., Dalton Trans.* **1987,** 747. (b) Schrock, R. R.; Parshall, G. W. *Chem. Rev.* **1976**, *76*, 243. (c) Davison, P. J.; Larrert, M. F.; Pearce, R. *Chem. Rev.* **1976**, *76*, 219.

12. (a) Collman, J. P.; Hegedus, L. S.; Norton, J. R.; Finke, R. G. *Principles and Applications of Organotransition Metal Chemistry*, 2nd ed. ; University Science Books : Mill Valley, L. A. , 1987. (b) Crabtree, R. H. *The Organometallic Chemistry of the Transition Metals*, John Wiley and sons, New York, 1988. (c) Puddephatt, R. J. *The Chemistry of the Metal-Carbon Bond*, Vol. I, Chapter 6, John Wiley and sons, 1982. (d) ref 2. (e) ref 8b and 11b.

13. (a) Parshell, G. W. *Homogeneous Catalysis*; John Wiley & Sons: New York; 1980; Chapter 3. (b) Cross, R. J. *The Chemistry of the Metal-Carbon Bond*; Hartley, F. R.; Patai, S., Eds.; John Wiley & Sons: New York; 1985; Vol.2, Chapter 8.

14. (a) Watson, P. L. *J. Am. Chem. Soc.* **1982**, *104*, 337. (b) Watson, P. L.; Roe, D. C. *J. Am. Chem. Soc.* **1982**, *104*, 6471. (c) Jordan, R. F.; Dasher, W. E.; Echols, S. F. *J. Am. Chem. Soc.* **1986**, *108*, 1718. (d) Jordan, R. F.; Bajgur, C. S.; Willett, R.; Scott, B. *J. Am. Chem. Soc.* **1986**, *108*, 7410. (e) Jeske, G.; Lauke, H.; Mauermann, H.; Swepston, P. N.; Schumann, H.; Marks, T. J. *J. Am. Chem. Soc.* **1985**, *107*, 8091. (f) Soto, J.; Steigerwald, M. L.; Grubbs, R. H. *J. Am. Chem. Soc.* **1982**, *104*, 4479. (g) Clawson, L.; Soto, J.; Buchwald, S. L.; Steigerwald, M. L.; Grubbs, R. H. *J. Am. Chem. Soc.* **1985**, *107*, 3377.

15. (a) Bryndza, H. E. *J. Am. Chem. Soc.,* **1986**, *108*, 4805. (b) Atwood, J. D. *Organometallics* , **1986**, *5*, 390.

16. (a) Wang, S.-Y. S.; Abboud, K. A.; Boncella, *J. Am. Chem. Soc.,* **1997**, *119*, 11990. (b) Huff, R. L.; Wang, S. Y.; Abboud, K. A.; Boncella, J. M. *Organometallics.*, **1997**, *16*, 1779. (c) Wang, S.-Y. S.; VanderLende, D. D.; Abboud, K. A.; Boncella, J. M. *Organometallics*, **1998**, in press.

17. (a) Thompson, M. E.; Baxter, S. M.; Bulls, A. R.; Burger, B. J.; Nolam, M. C.; Santarsiero, W. P.; Bercaw, J. E. *J. Am. Chem. Soc.,* **1987**, *109*, 203. (b) Fendrick, C. M.; Marks, T. J. *J. Am. Chem. Soc.,* **1986**, *108*, 425. (c) Watson, P. L.; Parshall, G. W. *Acc. Chem. Res.* **1985**, *18*, 51.

18. (a) Buchwald, S. L. and Nielsen, R. B. *J. Am. Chem. Soc.* **1988**, *110*, 3171-3175. (b) Freundlich, J. S., Schrock, R. R., and Davis, W. M. *J. Am. Chem. Soc.* **1996**, *118*, 3643-3655.

19. Dawoodi, Z.; Green, M. L. H.; Mtetwa, V. S. B.; Prout, K.; Schultz, A. J. Williams, M.; Koetzle, T. F. *J. Chem. Soc. Dalton Trans.,* **1986**, 1629.

20. Fellmann, J. D.; Schrock, R. R.; Trificante, D. D. *Organometallics*, **1982**, *1*, 481.

21. Buchwald, S. L.; Lum, R. T.; Dewan, J. C. *J. Am. Chem. Soc.* **1986**, *108*, 7441.

22. Erker, G. *J. Organomet. Chem.* **1977**, *134*, 189-202. (b) Erker, G.; Kropp, K. *Organometallics*, **1982**, *1*, 1246.

23. Fagan, P. J.; Marinquez, J. M.; Maatta, E. A.; Seyam, A. M.; Marks, T. T. *J. Am. Chem. Soc.* **1981**, *103*, 6650.

24. McLain, S. J.; Schrock, R. R.; Sharp, P. R.; Churchill, M. R.; Youngs, W. J. *J. Am. Chem. Soc.* **1979**, *101*, 263.

25. Kwart, H. *Acc. Chem. Res.* **1982**, *15*, 401.

26. Ozawa, F.; Ito, T.; Yamamoto, A. *J. Am. Chem. Soc.* **1980**, *102*, 6457.

27. Ikariya, T.; Yamamoto, A. *J. Organomet. Chem.* **1976**, *120*, 257.

28. (a) Whitesides, G. M. *Pure Appl. Chem.* **1981**, *53*, 287. (b) McCarthy, T. J.; Nuzzo, R. G.; Whitesides, G. M. *J. Am. Chem. Soc.* **1981**, *103*, 1676, 3396.

29. Burger, B. J.; Thompson, M. E.; Cotter, W. D.; Bercaw, J. E. *J. Am. Chem. Soc.* **1990**, *112*, 1566.

30. Evans, J.; Schwarts, J.; Urguhart, P. W. *J. Organomet. Chem.* **1974**, *81*, C37.

31. (a) Smith, K.-T.; Tilset, M.; Kristjansdottri, S. S.; Norton, J. R. *Inorg. Chem.*, **1995**, *34*, 6497. (b) Sorokin, A.; Robert, A.; Meunier, B. *J. Am. Chem. Soc.* **1993**, *115*, 7293. (c) Kwart, H.; Sarnar, S. F.; Slutsky, J. *J. Am. Chem. Soc.* **1973**, *95*, 5242.

32. Grubbs, R. H.; Miyashita, A. *J. Am. Chem. Soc.* **1978**, *100*, 7416.

33. Ozawa, F.; Yamamoto, A.; Ikariya, T.; Grubbs, R. H. *Organometallics* **1982**, *1*, 1481.

34. (a) McDermott, J. X.; White, J. F.; Whitesides, G. M. *J. Am. Chem. Soc.* **1976**, *98*, 6521. (b) McDermott, J. X.; White, J. F.; Whitesides, G. M. *J. Am. Chem. Soc.* **1973**, *95*, 4451.

35. Brown, M. P.; Hollings, A.; Houston, K. J.; Puddephatt, R. J.; Rashidi, M. *J. Chem. Soc.* **1976**, 786.

36. McLain, S. J.; Wood, C. D.; Schrock, R. R. *J. Am. Chem. Soc.* **1979**, *101*, 4558.

37. (a) McDermott, J. X.; Wilson, M. E.; Whitesides, G. M. *J. Am. Chem. Soc.* **1976**, *98*, 6529. (b) McDermott, J. X.; Whitesides, G. M. *J. Am. Chem. Soc.* **1974**, *96*, 947.

38. Foley, P.; DiCosimo, R.; Whitesides, G. M. *J. Am. Chem. Soc.* **1980**, *102*, 6713.

39. Miller, T. M.; Whitesides, G. M. *Organometallics* **1986**, *5*, 1473.

40. Goddard, R. J.; Hoffmann, R.; Eluvanthingal, D. J. *J. Am. Chem. Soc.,* **1980**, *102*, 7667.

41. (a) Ivin, K. J. *Ring Opening Polymerization,* Elsevier Science Pub. New York, 1984. (b) Dragutan, V. ; Balaban, A. T. ; Dimonie M. *Olefin Metathesis and Ring-Opening Polymerizations of Cyclo-Olefins*; 2nd ed. ; Wiley-Interscience : Bucharest, 1985. (c) Schrock, R. R. *Acc. Chem. Res.* **1990**, *23*, 158

42. Wagener, K. B. ; Boncella, J. M. ; Nel, J. G. *Macromolecules* **1991**, *24*, 2649.

43. (a) Vaughan, W. M. Ph.D dissertation, 1995, University of Florida. (b) Polse, J. L.; Anderson, R. A.; Bergman, R. G. *J. Am. Chem. Soc.,* **1996**, *118*, 8737. (c) Chamberlian, L. R.; Rothwell, I. P.; Huffmann, J. C. *J. Am. Chem. Soc.,* **1986**, *108*, 1502. (d) McDade, C.; Green, J. C.; Bercaw, J. E. *Organometallics* , **1982**, *1*, 1629.

44. Tran, E.; Legzdins, P. *J. Am. Chem. Soc.,* **1997**, *119*, 5071.

45. (a) Bruno, J. W.; Smith, G. M.; Marks, T. J.; Fair, C. K.; Schultz, A. J.; Williams, J. B. *J. Am. Chem. Soc.,* **1986**, *108*, 40. (b) Fendrick, C. M.; Marks, T. J. *J. Am. Chem. Soc.,* **1986**, *108*, 425. (c) Ibers, J. A.; DiCosimo, R.; Whitesides, G. M. *Organometallics* , **1982**, *1*, 13. (d) Tulip, T. H.; Thorn, D. L. *J. Am. Chem. Soc.,* **1981**, *103*, 2448.

46. Bercaw, J. E.; Marvich, R. H.; Bell, L. G.; Brintzinger, H. H. *J. Am. Chem. Soc.,* **1972**, *94*, 1219.

47. Abis, L.; Sen, A.; Halpern, J. *J. Am. Chem. Soc.,* **1978**, *100*, 2915.

48. (a) Green, M. L. H.; O'Hare, D. *Pure Appl. Chem.* **1985**, *57*, 1897. (b) Janowicz, A. H.; Bergman, R. G. *J. Am. Chem. Soc.,* **1982**, *104*, 352. (c) Hoyano, J. K.; Graham, W. A. G. *J. Am. Chem. Soc.,* **1982**, *104*, 3723. (d) Crabtree, R. H. *Chem. Rev.* **1985**, *85*, 245.

49. Foo, T.; Bergman, R. G. *Organometallics* , **1992**, *11*, 1811.

50. (a) VenderLende, D. D.; Abboud, K. A.; Boncella, J. M. *Organometallics* , **1994**, *13*, 3378. (b) Vanderlende, D. D.; Abboud, K. A.; Boncella, J. M. *Polymer Preprints* **1994**, *35*, 691.

51. (a) Aoyagi, K.; Kalai, K.; Gantzel, P. K.; Tilley, T. D. *Organometallics* **1996**, *15*, 923. (b) Aoyagi, K.; Kalai, K.; Gantzel, P. K.; Tilley, T. D. *Polyhedron* **1996**, *15*, 4299.

52. Pindado, G. J.; Thornton-Pett, M.; Bochmann, M. *J. Chem. Soc., Dalton Trans.,* **1998**, 393.

53. Nugent, W. A.; Mayer, J. M. *Metal-Ligand Multiple Bonds*, Wiley, New York, 1988.

54. D. E. Wigley, *Prog. Inorg. Chem.,* **1994**,*42* , 239.

55. (a) ven der Schaaf, P. A.; Abbenhuis, R. A. T. M.; Grove, D. M.; Smeets, W. J. J.; Spek, A. L.; van Koten, G. *J. Chem. Soc., Chem. Commun.,* **1993**, 504. (b) Legzdins, P.; Phillips, E. C.; Rettig, S. J.; Trotter, J.; Veltheer, J. E.; Yee, V. C. *Organometallics,* **1992**,*11* , 3104. (c) Eagle, A. A.; Young, C. G.; Tiekink, E. R. T.*Organometallics,* **1992**,*11* , 2934. (d) Zhang, C.; Schlemper, E. O.; Schrauzer, G. N. *Organometallics,* **1990**, *9* , 1016. (e) Schrock, R. R.; DePue, R. T.; Feldman, J.; Yap, K. B.; Yang, D. C.; Davis, W. M.; Park, L.; DiMare, M.;Schofield, M.; Anhaus, J.; Walborsky, E.; Evitt, E.; Kruger, C.; Betz, P. *Organometallics,* **1990**,*9* , 2262. (f) J.W. Faller, R.R. Kucharczyk, and Y. Ma, *Inorg. Chem.,* **1990**, *29* , 1662. (g) Fischer, J.; Kress, J.; Osborn, J. A.; Ricard, L.; Wesolek, M. *Polyhedron,* **1987**, *6* , 1839. (h) Churchill, M.R.; Youngs, W.J. *Inorg. Chem.,* **1979**, *18* , 2454. (i) Fletcher, S. R.; Skapski, A. C. *J. Organomet. Chem.,* **1973**,*59* , 299.

56. Pedersen, S. F.; Schrock, R. R. *J. Am. Chem. Soc.*, **1982**, *104*, 4783.

57. Wang, S.-Y. S.,; Boncella, J. M.; Abboud, K. A. *Acta Cryst.* **1997**, **C**53, 436.

58. LaMar, G. N. *J. Chem. Educ.* **1974**, *51*, 633.

59. Holmes, R. R. *Prog. Inorg. Chem.* **1984**, *32*, 119.

60. Rossi, A. R.; Hoffmann, R. *Inorg. Chem.* **1975**, *14*, 365.

61. (a) Dunn, S. C.; Mountford, P.; Shishin, O. V. *Inorg. Chem.* **1996**, *35*, 1006. (b) Fryzuk, M. D.; Mao, S. S. H.; Duval, P. B. *Polyhedron*, **1995**, *14*, 11. (c) Hsiao, T. Y.; Kuo, P. L.; Lai, C. H. *Organometallics,* **1993**, *12* , 1094.

62. Berry, R. S. *J. Chem. Phys.* **1960**, *32*, 933.

63. Holmes, R. R. *Pentacoordinated Phosphorus*, Vol. I, ACS Monogram, 175, A.C.S., Washington, D. C., **1980**. P.18.

64. Holmes, R. R. *Pentacoordinated Phosphorus*, Vol. II, ACS Monogram, 175, A.C.S., Washington, D. C., **1980**. P.226.

65. Ugi, I.; Marquarding, D.; Klusacek, H.; Gillespie, P.; Ramirez, F. *Acc. Chem. Res.* **1971**, *4*, 288.

66. Frankcombe, K.; Cavell, A.; Orrell, K. G.; Osborne, A. G.; Sik, V. *J. Chem. Soc., Chem. Commun.*, **1996**, 781.

67. Casares, J. A.; Espinet, P. *Inorg. Chem.* **1997**, *36*, 5428.

68. J. Sandström, *Dynamic NMR Spectroscopy*, Academic Press, New York, 1982.

69. Boncella, J. M.; Wang, S.-Y.S.; VanderLende, D. D.; Huff, R. L.; Vaughan, W. M.; Abboud, K. A. *J. Organomet. Chem.* **1997**, *530*, 59.

70. Albright, T. A.; Burdett, J. K.; Whangbo, M. H. *Orbital Interactions in Chemistry*, Wiley, New York, 1985.

71. (a) Treichel, P. M. *Adv. Organomet. Chem.* **1973**, *11*, 88. (b) L. D. Durfee and I. P. Rothwell, *Chem. Rev.*, **1988**, *88*, 1059. (c) Motz, P. L.; Alexander, J. J.; Ho, D. M. *Organometallics.*, **1989**, *8*, 2589. (d) Scott, M. J.; Lippard, S. J. *Organometallics.*, **1997**, *16*, 5857. (e) Lockwood, M. A.; Fanwick, P. E.; Rothwell, I. P. *Organometallics.*, **1997**, *16*, 3574. (f) Kloppenburg, L.; Petersen, J. L. *Organometallics.*, **1997**, *16*, 3548.

72. (a) Singleton, E.; Oosthuizen, H. E. *Adv. Organomet. Chem.* **1983**, *22*, 209. (b) Yamamoto, Y. *Coord. Chem. Rev.* **1980**, *32*, 193. (c) Yamamoto, Y.; Yamazaki, H. *Coord. Chem. Rev.* **1972**, *8*, 225.

73. (a) Chiu, K. W.; Jones, R. A.; Wilkinson, G.; Galas, A. M. R.; Hursthouse, M. B. *J. Chem. Soc., Dalton Trans.* (1981) 2090. (b) Valero, C.; Grehl, M.; Wingbermühle, D.; Kloppenburg, L.; Carpenetti, D.; Erker, G.; Petersen, J. L. *Organometallics*, *13* (1994) 415.

74. Kuniyasu, H.; Sugoh, K.; Su, M. S.; Kurosawa, H. *J. Am. Chem. Soc.* , **1997**, *119* , 4669.

75. (a) Tanase, T.; Ohizumi, T.; Kobayashi, K.; Yamamoto, Y. *Organometallics.*, **1996**, *15*, 3404. (b) ref 23(b).

76. Vaughan, W. M.; Abboud, K. A.; Boncella, J. M. *J. Am. Chem. Soc.* , **1995**, *117* , 11015.

77. Bishop III, K. C. *Chem. Rev.* **1976**, *76*, 461.

78. Chevrier, B.; Weiss, R.; Lange, M.; Chottard, J. C.; Mansuy, D. *J. Am. Chem. Soc.,* **1981**, *103*, 2399.

79. Schrock, R. R.; Fellmann, J. D. *J. Am. Chem. Soc.,* **1978**, *100*, 3359.

80. Schrock, R. R.; Meakin, P. *J. Am. Chem. Soc.,* **1974**, *96*, 5288.

81. Li, L.; Hung, M.; Xue, Z. *J. Am. Chem. Soc.,* **1995**, *117*, 12746.

82. Schrock, R. R. *J. Am. Chem. Soc.,* **1975**, *97*, 6577.

83. Grubbs, R. H. *Comprehensive Organometallic Chemistry*; G. Wilkinson and F. G. A. Stone, Eds.; Pergamon Press: Oxford, 1982; Vol. 8; pp499.

84. Herrison, J. L.; Chauvin, Y. *Makromol. Chem.* **1970**, *141*, 161.

85. (a) Mocella, M. T.; Busch, M. A.; Muetterties, E. L. *J. Am. Chem. Soc.,* **1976**, *98*, 1283. (b) Graff, G. M.; McNeils, E. *J. Catal.* **1975**, *38*, 482.

86. (a) Schrock, R. R. *Reactions of Coordinated Ligands*; Braterman, P. R., Ed.; Plenum: New Youk, 1986; p 221. (a) Calderon, N.; Lawrence, J. P.; Ofstead, E. A. *Adv. Organomet. Chem.* **1979**, *17*, 449. (b) Grubbs, R. H. *Prog. Inorg. Chem.* **1978**, *24*, 1.

87. (a) Rocklage, S. M.; Fellmann, J. D.; Rupprecht, G. A.; Messerle, L. W.; Schrock, R. R. *J. Am. Chem. Soc.,* **1981**, *103*, 1440. (b) McLain, S. J.; Wood, C. D.; Schrock, R. R. *J. Am. Chem. Soc.,* **1977**, *99*, 3519.

88. (a) Robbins, J.; Bazan, G. C.; Murdzek, J. S.; O'Regan, M. B.; Schrock, R. R. *Organometallics.*, **1991**, *10*, 2902. (b) Schrock, R. R.; Murdzek, J. S.; Bazan, G. C.; Robbins, J.; DiMare, M.; O'Regan, M. B. *J. Am. Chem. Soc.,* **1990**, *112*, 3875. (c) Feldman, J.; Murdzek, J. S.; Davis, W. M. Schrock, R. R. *Organometallics.*, **1989**, *8*, 2260.

89. Gassman, P. G.; Johnson, T. H. *J. Am. Chem. Soc.,* **1977**, *99*, 622.

90. (a) Schrock, R. R.; Sharp, P. R. *J. Am. Chem. Soc.,* **1978**, *100*, 2389. (b) ref 8.

91. Schwartz, J.; Gell, K. I. *J. Organomet. Chem.* **1980**, *184*, C1.

92. (a) Fox, H. H.; Lee, J.-K.; Park, L. Y.; Schrock, R. R. *Organometallics.*, **1993**, *12*, 759. (b) ref 17a and 17b.

93. (a) Berry, D. H.; Koloski, T. S.; Carroll, P. *Organometallics.*, **1990**, *9*, 2952. (b) ref 19a.

94. VanderLende, D. D. Ph.D dissertation, 1994, University of Florida.

95. Chisholm, M. H.; Huffman, J. C.; Hampden-Smith, M. J. *J. Am.Chem. Soc.* **1989**, *111*, 5284.

96. Robbins, J.; Bazan, G. C.; Murdzek, J. S.; O'Regan, M. B.; Schrock, R. R. *Organometallics.*, **1991**, *10*, 2902.

97. Lappert, M. F.; Power, P. P.; Sanger, A. R.; Srivastava, R. C. *Metal and Metalloid Amides* , John Wiley, New York, 1980, pp 244 - 249.

98. Feldman, J.; Davis, W. M.; Thomas, J. K.; Schrock, R. R. *Organometallics* **1990**, *9*, 2535.

99. (a) Gibson, V. C.; Poole, A. *J. Chem. Soc., Chem. Commun.,* **1995**, 2261. (b) Grubbs, R. H.; Miyashita, A. *J. Am. Chem. Soc.* **1978**, *100*, 1300.

100. (a) McLain, S. J.; Sancho, J.; Schrock, R. R. *J. Am. Chem. Soc.* **1980**, *102*, 5610. (b) Schrock, R. R.; McLain, S. J.; Sancho, J. *J. Pure Appl. Chem.* **1980**, *52*, 729.

101. Thorn, D. L.; Hoffman, R. *J. Am. Chem. Soc.* **1978**, *100*, 2079.

102. (a) Rothwell, I. P. *Polyhedron* **1985**, *4*. 177. (b) ref 48a.

103. (a) McDade, C.; Green, J. C.; Bercaw, J. E. *Organometallics*, **1982**, *1*, 1629. (b) Bulls, A. R.; Schaefer, W. P.; Serfas, M.; Bercaw, J. E. *Organometallics*, **1987**, *6*, 1219. (c) Chang, B. H.; Tung, H. S.; Brubaker, Jr., C. H. *Inorg. Chim. Acta*, **1981**, *51*, 143.

104. (a) Komiya, S.; Morimoto, Y. Yamamoto, A.; Yamamoto, T. *Organometallics*, **1982**, *1*, 1528-1536. (b) Whitesides, G. M.; Gaarch, J. F.; Stedronsky, E. R. *J. Am. Chem. Soc.* **1979**, *101*, 3659. (c) Boekel, C. P.; Teuben, J. H.; De Liefde Meijer, H. J. *J. Organomet. Chem.* **1976**, *120*, 257-284. (d) Erker, G.; Kropp, K. *J. Am. Chem. Soc.* **1979**, *101*, 3659. (e) Fagan, P. J.; Marinquez, J. M.; Maatta, E. A.; Seyam, A. M.; Marks, T. T. *J. Am. Chem. Soc.* **1981**, *103*, 6650. (f) Schock, L. E.; Brock, C. P.; Marks, T. J. *Organometallics*, **1987**, *6*, 232-241.

105. (a) Bruno, J. M.; Smith, G. M.; Marks, T. J.; Fair, C. K.; Schultz, A. J.; Williams, J. M. *J. Am. Chem. Soc.* **1986**, *108*, 40. (b) Simpson, S. J.; Turner, H. W.; Anderson, R. A. *Inorg. Chem.*, **1981**, *20*, 2991.

106. Buchwald, S. L.; Kreutzer, K. A.; Fisher, R. A. *J. Am. Chem. Soc.* **1990**, *112*, 4600.

107. Clark, G. R.; Nielson, A. J.; Richard, C. E. F.; Ware, D. C. *J. Chem. Soc., Dalton Trans.* **1990**, 1173.

108. Ortiz, C.; Boncella, J. M. unpublished results.

109. Visciglio, V. M.; Fanwick, P. E.; Rothwell, I. P. *J. Chem. Soc., Chem. Commun* **1992**,1505.

110. Rocklage, S. M.; Schrock, R. R. *J. Am. Chem. Soc.* **1982**, *104*, 3077.

111. Clark, G. R.; Nielson, A. J.; Richard, C. E. F.; Ware, D. C. *J. Chem. Soc., Chem. Commun.* **1989**, 1343.

112. (a) Rietveld, M. H. P.; Teunissen, W.; Hagen, H.; ven de Water, L.; Grove, D. M.; van der Schaaf, P. A.; Mühlebach, A.; Kooijman, H.; Smeets, W. J. J.; Veldman, N.; Spek, A. L.; van Koten, G. *Organometallics* **1997**, *16*, 1674. (b) Fernández, F. J.; Gómez-Sal, P.; Maneanero, A.; Royo, P.; Jacobson, H.; Berke, H. *Organometallics* **1997**, *16*, 1553. (c) Fanwick, P.E.; Rothwell, I. P.; Kriley, C. E.

Polyhedron **1996**, *15*, 2403. (d) Wehman-Ooyevaar, I. C. M.; Kapteijn, G. M.; Grove, D. M.; Smeets, W. J. J.; Spek, A. L.; van Koten, G. J. *J. Chem. Soc. Dalton Trans.* **1994**, 703. (e) Clark, G. R.; Nielson, A. J.; Richard, C. E. F.; Ware, D. C. *J. Chem. Soc., Dalton Trans.* **1990**, 1173. (f) Su, F.-M.; Cooper, C.; Geib, S. J.; Rheingold, A. L.; Mayer, J. M. *J. Am. Chem. Soc.* **1986**, *108*, 3545. (g) Cohen, S. A.; Auburn, P. R.; Bercaw, J. E. *J. Am. Chem. Soc.* **1983**, *105*, 1136. (h) Schultz, A. J.; Brown, R. K.; Williams, J. M.; Schrock, R. R. *J. Am. Chem. Soc.* **1981**, *103*, 169. (i) Guggenberger, L. J.; Meakin, P.; Tebbe, F. N. *J. Am. Chem. Soc.* **1974**, *96*, 5420.

113. Whitesides, G. M.; Gaasch, J. F.; Stedronsky, E. R. *J. Am. Chem. Soc.* **1972**, *94*, 5258.

114. Reger, D. L.; Culberston, E. C. *J. Am. Chem. Soc.* **1976**, *98*, 2789.

115. Wilkins, R. G. *Kinetics and Mechanism of Reactions of Transition Metal Complexes* 2nd Ed., VCH, New York, N.Y., 1991.

116. (a) Wood, C. D.; McLain, S.J.; Schrock, R. R. *J. Am. Chem. Soc.* **1979**, *101*, 3210. (b) Legzdens, P.; Veltheer, J. E.; Young, M. A.; Batchelor, R. J.; Einstein, F. W. B. *Organometallics*, **1995**, *14*, 407. (c) Vaughan, W. M.; Abboud, K. A.; Boncella, J. M. *J. Am. Chem. Soc.* **1995**, *117*, 11015.

117. (a) Doherty, N. M.; Bercaw, J. E. *J. Am. Chem. Soc.* **1985**, *107*, 2670-82. (b) Burger, B. J.; Santarsiero, B. D.; Trimmer, M. S.; Bercaw, J. E. *J. Am. Chem. Soc.* **1988**, *110*, 3134. (c) Burger, B. J.; Thompson, M. E.; Cotter, W. D.; Bercaw, J. E. *J. Am. Chem. Soc.* **1990**, *112*, 1566-77. (d) Halpern, J.; Okamoto, T. *Inorg. Chim. Acta*, **1984**, *89*, L53.

118. Ozawa, F.; Ito, T.; Yamamoto, A. *J. Am. Chem. Soc.* **1980**, *102*, 6457.

119. Schock, L. E.; Brock, C. P.; Marks, T. J. *Organometallics*, **1987**, *6*, 232-241.

120. Luinstra, G. A.; Teuben, J. H. *Organometallics*, **1992**, *11*, 1793-1801.

121. (a) Raftery, M. J,; Bowie, J. H.; Sheldon, J. C. *J. Chem. Soc., Perkin Trans. II*, **1988**, 563. (b) Orfanopoulos, M.; Smonou, I.; Foote, C. S. *J. Am. Chem. Soc.* **1990**, *112*, 3607.

122. (a) Lewis, G. N.; Randall, M. *Thermodynamics*, John Wiley and sons, New York, 1961. (b) Pitzer, K. S. *J. Chem. Phys.*, **1946**, *14*, 239. (c) Kilpatrick, J. E.; Pitzer, K. S. *J. Chem. Phys.*, **1949**, *17*, 1064.

123. Kiel, W. A.; Lin, G. -Y.; Gladysz, J. A. *J. Am. Chem. Soc.* **1980**, *102*, 3299.

124. Burk, M. J.; McGarth, M. P.; Crabtree, R. H. *J. Am. Chem. Soc.* **1988**, *110*, 620.

125. (a) Hlatky, G. G.; Crabtree, R. H. *Coord. Chem. Rev.*, **1985**, *65*, 1. (b) Moore, D. S.; Robinson, S. D. *Chem. Soc. Rev.*, **1983**, 415.

126. (a) Bau, R., Ed. *Transition Metal Hydrides*, Advances in Chemistry Series, No. 167, 1978. (b) Kaesz, H. D.; Saillant, R. B. *Chem. Rev.*, **1972**, *72*, 231. (c) ref 2.

127. (a) James, B. R. *Comprehensive Organometallic Chemistry*, Vol. 8, Chapter 51. Pergamon, New York, 1982. (b) ref 12(a). (c) ref 2.

128. Clark, J. R.; Fanwick, P. E.; Rothwell, I. P. *J. Chem. Soc., Chem. Commun* **1993**, 1233.

129. McNeese, T. J.; Mueller, T. E.; Wierda, D. A.; Darensbourg, D. J.; Delord, T. J. *Inorg. Chem.*, **1985**, *24*, 3465.

130. a) Crabtree, R. H. *Comprehensive Coordination Chemistry*, Wilkinson, G.; Gillard, R.; McCleverty, J. A. Eds.; Pergamon Press: New York, 1987; Chapter 19, Vol. 2. (b) Conner, K. A.; Walton, R. A. *Comprehensive Coordination Chemistry*, Wilkinson, G.; Gillard, R.; McCleverty, J. A. Eds.; Pergamon Press: New York, 1987; Chapter 43, Vol. 4. (c) LaPointe, R. E.; Wolczanski, P. T.; VanDuyne, G. D. *Organometallics*, **1985**, *4*, 1810. (d) LaPointe, R. E.; Wolczanski, P. T. *J. Am. Chem. Soc.*, **1986**, *108*, 3535.

131. Kubas, G. J.; Ryan, R. R.; Swanson, B. I.; Vergamini, P. J.; Wasserman, H. J. *J. Am. Chem. Soc.*, **1984**, *106*, 451.

132. Bianchini, C. *J. Am. Chem. Soc.*, **1987**, *109*, 5548.

133. Jessop, P. G.; Morris, R. H. *Coord. Chem. Rev.*, **1992**, *121*, 155.

134. Crabtree, R. H. *Inorg. Chim. Acta,* **1986**, *125*, 27.

135. Bullock, R. M.; Headford, C. E. L.; Hennessy, K. M.; Kegley, S. E.; Norton, J. R. *J. Am. Chem. Soc.*, **1989**, *111*, 3897.

136. (a) Howdle, S. M.; Healy, M. A.; Poliakoff, M. *J. Am. Chem. Soc.*, **1990**, *112*, 4804. (b) Luo, X. -L.; Crabtree, R. H. *J. Am. Chem. Soc.*, **1989**, *111*, 2527. (c) Rabaa, H.; Saillard, J. Y. *J. Organomet. Chem.*, **1987**, *330*, 397.

137. Halpern, J.; Okamoto, T.; Zakhariev, A. *J. Mol. Catal.*, **1976**, *2*, 65.

138. Wang, S. -Y. S.; Gomez, F.; Wagener, K. B.; Boncella, J. M. unpublished result.

139. (a)*Comprehensive Organometallic Chemistry*; G. Wilkinson and F. G. A. Stone, Eds.; Pergamon Press: Oxford, 1982; Vol. 3; Chapters 26.2, 27.2, and 28.2. (b) *Comprehensive Organometallic Chemistry*; G. Wilkinson and F. G. A. Stone, Eds.; Pergamon Press: Oxford, 1995; Vol. 5; Chapters 8.

140. (a) Price, J. T.; Sorensen, T. S. *Can. J. Chem.* **1968**, *46*, 515. (b) Emanuel, R. V.; Randall, E. W. *J. Chem. Soc. (A)*, **1969**, 3002. (c) Khankkarova, V. S.; Gubin, S. P.; Kvasov, B. A. *J. Organomet. Chem.*, **1970**, *23*, 509.

141. Visciglio, V. M.; Fanwick, P. E.; Rothwell, I. P. *J. Chem. Soc. Chem. Commun.*, **1992**, 1505.

142. Haward, M. T.; George, M. W.; Hamley, P.; Poliakoff, M. *J. Chem. Soc. Chem. Commun.*, **1991**, 1101.

143. (a) McLain, S. J.; Wood, C. D.; Schrock, R. R. *J. Am. Chem. Soc.* **1979**, *101*, 4558. (b) Grubbs, R. H.; Miyashita, A. *J. Am. Chem. Soc.* **1978**, *100*, 7416.

144. *Comprehensive Organometallic Chemistry*; G. Wilkinson and F. G. A. Stone, Eds.; Pergamon Press: Oxford, 1982; Vol. 8, Chapter 51.

145. Collman, J. P.; Hegedus, L. S.; Norton, J. R.; Finke, R. G. *Principles and Applications of Organotransition Metal Chemistry*, 2nd ed. ; University Science Books : Mill Valley, L. A. , 1987; Chapter 10.

146. (a) Dawans, F.; Morel, D. *J. Mol. Catal.* **1977**, *3*, 403. (b) Halpern, J. *J. Mol. Catal.* **1976**, *2*, 65.

147. (a) Chan, A. C. S.; Halpern, J. *J. Am. Chem. Soc.* **1980**, *102*, 838. (b) Halpern, J.; Riley, D. P.; Chan, A. C. S.; Pluth, J. J. *J. Am. Chem. Soc.* **1977**, *99*, 8055.

148. *Inorganic Reactions and Methods*, Zuckerman, J. J.; Norman, A. D. Eds.; VCH Publishers, New York, 1991; Vol. 16.

149. Kawakami, K.; Mizoroki, T.; Ozaki, A. *Chem. Lett.*, **1976**, 847.

150. Cais, M.; Frantel, E. N.; Rejoan, A. *Tetrahedron Lett.*, **1968**, 1919.

151. Sisak, A.; Ungvary, F. *Chem. Ber.*, **1976**, *109*, 531.

152. Fehr, C. *Helv. Chim. Acta*, **1983**, *49*, 3849.

153. (a) Pidcock, A.; Smith, J. D.; Taylor, B. W. *J. Chem. Soc. (A)*, **1969**, 1604. (b) Jones, C. E.; Coskran, K. J. *Inorg. Chem.*, **1971**, *10*, 55.

154. Nasielski, J.; Kirsch, P.; Wilputte-Steinert, L. *J. Organomet. Chem.*, **1971**, *27*, C13.

155. Connor, J. A. *Top. Curr. Chem.*, **1977**, *71*, 71.

156. Strohmeier, W.; Muller, R. *Z. Phys. Chem.*, **1964**, *40*, 86.

157. Sheldrick, G. M. *SHELXTL.* Nicolet XRD Corporation, Madison, Wisconsin, USA, 1995.

BIOGRAPHICAL SKETCH

Shu-Yu Steve Wang was born on December 27, 1967, in Taipei, Taiwan. It was fate that led him to be a chemist. He was accepted by National Taiwan University at 1986, where he spent lots of time in ballroom dancing and met Becky Chiu who became his wife in May 1994. His undergraduate work at NTU was focused on molecular beam reaction kinetics under the supervision of Professor Shen-Maw Lin at Academia Sinica. He received his B. S. in 1990 and was enlisted in the Chinese Air Force, working at the Quality Control Department for two years. Despite related experience in physical and analytical chemistry, he decided to actually work on something "visible." He started his graduate work at the University of Florida in 1993. He joined the research group of Dr. James M. Boncella where he spent five years exploring the fascinating world of organometallic chemistry. Three years after his marriage, their first son, Kyle, was born in February of 1997. After completion of his Ph. D. degree in organic/organometallic chemistry in April of 1998, Steve will assume a position as a research scientist at Sinon corporation, pharmaceutical division, in Taichung, Taiwan.

I certify that I have read this study and that in my opinion it conforms to acceptable standards of scholarly presentation and is fully adequate, in scope and quality, as a dissertation for the degree of Doctor of Philosophy.

James M. Boncella, Chairman
Associate Professor of Chemistry

I certify that I have read this study and that in my opinion it conforms to acceptable standards of scholarly presentation and is fully adequate, in scope and quality, as a dissertation for the degree of Doctor of Philosophy.

Lisa A. McElwee-White
Professor Chemistry

I certify that I have read this study and that in my opinion it conforms to acceptable standards of scholarly presentation and is fully adequate, in scope and quality, as a dissertation for the degree of Doctor of Philosophy.

David E. Richardson
Professor of Chemistry

I certify that I have read this study and that in my opinion it conforms to acceptable standards of scholarly presentation and is fully adequate, in scope and quality, as a dissertation for the degree of Doctor of Philosophy.

Kenneth B. Wagener
Professor of Chemistry

I certify that I have read this study and that in my opinion it conforms to acceptable standards of scholarly presentation and is fully adequate, in scope and quality, as a dissertation for the degree of Doctor of Philosophy.

Anthony B. Brennan
Associate Professor of Materials
Science and Engineering

This dissertation was submitted to the Graduate Faculty of the Department of Chemistry of the College of Liberal Arts and Sciences and to the Graduate School and was accepted as partial fulfillment of the requirements for the degree of Doctor of Philosophy.

May, 1998

Dean, Graduate School